UNIVERSITAT DE BARCELONA

Multitarget strategies in search of novel drug candidates against Alzheimer's disease

Caterina Pont Masanet

UNIVERSITAT DE BARCELONA

FACULTAT DE FARMÀCIA I CIÈNCIES DE L'ALIMENTACIÓ

Departament de Farmacologia, Toxicologia i Química Terapèutica

Unitat de Química Farmacèutica

MULTITARGET STRATEGIES IN SEARCH OF NOVEL DRUG CANDIDATES AGAINST ALZHEIMER'S DISEASE

Caterina Pont Masanet

Barcelona, 2019

UNIVERSITAT DE BARCELONA

Facultat de Farmàcia i Ciències de l'Alimentació

Programa de doctorat:

Química Orgànica

MULTITARGET STRATEGIES IN SEARCH OF NOVEL DRUG CANDIDATES AGAINST ALZHEIMER'S DISEASE

Memòria presentada per Caterina Pont Masanet per optar al títol de Doctor per la Universitat de Barcelona

Director i tutor:

Dr. Diego Muñoz-Torrero López-Ibarra

Doctoranda:

Caterina Pont Masanet

Barcelona, 2019

El treball experimental recollit en aquesta memòria ha estat realitzat al Laboratori de Química Farmacèutica de la Facultat de Farmàcia i Ciències de l'Alimentació de la Universitat de Barcelona sota la direcció del doctor Diego Muñoz-Torrero.

La present Tesi Doctoral ha estat possible gràcies a la concessió d'una beca per a la Formació de Personal Investigador (FI-DGR2016), atorgada per la *Generalitat de Catalunya* mitjançant l'*Agència de Gestió d'Ajuts Universitaris i de Recerca* (febrer-setembre de 2016) i a la concessió d'una beca de Formació de Professorat Universitari (FPU2015) atorgada pel *Ministerio de Educación, Cultura y Deporte* (setembre 2016 – octubre 2019).

El present treball ha estat finançat pel *Ministerio de Economía y Competitividad, Agencia Estatal de Investigación* i *Fondo Europeo de Desarrollo Regional (FEDER)* (SAF2014-57094-R, SAF2017-82771-R) i la *Generalitat de Catalunya* (2014SGR52, 2017SGR106).

Summary

Alzheimer's disease (AD) is the most common form of dementia and one of the most important health-care problems in the world, due to its high prevalence and unaffordable personal and economic impact. Moreover, current commercialised treatments are only symptomatic, but are not capable of preventing, curing or even delaying the disease progression. Because AD arises from a complex network of pathological events, such as dysfunction in neurotransmitter systems (mainly cholinergic and glutamatergic), β-amyloid and tau proteins disorders, oxidative stress or neuroinflammation, amongst others, the traditional medicinal chemistry paradigm of "one molecule-one target" is increasingly regarded as clearly ineffective. On the contrary, it becomes evident that a more comprehensive, complex pharmacological approach is needed to tackle AD. As a consequence, the use of multitarget directed ligands, where one single molecule is able to interact simultaneously with multiple targets of the pathological network, is emerging as a promising and more realistic way to confront this disease. In this context, the purpose of the present Thesis was the design, synthesis and biological evaluation of three novel families of compounds, endowed with multitarget biological profile, in order to find novel treatments for AD: 1) firstly, a new series of compounds designed by substitution of the rhein subunit of a rhein–huprine hybrid lead, previously developed in our group, by more simplified scaffolds, with the aim of finding optimized hybrids with reduced lipophilicity and better drug-like properties, while maintaining favourable activities against cholinesterases, BACE1, β-amyloid and tau aggregation, and antioxidant properties; 2) secondly, a novel family of huprine-derived hybrids, designed to perform a dual binding site interaction within BACE1 through the linkage of a huprine moiety to new scaffolds, selected by their predicted binding affinities towards a secondary transient pocket in BACE1, which were expected to combine cholinesterases and BACE1 inhibitory activities, as well as activity against β-amyloid and tau aggregation, and antioxidant properties; 3) finally, a family of huprine–TPPU and tacrine–TPPU hybrids, which were designed to be dual inhibitors of acetylcholinesterase (AChE) and soluble epoxide hydrolase (sEH). The blood–brain barrier permeability was also assessed for all these compounds, as it is a crucial factor for drugs acting in the central nervous system, while other important physicochemical and pharmacokinetic parameters, such as solubility and microsomal stability were determined for the latter series of compounds. Also, the toxicity of some compounds was evaluated. Finally, using the same assay that was employed for the determination of the β-amyloid and tau antiaggregating activity of the first two families and other compounds synthesised by our group, we demonstrated that a single compound can be able of inhibiting the aggregation of different types of amyloid-prone proteins, with these results supporting the notion that common mechanisms exist for the aggregation of different amyloidogenic proteins and that a generic treatment of conformational diseases is possible.

Abbreviations

AA	Arachidonic acid
Aβ	β-Amyloid peptide
$Aβ_{40}$	β-Amyloid peptide 1–40
$Aβ_{42}$	β-Amyloid peptide 1–42
ABD	Agonist binding domain
ACE	Angiotensin-converting enzyme
AcetylCoA	Acetyl coenzyme A
ACh	Acetylcholine
AChE	Acetylcholinesterase
AChEI	Acetylcholinesterase inhibitor
AD	Alzheimer's disease
ADAM	A disintegrin and metalloprotease
AICD	APP intracelular domain
AMPA	α-Amino-3-hydroxy-5-methyl-4-isoxazolepropionic acid
ApoE	Apolipoprotein E
APP	Amyloid precursor protein
ARE	Antioxidant response element
ATD	Amino-terminal domain
BACE1	β-Secretase; β-Site amyloid precursor protein cleaving enzyme 1
BBB	Blood–brain barrier
BCh	Butyrylcholine
BChE	Butyrylcholinesterase
BChEI	Butyrylcholinesterase inhibitor
BS1	Binding site 1 (BACE1)
BS2	Binding site 2 (BACE1)
CAS	Catalytic anionic site
CAT	Choline acetyltransferase
Cdk5	Cyclin-dependent kinase 5
CNS	Central nervous system
COX	Cyclooxygenase
CR	Congo red
CREB	Cyclic adenine monophosphate response element binding protein
CSF	Cerebrospinal fluid

CYP	Cytochrome P450
DHET	Dihydroeicosatrienoic acid
DMF	*N,N*-Dimethylformamide
DMSO	Dimethyl sulfoxide
DPPH	2,2-diphenyl-1-picrylhydrazyl
E. coli	*Escherichia coli*
EAAT	Excitatory amino acids transporter
ECE-1	Endothelin-converting enzyme 1
EDC	1-Ethyl-3-(3-dimethylaminopropyl)carbodiimide
EDTA	Ethylenediaminetetraacetic acid
EET	Epoxyeicosatrienoic acid
EOAD	Early-onset Alzheimer's disease
ER	Endoplasmic reticulum
Et	Ethyl
Et_3N	Triethylamine
Et_2O	Diethyl ether
EtOAc	Ethyl acetate
FgHET-s	prion-forming domain in filamentous fungus *Fusarium graminium*
GSK-3β	Glycosen synthase kinase 3β
*h*AChE	Human acetylcholinesterase
*h*BChE	Human butyrylcholinesterase
hIAPP	Human islet amyloid polypeptide
HETE	Hydroxyeicosatetranoic acid
HOBt	1-Hydroxybenzotriazole
HTVS	High throughput virtual screening
HRMS	High-resolution mass spectrometry
IB	Inclusion body
IDE	Insulin degrading enzyme
IgG1	Immunoglobulin G1
IL	Interleukin
IPTG	1-Thio-*β*-D-galactopyranoside
LBD	Ligand binding domain
LD_{50}	Letal concentration killing 50% individuals
LOAD	Late-onset Alzheimer's disease
LOX	Lipoxygenase
LTP	Long-term potentiation

mAb	Monoclonal antibody
mAChR	Muscarinic acetylcholine receptor
MAPK	Mitogen-activated protein kinase
MCM	Multiple-compound medication
MD	Molecular dynamics
Me	Methyl
MeOH	Methanol
MMP9	Matrix metalloproteinase 9
MMT	Multiple-medication therapy
Ms	Mesyl
MTDL	Multitarget-directed ligands
MW	Molecular weight
nAChR	Nicotinic acetylcholine receptor
NEP	Neprilysin
NFTs	Neurofibrillary tangles
NMDA	*N*-Methyl-D-aspartate
NMDAR	*N*-Methyl-D-aspartate receptor
NMP	*N*-Methyl-2-pyrrolidone
NMR	Nuclear magnetic resonance
NO	Nitric oxide
NORT	Novel Object Recognition Test
Nrf2	Nuclear receptor factor 2
NSAID	Non-steroid antiinflammatory
P_e	Permeability
PaHET-s	prion-forming domain in filamentous fungus *Podospora anserina*
PAMPA	Parallel artificial membrane permeability assay
PAS	Peripheral anionic site
PBS	Phosphate-buffered saline
PET	Positron emission tomography
PFD	Prion-forming domain
P-gp	P-glycoprotein
PHF	Paired helical filaments
PrP	Prion protein
PSEN	Presenilin
PSEN1 / PS1	Presenilin 1
PSEN2	Presenilin 2

*p*TSA	*p*-Toluenesulfonic acid
PV	Pyrocatechol violet
p3	p3 Peptide fragment
QM	Quantum mechanics
RNS	Reactive nitrogen species
ROC	Receiver operating characteristic curve
ROS	Reactive oxygen species
r. t.	Room temperature
SAPK	Stress-activated protein kinase
sAPPα	Secreted amyloid precursor protein-alpha form
sAPPβ	Secreted amyloid precursor protein-beta form
SAR	Structure–activity relationship
sEH	Soluble epoxyde hydrolase
SF	Straight filaments
SynH	Human synuclein
SynM	Mouse synuclein
tau	Tubulin-associated protein
THF	Tetrahydrofuran
Th-S	Thioflavin-S
Th-T	Thioflavin-T
TLC	Thin-layer chromatography
TMD	Trans-membrane domain
TNF-α	Tumor necrosis factor α
TTR	Transthyretin
XP	Extra precision
VS	Virtual screening

Table of contents

CHAPTER 1

Introduction

1.1 Dementia and Alzheimer's disease

Dementia was the fifth leading cause of death in the world in 2016, being responsible for almost 2 million deaths.[1] In 2018, there were approximately 50 million people suffering from dementia worldwide. Worryingly, this figure is estimated to increase to 82 million people in 2030 and to more than 152 million by 2050, along with the increase of average life expectancy in the world. Moreover, dementia has also a huge economic impact, with a total estimated worldwide cost of US$ 1 trillion, which will rise to US$ 2 trillion by 2030.[2]

Alzheimer's disease (AD) is the most common neurodegenerative disorder, accounting for 60-80% of all dementia cases. Many patients also present additional symptoms related to other dementias, which is called mixed dementia. AD is thought to begin about 20 years before symptoms appear. The most common symptoms pattern begins with gradual difficulties to remember new information. This is due to the death or malfunction of the first neurons, located in brain regions involved in thinking, learning and memory (cognitive function). Apathy and depression appear also often as early symptoms. As the disease progresses, neurons in other parts of the brain are damaged and destroyed, causing impaired communication, disorientation, confusion, poor judgement and behavioural changes. In the final stages of the disease, difficulties in speaking, swallowing and walking appear. At this point, patients are bed-bound and require continuous care. Being bed-bound makes them vulnerable to several conditions and infections, that are often a contributing case of death to patients with AD.[3,4]

Although AD is an age-related disease, it develops over a long preclinical period of several decades, which raises the question of the extent to which risk factors assessed during life can contribute in the development of this neurodegenerative disorder. Several studies have confirmed that there is strong evidence that regular physical activity and management of cardiovascular risk factors (such as diabetes or obesity) reduce the risk of cognitive impairment and may reduce the risk of suffering from dementia.[3,5]

---

[1] *Global Health Estimates 2016: Deaths by Cause, Age, Sex, by Country and by Religion, 2000-2016*. Geneva, World Health Organization, **2018**.

[2] C. Patterson. *World Alzheimer Report 2018: The state of the art of dementia research: New frontiers. Alzheimer's Disease International* **2018.**

[3] Alzheimer's Association. *Alzheimer's & Dementia* **2018**, *14*, 367–429.

[4] Alzheimer's Association. *Alzheimer's & Dementia* **2019**, *15*, 321–387.

[5] P. Scheltens, K. Blennow, M. M. B. Breteler, B. de Strooper, G. B. Frisoni, S. Salloway, W. M. Van der Flier. *Lancet* **2016**, *388*, 505–517.

Based on its age of onset, AD is classified into early-onset AD (EOAD, onset <65 years), which accounts for 1-5% of all cases, and late-onset AD (LOAD, onset ≥65 years) accounting for >95% of patients. Although they are clinically indistinguishable, EOAD is generally associated with a more rapid rate of progression and a Mendelian pattern of inheritance.[6] Genetics play a vital role in the risk and pathogenesis of AD. The genetics of AD are complicated because it is a highly heterogeneous disorder. Thus far, four genetic risk factors have been definitely implicated in the etiology of AD. Three genes encoding amyloid precursor protein (APP) and presenilin 1 and 2 (PSEN1 and PSEN2) have been firmly implicated in the pathophysiology of EOAD. Mutations in these genes are autosomal dominantly inherited (causing familial AD and early-onset disease) and may affect the cleavage of APP, resulting in overproduction and aggregation of β-amyloid peptide 1–42 ($A\beta_{42}$).[5-7]

On the contrary, genes involved in LOAD increase risk in a non-Mendelian fashion (called sporadic AD). The strongest genetic risk factor for LOAD involves the gene encoding apolipoprotein E (ApoE), involved in the transportation of lipids and cholesterol. The risk of suffering the disease is >50% for ApoE4 homozygotes and 20-30% for ApoE3 and ApoE4 heterozygotes. Mutations in ApoE may influence the synthesis, clearance and aggregation of Aβ. In order to identify new AD loci, several genome-wide association studies have identified more than 20 genetic loci associated with risk of AD. Those genes belong to pathways implicated in immune system and inflammatory responses, cholesterol and lipid metabolism, or endosomal-vesicle recycling. However, less convincing evidence has been found of their contribution to the individual risk for AD.[6,7]

1.2 Pathogenesis of Alzheimer's disease

AD is named after Dr. Alois Alzheimer. In 1907, Dr. A. Alzheimer described the occurrence of "military bodies" and "dense bundles of fibrils" in the autopsy of a cerebral cortex of a 56-year-old woman, who was previously diagnosed with dementia. However, it was not until 60-70 years later that new significant developments were reported and AD was recognized as the most common cause of dementia.[8,9] Since then, our knowledge of AD has increased dramatically.

---

[6] C. Reitz, R. Mayeux. *Biochem. Pharmacol.* **2014**, *88*, 640–651.
[7] W. Shao, D. Peng, X. Wag. *J. Clin. Neurosci.* **2017**, *45*, 1–8.
[8] a) A. Alzheimer. *Allgemeine Zeitschrift für Psychiatrie und Phychisch-Gerichtliche Medizin* **1907**, *64*, 146–148. b) A. Rainulf, H. Stelzmann, N. Scnitzlein, F. R. Murtagh. *Clin. Anat.* **1995**, *8*, 429–431.
[9] R. E. Tanzi, L. Bertram. *Cell* **2005**, *120*, 545–555.

Despite all the research around AD for several years, the etiology of this disorder is still unclear. However, two characteristic histopathological hallmarks are now clearly defined, namely the senile plaques (Dr. Alzheimer's military bodies) and neurofibrillary tangles (NFTs, Dr. Alzheimer's dense bundles of fibrils) (**Figure 1.1)**, together with the degeneration of the neurons and synapses. These structures are mainly composed of extracellular accumulations of β-amyloid peptide (Aβ) and helical filaments of hyperphosphorylated tau (tubulin-associated unit) protein inside neurons, respectively, and may be observed 10 to 15 years before the first symptoms appear.[3,4,8,9] As there is little known about the sequence of molecular mechanisms of these events, it still remains unclear which of them occurs first, or whether or not they are at the root of the pathogenesis of AD.[10]

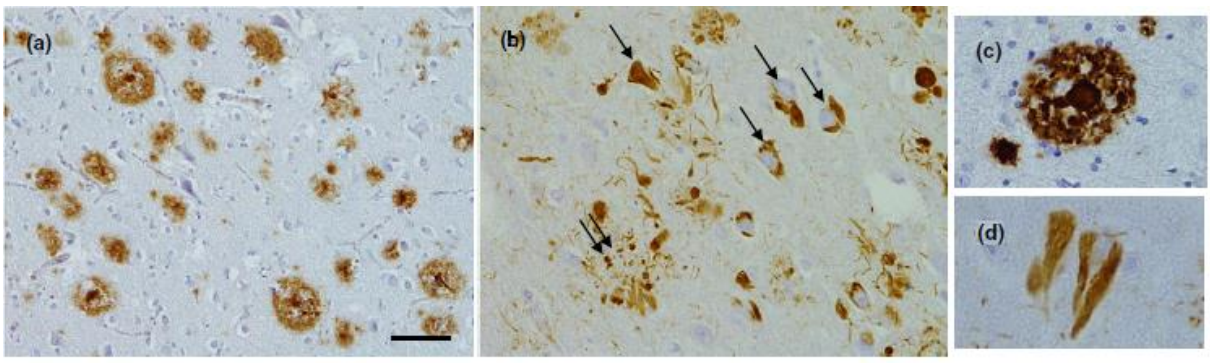

Figure 1.1. Immunohistochemistry of the frontal cortex of AD patients. (a) senile plaques formed by extracellular deposits of Aβ, surrounded by dystrophic neurites. An Aβ cored plaque is shown at higher magnification in (c) showing a central core. (b) neurofibrillary tangles (NFTs, arrows, shown at higher magnification in (d)) and neuritic plaques (double arrows) formed by aggregates of hyperphosphorylated tau protein. The bar represents 50 µm in (a); 25 µm in (b) and (c); 15 µm in (d). (Image adapted from: C. A. Lane, J. Hardy, J. M. Schott. *Eur. J. Neurol.* **2018**, *25*, 59–70).

Thus far, several pathogenic mechanisms underlying these changes have been studied, including Aβ aggregation and deposition into senile plaques, tau hyperphosphorylation with NFTs formation, neurovascular dysfunction and other mechanisms, such as neuroinflammatory processes or oxidative stress, which have led to the formulation of several hypotheses about the pathogenesis of AD.[11,12]

[10]P. Nelson, I. Alafuzoff, E. Bigio, C. Bouras, H. Braak, N. Cairns, R. Castellani, B. Crain, P. Davies. *J. Neuropathol. Exp. Neurol.* **2012**, *71*, 362–381.
[11]K. Blennow, M. J. de Leon, H. Zetterberg. *Lancet* **2006**, *368*, 387–403.
[12]P. Sharma, P. Srivastava, A. Seth, P. N. Tripathi, A. G. Banerjee, S. K. Shrivastava. *Prog. Neurobiol.* **2019**, *174*, 53–89.

1.2.1 Cholinergic hypothesis

The cholinergic hypothesis is based on cholinergic dysfunction, a common feature in AD patients. It came into existence in the mid-1970s, when reduced levels of the enzyme choline acetyltransferase (CAT) were reported in the brain of people who died of AD.[13,14] CAT is responsible for the synthesis of acetylcholine (ACh), which is a neurotransmitter in the brain with a relevant role in neuromodulation of learning, memory, and cognitive functions. This hypothesis postulated that degeneration of cholinergic neurons and associated loss of cholinergic neurotransmission in the cerebral cortex and other areas of the brain contributed significantly to deterioration in cognitive functions, perception, comprehension, reasoning and short-term memory in patients with AD.[15,16]

Impairment in the ACh neurotransmission is caused by dysregulation at different levels of synapses: first of all, a deficit in ACh synthesis caused by a reduced expression of CAT; secondly, a decreased availability of ACh in synapse, due to high affinity choline uptake by the presynaptic neuron, reduced ACh release and ACh metabolism by acetylcholinesterase (AChE) and butyrylcholinesterase (BChE); and finally, a loss of nicotinic ACh receptors (nAChRs), a ligand gated ion channel responsible for action potential transmission to the postsynaptic neuron, caused by a decrease in binding parameters, but not a decrease in muscarinic ACh receptors (mAChRs), which activate G protein signalling pathway **(Figure 1.2)**.[17-19]

1.2.2 Amyloid hypothesis

Also called “amyloid cascade hypothesis”, this model states that neurodegeneration in AD is caused by abnormal formation of Aβ plaques and its extracellular accumulation in various areas of the brain. Postulated several years ago, this hypothesis has become the dominant theory of AD pathogenesis and has guided the development of many potential treatments since then.[20-23]

---

[13]D. M. Bowen, C. B. Smith, P. White, A. N. Davison. *Brain* **1976**, *99*, 459–496.
[14]P. Davies, A. J. F. Maloney. *Lancet* **1976**, *2*, 1403.
[15]A. Blokland. *Brain Res. Rev*. **1995**, *21*, 285–300.
[16]R. T. Bartus, R. L. Dean 3rd, B. Beer, A. S. Lippa. *Science* **1982**, *217*, 408–414.
[17]P. Francis, A. Palmer, M. Snape, G. Wilcock. *J. Neurol. Neurosurg. Psychiatry* **1999**, *66*, 137–147.
[18]G. Benzi, A. Moretti. *Eur. J. Pharmacol.* **1998**, *346*, 1–13.
[19]D. Volpato, U. Holzgrabe. *Molecules* **2018**, *23*, 3230.
[20]J. A. Hardy, G. A. Higgins. *Science* **1992**, *256*, 184–185.
[21]J. Hardy, D. Allsop. *Trends in Pharmac.* **1991**, *12*, 383–388.
[22]D. J. Selkoe. *Neuron* **1991**, *6*, 487–498.
[23]D. J. Selkoe, J. Hardy. *EMBO Mol. Med.* **2016**, *8*, 595–608.

According to this theory, AD is caused by an imbalance between Aβ production and clearance, thus leading to increased amounts of Aβ, which coexist in several forms such as monomers, oligomers, insoluble fibrillary polymers and plaques in the brain.[20-25]

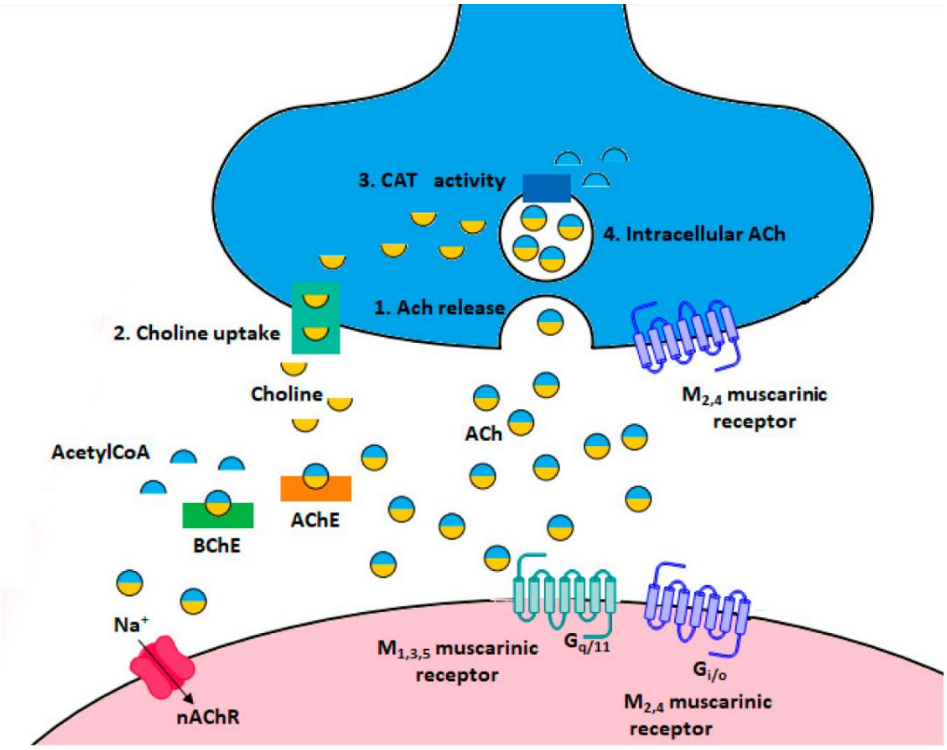

Figure 1.2. Major steps in the cholinergic neurotransmission: biosynthesis, storage, release, hydrolysis of ACh and neurotransmitter locations are illustrated (Image adapted from: C. A. Lane, J. Hardy, J. M. Schott. *Eur. J. Neurol.* **2018**, *25*, 59–70).

Aβ peptide is formed by proteolytic cleavage of the amyloid precursor protein (APP). APP is a transmembrane protein, which is crucial for neuronal plasticity and synapse formation.[26] There are two metabolic pathways of APP (**Figure 1.3**). In the non-amyloidogenic pathway, APP is cleaved sequentially by α- and γ-secretase, leading to soluble forms of APP (sAPPα) with neuroprotective effects. In contrast, in the amyloidogenic pathway, APP is cleaved through the sequential action of β- and γ-secretase, leading to fragments of Aβ of 39–43 amino acids, which are highly insoluble and tend to aggregate.[27-29]

[24]J. Hardy, D. J. Selkoe. *Science*, **2002**, *297*, 353–356.
[25]C. Morgan, M. Colombres, M. T. Nuñez, N. C. Inestrosa. *Prog. Neurobiol.* **2004**, *74*, 323–349.
[26]T. Mohamed, A. Shakeri, P. P. N. Rao. *Eur. J. Med. Chem.* **2016**, *113*, 258–272
[27]D. J. Selkoe, D. Schenk. *Annu. Rev. Pharmacol. Toxicol*. **2003**, *43*, 545–584.
[28]G. Thinakaran, E. H. Koo. *J. Biol. Chem.* **2008**, *283*, 29615–29619.
[29]K. Sambamurti, N. H. Greig, D. K. Lahiri. *Neuromol. Med.* **2002**, *1*, 1–31.

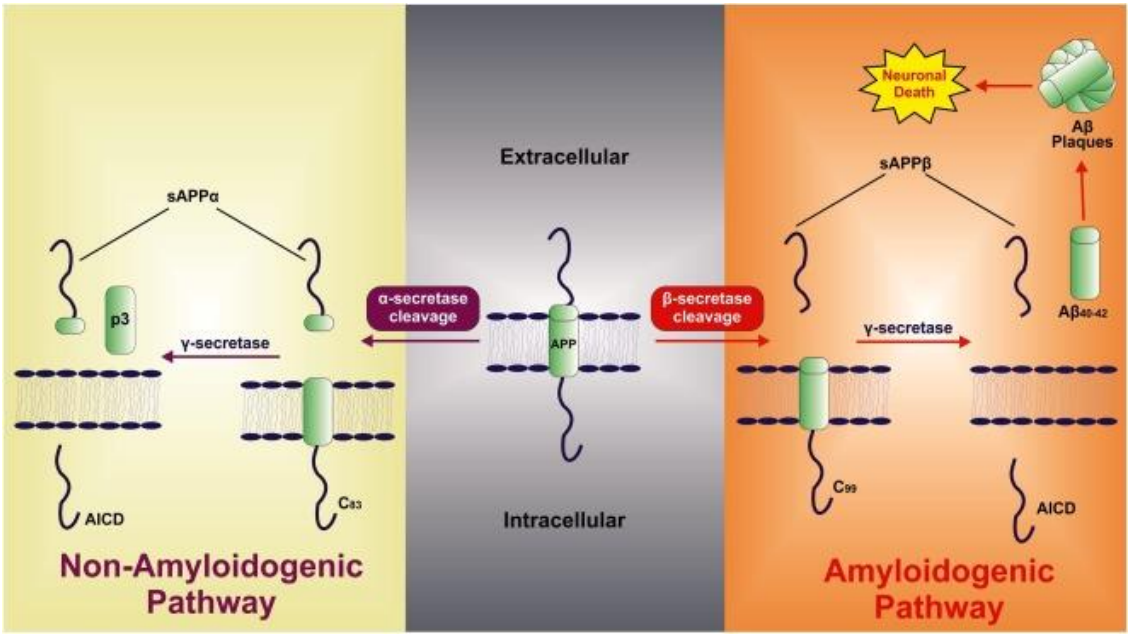

Figure 1.3. Schematic representation of APP metabolism through amyloidogenic and non-amyloidogenic pathways. APP- Amyloid precursor protein; sAPPα- Soluble amyloid precursor protein-α; sAPPβ- Soluble amyloid precursor protein-β; AICD- APP intracellular domain; p3- p3 peptide fragment; C83 and C99- C-terminal fragments of 83 and 99 peptide residues, respectively. (Image source: P. Sharma, P. Srivastava, A. Seth, P. N. Tripathi, A. G. Banerjee, S. K. Shrivastava. *Prog. Neurobiol.* **2019**, *174*, 53–89).

It must be said that both APP metabolic pathways are part of a normal physiology and that healthy brains have effective post-APP processing mechanisms to handle the byproducts.[29] In AD, APP metabolism shifts from primarily non-amyloidogenic to mostly amyloidogenic, resulting in an imbalance between production and clearance of released Aβ fragments.[30] Among them, the Aβ peptide of 40 amino acids ($A\beta_{1-40}$ or $A\beta_{40}$) is the most prevalent isoform, followed by $A\beta_{1-42}$ ($A\beta_{42}$) which is hydrophobic and aggregates at a faster rate.[31] $A\beta_{42}$ auto-assembly can result in various levels of aggregation, finally leading to amyloid dense plaques.[32] These plaques were originally considered to be critical to the development of AD. Nonetheless, it is now thought that soluble Aβ oligomers may be the most neurotoxic forms, causing synaptic dysfunction, microglia activation, cytokine release, astrocytosis and inflammatory responses, leading to a complex cascade of events that cause a widespread neuronal deficit and cognitive dysfunctions (**Figure 1.4**).[20,33]

[30]Y. W. Zhang, R. Thompson, H. Zhang, H. Xu. *Mol. Brain* **2011**, *4*, 3.
[31]D. M. Walsh, D. J. Selkoe. *J. Neurochem.* **2007**, *101*, 1172–1184.
[32]C. C. Chang, J. C. Althaus, C. J. Carruthers, M. A. Sutton, D. G. Steel, A. Gafni. *PLoS One* **2013**, *8*, e82139.
[33]C. A. Lane, J. Hardy, J. M. Schott. *Eur. J. Neurol.* **2018**, *25*, 59–70.

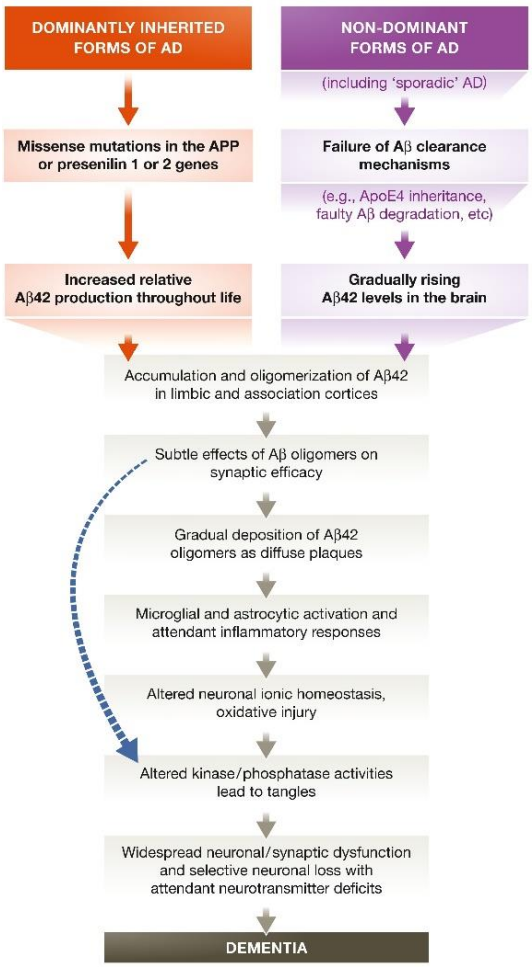

Figure 1.4. The sequence of major pathogenic events leading to AD proposed by the amyloid cascade hypothesis. The curved blue arrow indicates that Aβ oligomers may directly injure the synapses and neurites of brain neurons, in addition to activating microglia and astrocytes (Image source: D. J. Selkoe, J. Hardy. *EMBO Mol. Med.* **2016**, *8*, 595–608).

Nevertheless, there are some limitations to the amyloid cascade hypothesis. According to this model, deposition of Aβ represents the initial pathological trigger and the first neurotoxic step, whereas soluble Aβ oligomers are thought to induce synaptic dysfunction,[34] resulting in NFT formation, neuronal death and, finally, dementia.[24] Thus, amyloid removal by immunization should protect against Aβ-mediated neurotoxicity and preserve cognitive function, which is not the case.[35] Moreover, Aβ peptide accumulation does not correlate well with extent of neuronal loss and cognitive impairment. Also, demonstrating direct Aβ peptide neurotoxicity has been difficult in several animal

[34]S. T. Ferreira, W. L. Klein. *Neurobiol. Learn. Mem.* **2011**, *96*, 529–543.
[35]C. Haass, D. J. Selkoe. *Nat. Rev. Mol. Cell. Biol.* **2007**, *8*, 101–112.

models, revealing the existence of key intermediates between amyloidosis and neurodegeneration.[36] In this scenario, tau pathology correlates much more closely with neuronal loss, both spatially and temporally than amyloid plaques.

1.2.3 Tau hypothesis

Another pathological hallmark of AD are NFTs, which are formed by accumulations of protein tau. Tau is a soluble microtubule-associated protein mainly found in neurons that plays an important role in neuronal development and axonal growth by stabilizing microtubule assembly and neuronal microtubules network.[37] Under normal conditions, tau is effectively regulated by a balance between microtubule-associated phosphatases and kinases, which maintain correct phosphorylation states of tau.[38] However, under pathological conditions overactivation of kinases (mainly GSK-3β, cdk5 and its activator subunit p25, and MAPK) and inactivation of phosphatases lead to hyperphosphorylation of protein tau. This hyperphosphorylated tau has reduced affinity towards microtubules and assembles itself into paired helical filaments (PHF) and straight filaments (SF), and the abnormal accumulation of these filaments generates NFTs inside neurons. The loss of normal tau function results in a pathological dysfunction of the structure and functions of the cytoskeleton. These affect neurons functions such as maintenance of their morphology, axonal transport, leading to synaptic dysfunction and neurodegeneration (**Figure 1.5**).[39-41]

---

[36]P. T. Nelson, I. Alafuzoff, E. H. Bigio, C. Bouras, H. Braak, N. J. Cairns, R. J. Castellani, B. J. Crain, P. Davies, K del Tedici, C. Duyckaerts, M. P. Frosch, V. Haroutunian, P. R. Hof, C. M. Hulette, B. T. Hyman, T. Iwatsubo, K. A. Jellinger, G. A. Jicha, E. Kövari, W. A. Kukull, J. B. Leverenz, S. Love, I. R. Mackenzie, D. M. Mann, E. Masliah, A. C. Mckee, T. J. Montine, J. C. Morris, J. A. Schneider, J. A. Sonnen, D. R. Thal, J. Q. Trojanowski, J. C. Troncoso, T. Wisniewski, R. L. Woltjer, T. G. Beach. *J. Neuropathol. Exp. Neurol.* **2012**, *71*, 362–381.

[37]a) A. Mietelska-Porowska, U. Wasik, M. Goras, A. Filipek, G. Niewiadomska. *Int. J. Mol. Sci.* **2014**, *15*, 4671–4713. b) S. Biswal, D. Sharma, K. Kumar, T. C. Nag, K. Barhwal, S. K. Hota, B. Kumar. *Neurobiol. Learn. Mem.* **2016**, *133*, 157–170.

[38]M. L. Billingsley, R. L. Kincaid. *Biochem. J.* **1997**, *323*, 577–591.

[39]M. P. Mazanetz, P. M. Fischer. *Nat. Rev. Drug Discov.* **2007**, *6*, 464–479.

[40]E. Kopke, Y. C. Tung, S. Shaikh, A. C. Alonso, K. Iqbal, I. Grundke-Iqbal. *J. Biol. Chem.* **1993**, *268*, 24374–24384.

[41]S. Roy, B. Zhang, V. M. Lee, J. Q. Trojanowski. *Acta Neuropathol.* **2005**, *109*, 5–13.

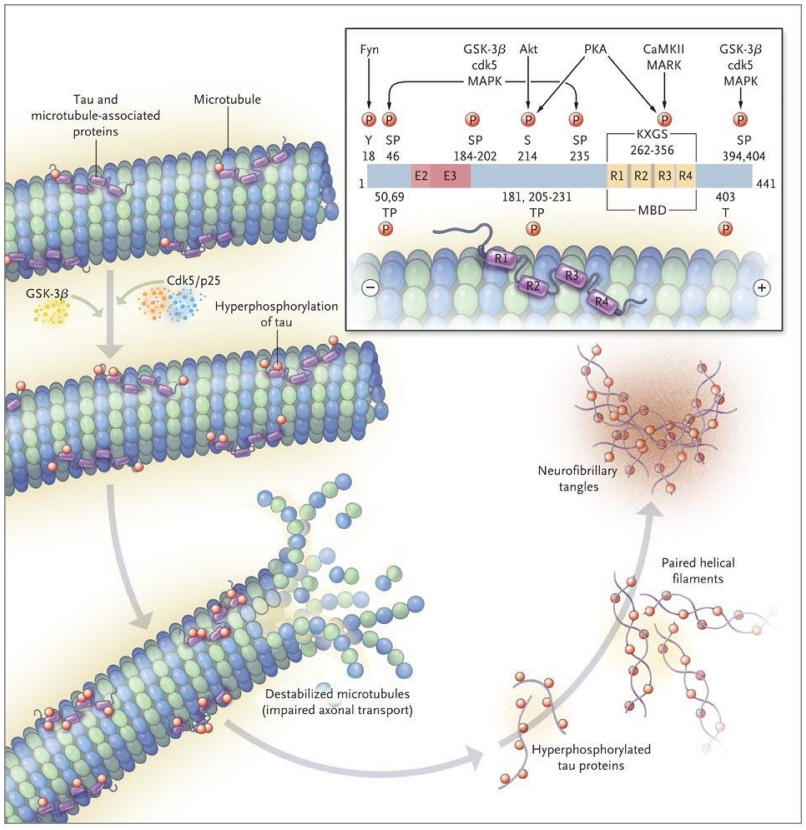

Figure 1.5. Structure of microtubule binding domain of tau protein with phosphorylation sites. The hyperphosphorylation of tau by GSK-3β, cdk5 and MAPK results into destabilization of microtubules, followed by detachment of tau and self-aggregation into PHFs and NFTs. (Image source: H. W. Querfurth, F. M. LaFerla, *N. Engl. J. Med.* **2010**, *362*, 329–344).

1.2.4 Glutamatergic excitotoxicity hypothesis

Glutamate is the major excitatory neurotransmitter in the central nervous system (CNS). It is present mostly in the hippocampus and cortex regions of the brain. Under physiological conditions, it plays a pivotal role in various neuronal functions, including synaptic transmission and plasticity, neuronal growth and differentiation, learning and long-term memory, through a phenomenon called long-term potentiation (LTP).[42] There are two types of glutamate receptors: metabotropic receptors (G-protein coupled) and ionotropic receptors (ion channel type). Among these, two ionotropic receptors are involved in the LTP, the α-amino-3-hydroxy-5-methyl-4-isoxazolepropionic acid (AMPA) receptor, permeable to Na^+, and the *N*-methyl-D-aspartate (NMDA) receptor, mainly permeable to

[42]D. A. Butterfield, C. B. Pocernich. *CNS Drugs* **2003**, 17, 641–652.

Ca^{2+}, although only the NMDA receptor is the final responsible for the LTP.[43] Under normal physiological conditions, glutamate binds to the NMDA receptor, and depolarization takes place, followed by magnesium ions mediated closing of the cationic channel to prevent the entry of Ca^{2+} in resting stage **(Figure 1.6)**.[43,44]

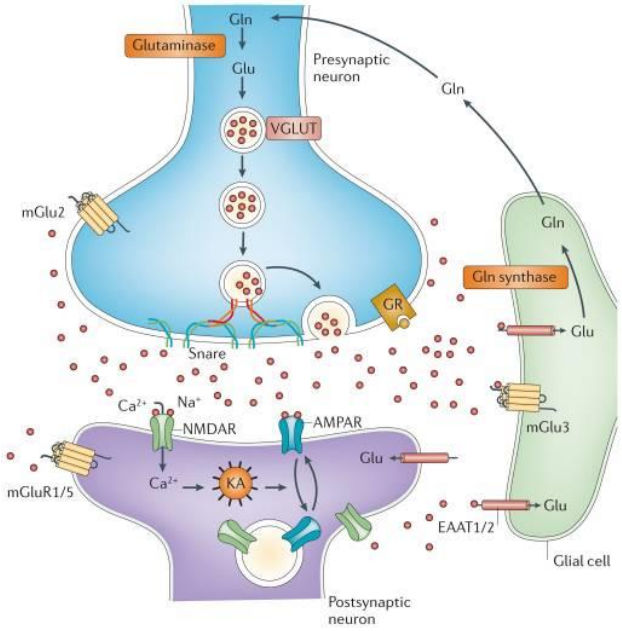

Figure 1.6. Scheme of glutamatergic transmission in normal brain. Glutamate is synthesized in presynaptic neurons and then released into the extracellular space, where glutamate binds to NMDA receptors and AMPA receptors at the postsynaptic neuron and to metabotropic receptors (mGluR1 to MGluR8) at both presynaptic and postsynaptic neurons and glial cells. The interaction between glutamate and NMDA receptors activates several metabolic pathways that finally lead to activation of LTP mechanisms. Excess of glutamate is cleared via excitatory amino acids transporters (EAATs) mainly on neighbouring glial cells. Within the glial cell, glutamate is converted into glutamine by glutamine synthetase and this glutamine is released and taken up by presynaptic neurons, where it will be again converted into glutamate by glutaminase. (Image source: M. Popoli, Z. Yan, B. S. McEwen, G. Sanacora *Nat. Rev. Neurosci.* **2012**, *13*, 22–344).

In AD, an overactivation of NMDA receptors takes place, probably due to an increased production of glutamate and a reduced uptake by glial cells. The overactivation of NMDA receptors causes the release of bound Mg^{2+} and allows the excessive entrance of Ca^{2+} into neurons, leading to an ionic dyshomeostasis. Overflow of Ca^{2+} into neurons further leads to mitochondrial dysfunction and activation of a signalling pathway mediated by CREB (cyclic AMP response element binding protein),

[43]C. Tabone, M. Ramaswami. *Neuron* **2012**, *74*, 767–769.
[44]J. W. Olney, D. F. Wozniak, N. B. Farber. *Arch. Neurol.* **1997**, *54*, 1234–1240.

which hampers neuronal transmission, damages nerve cells and finally causes neurodegeneration, neuritic injury and cell death. The latter process is called glutamatergic excitotoxicity, defined as cell death caused by the toxicity of an excessive action of excitatory glutamate.[44-47]

1.2.5 Oxidative stress and mitochondrial dysfunction hypothesis

Oxidative stress can be defined as a marked imbalance between reactive oxygen species (ROS) and their removal by the antioxidant systems.[48] There is strong evidence that free radicals play a significant role in neurodegeneration. Dysfunctional mitochondria release oxidizing free radicals, and in AD or in a normal aging brain, where the endogenous antioxidant system progressively decays, these free radicals cause considerable oxidative stress. Neuronal cells are more vulnerable to free radicals associated damage as a consequence of high oxygen consumption and lack of antioxidant enzymes availability compared to other organs.[49,50]

There are several factors that can initiate oxidative damage in the brain. In AD, Aβ is a prime initiator of this damage. Aβ plaques directly interfere with the electron transport chain in mitochondria, producing superoxide radicals, which are converted into hydrogen peroxide or react with nitric oxide, thus forming reactive nitrogen species (RNS). Mitochondrial hydrogen peroxide readily diffuses into the cytosol and participate in metal ion-catalysed radical formation, with free divalent transition metal ions (mainly iron, copper and zinc) and aluminium being especially involved in this process. These ROS and RNS damage several molecular targets, such as membrane lipids, DNA and several enzymes and proteins, finally causing oxidative cell injury and cell death **(Figure 1.7)**.[49,51,52]

---

[45]A. F. Teich, R. E. Nicholls, D. Puzzo, J. Fiorito, R. Purgatorio, O. Arancio. *Neurotherapeutics* **2015**, *12*, 29–41.
[46]D. Y. Zhu, L. Lau, S. H. Liu, J. S. Wei, Y. M. Lu. *Proc. Natl. Acad. Sci. U.S.A.* **2004**, *101,* 9453–9457.
[47]M. Parsons, L. Raymond. *Neuron* **2014**, *82*, 279–293.
[48]B. Halliwell. *Drugs Aging* **2001**, *18*, 685–716.
[49]H. W. Querfurth, F. M. LaFerla, *N. Engl. J. Med.* **2010**, *362*, 329–344.
[50]J. T. Coyle, P. Puttfarcken. *Science* **1993**, *262*, 689–695.
[51]J. S. Aprioku. *J. Reprod. Infertil.* **2013,** *14*, 158.
[52]K. Nowotny, T. Jung, A. Höhn, D. Weber, T. Grune. *Biomolecules* **2015,** *5*, 194–222.

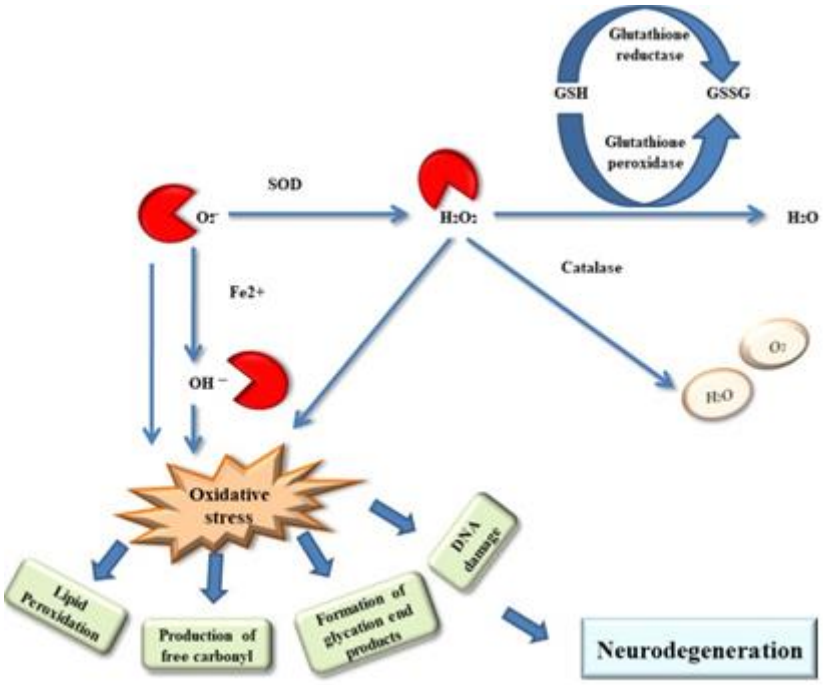

Figure 1.7. Oxidative stress and mitochondrial dysfunction in AD. (Image source: K. Kumar, A. Kumar, R. M. Reegan, R. Desmukh. *Biomed. Pharmacoter.* **2018**, *98*, 297–307).

1.2.6 Neuroinflammation hypothesis

An association between AD and inflammation was described several decades ago. During AD progression, amyloid plaques and NFT have been reported to activate microglia and astrocyte cells. Initially, microglia phagocytes and degrades Aβ. However, overactivation of microglia increases the expression of proinflammatory cytokines and chemokines, mainly interleukin-1 (IL-1), interleukin-6 (IL-6) and tumor necrosis factor α (TNF- α) **(Figure 1.8)**.[49,53] In addition, reactive astrocytes accumulate around Aβ plaques and help in their degradation, thus appearing to act in a neuroprotective manner, but they also secrete several pro-inflammatory mediators and stimulate the release of nitric oxide (NO) that helps to further increase the neuro-inflammatory response and leading to neuronal damage.[53-55]

[53]W. J. Streit. *Front. Aging Neurosci*. **2010**, *2*, 1– 5.
[54] J. M. Rubio-Perez, J. M. Morillas-Ruiz. *Sci. World J.* **2012**, *2012*, 1–15.
[55]C. M. Henstridge, B. T. Hyman, T. L. Spire-Jones. *Nat. Rev. Neurosci.* **2019**, *20*, 94–108.

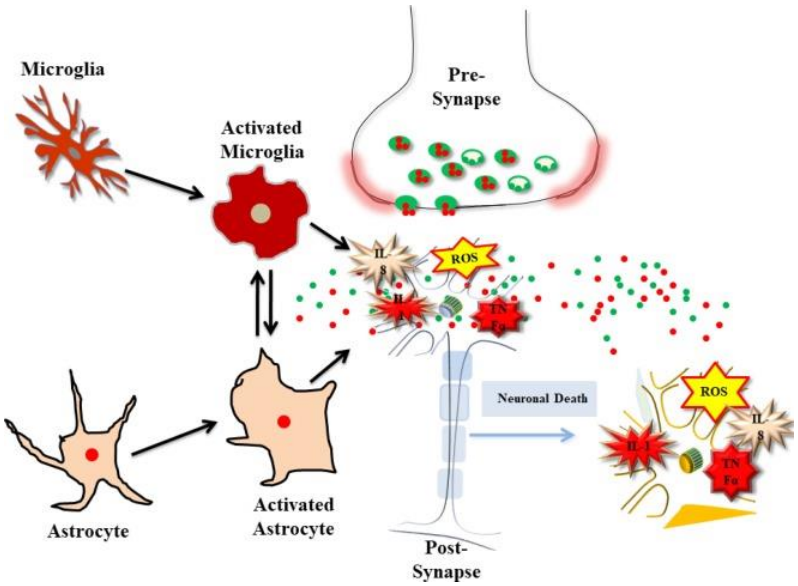

Figure 1.8. Process of neuroinflammation in AD progression. Overactivated microglia and astrocytes release high concentrations of pro-inflammatory cytokines, consequently leading to inflammation and neuronal damage. (Image source: K. Kumar, A. Kumar, R. M. Reegan, R. Desmukh. *Biomed. Pharmacoter.* **2018**, *98*, 297–307).

1.2.7 Biometal dyshomeostasis hypothesis

Strictly related to the oxidative stress hypothesis, there is enough evidence that redox active metals, mainly iron, copper and zinc, may have an important role in the production of ROS through the Fenton's reaction. Copper, zinc and iron have been found accumulated in the amyloid plaques and NFTs of AD brains. Apart from creating oxidative stress through ROS formation, copper, together with other metal ions, can influence protein aggregation. Copper forms a high affinity complex with Aβ, promoting its aggregation and neurotoxicity.[56]

Iron dyshomeostasis has been strongly related to the pathogenesis of AD. Iron is important for the maintenance of the high energy and metabolic requirements of neuronal tissues. However, in AD there is pathological accumulation of iron in the hippocampus and cerebral cortex, generally co-located with NFTs and senile plaques. When dysregulated, iron can act as a catalyst in the Fenton and Haber-Weiss reactions and drive the formation of different ROS, apart from increasing lipid peroxidative stress. When associating with Aβ, it also enhances Aβ aggregation by promoting covalent binding and may generate hydrogen peroxide, exacerbating the oxidative damage. Also, the

[56]A. Cavalli, M. L. Bolognesi, A. Minarini, M. Rossini, V. Tumiatti, M. Recanatini, C. Melchiorre. *J. Med. Chem.* **2008**, *51*, 347–372.

coexistence of ROS and iron within the mitochondria makes these organelles particularly sensitive to oxidative damage. Apart from that, iron-induced oxidative stress has been shown to initiate several apoptotic signalling pathways in neurons and its oxidative damage to proteins and lipids can cause synaptic dysfunction and neuronal death.[57,58]

1.2.8 Neurovascular hypothesis

The brain is an organ extremely energy-dependent, relying upon blood vessels for delivering oxygen and nutrients and for waste removal. Strong epidemiological evidence has shown correlation between vascular risk factors and risk of suffering AD. It has been proposed that neurovascular damage starts a cascade that ends in reduced cerebral blood flow and blood–brain barrier (BBB) disruption. When followed by Aβ pathology, it leads to AD, due to a defective clearance of Aβ from the brain to the periphery, which appears to be the main form of removing Aβ from the brain. In addition to impaired protein clearance, impaired delivery of nutrients to neurons, hypoperfusion, hypoxia and a critical breakdown of the BBB also take place. Finally, vascular injury and parenchymal inflammation occur, perpetuating the brain injury and contributing to AD pathogenesis.[55,59]

1.2.9 Insulin-resistance hypothesis

Another metabolic disturbance in AD that is becoming of great importance involves insulin signalling in the brain. The evidences suggested that 80% of people with AD had insulin resistance or type 2 diabetes.[60] Also, glucose intolerance and type 2 diabetes are considered to be risk factors for dementia. Insulin has been found to regulate processes such as neuronal survival, energy metabolism and plasticity by acting as a growth factor for neurons. Resistance to insulin signalling leads to energy-deficient neurons, making them vulnerable to oxidation or metabolic damage and also causing synaptic plasticity impairment. In addition, high serum glucose levels directly damage the hippocampus, by up-regulating GSK-3β and other kinases and by reducing levels of insulin-degrading enzyme in the brain.[12,49]

---

[57]A. Carocci, A. Catalano, M. S. Sinicropi, G. Genchi. *Biometals* **2018**, *31*, 715–735.
[58]D. J. R. Lane, S. Ayton, A. I. Bush. *J. Alzheimers Dis.* **2018**, *64*, 5379–5395.
[59]J. T. O'Brien, T. Erkinjuntti, B. Reisberg, G. Roman, T. Sawada, L. Pantoni, J. V. Bowler, C. Ballard, C. DeCarli, P. B. Gorelick, K. Rockwood, A. Burns, S. Gauthier, S. T. DeKosky. *Lancet Neurol.* **2003**, *2*, 89–98.
[60]B. Kim, E. L. Feldman, *Exp. Mol. Med.* **2015**, *47*, e149.

1.3 Pathological network of AD

In light of the aforementioned different mechanisms, it is evident that AD is a multifactorial disease, which makes it extremely challenging to find an effective treatment. Moreover, the different pathological pathways do not work separately but through a robust network whereby the disease always finds an alternative pathway to continue its progress. As a consequence, we must understand AD as a *pathological network*, where several key proteins and neuronal pathways are interconnected, even though some of these connexions still remain unclear.

From this point of view, it cannot be assumed that any of the previous mentioned hypotheses is exclusive. On the contrary, it should be elucidated how they are interconnected in order to generate a comprehensive map of connectivity between all those pathways. This should be the most relevant first step when trying to understand how AD network works, what is the starting point that triggers the onset of the disease and through which mechanisms it continues its development (**Figure 1.9**).

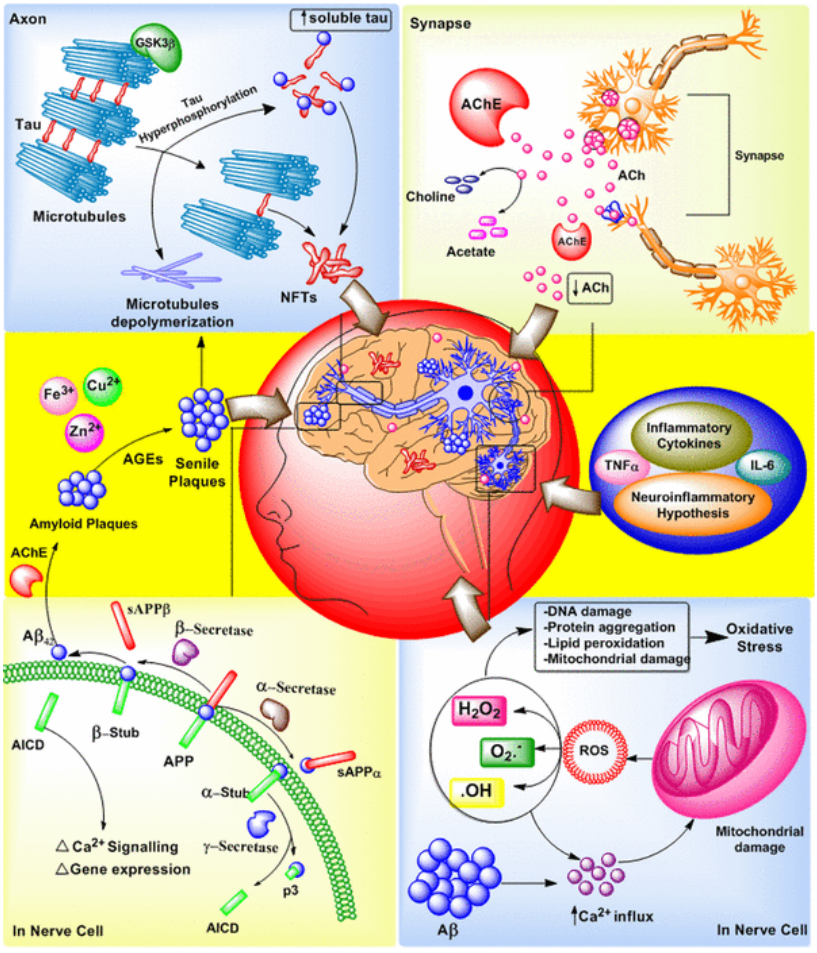

Figure 1.9. Map of the pathological network of AD. Only the most important pathways are represented. (Image source: M. Singh, M. Kaur, N. Chadha, O. Silakari. *Mol. Divers.* **2016**, *20*, 271–297).

Nowadays, there is enough evidence suggesting that Aβ, either in its oligomeric form or in the form of senile plaques, can be the triggering event in the pathogenesis of AD, playing a central role in the course of the disease (**Figure 1.10**). Aβ may exert its neurotoxic effect through different ways, including disruption of the mitochondrial function through the binding of Aβ to alcohol dehydrogenase protein, induction of apoptotic genes via inhibition of Wnt and insulin signalling, formation of ion channels, stimulation of the stress-activated protein kinases (SAPK) pathway or activation of microglia cells leading to expression of proinflammatory genes, an increase in ROS, and eventually neurotoxicity and death.[61-66]

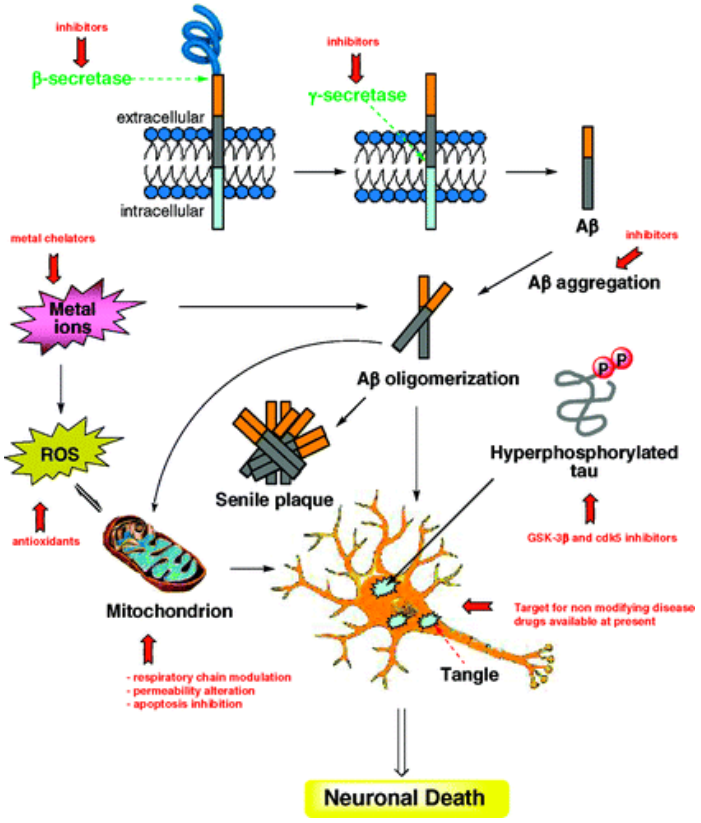

Figure 1.10. Possible molecular causes of neuronal death and protective mechanisms (in red) in AD. (Image source: M. Singh, M. Kaur, N. Chadha, O. Silakari. *Mol. Divers.* **2016**, *20*, 271–297).

---

[61]J. W. Lustbader, M. Cirilli, C. Lin, H. W. Xu, K. Takuma, N. Wang, C. Caspersen, X. Chen, S. Pollak, M. Chaney, F. Trinchese, S. Liu, F. Gunn-Moore, L. F. Lue, D. G. Walker, P. Kuppusamy, Z. L. Zewier, O. Arancio, D. Stern, S. S. Yan, H. Wu. *Science* **2004**, *304*, 448–452.

[62]A. Caricasole, A. Copani, A. Caruso, F. Caraci, L. Lacovelli, M. A. Sortino, G. C. Terstappen, F. Nicoletti. *Trends Pharmacol. Sci.* **2003**, *24*, 233–238.

[63]L. Xie, E. Helmerhorst, K. Taddei, B. Plewright, W. Van Bronswijk, R. Martins. *J. Neurosci.* **2002**, *22*, RC221.

[64]B. L. Kagan, Y. Hirakura, R. Azimov, R. Azimova, M. C. Lin. *Peptides* **2002**, *23*, 1311–1315.

[65]E. Tamagno, M. Parola, M. Guglielmotto, G. Santoro, P. Bardini, L. Marra, M. Tabaton, O. Danni. *Free Radical Biol. Med.* **2003**, *35*, 45–58.

[66]M. E. Bamberger, G. E. Landreth. *Microsc. Res. Tech*. **2001**, *54*, 59–70.

In the context of this PhD Thesis, the most relevant pathway connections have been addressed, including amyloid and tau pathologies, cholinergic neurotransmitter system, BACE1 inhibition, neuroinflammation and oxidative stress through ion metal chelation.

1.3.1 Connection between cholinergic and amyloid hypotheses

These two hypotheses are the most widely accepted by the scientific community. Consequently, they have been extensively studied for decades. It has been demonstrated that AChE (and BChE to a lower extent) is consistently increased in regions around amyloid plaques and NFTs in all stages of the disease.[67] Several studies suggest that AChE may directly interact with Aβ, thereby promoting Aβ aggregation and deposition to form plaques. This association leads to AChE-Aβ complexes, inducing alterations in some of the enzyme properties and increasing the neurotoxicity of Aβ fibrils.[68] The way AChE interacts with Aβ is through the peripheral anionic site (PAS) of AChE. The role of the PAS is to provide a seeding location for small Aβ oligomers. This seeding process further promotes the aggregation and formation of the complexes, which have been proved to be more neurotoxic that Aβ complexes alone (**Figure 1.11**). One of the earliest effects of AChE–Aβ complexes is the increase in intracellular calcium, which leads to channel opening and the loss of mitochondrial membrane potential and further loss of viability. [68-70]

In addition, it has also been reported that Aβ increases AChE expression. $A\beta_{42}$ has been demonstrated to induce enhancement of AChE expression through its action on α7 nicotinic acetylcholine receptors (nAChR), indicating that the local increase of AChE around amyloid plaques may be a result of a direct action of Aβ at those receptors.[71] Moreover, deposits of Aβ fibrils trigger a local immune reaction through the induction of proinflammatory cytokines (this process will be further explained in **Section 1.3.2**), which has been assumed to be a major contribution to neuronal dysfunction. Particularly, basal forebrain cholinergic cells have been found to be especially vulnerable to these inflammation processes (**Figure 1.11**).[68,72]

---

[67]M. M. Mesulam, M. A. Moran. *Ann. Neurol.* **1987**, *22*, 223–228.
[68]R. Schliebs. *Neurochem. Res.* **2005**, *30*, 895–908.
[69]M. C. Dinamarca, J. P. Sagal, R. A. Quintanilla, J. A. Godoy, M. S. Arrazola, N. C. Inestrosa. *Mol. Neurodegener.* **2010**, *5,* 4.
[70]F. J. Muñoz, N. C. Inestrosa. *FEBS Lett.* **1999**, *450*, 205–209.
[71]L. R. Fodero, S. S. Mok, D. Losic, L. L. Martin, M. I. Aguilar, C. J. Barrow, B. G. Livett, D. H. Small. *J. Neurochem.* **2004**, *88*, 1186–1193.
[72]L. B. Willard, B. Hauss-Wegrzyniak, G. L. Wenk, *Neuroscience* **1999**, *88*, 193–200.

Taken together, a disturbance in the homeostasis between cholinergic function and APP metabolism should result into deleterious consequences by favouring the amyloidogenic route of APP and the formation of senile plaques and inducing local neuroinflammation, which will translate in cholinergic functions damage.

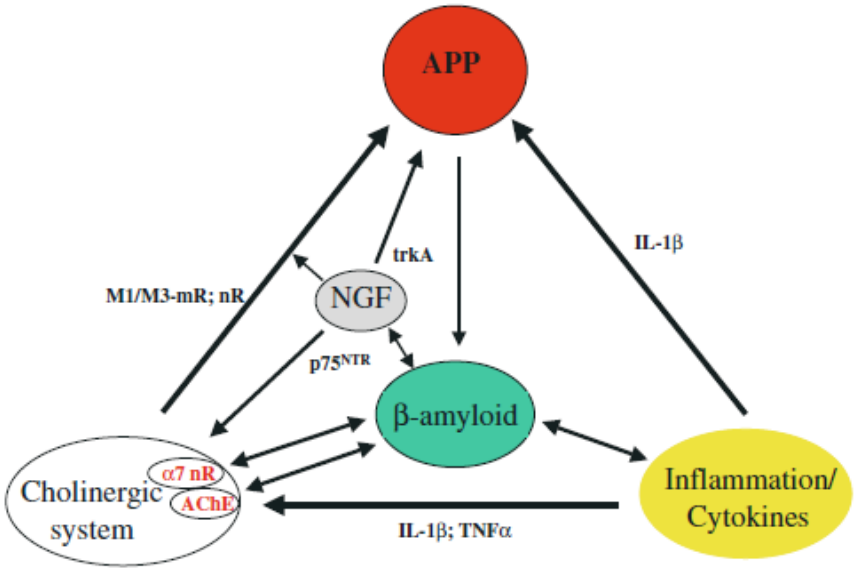

Figure 1.11. Connexion between cholinergic neurotransmission, metabolism of APP and Aβ-induced production of proinflammatory cytokines. (Image source: R. Schliebs. *Neurochem. Res.* **2005**, *30*, 895–908).

1.3.2 Connection between amyloid and neuroinflammation hypotheses

It has been postulated that senile plaques in brains of AD patients are associated with reactive astrocytes and activated microglial cells, promoting the expression of a number of inflammatory cytokines, such as IL-1 or TNF-α.[73] As mentioned before, this neuroimmunological cascade attacks the basal forebrain cholinergic cells, which are extremely vulnerable to inflammation.[72] Besides this, IL-1 has also been found to up-regulate the expression of APP, to stimulate the amyloidogenic pathway of APP as well as to induce expression and phosphorylation of tau protein.[68,74,75] Also, Aβ-mediated up-regulation of IL-1β in reactive astrocytes surrounding plaques is accompanied by a glial expression of BACE1.[76]

[74]P. Eikelenboom, W. A. van Gool. *J. Neural Transm.* **2004**, *111*, 281–294.
[75]J. D. Buxbaum, M. Oishi, H. I. Chen, R. Pinkas-Kramarski, E. A. Jaffe, S. E. Gandy, P. Greengard. *Proc. Natl. Acad. Sci. U.S.A.* **1992**, *89*, 10075–10078.
[76]J. T. Rogers, L. M. Leiter, J. McPhee, C. M. Cahill, S. S. Zhan, H. Potter, L. N. Nilsson. *J. Biol. Chem.* **1999**, *274*, 6421–6431.

1.3.3 Connection between amyloid and tau hypotheses

Some studies suggest a toxic interrelation between Aβ and tau, such as Aβ synaptotoxicity mediated by tau, whereby Aβ-promoted endogenous hyperphosphorylation of tau leads to decreased microtubule binding[77] and release of tau from the axon to the dendritic compartment by retrograde axonal transport.[78] A conformational rearrangement occurs in some part of this unfolded tau protein, finally leading to tau aggregation in the form of intracellular fibrils.[79]

1.3.4 Connection between amyloid and other hypotheses

One of the major sources of oxidative stress in AD is that associated with Aβ peptide. Some studies have demonstrated that Aβ oligomers can induce free radical generation, even in the presence of metal chelators, indicating that this induction is independent of redox metals.[80,81] Moreover $A\beta_{25-35}$, $A\beta_{40}$ and $A\beta_{42}$ were shown to induce significant increase in protein oxidation (carbonyl formation) in cortical synaptosomes, cultured hippocampal neurons, neuron cultures and astrocytes.[82] Besides, Aβ can also lead to lipid peroxidation, affecting lipid structure and causing membrane disruption, pore formation and neuronal damage.[82,83] On the contrary, lipid constitution and its physicochemical properties can induce conformational changes in Aβ, catalysing the formation of diverse oligomers.[83]

Another effect of Aβ is the induction of depression of glutamatergic synaptic transmission in hippocampal pyramidal neurons, triggering the loss of function. $A\beta_{42}$ oligomers can induce a toxic overactivation of NMDA receptors by driving an abnormal conformation of the receptor, where the Mg^{2+} blockade function is no longer effective. Consequently, it leads to the loss of NMDA receptor function and reduced LTP.[84,85]

---

[77]T. Maas, J. Eidenmüller, R. Brandt. *J. Biol. Chem.* **2000**, *275*, 15733–15740.
[78]X. Li, Y. Kumar, H. Zempel, E. M. Mandelkow, J. Biernat, E. Mandelkow. *EMBO J.* **2011**, *30*, 4825–4837.
[79]F. Hernandez, J. Avila. *Cell. Mol. Life Sci.* **2007**, *64*, 2219–2233.
[80]S. Varadarajan, S. Yatin, M. Aksenova, D. A. Butterfield. *J. Struct. Biol.* **2000**, *130*, 184–208.
[81]S. Varadarajan, J. Kanski, M. Aksenova, C. Lauderback, D. A. Butterfield. *J. Am. Chem. Soc.* **2001**, *123*, 5625–5631.
[82]D. A. Butterfield, D. Boyd-Kimball. *J. Alzheimers Dis.* **2018**, *62*, 1345–1367.
[83]V. Rangachari, D. N. Dean, P. Rana, A. Vaidya, P. Ghosh. *BBA Biomembranes* **2018**, *1860*, 1652–1662.
[84]F. De Felice, P. Velasco, M. Lambert, K. Viola, S. Fernandez. S. Ferreira, L. Klein. *J. Biol. Chem.* **2007**, *282*, 11590–11601.
[85]R. Malinow. *Curr. Opin. Neurobiol.* **2012**, *22*, 559–563.

1.4 Current therapeutics and novel approaches in the treatment of AD

The current therapeutic arsenal for AD is dominated by a group of drugs that are only symptomatic, but they are not capable of curing or modifying the progression of the disease. There are only five commercialised drugs for the treatment of AD and all of them are aimed to re-establish functional neurotransmission. Four of them, based on the "cholinergic hypothesis", are acetylcholinesterase inhibitors while the other is an NMDA receptor uncompetitive antagonist, based on the "glutamatergic hypothesis". Research advances on the molecular pathogenesis of AD have also led to new drug candidates with disease-modifying potential. However, thus far none of them have succeeded in clinical trials.[11]

1.4.1 Modulating neurotransmission

1.4.1.1 Acetylcholinesterase inhibitors (AChEIs)

Targeting the cholinergic system has been always the favourite approach among the scientific community. Human AChE (*h*AChE) is a 583 amino acid enzyme, which is responsible for the hydrolysis of the neurotransmitter ACh. First, ACh binds to the outer part of the active site gorge of the enzyme, called peripheral anionic site (PAS), rich in aromatic residues, which is in charge of early binding and guiding the substrate through the 20 Å-long gorge towards the catalytic anionic site (CAS), at the bottom, where the hydrolysis of ACh takes place (**Figure 1.12**). The CAS consists of a catalytic triad, which is formed by residues Ser203, His447, and Glu334 (Ser220, His440, and Glu 327, respectively, in *Torpedo californica* AChE, the first crystallized and studied AChE), responsible for the hydrolysis, and a neighbouring anionic hydrophobic site, which helps to stabilize the positive charge of the quaternary ammonium group of ACh by cation-π interactions and orients its acetyl group to the catalytic triad. [12,86,87]

[86] J. S. de Almeida, S. F. de A. Cavalcante, R. Dolezal, K. Kuca, K. Musilek, D. Jun, T. C. França. *J. Biomol. Struct. Dyn.* **2018**, *37*, 1–8.

[87] a) H. Dvir, I. Silman, M. Harel, T. L. Rosenberry, J. Sussman. *Chem. Biol. Interact.* **2010**, *187*, 10–22. b) G. Kryger, M. Harel, K. Giles, L. Toker, B. Velan, A. Lazar, C. Kronman, D. Barak, N. Ariel, A. Shafferman, I. Silmanb and J. L. Sussman. *Acta Cryst*. **2000**, *D56*, 1385–1394.

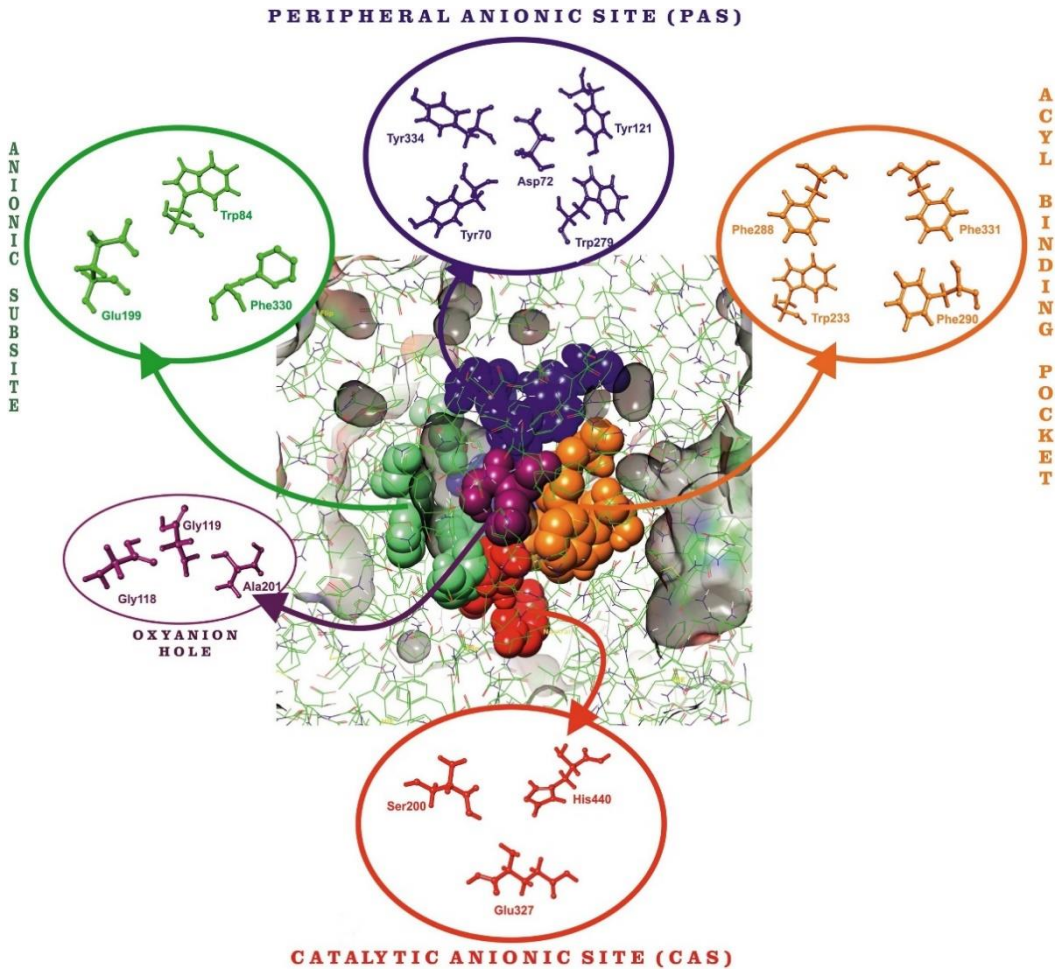

Figure 1.12. Schematic representation of *Torpedo californica* AChE (PDB ID: 1EVE) with details of the CAS and the PAS. Other subunits, such as anionic subsite, acyl binding pocket and oxyanion hole are shown. (Image source: P. Sharma, P. Srivastava, A. Seth, P. N. Tripathi, A. G. Banerjee, S. K. Shrivastava. *Prog. Neurobiol.* **2019**, *174*, 53–89).

AChEIs prevent the hydrolysis of ACh, thereby increasing the levels of this neurotransmitter in neuronal cells.[88] Until now, four AChEIs have been approved as anti-Alzheimer drugs, namely tacrine, **1** (marketed in 1993, **Figure 1.13**), donepezil, **2** (marketed in 2001), rivastigmine, **3** (marketed in 2000) and galantamine, **4** (marketed in 2001).[89] Nevertheless, tacrine was withdrawn from the market due to hepatotoxicity issues.[90] Donepezil is a selective inhibitor of AChE, whereas rivastigmine inhibits AChE and BChE with similar affinity and galantamine is also an allosteric modulator of presynaptic nicotinic receptors, which probably contributes to their clinical benefits.[11,91]

[88]V. N. Talesa. *Mech. Ageing Dev.* **2001**, *122*, 1961–1969.
[89]Y. Madav, S. Wairkar, B. Prabhakar. *Brain Res. Bull.* **2019**, *146*, 171–184.
[90]J. Patocka, D. Jun, K. Kuca. *Curr. Drug Metab.* **2008**, *9*, 332–335.
[91]J. Coyle, P. Kershaw. *Biol. Psychiatry* **2001**, *49*, 289–299.

It has been demonstrated that irreversible AChEIs may deteriorate the cholinergic synaptic transmission permanently, causing severe side effects.[92] Tacrine, donepezil and galantamine are reversible AChEIs, whilst rivastigmine is considered a pseudoirreversible AChEI, since it contains a carbamate group that reacts with Ser203, leading to a carbamoylated AChE, whose activity is slowly recovered after hydrolysis of the serine carbamate.[93] Donepezil, galantamine and rivastigmine have proven beneficial effects on cognitive, functional and behavioural symptoms in mild to severe AD and a good safety profile, with limited side effects such as gastrointestinal symptoms. There is no evidence that one drug is more efficacious than another.[94] Consequently, they are the first-line treatment against AD, along with memantine. Nevertheless, on long-term administration, they failed to reduce the risk or delay the onset of AD, being considered for this reason as symptomatic treatments.[95,96]

The analysis of the X-Ray structure of the marketed AChEIs within AChE showed that tacrine, **1**, rivastigmine, **3**, and galantamine, **4**, clearly interact at the CAS of the enzyme whereas donepezil, **2**, spans the whole length of the active site gorge, simultaneously interacting with both the CAS and the PAS, thus exhibiting a dual site binding (**Figure 1.13**).[97]

Down the years, research to find new AChEIs have continued and many potential candidates came under clinical trials, even though all of them have failed at certain stages. Many of them, such as metrifonate, have failed due to their safety profile but the majority of them have failed because of lack of efficacy, such as tesofensine. Although current therapies have only modest benefits and research and clinical outcomes indicated that AChEIs have not been able to modify the disease progression, the truth is that, until now, no alternatives to these drugs have been found and more intense research efforts in this direction is still a requisite.[12,98,99]

---

[92]M. B. Colovic, D. Z. Krstic, T. D. Lazarevic-Pasti, A. M. Bondzic, V. M. Vasic. *Curr. Neuropharmacol.* **2013**, *11*, 315–335.
[93]E. Giacobini. *Pharmacol. Res.* **2004**, *50*, 433–440.
[94]J. S. Birks. *Cochrane Database Syst Rev* **2006**, *1*, CD005593.
[95]R. Raschetti, E. Albanese, N. Vanacore, M. Maggini. *PLoS Med.* **2007**, *4*, e338.
[96]A. Contestabile. *Behav. Brain Res.* **2011**, *221*, 334–340.
[97]D. Muñoz-Torrero. *Curr. Med. Chem.* **2008**, *15*, 2433–2455.
[98]M. Mehta, A. Adem, M. Sabbagh. *Int. J. Alzheimers Dis.* **2012**, *2012*, 728983.
[99]A. Astrup, S. Madsbad, L. Breum, T. J. Jensen, J. P. Kroustrup, T. M. Larsen. *Lancet* **2008**, *372*, 1906–1913.

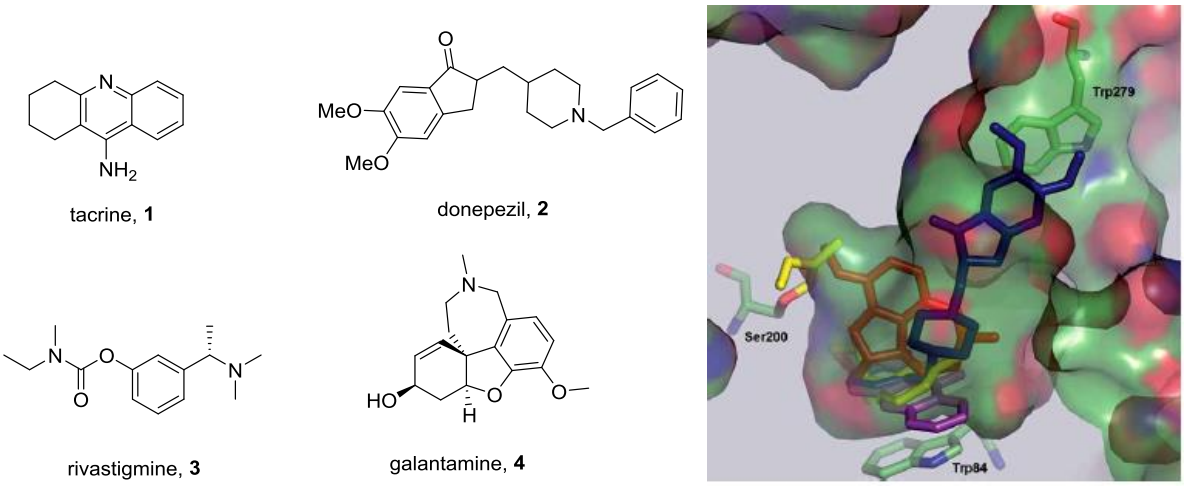

Figure 1.13. Left: structure of the four FDA-approved AChEIs. Right: Binding mode of these drugs in the gorge of *Torpedo californica* AChE: tacrine, **1** (PDB ID: 1ACJ, magenta), donepezil, **2** (PDB ID: 1EVE, blue), rivastigmine, **3** (PDB ID: 1GQR, yellow), galantamine, **4** (PDB ID: 1DX6, orange). (Right image source: D. Muñoz-Torrero. *Curr. Med. Chem.* **2008**, *15*, 2433–2455).

1.4.1.2 Butyrylcholinesterase inhibitors

It is noteworthy to mention that there is another type of cholinesterase (ChE) responsible for ACh degradation, apart from AChE. Butyrylcholinesterase (BChE), present in the central and peripheral nervous system, also plays this role. BChE also has a high presence in peripheral regions and is the main cholinesterase in plasma. Therefore, inhibition of BChE might be associated with peripheral side effects. Functionally, both enzymes hydrolyse ACh efficiently, even though AChE degrades ACh much faster than butyrylcholine (BCh) whereas BChE hydrolyses ACh much more slowly than BCh.[100,101] In normal conditions, AChE hydrolyses the majority of Ach, with BChE playing only a secondary role. However, in AD patients, the brain activity of AChE decreases as the disease progresses, whereas the expression of BChE is increased, thus gaining importance with AD progress and playing a significant role in degrading ACh.[102,103]

[100]W. Krall, J. Sramek, N. Cutler. *Ann. Pharmacother.* **1999**, *33*, 441–450.
[101]L. Savini, A. Gaeta, C. Fattorusso, B. Catalanotti, G. Campiani, L. Chiasserini, C. Pellerano, E. Novellino, D. McKissic, A. Saxena. *J. Med. Chem.* **2003**, *46*, 1–4.
[102]G. Reid, N. Chilukuri, S. Darvesh. *Neuroscience* **2013**, *234*, 53–68.
[103]M. Mesulam, A. Guillozet, P. Shaw, B. Quinn. *Neurobiol. Dis.* **2002**, *9*, 88–93.

Structurally, both ChEs are similar, sharing more than 65% of their amino acid sequence.[104] The basic difference is present at the gorge of BChE, which presents less hydrophobic aromatic residues (only six compared to fourteen in AChE).[105] Although substantial progress has been made in the development of BChEIs (specific or dual AChE–BChE inhibitors), there are still several controversies such as whether specific BChE inhibition may cause peripheral cholinergic side effects or specific AChEIs devoid of BChE inhibitory activity may not be disease-modifying.[12]

1.4.1.3 NMDA receptor antagonists

NMDA receptors (NMDARs) have been always of interest as potential pharmacological drug targets in the brain, due to their implication in several CNS disorders, such as Parkinson's disease, Huntington's disease or AD. This receptor is a ionotropic ion channel that exists in the form of an heterotetramer, mainly composed of two copies of GluN1 and two of GluN2. It is activated upon concurrent binding of glycine to GluN1 and L-glutamate to GluN2, and relief of a Mg^{2+} blockade of the channel pore by membrane depolarization.[106,107] Opening of the NMDAR results in an influx of Ca^{2+} ions inside the neurons, which triggers several signal transduction cascades that control neural connectivity and neuroplasticity.[107]

The X-ray structure of the NMDA receptor shows that it has two extracellular domains, the N-terminal domain (amino-terminal domain or ATD) and the agonist binding domain (ABD), and a transmembrane domain (TMD, **Figure 1.14**). The ATD contributes to control the opening/closing rate and contains allosteric modulator binding sites; the ligand binding domain (LBD) contains the binding sites for Mg^{2+}, glycine and glutamate; the TMD comprises the architecture of the pore and the C-terminal domains are associated with intracellular proteins that trigger signalling pathways.[106,107]

---

[103] M. Mesulam, A. Guillozet, P. Shaw, B. Quinn. *Neurobiol. Dis.* **2002**, *9*, 88–93.
[104] Y. Nicolet, O. Lockridge, P. Masson, J. C. Fontecilla-Camps, F. Nachon. *J. Biol. Chem.* **2003**, *278*, 41141–41147.
[105] S. Darvesh, D. A. Hopkins, C. Geula. *Nat. Rev. Neurosci.* **2003**, *4*, 131–138.
[106] C. H. Lee, W. Lü, J. C. Michel, A. Goehring, J. Du, X. Song, E. Gouaux. *Nature* **2014**, *511*, 191–197.
[107] E. Karakas, H. Furukawa. *Science* **2014**, *344*, 992–997.

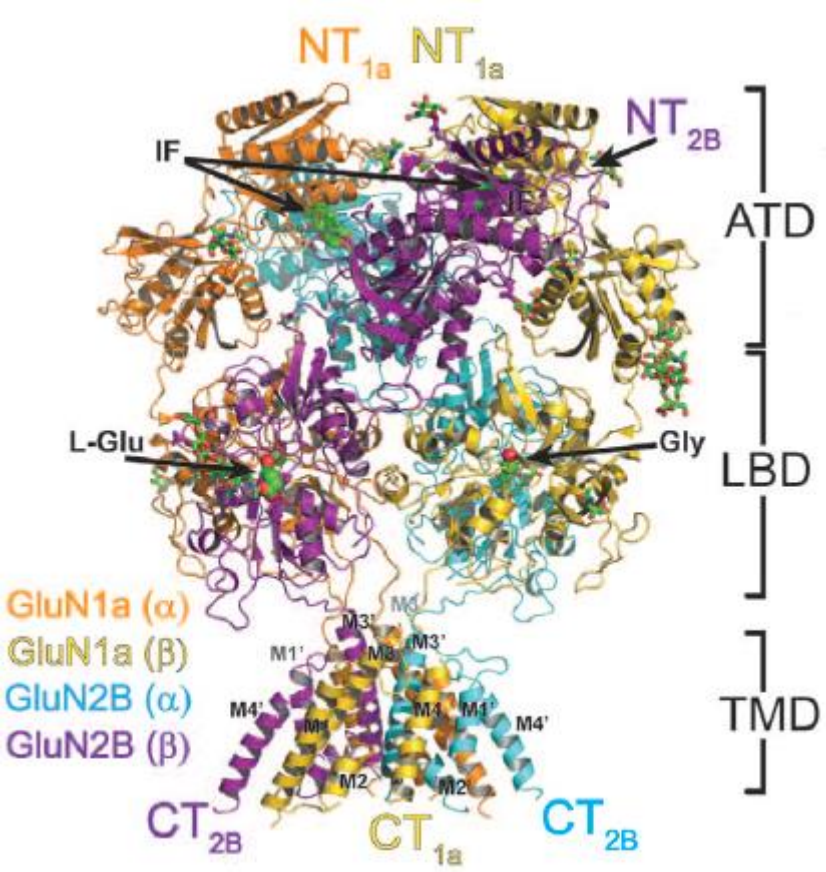

Figure 1.14. Overall structure of heterotetrameric GluN1a-GluN2B NMDA receptor. GluN1a and GluN2B subunits, labelled as GluN1a (α), GluN1a (β), GluN2B(α), GluN2B(β) are coloured in orange, yellow, cyan, and purple, respectively. The amino (NT) and carboxy (CT) termini are located on top and bottom, respectively. Ifenprodil (IF), located at the GluN1a-GluN2B ATD heterodimer interfaces, and agonists, glycine (Gly) and L-glutamate (L-Glu), lodged at the LBD clamshells, are shown in green spheres. (Image adapted from: E. Karakas, H. Furukawa. *Science* **2014**, *344*, 992–997).

Apart from the commercialized AChEIs mentioned in **Section 1.4.1.1**, there is also an NMDA receptor antagonist that is approved for the treatment of AD, memantine, **5**, marketed in 2002 (**Figure 1.15**). Traditionally, competitive inhibitors of glutamate for the agonist binding site also block the normal physiological functions.[108] Memantine is a low affinity uncompetitive NMDA receptor antagonist, which is approved for use in moderate to severe AD, with some evidence that it also reduces the likelihood of patients developing agitation.[109] Experimental evidences show that memantine improves spatial learning, protects neurons from Aβ induced toxicity, decreases apoptosis

[108]S. A. Lipton. *Nat. Rev. Drug Discov*. **2006**, *5*, 160–170.
[109]R. McShane, A. Areosa Sastre, N. Minakaran. *Cochrane Database Syst. Rev.* **2006**, *2*, CD003154

and free radical mediated damage and restores synaptic degeneration.[110] Moreover, in combination therapy with donepezil, memantine has shown positive effects on symptoms relative to donepezil alone.[111]

Memantine works by preferentially blocking open NMDA channels (**Figure 1.15**). Its moderate affinity and voltage dependency property allows it to block the overactivation of NMDA receptors. Also, evidences show that memantine-mediated blockade is relieved by high glutamate concentrations in the synaptic cleft. Hence, when a physiological impulse arrives, glutamate can override the memantine blockade, enabling the physiological transmission.[111] Thus, memantine blocks the neurotoxicity of glutamate without interfering in the physiological conditions.

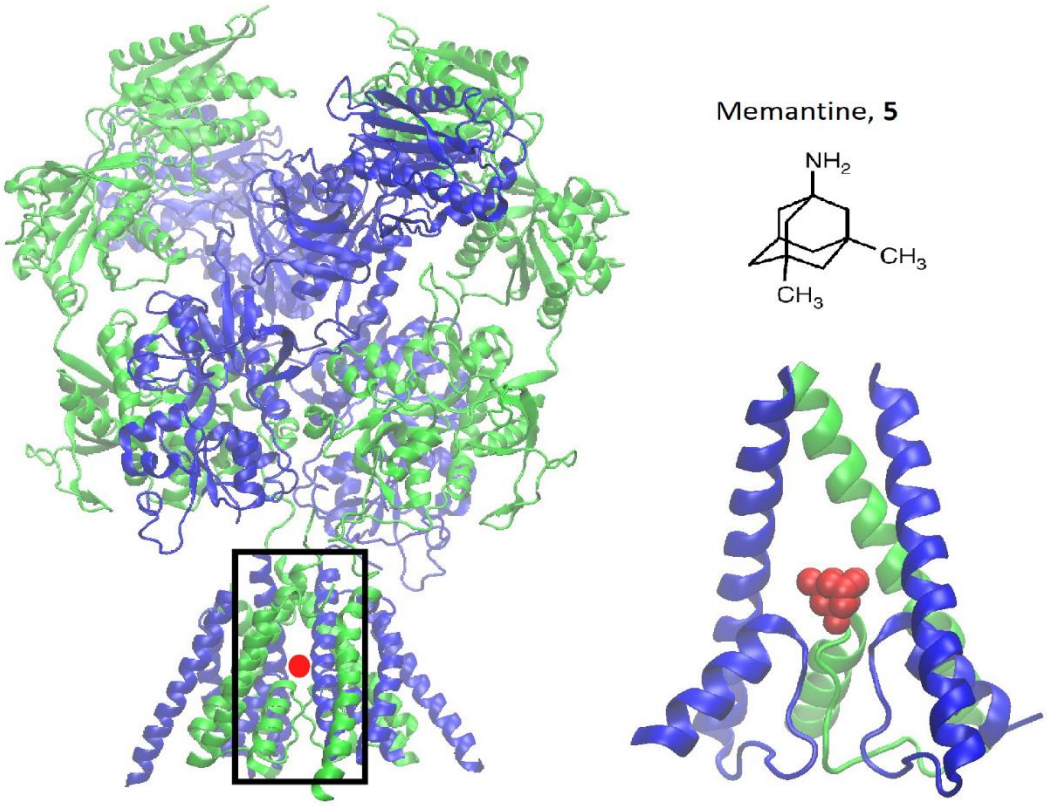

Figure 1.15. NMDAR channel blocked by memantine. Left: general view of the channel (PDB ID: 4TML) with a red dot at the likely approximate location of memantine binding site. The black box indicates the area of the receptor expanded in the left side. Right: Top, structure of memantine. Bottom, a view of the channel region with memantine (red spheres) blocking the channel. GluN1 subunits are shown in green and GluN2 subunits in blue. (Image source: J. Johnson, N. Glasgow, N. Povysheva. *Curr. Opin. Pharmacol.* **2015**, *20*, 54–63).

[110]P. N. Tariot, M. R. Farlow, G. T. Grossberg, S. M. Graham, S. McDonald, I. Gergel. *JAMA* **2004**, *291*, 317–324.
[111]J. J. Miguel-Hidalgo, I. A. Paul, V. Wanzo, P. K. Banerjee. *Eur. J. Pharmacol.* **2012**, *692*, 38–45.

1.4.2 Aβ directed strategies

The clinical trials landscape for the past 20 years has been dominated by the amyloid cascade hypothesis, even though a large number of major phase 3 clinical trials targeting Aβ have failed, prompting scepticism about this hypothesis. Nevertheless, it is important to note that many of these studies have been complicated due to concerns in target engagement and patient selection.[112] Not only did a proportion of patients recruited not have evidence of AD pathology, but also most studies were for late-stage AD patients, by which time Aβ may no longer be an appropriate target.[23] Nowadays it is considered possible that Aβ-targeted strategies will need to be applied at very early stages of AD, long before symptoms began.[55] There are several ways to tackle Aβ pathogenesis in AD (**Figure 1.16**), which are presented below.

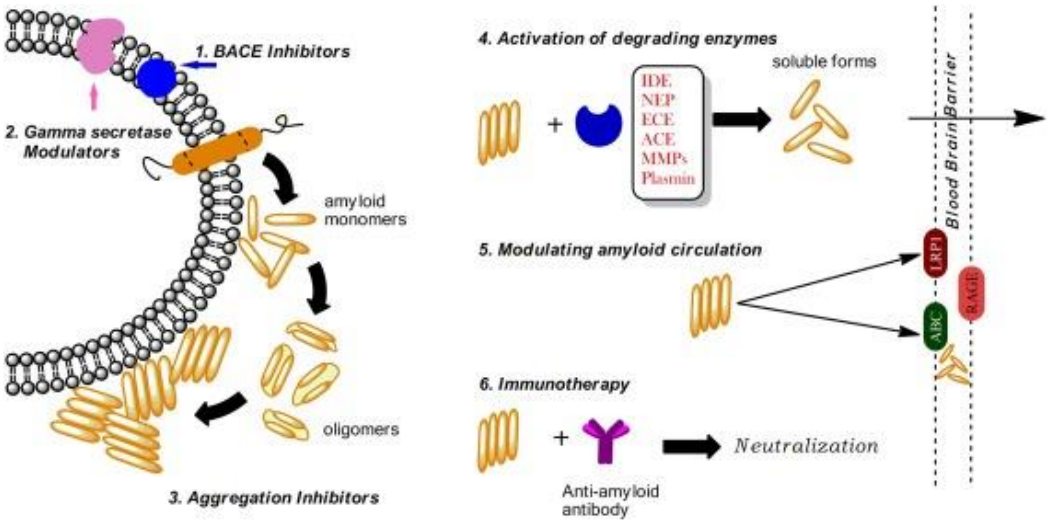

Figure 1.16. Different approaches targeting Aβ: inhibition of its synthesis (1 and 2), prevention of its aggregation (3), increasing its clearance (4 and 5) and Aβ immunotherapy (6). (Image source: Y. Madav, S. Wairkar, B. Prabhakar. *Brain Res. Bull.* **2019**, *146*, 171–184).

1.4.2.1 Inhibition of Aβ synthesis

There are several approaches to reduce the formation of Aβ peptide, with the inhibition of β-secretase (BACE1) and γ-secretase being the mostly pursued. As mentioned before, both enzymes are responsible for the amyloidogenic cleavage of APP to form Aβ fragments. Another important approach is enhancement of α-secretase activity, which starts the non-amyloidogenic pathway of APP cleavage.

[112]E. Karran, J. Hardy. *Ann. Neurol.* **2014**, *76*, 185–205.

β-secretase (BACE1) inhibition

BACE is a transmembrane aspartic protease. It has two isoforms, BACE1, mainly found in the brain and responsible for APP cleavage, and BACE2, which is more prominent in peripheral tissues such as kidneys or pancreas than in brain. As a consequence, the selectivity of the compounds for BACE1 over other proteases is a major challenge in developing these inhibitors.[89,113] BACE1 is a glycosylated enzyme found to be most active in acidic conditions.[114] It presents a catalytic dyad of aspartate residues (Asp32 and Asp228) responsible for the hydrolytic cleavage, that is placed in a flexible flap, which guides the substrate into the catalytic site, enabling the adoption of the reactive conformation and being responsible for the specificity of the enzyme.[115,116]

There are various issues that need to be addressed when designing potential BACE1 inhibitors. Firstly, the complete inhibition of its activity might lead to phenotypical defects in learning and memory.[117] Moreover, these inhibitors must be able to cross the BBB to cleave APP in the endosomes of neurons.[118] In the last years, several BACE1 inhibitors have entered clinical trials. The first generation of BACE1 inhibitors, such as *BI 1181181*, failed because of low oral bioavailability and low BBB penetration. Second-generation BACE1 inhibitors, such as *RG7129*, *LY2811376* and *LY2886721* (**Figure 1.17**) also failed in clinical trials because of liver toxicity. More recently, third-generation BACE1 inhibitors have shown satisfactory pharmacokinetics and encouraging clinical data in ongoing studies, including elenbecestat (*E2609*, **Figure 1.17**) (Phase III), *AZD3293* (Phase III), *CNP520* (Phase II/III), *JNJ-54861911* (Phase II/III). Although *verubecestat* (*MK-8931*, **Figure 1.17**) reduces CNS Aβ in animal models and in AD patients, its Phase III clinical study in mild-to-moderate AD patients was discontinued in 2017 because of lack of efficacy.[119]

[113]R. Vassar, B. D. Bennett, S. Babu-Khan, S. Kahn, E. A. Mendiaz, P. Denis, D. B. Teplow, S. Ross, P. Amarante, R. Loeloff. *Science* **1999**, *286*, 735–741.
[114]J. Yuan, S. Venkatraman, Y. Zheng, B. M. McKeever, L. W. Dillard, S. B. Singh. *J. Med. Chem.* **2013**, *56*, 4156–4180.
[115]M. Hernández-Rodríguez, J. Correa-Basurto, A. Gutiérrez, J. Vitorica, M. C. Rosales- Hernández. *Eur. J. Med. Chem.* **2016**, *124*, 1142–1154.
[116]L. Hong, J. Tang. *Biochemistry* **2004**, *43*, 4689–4695.
[117]B. Hitt, S. Riordan, L. Kukreja, W. Eimer, T. Rajapaksha, R. Vassar. *J. Biol. Chem.* **2012**, *287*, 38408–38425.
[118]K. W. Menting, J. A. Claassen. *Front. Aging Neurosci.* **2014**, *6*, 1–19.
[119]S. Hung, W. Fu. *J. Biomed. Sci.* **2017**, *24*, 1–47.

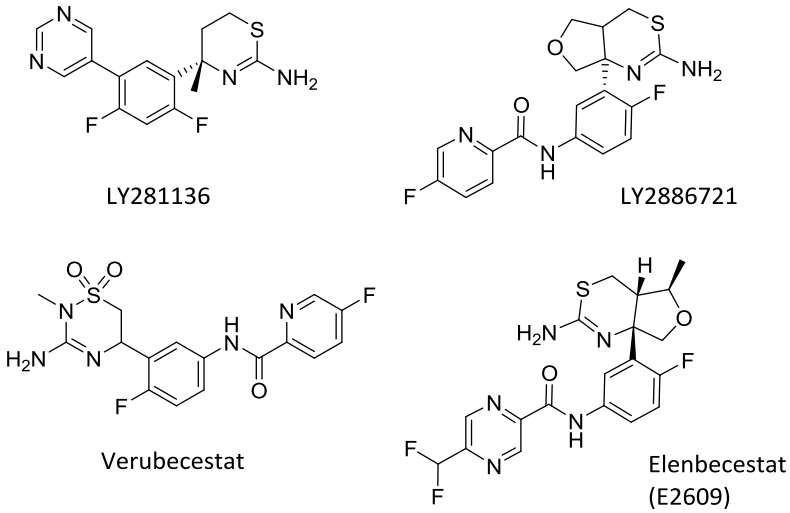

Figure 1.17. Structure of some BACE1 inhibitors.

γ-secretase inhibition

γ-secretase is responsible for the final cleavage of APP, either in the amyloidogenic or non-amyloidogenic pathways. This enzyme is a complex of four integral membrane proteins: presenilins (PS1 and PS2), nicastrin, Aph-1 and Pen-2.[120] This complex cleaves various substrates, apart from APP. It is involved in the Notch signalling pathway, which plays a critical role in the development and cellular growth of neurons. Disruption of Notch signalling may lead to intolerable toxic reactions to several systems.[121,122] Therefore, the design of γ-secretase inhibitors that can specifically inhibit APP processing and no other vital processes is extremely challenging.

[120]G. He, W. Luo, P. Li, C. Remmers, W. J. Netzer, J. Hendrick, K. Bettayeb, M. Flajolet, F. Gorelick, L. P. Wennogle. *Nature* **2010**, *467*, 95–98.
[121]J. D. Grill, J. L. Cummings. *Expert Rev. Neurother.* **2010**, *10*, 711–728.
[122]C. M. Carroll, Y. M. Li. *Brain Res. Bull.* **2016**, *126*, 199–206.

A number of γ-secretase inhibitors are currently under research. *Semagacestat* (LY450139) and *DAPT* (**Figure 1.18**) were some of the few inhibitors that reached late phase of clinical trials, but unfortunately both failed due to their severe toxic reactions, related to disruption of Notch signalling.[123] Moreover, *semagacestat* also caused worsening of the symptoms in some patients.[119] *Avagacestat* (**Figure 1.18**) was discontinued in a Phase II clinical trial after causing serious adverse events such as cerebral microbleeds, dose-dependent glycosuria, and nonmelanoma skin cancer.[119] The small molecule, selective γ-secretase modulator *EVP-0962* reduces $A\beta_{42}$ production by shifting the APP cleavage toward the production of shorter and less toxic Aβ peptides, without affecting Notch cleavage. Although *EVP-0962* showed promise in transgenic Alzheimer's models, it was discontinued in Phase II clinical trials.[119] Having all of these failures into account, future directions should be focused towards the development of stabilizers of γ-secretase, which could stabilize the interaction of the enzyme with the Aβ peptide and generate less toxic fragments.[124] A combination of γ-secretase modulator along with BACE1 inhibitor has shown an additive effect in the reduction of Aβ production with minor adverse effects.[125]

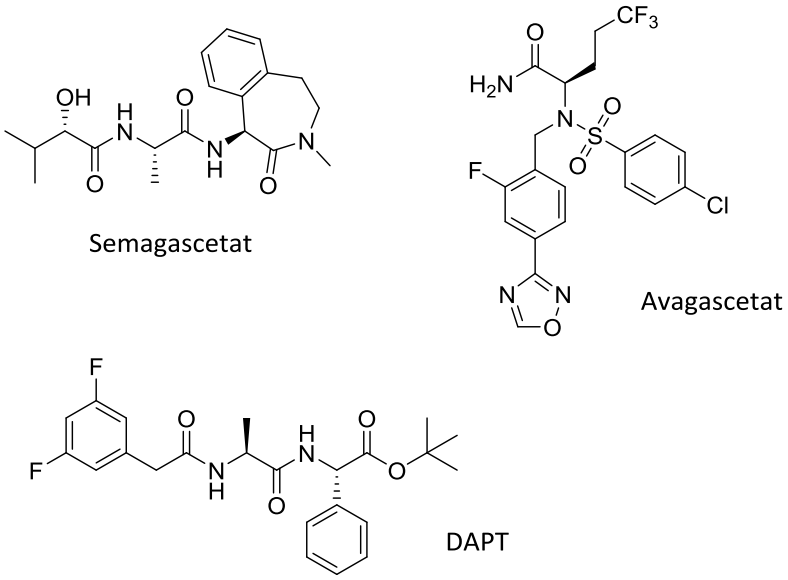

Figure 1.18. Structure of some γ-secretase inhibitors.

[123]S. C. Mayer, A. F. Kreft, B. Harrison, M. Abou-Gharbia, M. Antane, S. Aschmies, K. Atchison, M. Chlenov, D. C. Cole, T. Comery. *J. Med. Chem.* **2008**, *51*, 7348–7351.
[124]R. J. Andrew, K. A. Kellett, G. Thinakaran, N. M. Hooper. *J. Biol. Chem.* **2016**, *291*, 19235–19244.
[125]K. Stromberg, S. Eketjall, B. Georgievska, K. Tunblad, K. Eliason, F. Olsson, A. C. Radesater, R. Klintenberg, P. I. Arvidsson, S. von Berg, J. Fälting, R. F. Cowburn, M. S. Dabrowski, *FEBS J.* **2015**, *282*, 65–73.

α-secretase activation

As mentioned before, α-secretase is the initial enzyme in the non-amyloidogenic APP cleavage pathway. Thus, up-regulation of its activity may preclude Aβ peptide formation. Several proteases, such as ADAM (A disintegrin and metalloprotease) family may promote α-secretase expression, increasing consequently α-secretase cleavage of APP.[126]

1.4.2.2 Prevention of Aβ aggregation

The approach of developing small molecules that interfere with Aβ–Aβ interactions and prevent its aggregation is gaining interest amongst researchers. Several sulfonated dyes, such as Congo red, bind to Aβ fibrils and reduce fibril formation and neurotoxicity.[127] Furthermore, several specific peptides with similar sequences to $A\beta_{42}$ have been developed, with the ability of recognising and binding Aβ peptides and alter its morphology, thereby reducing Aβ cellular toxicity.[128] These peptide derivatives present various issues associated with administration, delivery and rapid degradation.[129] Finally, some small molecules have been also developed as aggregation inhibitors, with the drawbacks of lack of specificity, toxicity and unknown mechanism of action.[129] One example of small molecule is *tramiprosate*, which binds $A\beta_{42}$, blocking its aggregation, and also seems to have anti-inflammatory effect. Even though it showed a reduction in global cognitive decline in Phase III clinical trials, *tramiprosate* was discontinued because of failure in reaching its primary endpoints.[130]

1.4.2.3 Increase of Aβ clearance

There are several proteases that degrade Aβ aggregates, along with other substrates, maintaining Aβ homeostasis in neurons.[131] The ones that play a major role are plasmin, neprilysin (NEP), insulin degrading enzyme (IDE), endothelin-converting enzyme (ECE-1), angiotensin-converting

---

[126] S. H. Barage, K. D. Sonawane. *Neuropeptides* **2015**, *52,* 1–18.
[127] A. Lorenzo, B. A. Yankner. *Proc. Natl. Acad. Sci. U.S.A.* **1994**, *91*, 12243–12247.
[128] B. Neddenriep, A. Calciano, D. Conti, E. Sauve, M. Paterson, E. Bruno, D. A. Moffet. *Open Biotechnol. J.* **2011**, *5*, 39–46.
[129] L. D. Estrada, C. Soto. *Curr. Top. Med. Chem.* **2007**, *7*, 115–126.
[130] a) P. S. Aisen, S. Gauthier, B. Vellas, R. Briand, D. Saumier, J. Laurin, D. Garceau. *Curr. Alzheimer Res.* **2007**, *4*, 473–478. b) C. Caltagirone, L. Ferrannini, N. Marchionni, G. Nappi, G. Scapagnini, M. Trabucchi. *Aging Clin. Exp. Res*. **2012**, *24*, 580–587.
[131] D. S. Wang, D. W. Dickson, J. S. Malter. *J. Biomed. Biotechnol.* **2006**, *2006*, 58406.

enzyme (ACE) and matrix metalloproteinase 9 (MMP9).[132] The levels of these Aβ degrading enzymes decline in AD patients, which may contribute to Aβ accumulation. The overexpression of these enzymes would be an alternative approach to reduce Aβ peptide concentration. Some small molecules that can activate these degrading enzymes have been identified. However, more studies are needed in order to assess the relative contribution of each enzyme to understand the key players involved in the amyloid cascade.[126]

1.4.2.4 Aβ immunotherapy

One of the most attractive approaches for the treatment of AD is the development of anti-Aβ immunotherapeutic agents. There are two approaches that can be used: active and passive immunization. In both cases, the ultimate goal is to prevent the formation of senile plaques and increase the degradation of Aβ peptide.

In the active immunization, the immune system is stimulated to produce its own antibodies through administration of a vaccine with the appropriate antigens. The success of this technique relies on the capacity of the body to create an antibody response. However, in elderly patients, the aging immune system may generate autoimmune side effects instead of producing the appropriate antibodies.[133] The first report of Aβ immunotherapy treatment was *AN-1792*, a synthetic full-length $A\beta_{42}$ peptide with QS-21 adjuvant. It was discontinued in Phase II because of severe meningoencephalitis developing in 6% of the patients. Next-generation vaccines are working to target more specific epitopes to induce a more controlled immune response. An active vaccination strategy that aims to elicit a strong antibody response while avoiding inflammatory T cell activation is *CAD106*, which uses the $A\beta_{1-6}$ peptide. *CAD106* is in Phase II/III in cognitively unimpaired individuals with 2 ApoE4 genes. *ACC-001* is an N-terminal $A\beta_{1-7}$ peptide fragment linked to inactivated diphtheria toxin as the carrier. *ACC-001* was discontinued in Phase II trials because of a strong autoimmune response. *Affitope AD02* contains six amino acids that mimic the N-terminus of Aβ and is in Phase II clinical trials.[119]

[132]N. N. Nalivaeva, C. Beckett, N. D. Belyaev, A. J. Turner. *J. Neurochem.* **2012**, *120*, 167–185.
[133]J. Godyn, J. Jonczyk, D. Panek, B. Malawska. *Pharmacol. Rep.* **2016**, *68,* 127–138.

Passive immunization consists of injecting directly the adequate antibodies in the body. It is currently the most widely pursued approach in clinical trials, because of the lower probability of side effects.[134] *Bapineuzumab*, a humanized form of murine monoclonal antibody (mAb) that binds the N-terminal epitope of Aβ, was terminated in two Phase III trials because of lack of efficacy. *AAB-003*, a derivative of bapineuzumab, completed Phase I trials in 2014. *GSK933776* is a humanized mouse IgG1 mAb directed against the N-terminus of Aβ, which has failed to show any clinical benefit. *Solanezumab* is a mAb directed against $A\beta_{16-24}$, which in Phase III clinical trials also failed to meet the primary endpoint. Now, *solanezumab* is being tested in a prevention study in asymptomatic older subjects, who have positive positron emission tomography (PET) scans for brain amyloid deposits. *Crenezumab* recognizes oligomeric and fibrillar Aβ species and amyloid plaques with high affinity, and monomeric Aβ with low affinity and is in Phase III study until 2020. *Gantenerumab* is a conformational antibody against Aβ fibrils that is being tested in Phase III clinical trials in patients with mild AD. *BAN2401* binds to large soluble Aβ protofibrils and is thought to lead to Aβ clearance or neutralize Aβ toxicity. It is currently in Phase II trials. *Aducanumab*, targeting aggregated but not monomeric Aβ, is currently in Phase III trials in patients with early AD.[119]

1.4.3 Tau directed strategies

Hyperphosphorylation of tau and its aggregation into NFTs are also pathological events that have attracted great interest in the search of anti-Alzheimer drug candidates. There can be broadly four major approaches to tackle the tau hypothesis (**Figure 1.20**), which are explained hereunder.

1.4.3.1 Inhibition of tau hyperphosphorylation

Kinases are the major family of proteins involved in hyperphosphorylating tau protein. In AD, increased levels of kinases are found in affected areas of the brain. There are several kinases involved in this process. The main focus has been on glycogen synthase kinase 3 (GSK3), one of the primary enzymes involved in tau hyperphosphorylation.[135] *Lithium* and *valproate* are inhibitors of GSK3 and both showed

[134] J. Moreth, C. Mavoungou, K. Schindowski. *Immun. Ageing* **2013**, *10*, 1–9.
[135] C. Gao, C. Hölscher, Y. Liu, L. Li. *Rev. Neurosci.* **2012**, *23*, 1–11.

some beneficial effects in small scale trials. However, both have failed to show efficacy in larger studies.[136] Tideglusib (**Figure 1.21**) is an irreversible inhibitor of GSK3β currently in Phase II clinical trials.[137]

Activation of protein phosphatases to increase the dephosphorylation of tau is another strategy under evaluation. The main dephosphorylating enzyme is protein phosphatase 2A and sodium selenite (Ve-015) is an activator of this enzyme which is currently in Phase II trials.[137]

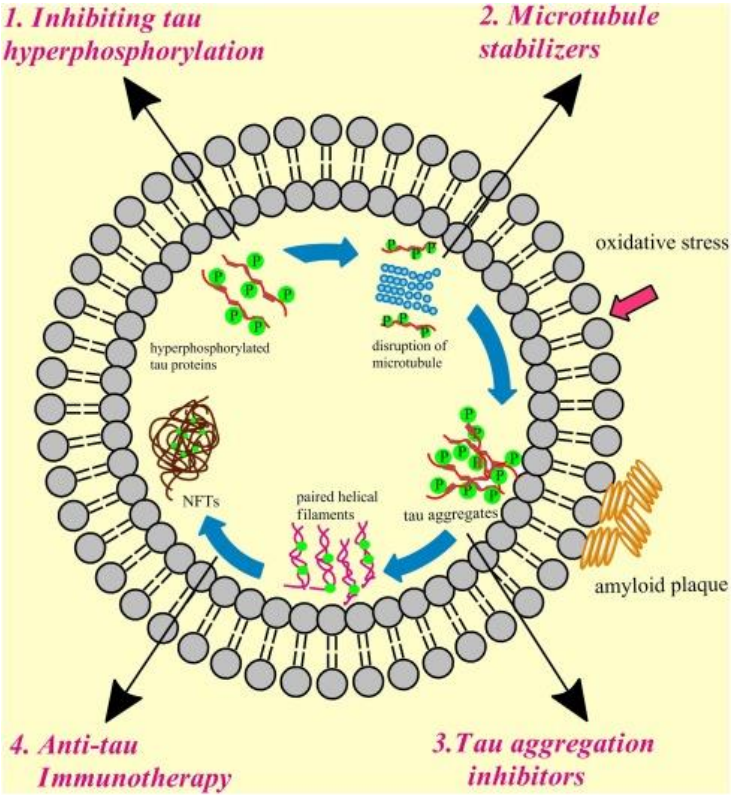

Figure 1.20. Different approaches targeting tau proteins: inhibition of its hyperphosphorylation (1), microtubule stabilization (2), prevention of its aggregation (3) and tau immunotherapy (4). (Image source: Y. Madav, S. Wairkar, B. Prabhakar. *Brain Res. Bull.* **2019**, *146*, 171–184).

[136]a) H. Hampel, M. Ewers, K. Burger, P. Annas, A. Mortberg, A. Bogstedt, L. Frolich, J. Schroder, P. Schonknecht, M. W. Riepe, I. Kraft, T. Gasser, T. Leyhe, H. J. Moller, A. Kurz, H. Basun. *J. Clin. Psychiatry* **2009***, 70*, 922–931. b) P. N. Tariot, P. Aisen, J. Cummings, L. Jakimovich, L. Schneider, R. Thomas, L. Becerra, R. Loy. *Alzheimers Dementia* **2009**, *5*, 84–85.
[137]R. Anand, K. D. Gill, A. A. Mahdi. *Neuropharmacology* **2014**, *76*, 27–50.

1.4.3.2 Microtubule stabilization

Various compounds with microtubule stabilizing effects are under development. *Epothilone D* administration showed significant amelioration in microtubule pathology in Phase I trials. However further evaluation of this compound was discontinued.[119,138] *Paclitaxel* improved fast axonal transport, microtubule density and motor function in tau-transgenic mice. Nevertheless, it failed to reach the clinics due to toxic side effects. *TPI 287* is currently in Phase I clinical trials for mild-to-moderate AD.[119]

1.4.3.3 Inhibition of tau aggregation

Oligomeric forms of tau act as a substrate for tau–tau binding, leading to tau aggregation, even though tau oligomers may not necessarily lead to tau aggregation.[139] Some benzimidazole derivatives showed a strong affinity to bind tau proteins, consequently disrupting tau–tau interactions. One of this derivatives, lansoprazole (**Figure 1.21**), was able to decrease tau pathology but it was found to increase amyloid deposition and aggregation, probably due to its γ-secretase modulating effect.[140] Derivatives of dye methylene blue have also shown to disrupt aggregation of tau, such as Rember™, which showed some improvement in AD-related symptoms but was discontinued in Phase II trials because of emergent side effects. TRx0237 (LMTM, **Figure 1.21**) is a second-generation methylene blue derivative with is currently in three Phase III clinical trials.[119]

1.4.3.4 Anti-tau immunotherapy

Some approaches to promote clearance of tau NFTs have emerged recently. Passive immunization with monoclonal antibodies against phosphorylated tau has shown benefits in tau transgenic animal models, leading to reduced motor impairment and decreased phosphorylation of tau and its aggregates.[141] Regarding the active immunization, it consists of the administration of phosphorylated tau fragments present in NFTs in order to generate an immune response against them.[142] *AADvac-1* vaccine, which contains synthetic $tau_{294-305}$ peptides, is in Phase II trials and *ACI-35*, which contains phosphorylated S396 and S404 tau fragments, is in Phase I trials.[119]

---

[138]K. R. Brunden, B. Zhang, J. Carroll, Y. Yao, J. S. Potuzak, A. M. Hogan, M. Iba, M. J. James, S. X. Xie, C. Ballatore, A. B. Smith 3rd, V. M. Lee, J. Q. Trojanowski. *J. Neurosci.* **2010**, *30*, 13861–13866.

[139]S. Wegmann, S. Nicholls, S. Takeda, Z. Fan, B. T. Hyman. *J. Neurochem* **2016**, *139*, 1163–1174.

[140]N. Badiola, V. Alcalde, A. Pujol, L. M. Munter, G. Multhaup, A. Lleo, M. Coma, M. Soler-Lopez, P. Aloy. *PLoS One* **2013**, *8*, e58837.

[141]A. Boutajangout, J. Ingadottir, P. Davies, E. M. Sigurdsson. *J. Neurochem* **2011**, *118*, 658–667.

[142]C. H. van Dyck. *Biol. Psychiatry* **2018**, *83*, 311–319.

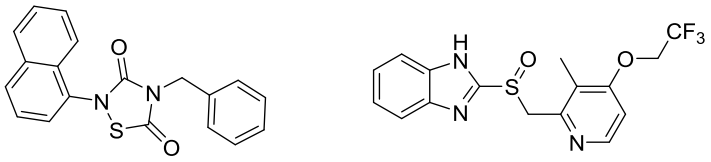

Tideglusib

Lansoprazole

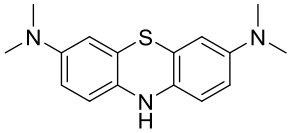

Methylene blue

Figure 1.21. Structure of some anti-tau compounds.

1.4.4 Oxidative stress directed strategies

The direct relationship between antioxidant therapies and improvement in cognitive dysfunctionalities has been well established.[143] Many exogenous antioxidants have been tested in AD. Administration of vitamin E in transgenic AD models led to reduced lipid peroxidation and plaque burden. However, supplementary trials in humans have not shown convincing evidence of their benefit.[144] Combination of vitamin E with donepezil did not provide additional benefit.[145] A Phase III trial combining vitamin E and memantine has been completed,[146] and also a Phase III study with vitamin E and selenium is currently ongoing. Several other ubiquitous antioxidants, such as flavonoids, carotenoids or curcumin, have also shown neuroprotective effects in experimental studies, but no significant differences in improving cognitive functions in humans have been found. Melatonin is another potent antioxidant currently in Phase II trials in the form of a prolonged release form.[137] Another way to fight against oxidative stress is facilitating the endogenous antioxidant defence. The primary endogenous antioxidant pathway is the nuclear receptor factor 2 (Nrf2) / antioxidant response element (ARE) cascade. Different compounds that can reestablish this pathway are under consideration.[147]

---

[143]F. Grodstein, J. Chen, W. C. Willett. *Am. J. Clin. Nutr.* **2003**, *77*, 975–984.

[144]N. Farina, M. G. Isaac, A. R. Clark, J. Rusted, N. Tabet. *Cochrane Database Syst. Rev.* **2012**, *11*, CD002854.

[145]R. C. Petersen, R. G. Thomas, M. Grundman, D. Bennett, R. Doody, S. Ferris, D. Galasko, S. Jin, J. Kaye, A. Levey, E. Pfeiffer, M. Sano, C. H. van Dyck, L. J. Thal. *N. Engl. J. Med.* **2005**, *352*, 2379–2388.

[146]M. W. Dysken, P. D. Guarino, J. E. Vertrees, S. Asthana, M. Sano, M. Llorente, M. Pallaki, S. Love, G. D. Schellenberg, J. R. McCarten, J. Malphurs, S. Prieto, P. Chen, D. J. Loreck, S. Carney, G. Trapp, R. S. Bakshi, J. E. Mintzer, J. L. Heidebrink, A. Vidal-Cardona, L. M. Arroyo, A. R. Cruz, N. W. Kowall, M. P. Chopra, S. Craft, S. Thielke, C. L. Turvey, C. Woodman, K. A. Monnell, K. Gordon, J. Tomaska, G. Vatassery. *Alzheimers Dementia* **2014**, *10*, 36–44.

[147]C. P. Ramsey, C. A. Glass, M. B. Montgomery, K. A. Lindl, G. P. Ritson, L. A. Chia, R. L. Hamilton, C. T. Chu, K. L. Jordan-Sciutto. *J. Neuropathol. Exp. Neurol.* **2007**, *66*, 75–85.

The aforementioned metal dyshomeostasis is another factor which can increase oxidative stress in AD. Biometals, such as Fe, Cu and Zn, are also responsible for promoting Aβ aggregation and deposition.[148] Therefore, metal chelators could be used to attenuate the deposition of Aβ.[149] Several metal chelators have been evaluated for amyloidopathy and tauopathy.[150] Clioquinol (PBT-1) specifically chelates Cu and Zn, preventing their interaction with Aβ. In Phase II trial, clioquinol administration decreased CSF Aβ levels but did not show improvements in cognitive functions. Consequently, Phase III trial was halted.[119]

1.4.5 Anti-inflammatory strategies

The abundant evidence for neuroinflammation in AD has prompted diverse studies with anti-inflammatory therapies. Several NSAIDs have been studied against AD. Numerous epidemiological data point to a reduced incidence of AD in NSAID users.[151] However, data from most clinical trials in AD and mild cognitive impairment have shown either neutral or harmful effects.[152] CHF 5074, a small molecule microglia modulator is in Phase II trial for mild cognitive impairment.[119]

1.5. Multitarget-directed ligands

In light of the aforementioned various complex mechanisms involved in the pathological network of AD and all the failures in finding effective therapies to stop the progression of the disease, it has become evident why the classical medicinal chemistry paradigm of “one molecule-one target” has met with such limited success. Consequently, a more comprehensive, complex pharmacological approach is needed to derive effective treatments.

---

[148]R. A. Cherny, C. S. Atwood, M. E. Xilinas, D. N. Gray, W. D. Jones, C. A. McLean, K. J. Barnham, I. Volitakis, F. W. Fraser, Y. S. Kim. *Neuron* **2001**, *30*, 665–676.

[149]P. A. Adlard, J. M. Parncutt, D. I. Finkelstein, A. I. Bush. *J. Neurosci.* **2010**, *30*, 1631–1636.

[150]P. A. Adlard, R. A. Cherny, D. I. Finkelstein, E. Gautier, E. Robb, M. Cortes, I. Volitakis, X. Liu, J. P. Smith, K. Perez, K. Laughton, Q. X. Li, S. A. Charman, J. A. Nicolazzo, S. Wilkins, K. Deleva, T. Lynch, G. Kok, C. W. Ritchie, R. E. Tanzi, R. Cappai, C. L. Masters, K. J. Barnham, A. I. Bush. *Neuron* **2008**, *59*, 43–55.

[151]C. Cornelius, J. Fastbom, B. Winblad, M. Viitanen. *Neuroepidemiology* **2004**, *23*, 135–143.

[152]S. A. Reines, G. A. Block, J. C. Morris, G. Liu, M. L. Nessly, C. R. Lines, B. A. Norman, C. C. Baranak. *Neurology* **2004**, *62*, 66–71.

In this context, different pharmacological approaches offer alternatives to overcome the problems associated with the use of single target drugs in complex diseases such as AD. The most commonly used approach is the so-called *multiple-medication therapy* (MMT, **Figure 1.22**), consisting in the combination of two or more drugs with different action mechanisms. However, this approach may suffer from patient compliance issues, especially in AD patients, and is associated with problems of bioavailability, pharmacokinetics and metabolism, as well as drug–drug interaction issues.[56,153] A related approach is the use of a *multiple-compound medication* (MCM, **Figure 1.22**) approach, where different drugs are incorporated into the same formulation, leading to simplified dosing regimens, and, hence, to improved patient compliance, but it still retains the other problems.[56,153]

Finally, a third strategy has emerged, which focuses on the use of a single compound that is able to hit multiple targets, which clearly presents multiple advantages over MMT or MCM. This approach, called *multitarget-directed ligand* therapy (MTDL, **Figure 1.22**), has a number of advantages, such as easier pharmacokinetics for ADME profile optimization, improved efficacy due to synergistic effects of simultaneous modulation of different targets, and improved safety by decreasing potential side effects and the risk of drug–drug interactions.[128,154] Nonetheless, this approach must face up important challenges in the drug discovery process. Firstly, the multitarget compound must interact with its multiple targets with comparable or balanced affinities. Also, potential drug promiscuity as a result of off-target effects might be an issue, which renders the design of these compounds a challenging task.[155,156] In any case, this new paradigm of MTDLs represents a new hope for AD and other multifactorial diseases, like cancer, diabetes or cardiovascular disease whose complex pathologies are difficult to tackle.

[153]B. Schmitt, T. Bernhardt, H. J. Moeller, I. Heuser, L. Frölich. *CNS Drugs* **2004**, *18*, 827–844.
[154]R. Morphy, Z. Rankovic. *J. Med. Chem.* **2005**, *48*, 6523–6543.
[155]E. Viayna, I. Sola, O. Di Pietro, D. Muñoz-Torrero. *Curr. Med. Chem.* **2013**, *20*, 1623–1634.
[156]A. Anighoro, J. Bajorath, G. Rastelli. *J. Med. Chem.* **2014**, *57*, 7874–7887.

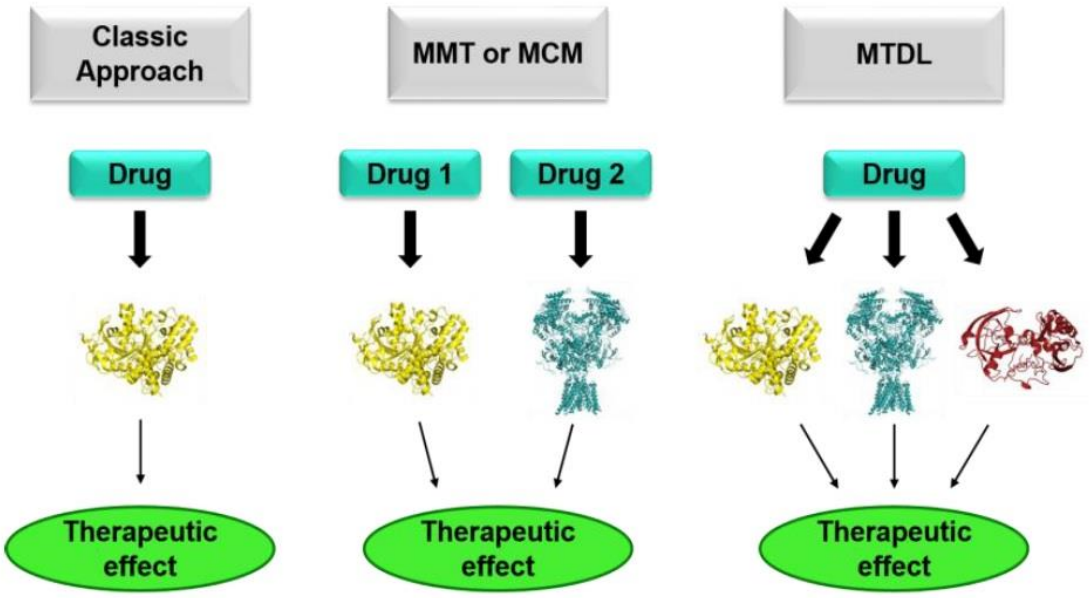

Figure 1.22. Different approaches to therapies against multifactorial diseases. Left: one-molecule-one-target strategy. Centre: multiple-medication therapy (MMT) or multiple-compound medication (MCM), where both drugs are applied in the same pill. Right: multitarget-directed ligand (MTDL) approach. (Image source: F. J. Pérez-Areales, D. Muñoz-Torrero, in *Recent Advances in Pharmaceutical Sciences VIII* (D. Muñoz-Torrero, Y. Cajal, J. M. Llobet (eds.), Transworld Research Network, Kerala, 2018, pp. 43–58).

1.6. Previous work in our research group

In the past years many research groups, including ours, have been working in the development of a large number of MTDLs with the purpose of finding disease-modifying drug candidates for the treatment for AD. In this section, some of the most recent work of our group in this field will be discussed.

MTDLs can be rationally designed through molecular assembly of two or more pharmacophore moieties from bioactive molecules, where each part is expected to retain the potential to interact with its specific target or its specific site in the same target.[157] An example of MTDLs hybrid molecules developed recently in our research group are the rhein–huprine hybrids, developed as part of Drs. Elisabet Viayna and Irene Sola's PhD Theses.[158]

[157]M. Decker. *Curr. Med. Chem.* **2011**, *18*, 1464–1475.
[158]E. Viayna, I. Sola, M. Bartolini, A. De Simone, C. Tapia-Rojas, F. G. Serrano, R. Sabaté, J. Juárez-Jiménez, B. Pérez, F. J. Luque, V. Andrisano, M. V. Clos, N. C. Inestrosa, D. Muñoz-Torrero. *J. Med. Chem.* **2014**, *57*, 2549–2567.

Huprines are a class of AChEIs developed in 1998 by Drs. Pelayo Camps and Diego Muñoz-Torrero, which turned out to be among the most potent reversible AChEIs reported so far.[159-161] They were designed by conjunctive approach using two well-known AChE CAS inhibitors, namely tacrine (**1**), the first marketed anti-Alzheimer drug, and (–)-huperzine A (**6**), an alkaloid isolated from *Huperzia serrata* with potent AChE inhibitory activity.[161] More than thirty different huprines were designed, synthesized and pharmacologically tested. The most potent members of this family are the so-called (–)-huprine Y, (–)-**7**, and (–)-huprine X, (–)-**8**, which are, in racemic form, up to 640- and 810-fold more potent *h*AChE inhibitors than the parent compounds tacrine and (–)-huperzine A, respectively (**Figure 1.23**).[161]

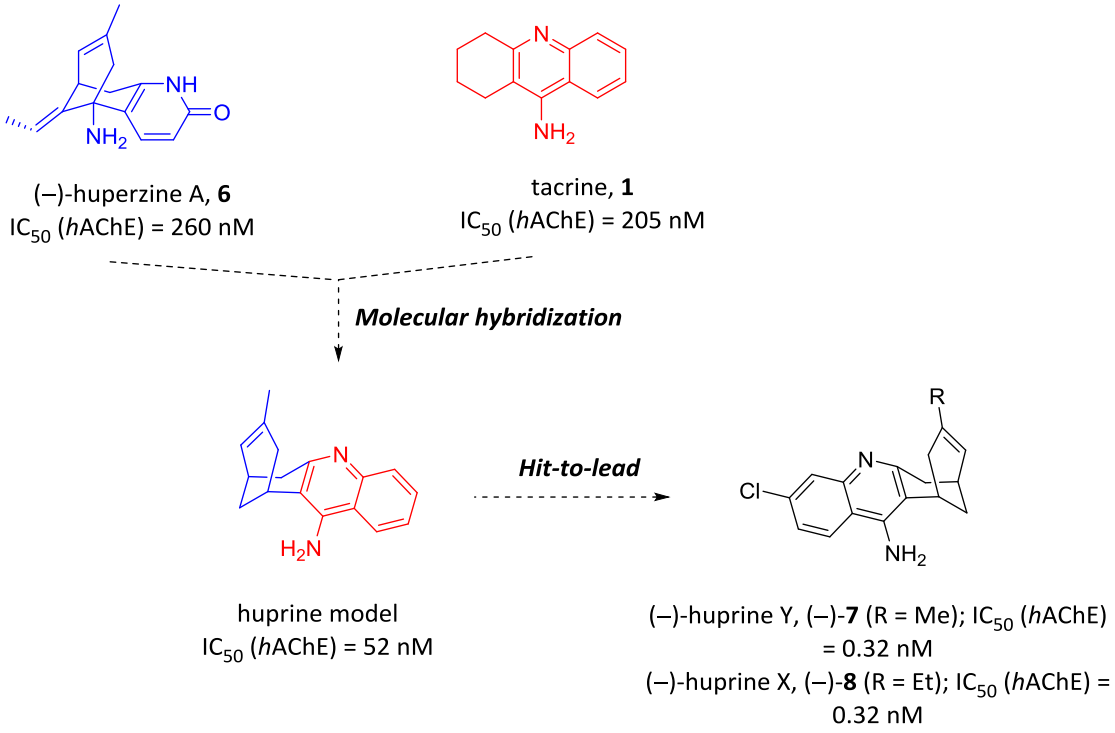

Figure 1.23. Design and development of huprines.

[159]A. Badia, J. E. Baños, P. Camps, J. Contreras, D. M. Görbig, D. Muñoz-Torrero, M. Simón, N. M. Vivas. *Bioorg. Med. Chem.* **1998**, *6*, 427–440.

[160]P. Camps, R. El Achab, D. M. Görbig, J. Morral, D. Muñoz-Torrero, A. Badia, J. E. Baños, N. M. Vivas, X. Barril, M. Orozco, F. J. Luque. *J. Med. Chem.* **1999**, *42*, 3227−3242.

[161]D. Muñoz-Torrero, P. Camps. *Exp. Opin. Drug Discov.* **2008**, *3*, 65–81.

The selection of rhein as a pharmacophore for designing new MTDLs by our group had its origin in the finding that compounds sharing a moiety of hydroxyanthraquinone displayed tau anti-aggregating properties *in vitro* with IC_{50} values in the low micromolar range.[162,163] The structurally related compound rhein, **9** (**Figure 1.24**), is a natural product from rhubarb (*Rheum rhabarbarum*), a product used in the traditional Chinese medicine.[164] In the context of Drs. Elisabet Viayna and Irene Sola's PhD Theses, a first generation of rhein–huprine hybrids was synthesised and biologically evaluated against several key targets of AD, with the lead compound being (±)–**10** (**Figure 1.20**).[158]

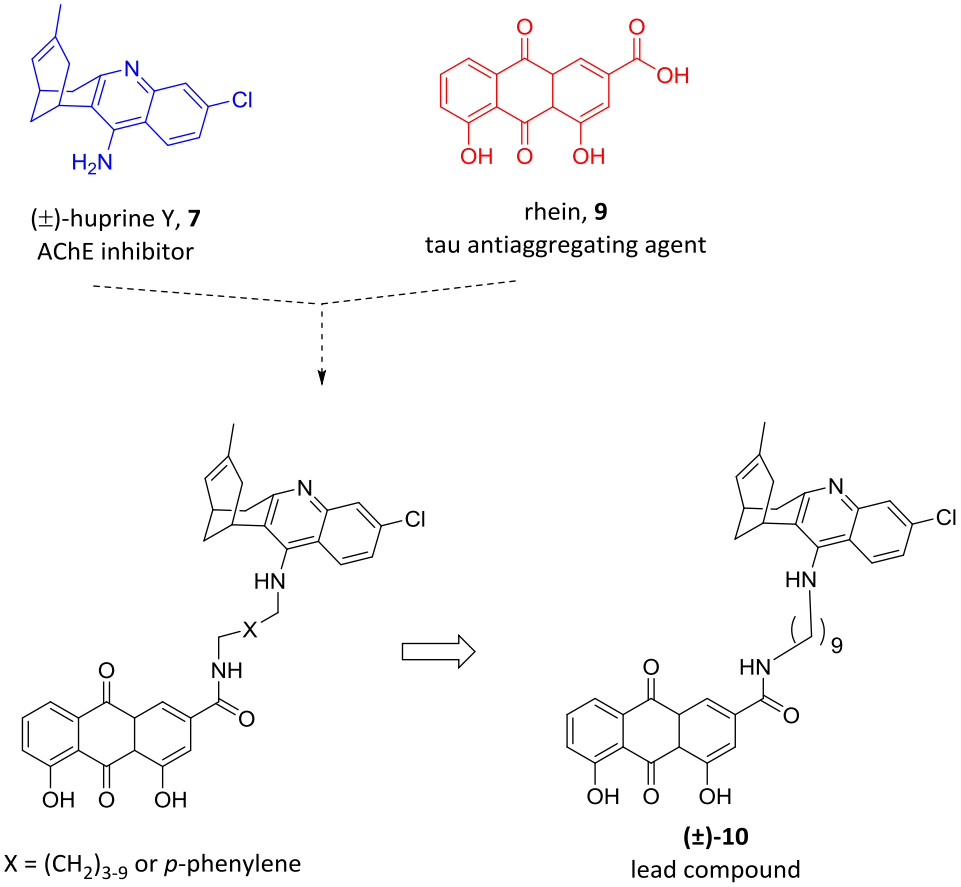

Figure 1.24. First generation of rhein–huprine hybrids, with their parent compounds (±)-huprine Y, **7**, and rhein, **9**, and the lead compound of the series, (±)–**10**.

[162]M. Pickhardt, Z. Gazova, M. V. Bergen, I. Khlistunova, Y. Wang, A. Hascher, E. -M. Mandelkow, J. Biernat, E. Mandelkow. *J. Biol. Chem.* **2005**, *280*, 3628–3635.

[163]B. Bulic, M. Pickhardt, B. Schmidt, E. -M. Mandelkow, H. Waldmann, E. Mandelkow. *Angew. Chem. Int. Ed.* **2009**, *48*, 1740–1752.

[164]X. Yang, G. Sun, C. Yang, B. Wang. *ChemMedChem* **2011**, *6*, 2294–2301.

These hybrids were endowed with a very interesting *in vitro* and *in vivo* multitarget profile, especially compound (±)–**10**, which presented cholinergic activity through the inhibition of *h*AChE (IC_{50} = 3.60 nM) and BChE (IC_{50} = 620 nM), Aβ and tau antiaggregating activity (48% and 30% inhibition at 10 μM, respectively) and, more surprisingly, a potent inhibitory activity against human BACE1 (IC_{50} = 120 nM). All these activities led to a significant Aβ lowering and cognition enhancing effect, especially by the dextrorotatory (7*R*,11*R*)-enantiomer, in a transgenic mouse model of AD (APP/PS1 mice).[158,165] With regard to the potent hAChE inhibitory activity, molecular modelling studies suggested, as expected, a dual binding mode of these compounds within the enzyme, i.e. a simultaneous interaction at both CAS and PAS of hAChE.[158] More interestingly, a dual site binding within BACE1 was also predicted by molecular modelling studies carried out by the group of Prof. F. Javier Luque, with the protonated huprine unit interacting with the aspartates catalytic dyad and the rhein moiety interacting with a thus far unknown secondary transient binding site.[158]

Given the pivotal role of oxidative stress in AD and considering the previous knowledge about AChEIs and MTDLs in our research group, more recently a new family of CR-6–chlorotacrine hybrids was developed as part of Dr. F. Javier Pérez Areales PhD Thesis. This project was developed in collaboration with the group of Prof. Àngel Messeguer (*Instituto de Química Avanzada de Cataluña*, IQAC-CSIC), with extensive knowledge in the development of antioxidants. This new series was designed to achieve a dual binding within both AChE and BACE1, apart from antioxidant activity, by combination of 6-chlorotacrine (**11**, **Figure 1.25**), a potent AChEI derived from tacrine, and a moiety derived from CR-6 (**12**), a potent antioxidant related to vitamin E, developed by Prof. Messeguer's group.[166] Several hybrids connected with different linkers were synthesised and biologically evaluated.[167]

[165]F. G. Serrano, C. Tapia-Rojas, F. J. Carvajal, P. Cisternas, E. Viayna, I. Sola, D. Muñoz-Torrero, N. C. Inestrosa. *Curr. Alzheimer Res.* **2016**, *13*, 1017–1029.

[166]L. Vázquez-Jiménez, M. Garrido, M. Miceli, E. Prats, A. Ferrer-Montiel, M. Teixidó, C. Jimeno, A. Messeguer. *Eur. J. Med. Chem.* **2016**, *123*, 788–802.

[167]F. J. Pérez-Areales, M. Garrido, E. Aso, M. Bartolini, A. De Simone, A. Espargaró, T. Ginex, R. Sabate, B. Pérez, V. Andrisano, F. J. Luque, I. Ferrer, F. Ciruela, A. Messeguer, D. Muñoz-Torrero, submitted.

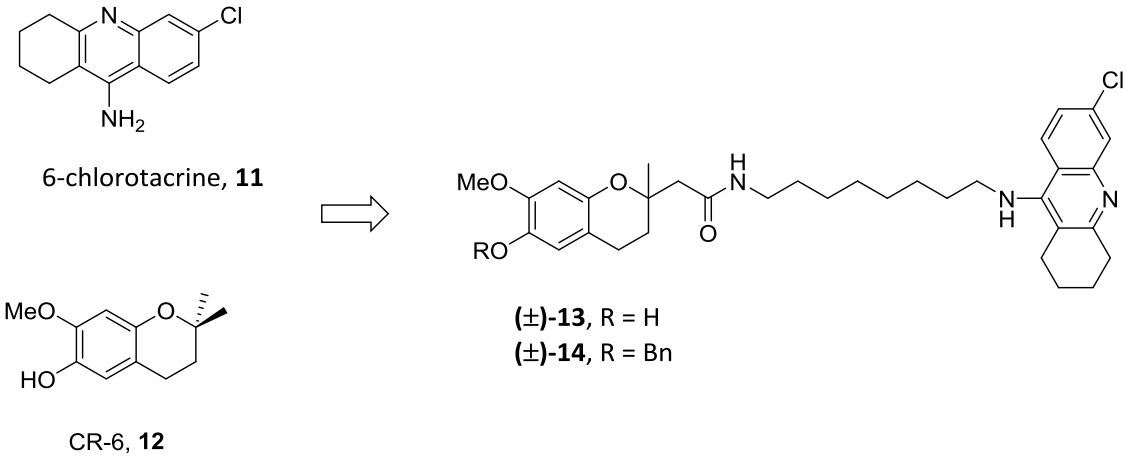

Figure 1.25. Lead compounds of the CR6–chlorotacrine family, **(±)–13** and **(±)–14**, and their parent compounds.

As expected by the rational design, these compounds seemed to display a dual binding mode within AChE and BChE, as confirmed by molecular dynamics simulations, which translated into a high inhibitory potency against both enzymes, reaching the subnanomolar range for hAChE inhibition. The BACE1 inhibitory potency was dependent on the length of the linker, being compounds **(±)–13** and **(±)–14** the most potent of the family, with an inhibitory potency of around 5 μM. All these hybrids exhibited significant *in vitro* Aβ42 and tau antiaggregating and antioxidant activities, and the majority of them were predicted to be able to cross the BBB.[167] The lead compounds exhibited a trend to improve cognition and decrease amyloid burden and some oxidative stress markers in APP/PS1 mice.

CHAPTER 2

Objectives

2.1 Modified rhein–huprine hybrids: design, synthesis and biological evaluation

As mentioned before, the lead compound of the first generation rhein–huprine hybrids, compound **10** (**Figure 2.1**), displayed a very interesting *in vitro* multi-target anti-Alzheimer profile and led to lowered central Aβ levels, reduced amyloid burden and neuroinflammation and improved cognition in a transgenic mouse model of AD *in vivo*. In a further lead optimization attempt, a second generation of these hybrids was synthesised in the frame of Dr. F. Javier Pérez Areales PhD Thesis. In that case, the huprine moiety of the lead **10** was modified in order to explore the effect of the pyridinic ring basicity on the different biological activities. However, these compounds presented lower inhibitory potencies than the previous lead. In the present work, we envisaged a third generation of rhein–huprine hybrids (general structure **I**, **Figure 2.1**), designed by modification of the rhein moiety of the lead **10**. The main aim of this work was replacing the rhein moiety by more simplified scaffolds with the hope of obtaining optimized hybrids with reduced molecular weight (MW) and lower lipophilicity to improve their physicochemical properties and pharmacokinetic profile, while retaining the multi–target profile of the lead **10**.

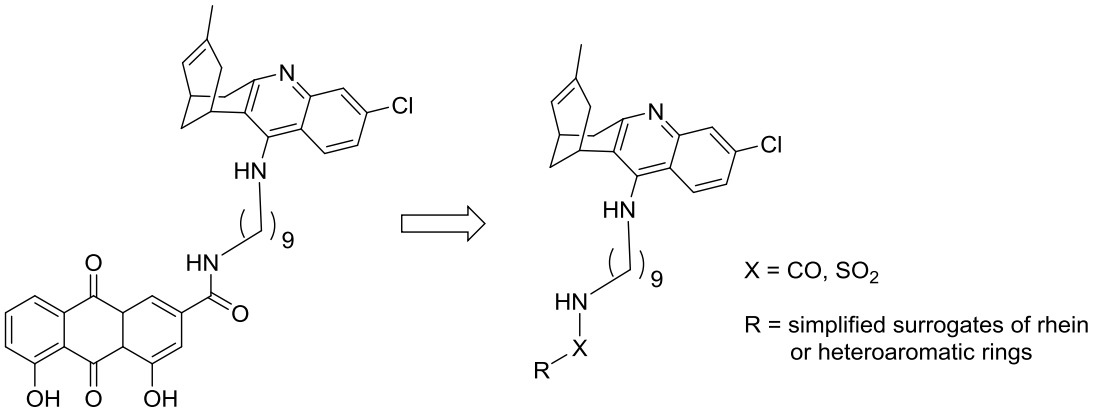

(±)-10 **(±)-I**

Figure 2.1. Structure of the lead compound of the first generation of rhein–huprine hybrids, **10**, and general structure proposed for the third generation (**I**).

This novel family of compounds was to be prepared using a general methodology, which comprised, as previously reported,[158] the alkylation of the racemic huprine with 9-bromononanenitrile, followed by a reduction to the corresponding aminononylhuprine, and the final acylation or sulfonylation with the corresponding carboxylic acids or sulfonyl chlorides.

2.2 Huprine–based BACE1 multisite inhibitors: design, synthesis and biological evaluation

Like in the previous section, the second objective of this work derives from the first generation of rhein–huprine hybrids, previously developed in our group. Further computational studies were performed on the interaction of the lead compound **10** within BACE1, in order to understand its binding mode, which led to an outstanding BACE1 inhibitory potency (IC_{50} = 120 nM). As a result of these studies, a novel transient druggable pocket was found, which appeared to accommodate the rhein subunit, whereas the huprine moiety was placed in the catalytic site. On the basis of these findings, a virtual screening (VS) campaign from the ZINC database led to the identification of a number of scaffolds with predicted binding affinity to this secondary floppy pocket of BACE1. In this work, we envisaged the synthesis of a novel class of hybrids, designed by combination of these putative secondary pocket binding scaffolds identified by virtual screening with a huprine moiety to display dual site binding within both BACE1 and AChE (general structures **II** and **III**, **Figure 2.2**).

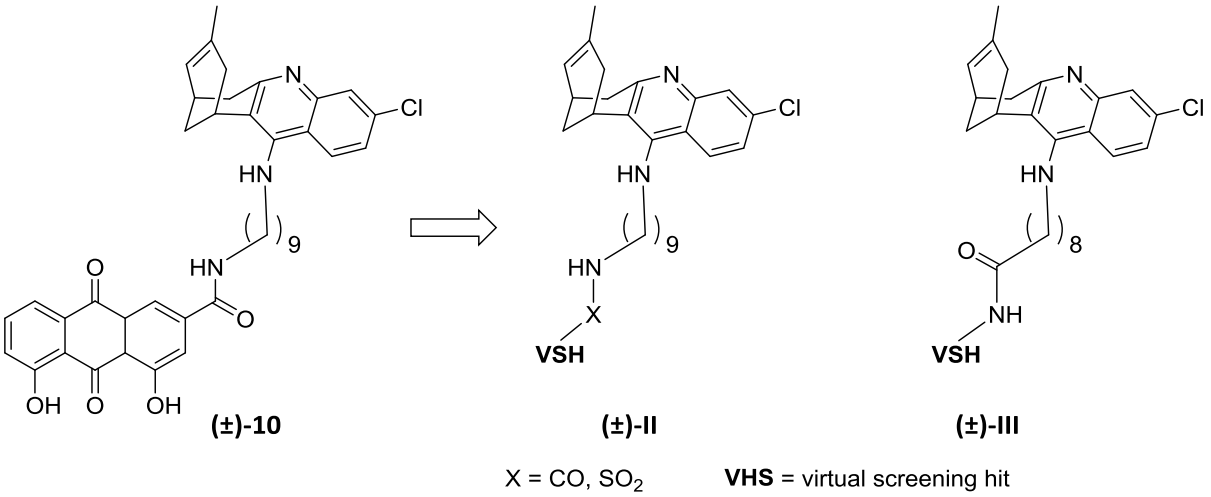

Figure 2.2. Structure of the lead compound of the first generation of rhein–huprine hybrids, **10**, and the general structures proposed for this new family of BACE1 multisite binding huprine–based hybrids (**II** and **III**).

This novel family of compounds was to be prepared using the methodology described for the previous work, which comprised the alkylation of racemic huprine with 9-bromononanenitrile, followed by reduction of the resulting cyanoalkylhuprine to the corresponding aminononylhuprine or hydrolysis to the carboxylic acid, and the final carboxamide or sulphonamide formation with the corresponding carboxylic acids, sulfonyl chlorides or amines.

2.3 Huprine–TPPU and 6-chlorotacrine–TPPU hybrids: design, synthesis and biological evaluation

Given the pivotal role that seems to play neuroinflammation in AD, we envisioned a new family of compounds, designed to simultaneous inhibit soluble epoxyde hydrolase (sEH), an enzyme involved in neuroinflammation, and AChE. Taking advantage of the knowledge in our research group about AChEIs, a collaborative work was planned with the group of Prof. Santiago Vázquez (*Universitat de Barcelona*), which has extensively worked during the last years in the search of sEH inhibitors of potential interest for the treatment of different diseases, such as acute pancreatitis or AD. The new family of hybrids was designed by combination of pharmacophores for both enzymes. On one side, we planned the use of 6-chlorotacrine and huprine Y as AChE inhibiting pharmacophores, which were to be combined with a unit of TPPU, a potent sEH inhibitor developed by the group of Prof. Bruce D. Hammock. Both pharmacophoric units should be connected through an appropriate linker to enable a dual site binding within AChE (general structure **IV** and compounds **(+)-16** and **(–)-16**, **Figure 2.3**).

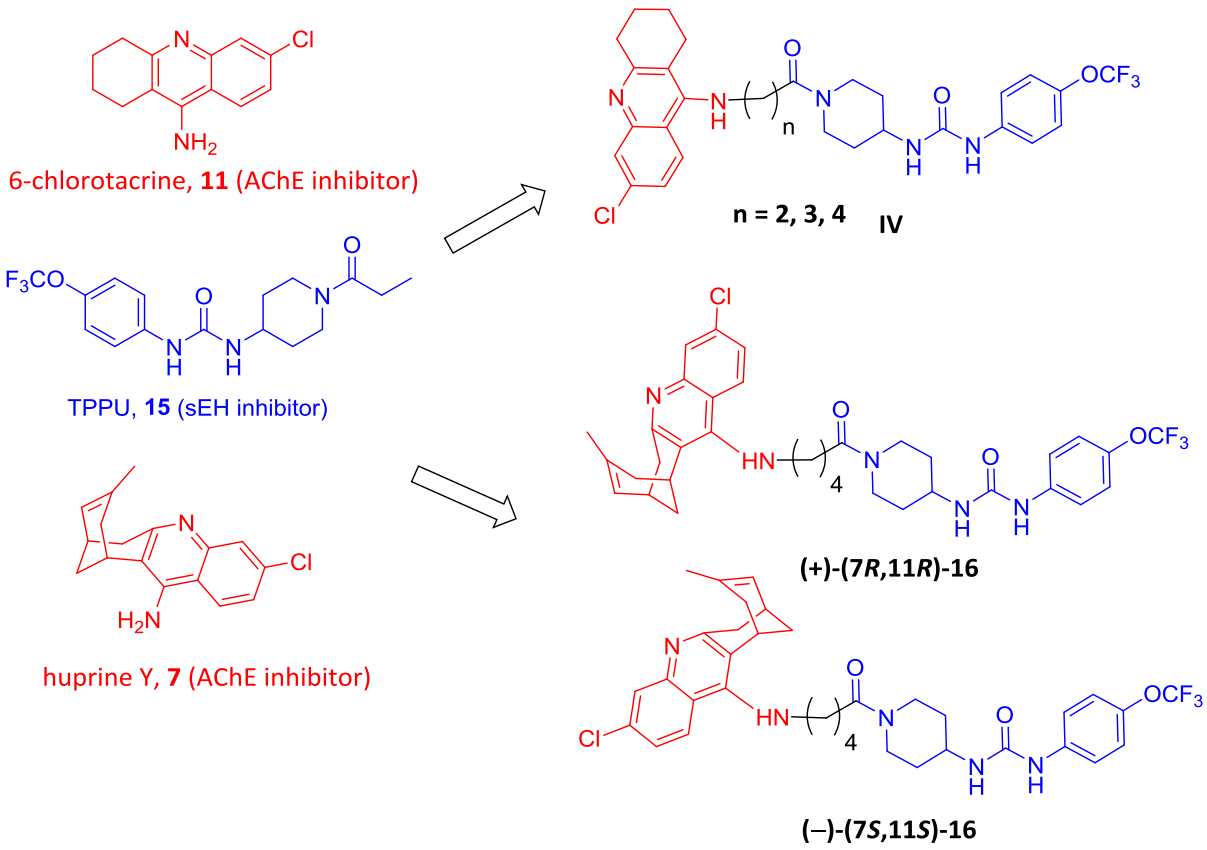

Figure 2.3. Structure of the parent AChEIs, huprine Y and 6-chlorotacrine, the parent sEHI, TPPU, and the structures proposed for this new family of hybrids (general structure **IV** and compounds **(+)-(7*R*,11*R*)-16** and **(–)-(7*S*,11*S*)-16**).

The synthesis of these hybrids was envisaged through two general methodologies. For the shorter tacrine–TPPU hybrids (**IV**, n = 2, 3), a nucleophilic aromatic substitution of 6,9-dichloro-1,2,3,4-tetrahydroacridine with the corresponding aminoalcohol was envisaged, followed by conversion of the alcohol to the corresponding mesylate and a nucleophilic substitution to obtain the corresponding nitrile. For the huprine–TPPU hybrids **16** and the longer tacrine–TPPU hybrid (**IV**, n = 4), an initial direct alkylation of huprine Y or 6-chlorotacrine with 5-bromovaleronitrile was planned. Hydrolysis of all these nitriles to the corresponding carboxylic acids and final amide coupling with the TPPU piperidine derivative was planned to get access to the target hybrids.

2.4 Biological evaluation of amyloidogenic proteins aggregation in *E. coli* cells

As mentioned in the Introduction section, aggregation of Aβ and tau into senile plaques and NFTs, respectively, are the main hallmarks of AD. Amyloid-prone proteins, including Aβ and tau, tend to aggregate spontaneously under pathological conditions, by induction of conformational changes, which lead to alignment of complementary β-sheets and formation of fibrils. For this reason, development of inhibitors of the aggregation of these proteins can be of great interest in AD and other amyloidogenic diseases.

Some years ago, in the frame of a research collaboration with the group of Dr. Raimon Sabaté (*Universitat de Barcelona*), a new methodology was developed for the fast, simple and inexpensive screening of Aβ and tau aggregation inhibitors using a simplified *in vivo* system, namely intact *Escherichia coli* cells that have been genetically modified to overexpress one amyloidogenic protein (Aβ and tau). Overexpression of the amyloidogenic protein is followed by its aggregation to form inclusion bodies, which can be stained with the dye thioflavin S (Th-S) to monitor the extent of the aggregation or the antiaggregating activity of an inhibitor by a fluorimetric assay. In this context, and taking into account that Aβ and tau aggregation were some of the pathological events to be targeted by the different families of compounds planned, the evaluation by myself of the Aβ and tau antiaggregating activities of the target compounds and other compounds contemporarily developed in our group in *E. coli* cells was also included as one of the objectives of this PhD Thesis.

Taking advantage of the experience gained in these assays, an additional, more ambitious objective was planned in this PhD Thesis, i.e. to demonstrate the feasibility of developing compounds that are active against all amyloidogenic proteins (amyloid pan-inhibitors). This objective arises from a credence that the aggregation of all amyloidogenic proteins proceeds through common mechanisms,

thus making feasible the development of common treatments against different conformational diseases. In order to validate this hypothesis, we planned the setting up of the aggregation assay in *E. coli* cells for other eleven different amyloidogenic proteins, apart from Aβ and tau, and the evaluation of three compounds with known antiaggregating properties against Aβ and tau, previously developed in our group, against the aggregation of all the thirteen different amyloidogenic proteins, which encompass all the major types of amyloid-based disorders (**Figure 2.4**).

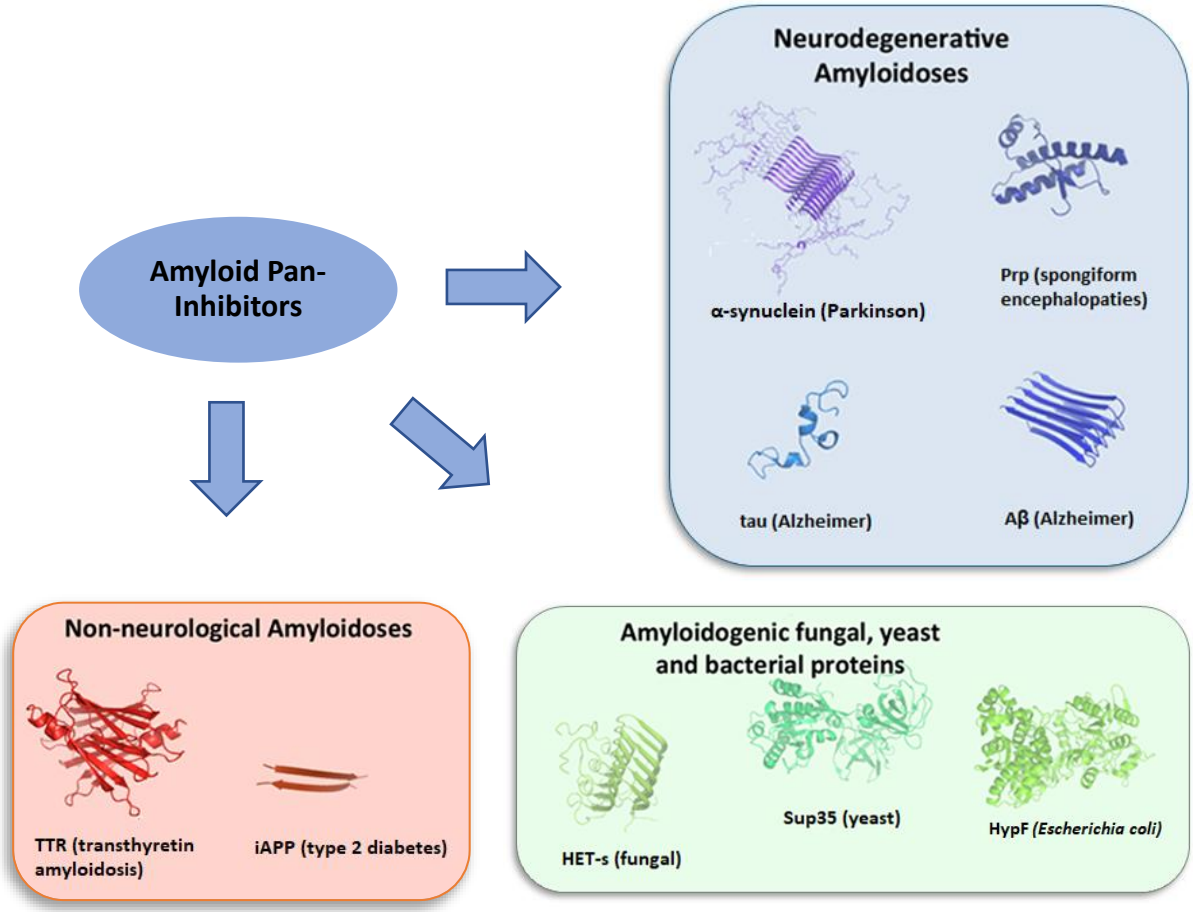

Figure 2.4. Hypothesis of the amyloid pan-inhibitors to be tested.

CHAPTER 3

Modified rhein–huprine hybrids

3.1 First generation rhein–huprine hybrids: computational studies

As mentioned in section **1.6**, a family of rhein–huprine hybrids was prepared as part of Drs. Elisabet Viayna and Irene Sola PhD Theses. The lead of the family, compound **10** showed a very interesting *in vitro* and *in vivo* multi-target anti-Alzheimer profile, displaying a potent *h*AChE inhibition (IC_{50} = 3.60 nM), a moderately potent *h*BChE (IC_{50} = 620 nM), Aβ and tau antiaggregating properties (48% and 30% inhibition at 10 μM, respectively) and, more strikingly, a potent inhibitory potency against *h*BACE1, in the nanomolar range (IC_{50} = 120 nM). To shed light on the binding mode of these compounds, molecular modelling studies within AChE and BACE1 were performed by the group of Prof. F. Javier Luque (*Universitat de Barcelona*).[158]

The binding mode of these compounds to AChE was firstly studied with compound **17** (**Figure 3.1**). Even though this compound was not the most potent of the series, it was chosen due to the limited number of rotatable bonds as compared with the lead, **10**. The results showed that the huprine moiety was placed in the CAS of AChE whereas the rhein unit was found to interact with the aromatic rings of Trp286 and Tyr72 in the PAS. These findings support the idea that the potent inhibitory activity of these hybrids against AChE stems from a dual site binding within this enzyme (**Figure 3.1**).[158]

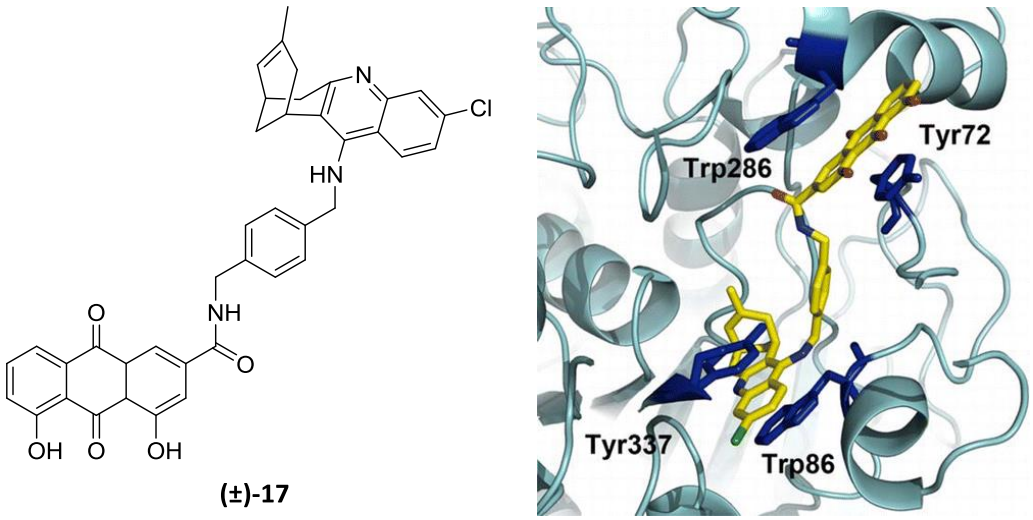

(±)-17

Figure 3.1. Structure of the *p*-phenylene-linked rhein–huprine hybrid **17** and its binding mode within AChE. (Image source: E. Viayna, I. Sola, M. Bartolini, A. De Simone, C. Tapia-Rojas, F. G. Serrano, R. Sabaté, J. Juárez-Jiménez, B. Pérez, F. J. Luque, V. Andrisano, M. V. Clos, N. C. Inestrosa, D. Muñoz-Torrero. *J. Med. Chem.* **2014**, *57*, 2549–2567).

With regard to the study of the binding mode within BACE1, as a first step, the druggable pockets present in the enzyme were examined with the aim of determining their ability to bind the huprine and hydroxyanthraquinone moieties of the hybrids. Two druggable pockets, namely BS1, which encompasses the catalytic site, and BS2, which includes unexplored subsites, were found to be suitable for binding of huprine and rhein moieties (**Figure 3.2**). In addition, the distance between these pockets was comprised between 7 and 11 Å, thus satisfying the geometrical criteria required for the tether in the rhein–huprine hybrids. In an analogous way as for AChE, molecular modelling studies for BACE1 were performed with the conformationally more restricted compound **17**. Calculations suggested a clear dual binding site mode, in which the huprine moiety is accommodated at the BS1 pocket, and the rhein unit fills the BS2 site (**Figure 3.2**). The huprine moiety seems to be tightly bound to BS1, as expected from the electrostatic stabilization between the protonated aminoquinoline system and the catalytic dyad (Asp32 and Asp228), whereas the bicyclic system of huprine fills a hydrophobic pocket near the catalytic dyad. On the other hand, the hydroxyanthraquinone moiety of **17** establishes an electrostatic interaction with Lys321, hydrogen bonds with the backbone of Phe322 and the side chain of Asn233, and hydrophobic contacts with Val309 (**Figure 3.2**). On the basis of these findings it was reasonable to expect that the larger flexibility afforded by the linker in the lead **10** should facilitate a proper accommodation to both BS1 and BS2 in BACE1, thus leading to a high inhibitory activity against this enzyme.

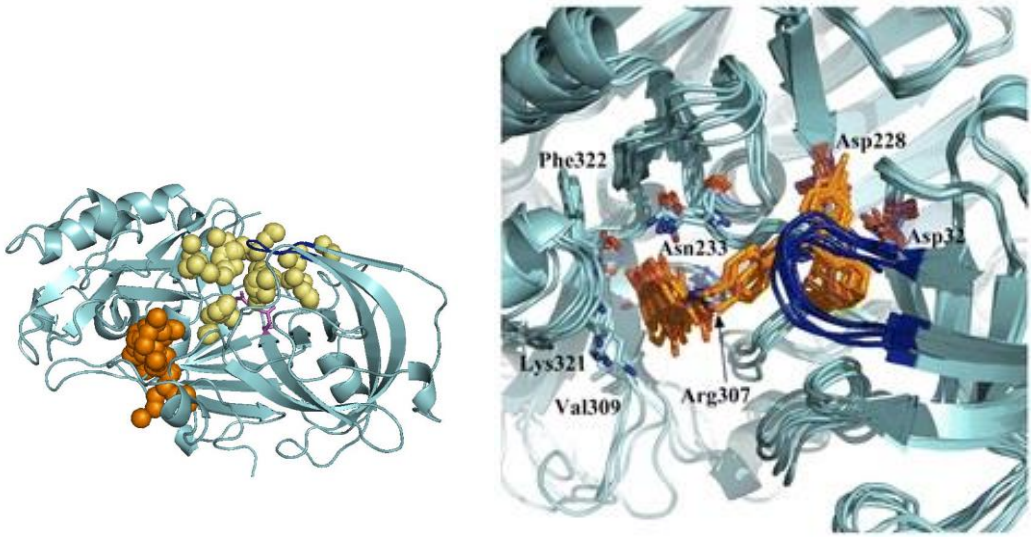

Figure 3.2. Left: representation of the two druggable pockets of BACE1, namely BS1 (yellow spheres), which is shaped by the "flap" (in dark blue), and BS2 (orange spheres), an unexplored secondary site. Right: superposition of four independent molecular dynamic simulations of **17** bound to BACE1. (Image source: E. Viayna, I. Sola, M. Bartolini, A. De Simone, C. Tapia-Rojas, F. G. Serrano, R. Sabaté, J. Juárez-Jiménez, B. Pérez, F. J. Luque, V. Andrisano, M. V. Clos, N. C. Inestrosa, D. Muñoz-Torrero. *J. Med. Chem.* **2014**, *57*, 2549–2567).

3.2 Second generation rhein–huprine hybrids: basicity modulation

More recently, a second series of these hybrids was developed in the frame of the PhD Thesis of Dr. F. Javier Pérez Areales.[168] These hybrids were designed by modification of the huprine chlorobenzene ring of the previous lead **10** by other aromatic or heteroaromatic rings (**Figure 3.3**), with the purpose of exploring the effect of the pyridinic ring basicity on the different biological activities, aiming to identify an optimized hybrid with favourable multi-target profile and reduced basicity and, thus, with expectable better bioavailability.

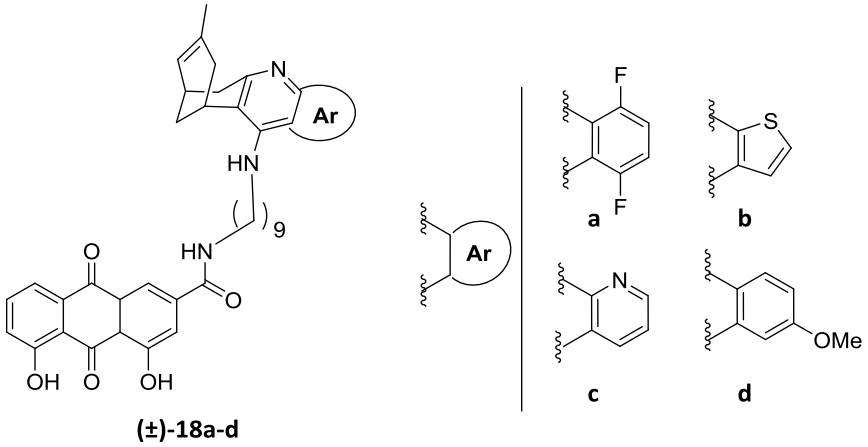

Figure 3.3. Structures of the second generation rhein–huprine hybrids.

Among the four compounds of the family, the parent modified huprines of two of them (compounds **(±)-18a** and **(±)-18b**, **Figure 3.3**) were predicted to present reduced basicity compared to huprine Y by high-level quantum mechanics (QM) studies (pK_a = 7.8 and 7.6, respectively, *versus* pK_a = 9.5 for huprine Y). The other two (compounds **(±)-18c** and **(±)-18d**) were predicted to be slightly more basic than huprine (pK_a = 10.1 for both of them). These new hybrids resulted to present decreased potency against *h*AChE and *h*BChE, in the low micromolar range, and against BACE1 (low micromolar or high nanomolar range for **(±)-18a** and **(±)-18b**, **(±)-18c** and **(±)-18d** were inactive). They presented similar antiaggregating potencies against tau and $A\beta_{42}$ peptide, good antioxidant activity, mainly due to the presence of the phenolic groups of rhein, and all of them were predicted to cross the BBB in a PAMPA-BBB assay.

[168] F. J. Pérez-Areales, N. Betari, A. Viayna, C. Pont, A. Espargaró, M. Bartolini, A. De Simone, J. F. R. Alvarenga, B. Pérez, R. Sabate, R. M. Lamuela-Raventós, V. Andrisano, F. J. Luque, D. Muñoz-Torrero. *Fut. Med. Chem.* **2017**, *9*, 965–981.

3.3 Design of modified rhein–huprine hybrids

In the light of the aforementioned results for the first and second generation of rhein–huprine hybrids, and once the tether length between both subunits and the huprine moiety had been optimized (in the first and the second series, respectively), in this PhD Thesis we considered the optimization of the rhein subunit. Rhein itself is highly lipophilic and insoluble in water[169], as it is the case of the first and second generation rhein–huprine hybrids, which, in addition have molecular weights over 500, which might compromise solubility, oral absorption, and penetration of these compounds through the BBB.[170] For this reason, we envisaged a novel series of huprine–modified rhein hybrids, using as a template the previous lead **10**, featuring the optimal huprine Y unit and nonamethylenic tether. By substitution of the rhein moiety by more simplified analogues, with reduced molecular weight and decreased lipophilicity, we aimed to further delineating the SAR around this moiety and to identify analogues with reduced size and favourable physicochemical and pharmacokinetic properties, and multitarget activity profile.

As mentioned before, the rhein subunit has been predicted to fill the BS2 pocket within BACE1. Further computational studies of the binding mode of compound **10** within the enzyme revealed that the hydroxyanthraquinone moiety adopts a well-defined binding mode in this secondary cavity of BACE1. The most relevant feature for this is a hydrogen bond interaction of the carbonyl group of the most hydrophobic edge of rhein with the guanidinium moiety of Arg307, which in turn forms a salt bridge interaction with Glu339, whereas the most hydrophilic edge of rhein is oriented towards the solvent (**Figure 3.4**).[171]

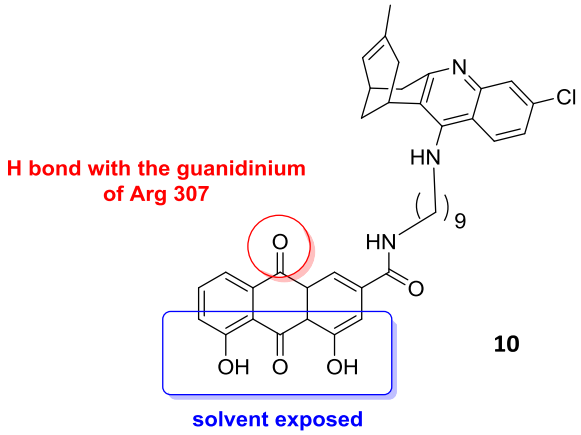

Figure 3.4. Structure of compound **10** with the main interaction of the rhein subunit at the secondary pocket of BACE1.

[169]J. Liu, G. Hu, R. Xu, Y. Qiao, H. -P. Wu, X. Ding, P. Duan, P. Tu, Y. -J. Lin. *J. Asian Nat. Prod. Res.* **2015**, *15*, 756–763.
[170]H. Pajouhesh, G. R. Lenz. *Neurotherapeutics* **2005**, *2*, 541–553.
[171]O. Di Pietro, J. Juárez-Jiménez, D. Muñoz- Torrero, C. A. Laughton, F. J. Luque. *PLoS ONE* **2017**, *12*, e0190327.

For all the hybrids designed, the general structure of the compounds (general structure **I**, **Figure 3.4**) comprises the racemic huprine with the nonamethylenic linker, which are the optimal features for these hybrids, and different substituents replacing the rhein moiety. These substituents can be distributed into three main groups: i) direct simplified surrogates of rhein, resulting from removal of substituents, ring contraction or ring opening (**Figure 3.5**), ii) analogues with one heteroaromatic ring (**Figure 3.6**), and iii) analogues with two aromatic rings, either fused or not (**Figure 3.7**). In all cases, these substituents should retain the ability to act as hydrogen bond acceptor (through a carbonyl group or an heteroatom in an heteroaromatic ring), which is the main feature required for the interaction with Arg307 at the BS2 of BACE1.

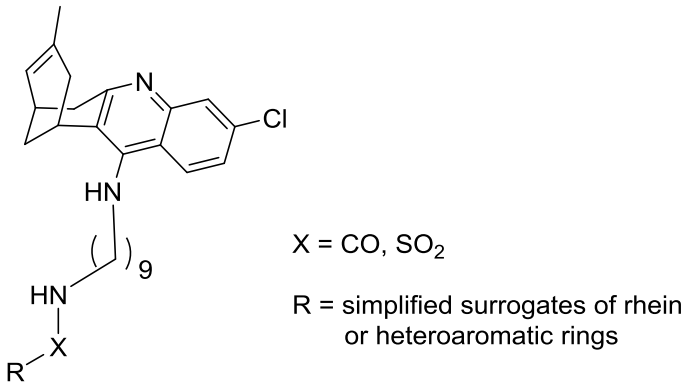

(±)-I

Figure 3.4. General structure of the huprine–modified rhein hybrids.

Group i) simplified surrogates of rhein (carbonyl as H bond acceptor)

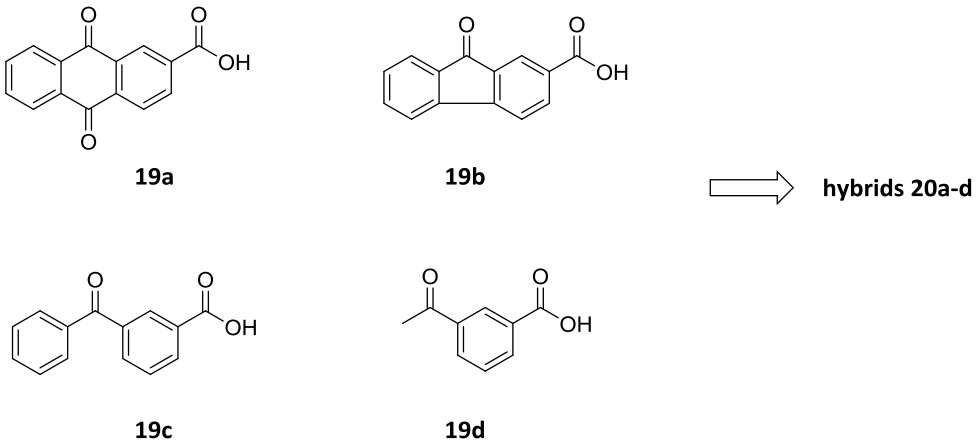

Figure 3.5. Parent substituents of group i) and compound numbers of the resulting hybrids.

Group ii) one heteroaromatic ring (heteroatom as H bond acceptor)

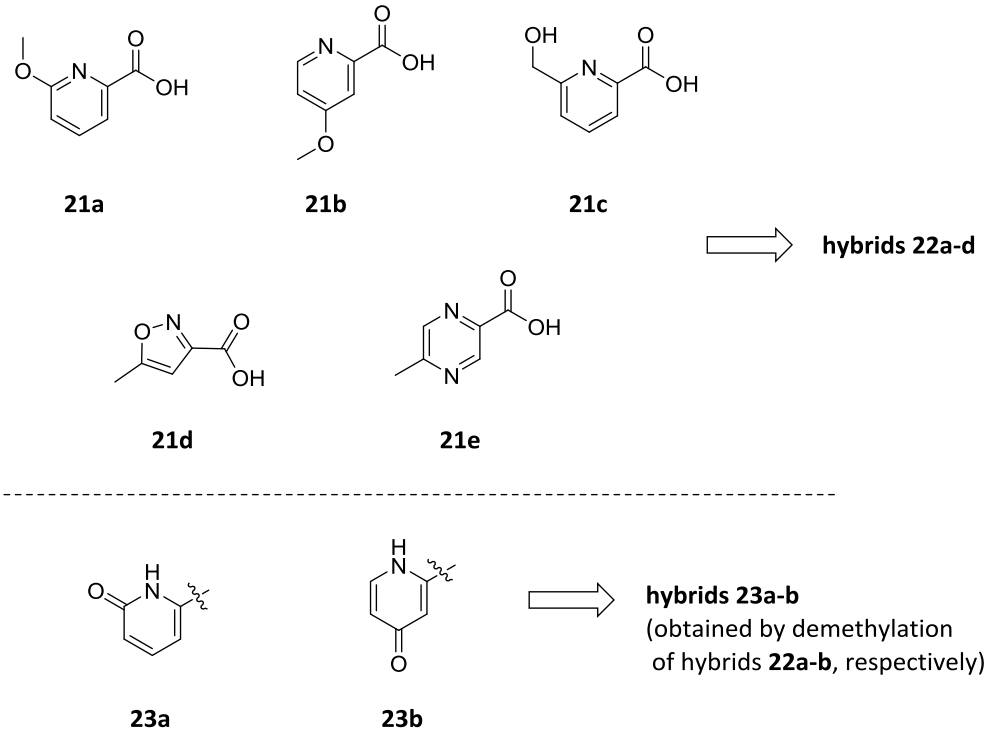

Figure 3.6. Parent substituents of group ii) and compound numbers of the resulting hybrids .

Group iii) two (hetero)aromatic rings (heteroatom as H bond acceptor)

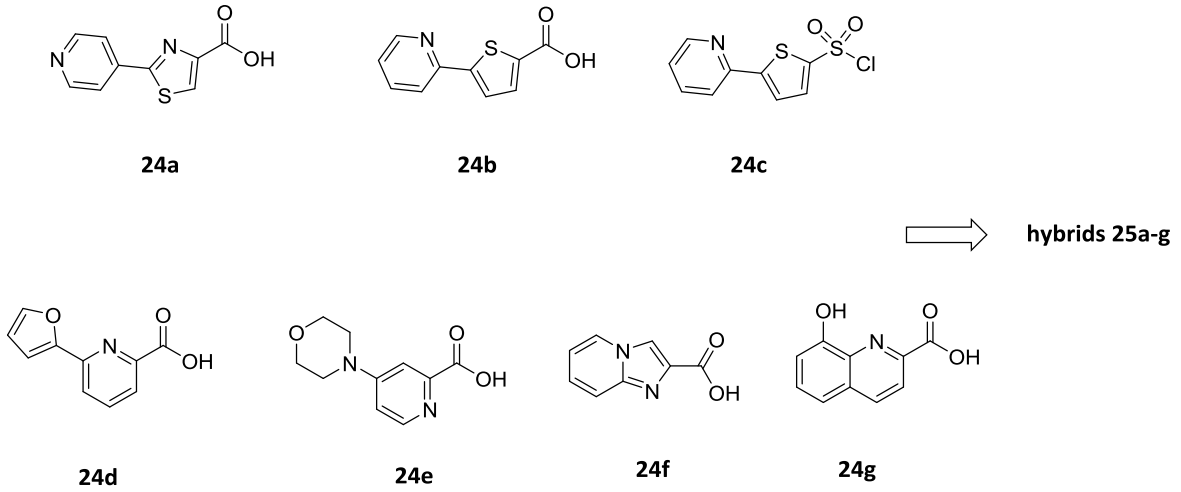

Figure 3.7. Parent substituents of group iii) and compound numbers of the resulting hybrids.

In the same way as compound **10**, these new compounds were expected to be dual inhibitors of AChE, with the huprine moiety being placed at the CAS and the new rhein-replacing substituents interacting with the PAS of the enzyme. We expected them to display a dual inhibition in BACE1 as well, as they were designed with this purpose. Apart from that, as discussed in section **1.2.7**, it is known that redox active metals may have an important role in oxidative stress through the production of ROS and can influence protein aggregation. In this way, some of the rhein-replacing scaffolds were selected in light of their potential metal chelating properties or radical scavenging capacity. Finally, these compounds were also expected to display Aβ and tau antiaggregating properties, like other huprine-based hybrids developed in our group.

3.4 Synthesis of modified rhein–huprine hybrids

For the preparation of these compounds, we first needed to prepare the linker intermediate, 9-bromononanenitrile, **27**, which was not commercially available. To obtain this intermediate, 1,8-dibromooctane, **26**, was treated with NaCN in DMF for 2 h at 35 °C. This product was previously purified in our group by a tedious microdistillation process under vacuum from a mixture with unreacted dibromoalkane and di-reaction byproduct, leading to very low yields (<10%). In the present Thesis, purification of the reaction crude by silica gel column chromatography led to compound **27** more rapidly and in much better yield, albeit still moderate (48%, **Scheme 3.1**). After that, alkylation of racemic huprine Y, **7**, with **27** in the presence of KOH in DMSO at r. t. overnight, led to nitrile **28** in good yield (73%, **Scheme 3.1**), after silica gel column chromatography purification.

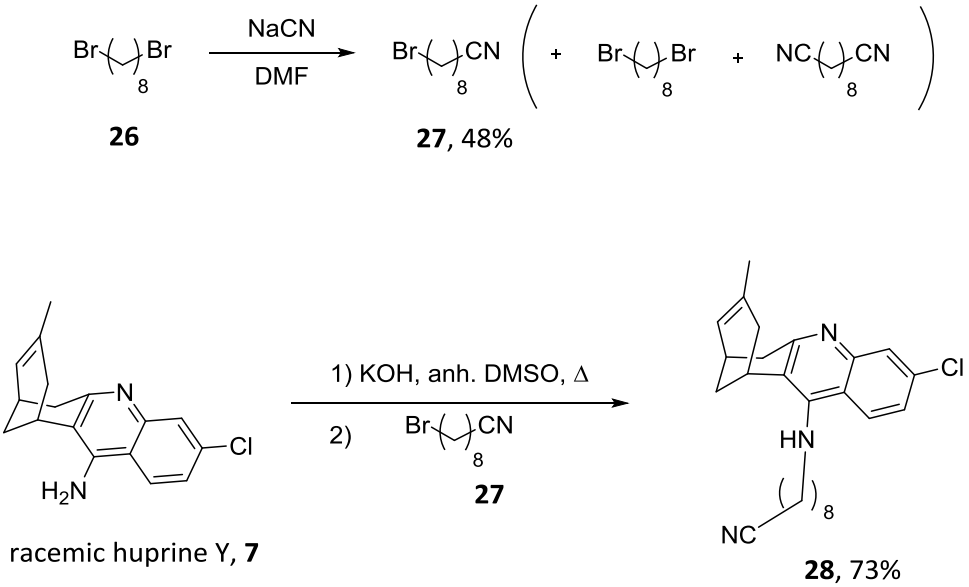

Scheme 3.1

In the following step, nitrile **28** was reduced by treatment with $LiAlH_4$ in Et_2O at r. t. overnight, to afford the corresponding aminononylhuprine, **29**, in a very good yield (96%) without further purification (**Scheme 3.2**).

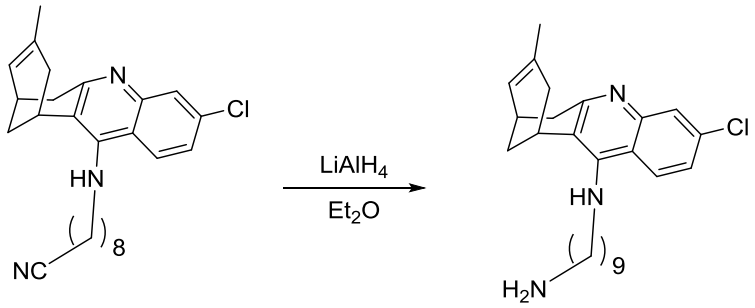

28 **29**, 96%

Scheme 3.2

Final amide coupling reaction between the corresponding carboxylic acid, **19a-d, 21a-e** and **24a,b,d-f**, and the primary amine **29** was performed in the presence of EDC, HOBt, and Et_3N in a mixture of EtOAc / DMF at r. t. overnight, to provide the desired hybrids, **20a-d, 22a-e** and **25a,b,d-f**, in moderate to good yields (53%-quantitative, **Scheme 3.3**), after silica gel column chromatography purification.

For 8-hydroxyquinoline-2-carboxylic acid, **24g**, direct coupling with aminononylhuprine, **29**, did not lead to the desired product, presumably due to the free hydroxy group. Alternatively, we performed the acetylation of the hydroxy group of **24g** by treatment with acetic anhydride and Et_3N in a mixture of CH_2Cl_2 / DMF, to afford the protected carboxylic acid, **30**, in good yield (89%, **Scheme 3.4**) after silica gel column chromatography purification, which was then coupled with the aminononylhuprine **29** in the same conditions as above (31% yield of amide). The resulting hybrid, **31** was then deprotected with $NaHCO_3$ in a mixture of MeOH / water to provide the target hybrid, **25g**, in good yield (93%).

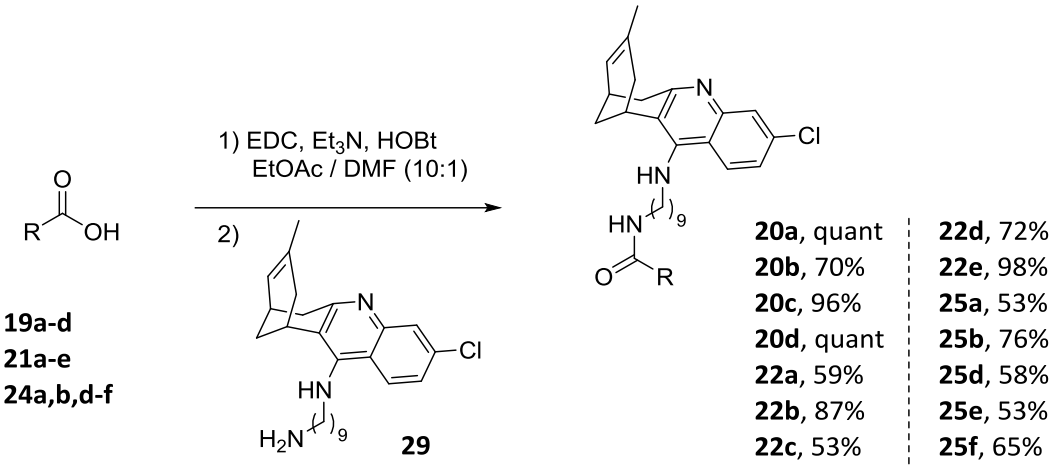

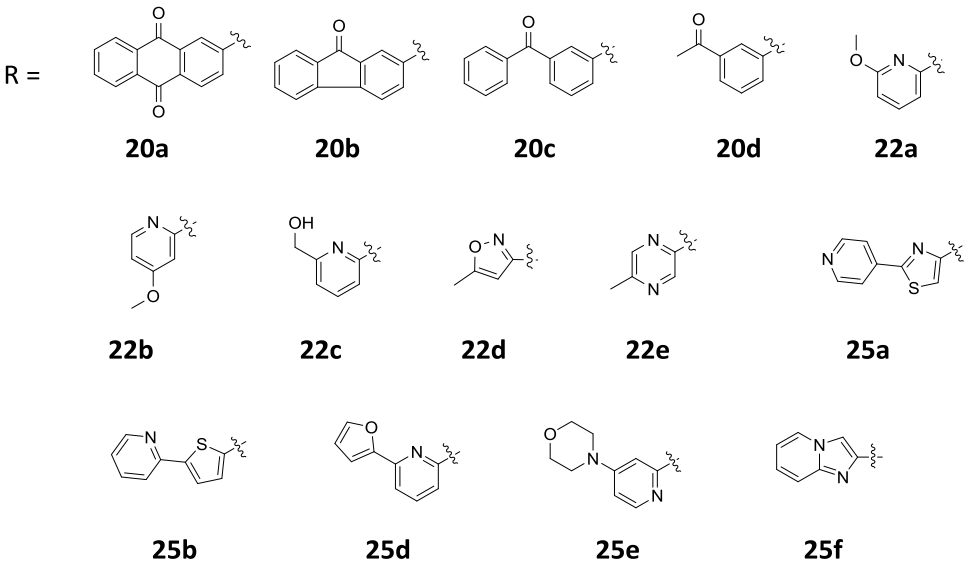

Scheme 3.3

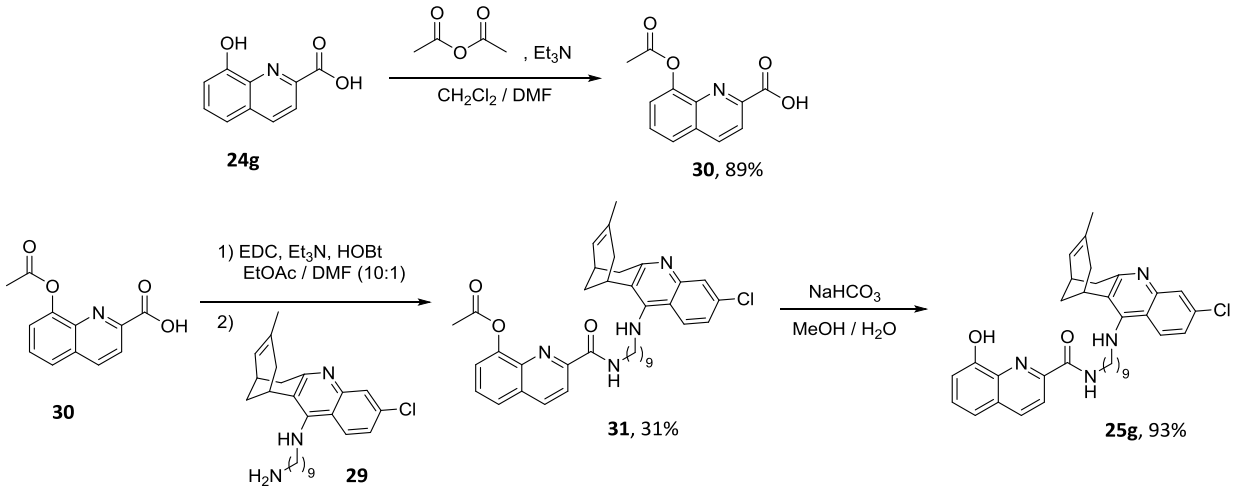

Scheme 3.4

Hybrids **23a-b**, which should be in tautomeric equilibrium with their corresponding pyridones, being these the most predominant forms, were obtained by demethylation of hybrids **22a-b** upon treatment with LiCl and *p*TSA in DMF at 120 °C for 5.5 h (for **23a**) or *N*-Methyl-2-pyrrolidone (NMP) at 120 °C for 2 h (for **23b**) in moderate yields (33 and 64%, respectively, **Scheme 3.5**).

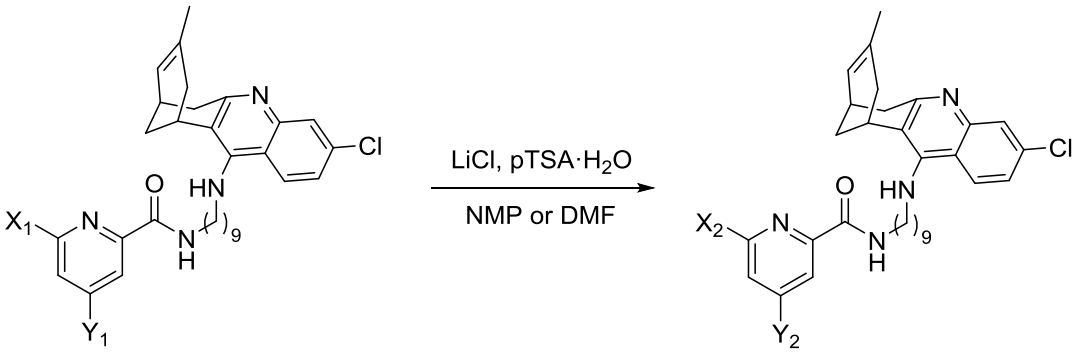

22a: X_1 = OMe, Y_1 = H
22b: X_1 = H, Y_1 = OMe

23a: X_1 = OH, Y_1 = H, 33%
23b: X_1 = H, Y_1 = OH, 64%

Scheme 3.5

Finally, sulphonamide-linked hybrid **25c** was obtained by coupling between commercially available sulphonyl chloride **24c** and aminononylhuprine **29** in the presence of Et_3N in DMF in good yield (85%, **Scheme 3.6**).

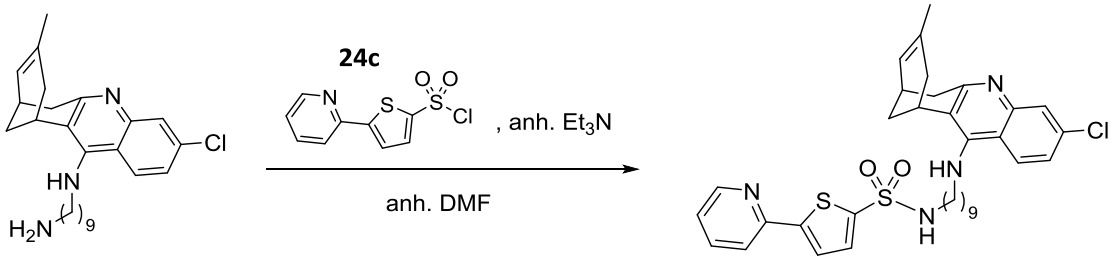

29

25c, 85%

Scheme 3.6

3.5 Pharmacological evaluation of modified rhein–huprine hybrids

3.5.1 Cholinesterases inhibitory activity

The anticholinesterase activities of the novel hybrids were evaluated by Dr. Manuela Bartolini (*Università di Bologna*). The inhibitory activity of the new hybrids, **20a-d**, **22a-e**, **23a-b** and **25a-g**, against recombinant *h*AChE and serum *h*BChE was evaluated by the method of Ellman *et al.*,[172] and compared with that of the parent racemic huprine Y, **7**, and rhein, **9**, and the lead compound of the first generation of hybrids **10**, under the same assay conditions (**Table 3.1**).

The novel hybrids have turned out to be very potent inhibitors of *h*AChE, with inhibitory activities in the low nanomolar or even subnanomolar range (0.66–17 nM, **Table 3.1**). All of them were in the same range of potencies than the previous lead **10** (IC_{50} ≈ 4 nM). Compounds **23a** and **23b** were the most potent of the series, with **23a** displaying a subnanomolar IC_{50} value.

These compounds were also potent inhibitors of *h*BChE, being the IC_{50} values of the majority of them also in the low nanomolar range (11–91 nM, **Table 3.1**), except for compounds **20a** and **20b**, which displayed IC_{50} values in the low micromolar or submicromolar range (IC_{50} = 1250 and 883 nM, respectively). Normally, huprine-derived hybrids are selective for AChE over BChE inhibition. This effect is attributed to the chlorine atom at position 3 of huprine Y, which is crucial for the inhibitory activity against *h*AChE, as it fills a hydrophobic pocket, but detrimental for the inhibitory activity against *h*BChE, due to the steric hindrance with Met437. This trend can be also observed in compounds **20a-b**, **22b,d,e**, **23a-b** and **25f**, which are clearly more potent against *h*AChE than *h*BChE (26- to 181-fold). However, compounds **20c,d**, **22a,c**, and **25a-e,g** exhibited comparable IC_{50} values for both enzymes, which may suggest that their rhein-replacing substituents play favourable interactions at the PAS of *h*BChE, thus compensating the detrimental effect of the chlorine atom of the huprine moiety at the CAS of the enzyme.

[172] G. L. Ellman, K. D. Courtney, V. Andres Jr., R. M. Featherstone. *Biochem. Pharmacol.* **1961**, *7*, 88–90.

Table 3.1. *h*AChE and *h*BChE inhibitory activities of rhein, hybrid **22b** (as free base) and the hydrochloride salts of huprine Y, the lead **10** and the new hybrids **20a-d**, **22a,c-e**, **23a,b** and **25a-g**.

Compound	*h*AChE[a] IC_{50} (nM)	*h*BChE[a] IC_{50} (nM)
20a	6.91 ± 0.77	1250 ± 130
20b	5.93 ± 0.26	883 ± 55
20c	11.6 ± 0.9	16.5 ± 1.9
20d	5.97 ± 0.93	12.7 ± 0.9
22a	7.18 ± 0.84	14.8 ± 0.7
22b	6.41 ± 0.90	70.0 ± 2.7
22c	2.15 ± 0.34	15.8 ± 1.2
22d	4.34 ± 0.42	48.5 ± 5.8
22e	2.19 ± 0.50	56.7 ± 5.9
23a	0.660 ± 0.098	44.9 ± 2.1
23b	1.11 ± 0.22	90.7 ± 4.0
25a	4.89 ± 0.36	38.8 ± 1.0
25b	5.25 ± 0.92	56.5 ± 4.4
25c	16.8 ± 2.2	15.2 ± 0.3
25d	13.3 ± 0.1	14.1 ± 1.0
25e	4.83 ± 0.71	34.8 ± 1.5
25f	2.31 ± 0.35	66.6 ± 3.7
25g	8.52 ± 0.03	11.0 ± 0.6
huprine Y	1.07 ± 0.05[b]	181 ± 15[b]
rhein	>10000[b]	17000 ± 4220[b]
10	3.60 ± 0.21[b]	620 ± 20[b]

[a] IC_{50} (nM) of human recombinant AChE and human serum BChE. Values are expressed as mean ± SEM of at least three experiments, each one performed in duplicate.
[b] Data from Ref. 158

3.5.2 BACE1 inhibitory activity

The assessment of BACE1 inhibitory activity for this new series was carried out by the group of Dr. Vincenza Andrisano (*Università di Bologna*). The inhibitory activity of the new hybrids, **20a-d**, **22a-e**, **23a-b** and **25a-g**, against recombinant *h*BACE1 was evaluated by employing Panvera peptide as substrate (**Table 3.2**). It is noteworthy to mention that for previous studies from our group, including the evaluation of the first generation of hybrids, another substrate, M-2420, was used. Problems associated with the fluorescence emission of the compounds and the substrate employed made it necessary the change of substrate and conditions of the assay.

The novel hybrids turned out to be less potent than the previous lead, **10**, with the compounds displaying IC_{50} values in the low micromolar range at best (4% – >80% inhibition at 15 μM, **Table 3.2**). The least potent compounds were **22c**, **23b** and **25a**, with percentages of inhibition lower than 10% at 15 μM. In contrast, compounds **20a**, **20b**, **25c**, and **25g** were the most potent compounds, with IC_{50} values of 3, 6, 3 and 3 μM, respectively. Comparing these values with the inhibitory activity of the lead compound **10** (IC_{50} = 120 nM),[158] it could be thought that the new hybrids do not conserve the potency of the lead, despite keeping a hydrogen bond acceptor for their interaction with the secondary pocket of BACE1. However, as mentioned above, the activity of compound **10** against *h*BACE1 was tested using a different substrate (M-2420 *versus* Panvera for the new hybrids). It is worth to say that when the lead **10** was reevaluated using Panvera substrate, an IC_{50} of 1.67 μM (**Table 3.2**) was found for this compound, i.e. a potency very close to that found for the best compounds of the novel series. In the light of these results, we can infer that the most potent compounds of this family, **20b**, **20c**, **25c**, and **25g**, have an inhibitory activity against *h*BACE1 in the same range as the lead **10**.

Table 3.2. *h*BACE1 inhibitory activities of rhein, hybrid **22b** (as free base) and the hydrochloride salts of racemic huprine Y, the lead **10** and the new hybrids **20a-d**, **22a,c-e**, **23a,b** and **25a-g**.

Compound	*h*BACE1 % inhibition[a] or IC_{50} (μM)[b]
20a	2.89 ± 0.50
20b	5.63 ± 0.01
20c	61.49 ± 0.36 %
20d	48.13 ± 0.32 %
22a	48.69 ± 5.31 %
22b	41.18 ± 3.17 %
22c	6.89 ± 0.36 %
22d	48.96 ± 0.01 %
22e	31.93 ± 0.39 %
23a	18.34 ± 3.94 %
23b	4.36 ± 0.11 %
25a	8.9 ± 0.7 %
25b	4.44 ± 0.07
25c	3.42 ± 0.18
25d	7.33 ± 1.99
25e	29.96 ± 3.4 %
25f	38.15 ± 4.44 %
25g	3.02 ± 0.03
huprine Y	14%[c,d]
rhein	na[c,e]
10	0.120 ± 0.90[c,f] 1.67[g]

[a] % inhibition at 15 μM.
[b] IC_{50} (μM) of human recombinant BACE1. Values are expressed as mean ± SEM of at least three experiments, each one performed in duplicate.
[c] Data from Ref. 158.
[d] 14% inhibition at 5 μM.
[e] Not active
[f] M-2420 as substrate.
[g] Panvera as substrate.

3.5.3 Aβ and tau antiaggregating activity

The AChE PAS binding site is well known to induce Aβ aggregation. As a consequence, dual binding site inhibitors of AChE are normally endowed with Aβ antiaggregating properties,[173] which arise from the direct blockade of the PAS or from a direct interaction with Aβ (blockade of spontaneous Aβ aggregation). In the latter case, spontaneous amyloid aggregation takes place by alignment of complementary β-sheets, forming fibrils.[174] The presence of aromatic planar moieties in the inhibitors can block this self-aggregation by interfering in the β-sheets alignment.

The evaluation of the inhibitory activity of the novel hybrids against the self-aggregation of $A\beta_{42}$ peptide and tau protein in intact *E. coli* cells was performed by myself under the supervision of Dr. Raimon Sabaté (*Universitat de Bacelona*). This assay consists of the overexpression of amyloid-prone proteins in bacteria and the measurement of its aggregation by a fluorimetric assay. The basis and the methodology of this assay will be better explained in Chapter **6** of this Thesis.

This new family of hybrids displayed in general good inhibitory potencies against $A\beta_{42}$ and tau self-aggregation (**Table 3.3**). Only two compounds, **22d** and **22e**, were found inactive whereas hybrids **20d**, **22b** and **23b** displayed moderate antiaggregating potencies against one or two of the studied proteins. The rest or the compounds were found to be potent inhibitors of the aggregation of both $A\beta_{42}$ and tau, all of them being clearly more potent than the parent compounds,racemic huprine, **7**, and rhein, **9**, and in the same order of potencies (against $A\beta_{42}$ aggregation) or slightly more potent (against tau aggregation) than the lead **10**. The fact that the majority of the new hybrids presented the same order of potencies against both proteins supports the existence of common mechanisms behind the aggregation of different amyloid-prone proteins, and the possibility of finding a common treatment against different amyloidogenic diseases.[174] Overall, the most potent antiaggregating agents of this family were **25b, 25c** and **25g**, with IC_{50} values that must be in the low micromolar range. The presence in these three compounds of several aromatic moieties with extended π-conjugated systems supports the idea that these systems play an important role in blocking the aggregation of these amyloidogenic proteins.

[173]E. Viayna, R. Sabaté, D. Muñoz-Torrero. *Curr. Top. Med. Chem.* **2013**, *13*, 1820–1842.
[174]S. Pouplana, A. Espargaró, C. Galdeano, E. Viayna, I. Sola, S. Ventura, D. Muñoz-Torrero, R. Sabate. *Curr. Med. Chem*. **2014**, *21*, 1152–1159.

.**Table 3.3.** $A\beta_{42}$ and tau antiaggregating activities of rhein, hybrid **22b** (as free base) and the hydrochloride salts of racemic huprine Y, the lead **10** and the new hybrids **20a-d**, **22a,c-e**, **23a,b** and **25a-g**.

Compound	$A\beta_{42}$ aggregation[a] (% inh. at 10 μM)	Tau aggregation[a] (% inh. at 10 μM)
20a	50.6 ± 1.1	47.1 ± 1.9
20b	45.5 ± 1.2	46.5 ± 1.5
20c	49.3 ± 1.3	43.6 ± 2.7
20d	28.8 ± 1.5	37.6 ± 1.3
22a	43.7 ± 2.6	48.2 ± 2.6
22b	20.2 ± 3.2	38.9 ± 1.9
22c	47.2 ± 2.6	38.3 ± 2.0
22d	na[b]	7.0 ± 3.2
22e	na[b]	5.2 ± 2.8
23a	44.8 ± 2.2	46.6 ± 3.0
23b	24.8 ± 3.3	45.0 ± 1.9
25a	41.9 ± 4.2	49.6 ± 1.5
25b	55.2 ± 2.8	51.9 ± 1.4
25c	52.5 ± 2.4	53.5 ± 2.2
25d	51.2 ± 3.4	48.0 ± 3.5
25e	49.4 ± 2.0	52.1 ± 1.6
25f	49.2 ± 1.9	46.6 ± 1.5
25g	52.8 ± 2.4	56.0 ± 3.1
huprine Y	na[b,c]	na[b,c]
rhein	49.9 ± 6.4[c]	40.8 ± 0.7[c]
10	47.9 ± 14.5[c]	29.6 ± 8.5[c]

[a] % inhibition at 10 μM in intact *E. coli* cells. Values are expressed as mean ± SEM of at least three independent experiments.
[b] Not active.
[c] Data from Ref. 158.

3.5.4 Antioxidant properties

As previously discussed in sections **1.2.5** and **1.2.7**, oxidative stress seems to play a pivotal role in the pathology of AD. Free radical formation is caused, amongst other reasons, by a dyshomeostasis at the CNS of some biometals, mainly iron, copper and zinc, which participate in metal ion-catalysed radical formation. Thus, both radical scavenging and metal-chelating properties are desired biological activities that are pursued for MTDLs, to better protect the brain from oxidative stress. In this context, this new family of compounds was evaluated for both properties, as some of the scaffolds were selected by their potential to be metal chelators.

3.5.4.1 Radical scavenging activity

The evaluation of the radical scavenging properties was assessed by the group of Prof. Michael Decker (*University of Würzburg*) in the frame of a collaboration with this group and that of Prof. Maria Laura Bolognesi (*Università di Bologna*) by a spectrophotometric assay using DPPH as substrate and ascorbic acid as a reference. The majority of the compounds exhibited weak radical scavenging properties, with activities in the range 31–79% at 500 μM (**Table 3.4**), whereas compound **22b** was found to be inactive. The only compound with moderate radical scavenging properties was **23b** (IC_{50} = 91 μM). Surprisingly, compound **25g**, bearing a phenolic moiety was found to be a weak radical scavenger (54% scavenging activity at 500 μM). Evaluation of compounds **20a-d** and **22d-e** is still pending.

Table 3.4. Radical scavenging activities of hybrid **22b** (as free base) and the hydrochloride salts of hybrids **20a-d**, **22a,c-e**, **23a,b** and **25a-g**.

Compound	% scavenging[a] or EC_{50} (μM)[b]
20a	nd[d]
20b	nd[d]
20c	nd[d]
20d	nd[d]
22a	52%
22b	na[d]
22c	36%
22d	nd[d]
22e	nd[d]
23a	31%
23b	91.15
25a	51%
25b	58%
25c	69%
25d	53%
25e	79%
25f	67%
25g	54%

[a] % DPPH radical scavenging activity at 500 μM.
[b] EC_{50} (μM) of radical scavenging activity. Values are the mean of at least three independent experiments.
[c] nd: not determined.
[d] na: not active.

3.5.4.2 Cu^{2+} chelating activity

As previously mentioned, copper ions are one of the most important metal ions related to AD pathology. The evaluation of the Cu^{2+} chelating properties of the novel hybrids was assessed by the group of Prof. Michael Decker (*University of Würzburg*) in the frame of a collaboration with this group and that of Prof. Maria Laura Bolognesi (Università di Bologna) by a spectrophotometric assay using pyrocatechol violet (PV) as substrate and EDTA as a reference.

Overall, the majority of the compounds presented good copper chelating properties. Hybrids **23a**, **23b**, **25f**, and **25g** were the most potent, with chelating activities (% of chelated Cu^{2+}) over 50% at all compound:Cu^{2+} ratios evaluated (or close to 50% in **23b** and **25g** at 0.5:1 ratio). Compounds **22b**, **22c**, **25a**, **25d**, and **25e** were found to be moderately potent chelators with activities over 50% only at high ratios (5:1 to 2:1). Surprisingly, **22b** and **25e** were able to chelate copper at a 2:1 ratio better than at a 5:1 ratio. Finally, hybrids **22a**, **25b**, and **25c** showed weak chelating activities, as their ability to chelate cupper ions was below 50% at all ratios evaluated.

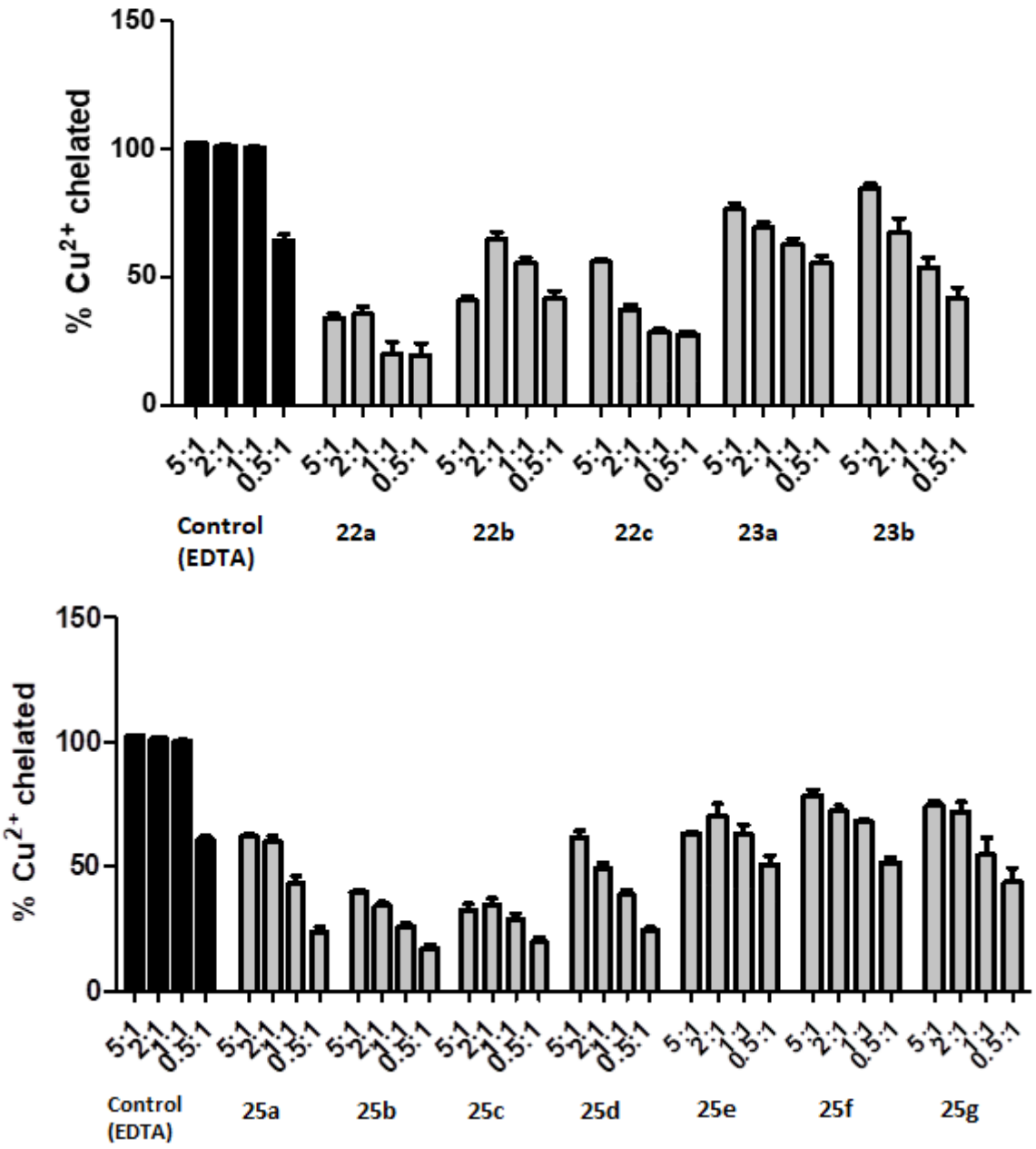

Figure 3.8. Copper (II) chelation properties of hybrid **22b** (as free base) and the hydrochloride salts of hybrids **22a,c**, **23a,b** and **25a-g** at different compound:Cu^{2+} ratios. Values are expressed as means ± SEM of at least three independent assays and referred to control samples with EDTA.

3.5.5 *In vitro* BBB permeation assay

In order to demonstrate the ability of the hybrids to cross the BBB and get access to the CNS, which is obviously a necessary condition for AD drugs, Dr. Belén Pérez (*Universitat Autònoma de Barcelona*) performed a PAMPA (Parallel Artificial Membrane Permeability Assay)-BBB assay, a well-established *in vitro* test that uses an artificial membrane model.[175] Previous results from *in vitro*, *ex vivo* and *in vivo* studies have shown that huprine Y and related hybrids can readily cross the BBB, leading to central effects.[158,176,177] The starting point for the design of the new hybrids described in this Chapter was the replacement of the large lipophilic rhein moiety of first and second generation rhein–huprine hybrids by smaller less lipophilic aromatic systems, leading to more druglike hybrids. To check whether these compounds could cross the BBB, their *in vitro* permeability (P_e) was determined and compared with that of huprine Y, **7**, rhein, **9**, and the lead **10**. Regarding the limits established for BBB penetration,[173] compounds with P_e (10^{-6} cm s^{-1}) > 5.2 would be expected to have high BBB penetration (CNS+), compounds with P_e (10^{-6} cm s^{-1}) < 1.9 would have low BBB penetration (CNS–) and compounds with 5.2 > P_e (10^{-6} cm s^{-1}) > 1.9 would present an uncertain BBB permeation (CNS±).

The majority of the new hybrids were predicted to have high BBB penetration, which should enable them to reach their multiple CNS targets (**Table 3.5**). Only compounds **22b** and **25b** were predicted to have uncertain permeation through the BBB whereas compounds **25c** and **25d** were predicted to have low BBB penetration.

---

[175]L. Di, E. Kerns, K. Fan, O. McConnell, G. Carter. *Eur. J. Med. Chem.* **2003**, *38*, 223–232.

[176]C. Galdeano, E. Viayna, I. Sola, X. Formosa, P. Camps, A. Badia, M. V. Clos, J. Relat, M. Ratia, M. Bartolini, F. Mancini, V. Andrisano, M. Salmona, C. Minguillón, G. C. González-Muñoz, M. I. Rodríguez-Franco, A. Bidon-Chanal, F. J. Luque, D. Muñoz-Torrero. *J. Med. Chem.* **2012**, *55*, 661–669.

[177]M. Hedberg, M. V. Clos, M. Ratia, D. Gonzalez, C. U. Lithner, P. Camps, D. Muñoz-Torrero, A. Badia, L. Giménez-Llort, A. Nordberg. *Neurodegener. Dis.* **2010**, *7*, 379–388.

Table 3.5. Permeability results for the PAMPA-BBB assay of rhein, hybrid **22b** (as free base) and the hydrochloride salts of huprine Y, the lead **10** and the new hybrids **20a-d**, **22a,c-e**, **23a-b** and **25a-g**.

Compound	P_e (10^{-6} cm s^{-1})[a]	Prediction
20a	9.2 ± 1.2	CNS+
20b	6.25 ± 0.8	CNS+
20c	7.4 ± 0.3	CNS+
20d	16.5 ± 1.1	CNS+
22a	8.5 ± 0.2	CNS+
22b	3.9 ± 0.2	CNS±
22c	11.6 ± 1.9	CNS+
22d	12.9 ± 0.9	CNS+
22e	5.9 ± 0.2	CNS+
23a	15.2 ± 0.8	CNS+
23b	11.3 ± 0.9	CNS+
25a	9.6 ± 0.3	CNS+
25b	2.6 ± 0.1	CNS±
25c	0.9 ± 0.01	CNS–
25d	1.7 ± 0.3	CNS–
25e	7.9 ± 0.3	CNS+
25f	12.3 ± 0.4	CNS+
25g	5.8 ± 0.03	CNS+
huprine Y	23.8 ± 2.7	CNS+
rhein	2.7 ± 0.1	CNS±
10	21.5 ± 0.7	CNS+

[a] Permeability values from the PAMPA-BBB assay. Values are expressed as mean ± SEM of three independent experiments.

3.5.6 Toxicological studies

Although tacrine has been proven to exert toxic side effects,[90] previous *in vivo* studies in our group have demonstrated that huprine and huprine-related hybrids do not present relevant toxicity.[158,167] In order to assess potential toxicity issues of this new family of compounds, two different assays were performed, a neurotoxicity assay in HT-22 neuronal cells and an acute toxicity assay in a zebra fish model.

3.5.6.1 Neurotoxicity

The evaluation of the neurotoxicity of these modified rhein–huprine hybrids was performed by the group of Prof. Michael Decker (*University of Würzburg*). The viability of HT-22 neuronal cells in the presence of the new hybrids was assessed through the MTT assay. Overall, this new series of hybrids were devoid of serious neurotoxic effects (**Figure 3.9**), as there was not a significant loss of cell viability at 25 μM in any of the cases. Only compounds **22a**, **22b** and **23b** were slightly neurotoxic at this concentration, albeit maintaining cell viabilities close to 80% in the three cases. The rest of compounds did not display neurotoxic effects at 25 μM. Evaluation of compounds **20a-d** and **22d-e** is still pending.

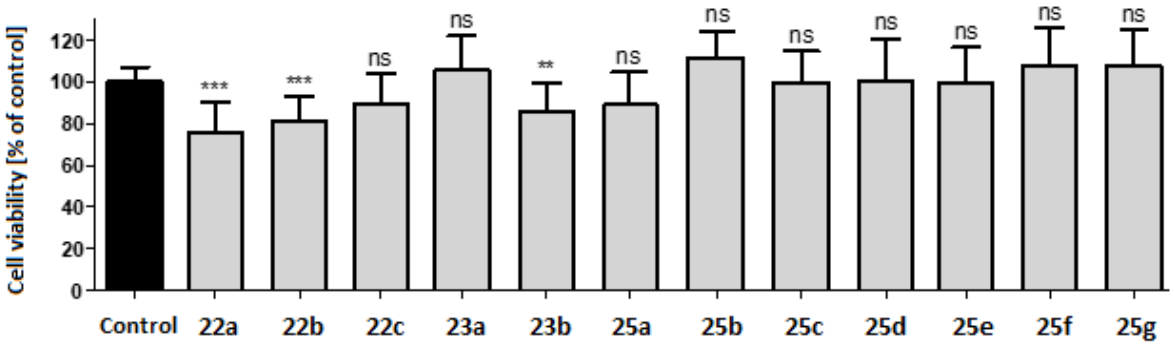

Figure 3.9. Cell viability of HT-22 neuronal cells in the presence of hybrid **22b** (as free base) and the hydrochloride salts of hybrids **22a,c**, **23a,b** and **25a-g**, at 25 μM. Results are shown as means ± SD of three independent experiments, each performed in sextuplicate, and referred to untreated control cells. Levels of significance: *p < 0.01; **p < 0.005; ***p < 0.001, ns: not significant.

3.5.6.2 Toxicity in a zebra fish model

Toxicological studies in zebra fish embryos for this new series of hybrids were performed by the group of Prof. Jesús Gómez and Dr. Marta Barenys (*Universitat de Barcelona*), following the OECD Guideline for Fish Embryo Acute Toxicity (FET) Test. The toxicity of the new hybrids was evaluated and compared with that of the parent huprine Y in the same assay conditions (**Table 3.6**). In some cases, precipitation of the compounds at high concentrations made it difficult to measure the LD_{50} (letal concentration killing 50% individuals), but a calculated LD_{50} was extrapolated from the results obtained at lower concentrations. In these cases, the NOAEC (no adverse effect concentration) was the maximum soluble concentration.

Amongst the compounds evaluated, hybrids **20a-d**, **25a** and **25c** did not elicit significant toxicity, presenting LD_{50} values in the high micromolar range (>100 μM for **20a**, **20b**, **20d** and **25c**, 98.1 μM for **25a** and 40 μM for **20c**). In contrast, compounds **22a**, **22d**, and **22e** were found to be toxic at low concentrations of around 1–2 μM (LD_{50} = 2.3, 0.9, and 1 μM, respectively). Finally, hybrids **25e** and **25g** were found to be moderately toxic with LD_{50} values of 18.6 and >10 μM, respectively, i.e. in the same range of toxicity than the parent huprine (LD_{50} = 20.9 μM).

Table 3.6. Toxicology results in zebra fish model of hybrid **22b** (as free base) and the hydrochloride salts of huprine Y and the new hybrids **20a-d**, **22a,c-e**, **23a-b** and **25a-g**.

Compound	LC_{50} (μM)[a]	NOAEC (μM)[b]
20a	>100[c]	25[d]
20b	>100[c]	25[d]
20c	40[c]	25[d]
20d	>100[c]	25[d]
22a	2.3	1.25
22b	nd[e]	nd[e]
22c	nd[e]	nd[e]
22d	0.9	0.625
22e	1	0.625
23a	nd[e]	nd[e]
23b	nd[e]	nd[e]
25a	98.1[c]	12.5[d]
25b	nd[e]	nd[e]
25c	>100[c]	12.5[d]
25d	nd[e]	nd[e]
25e	18.6[c]	10[d]
25f	nd[e]	nd[e]
25g	>10[c]	5[d]
huprine Y	20.9	12.5

[a] LC_{50} in zebra fish embryos. Values are the result of at least three independent experiments.
[b] No adverse effect concentration.
[c] Calculated LC_{50}
[d] Maximum soluble concentration
[e] nd: not determined

CHAPTER 4

Huprine–based BACE1 multisite inhibitors

4.1 First generation rhein–huprine hybrids: further computational studies within BACE1

The critical role of BACE1 in the formation of neurotoxic Aβ in the brain, makes it an important and attractive target in the search of an efficacious treatment of AD. The first family of rhein–huprine hybrids (sections **1.6** and **3.1**), previously synthesised in our group, displayed a very interesting multitarget profile, including a surprisingly potent inhibitory potency against BACE1. The initial molecular modelling studies of the interaction of these compounds with AChE and BACE1 were made with compound **17** (**Figure 4.1**), which was not one of the most potent of the series but presented a more rigid structure, making it easier to be studied by computational techniques. However, the lead of the family was compound **10** (**Figure 4.1**), which also presented the best potency against BACE1 (IC_{50} = 120 nM). For this reason, the binding mode of compound **10** within BACE1 was later studied as part of the PhD Thesis of Dr. Ornella Di Pietro, in order to shed light on the possible interactions accounting for such inhibitory potency.

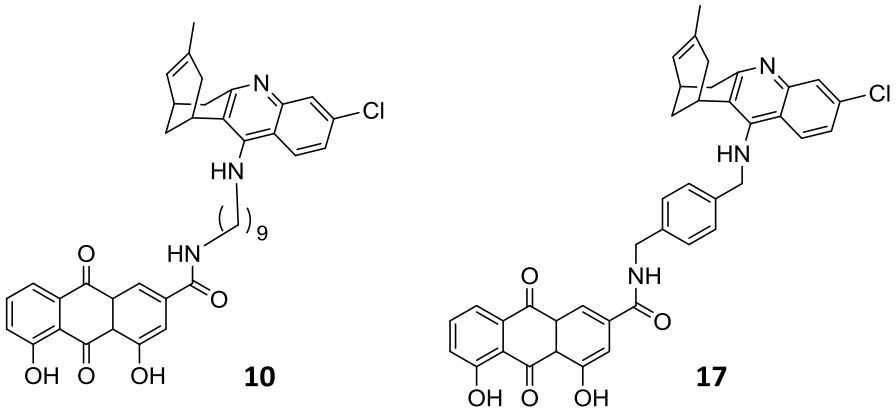

Figure 4.1. Chemical structures of first generation rhein–huprine hybrids **10** and **17**.

BACE1 active site is an open, long cleft formed around the catalytic dyad (Asp32 and Asp228). The binding site cleft is partially covered by a highly flexible antiparallel hairpin-loop, known as the *flap*.[178,179] Examination of crystal structures of BACE1 revealed that there was no appropriate binding site large enough to accommodate compound **10**. Nonetheless, the fact that both parent compounds, huprine and rhein, were almost inactive (14% inhibition at 5 μM for huprine, rhein was inactive), suggested the idea that compound **10** might perform a multisite binding within BACE1. Indeed, the inhibitory potencies of the family are highly dependent on the length of the tether, which suggests

[178]R. Friedman, A. Caflisch. *Proteins* **2010**, *78*, 1575–1582.
[179]A. A. Gorfe, A. Caflisch. *Structure* **2005**, *13*, 1487–1498.

that the precise spatial arrangement in the BACE1 cleft afforded by the nonamethylenic tether of compound **10** triggers a highly synergistic cooperative effect. [171]

As discussed in section **3.1**, the computational studies performed in the PhD Thesis of Dr. Ornella Di Pietro predicted the interaction of the protonated aminoquinoline ring of the huprine moiety of the lead **10** with the catalytic dyad. Given the strong dependency of the inhibitory potency on the linker length, it was hypothesised that the rhein moiety of **10** was capable of filling a peripheral "floppy" pocket in the region delimited by the high flexible loops formed by residues 8–14, 154–169, and 307–318. The analysis of the protein dynamics, together with studies of pocket druggability, allowed us to detect the transient formation of a secondary binding site at the edge of the catalytic cleft, delimited by the previously mentioned loops. This secondary floppy pocket apparently enabled the binding of multisite inhibitors targeting catalytic and secondary sites (**Figure 4.2**). [171]

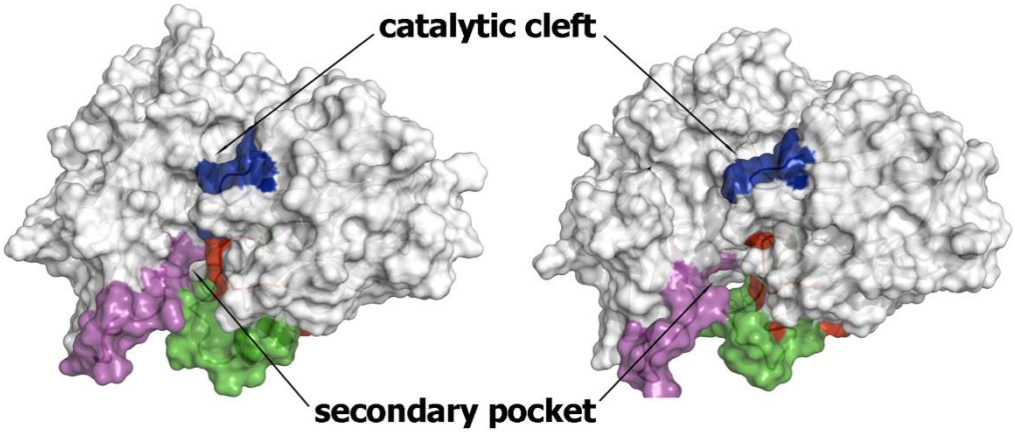

Figure 4.2. Representative snapshots of BACE1 with the loop 8–14 in the *out* conformational state. The flap region of the active site is shown in blue, and the loops defined by residues 8–14, 154–169, and 307–318 are shown in red, green and magenta, respectively. (Image source: O. Di Pietro, J. Juárez-Jiménez, D. Muñoz-Torrero, C. A. Laughton, F. J. Luque. *PLoS ONE* **2017**, *12*, e0190327).

Molecular dynamics (MD) simulations of compound **10** bound to BACE1 were then performed to confirm this hypothesis. It was found that the huprine moiety was tightly bound to the active site in all cases. Apart from the strong electrostatic stabilization arising from the hydrogen bond interaction between the protonated aminoquinoline system and the catalytic dyad (Asp32), the aminoquinoline system filled a hydrophobic pocket formed by residues Leu30, Tyr71, Phe108, Trp115 and Ile118. Finally, the chlorine atom filled a subpocket formed by the side chains of Tyr198 and Ile226 (**Figure 4.3**). On the other hand, the hydroxyanthraquinone moiety of rhein adopted a well-defined binding mode in the secondary cavity (**Figure 4.3**). As mentioned previously in section **3.3**, the most relevant

interaction was the hydrogen bond between the carbonyl unit of rhein and the guanidinium group in Arg307, which in turn formed a salt bridge interaction with Glu339. Moreover, the carbonyl located in the opposite edge of rhein formed an electrostatic stabilization with the main chain NH group of Glu310, which was in turn stabilized by the interaction between the side chains of Glu310 and Ser10, thus favouring the binding of rhein to the secondary pocket. Finally, this pattern of interactions was not affected by the specific arrangement imposed to the amide group in the tether in any of the simulations.[171]

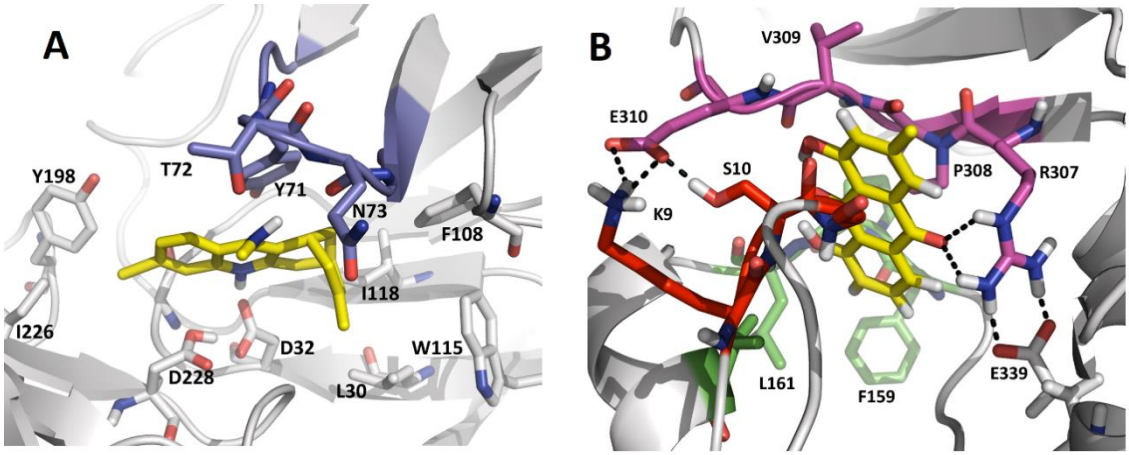

Figure 4.3. A) Representative view of the binding mode of the huprine moiety of compound **10**. The residues in the flap loop are shown in blue. For the sake of clarity, the methylenic chain and the rhein moiety have been deleted. **B)** Representative view of the binding mode of the rhein moiety of compound **10**. Residues in the loops 8–14, 154–169, and 307–318 are shown in red, green and magenta, respectively. For the sake of clarity, the methylenic chain and the huprine moiety have been deleted. (Image source: O. Di Pietro, J. Juárez-Jiménez, D. Muñoz- Torrero, C. A. Laughton, F. J. Luque. *PLoS ONE* **2017**, *12*, e0190327).

4.2 Virtual screening over the transient secondary pocket of BACE1

In the light of the results derived from the molecular dynamics simulations of the lead **10** within BACE1, a virtual screening campaign over the freshly discovered secondary pocket of BACE1 was performed by the group of Prof. F. Javier Luque (*Universitat de Barcelona*). An initial database of 283130 compounds, coming from the ZINC database, was prepared and screened over two protein structures from BACE1 (namely BACE1_state1 and BACE1_state2), both derived from the previous molecular dynamics simulations. These two structures differed in the orientation adopted by the side chain of Arg307 at the peripheral site of BACE1.

Virtual screening was performed in two steps by using the Glide module of the Schrödinger suite:

1. **HTVS** (High Throughput Virtual Screening): a preliminary screening with a low precision docking algorithm where only solutions/poses with GScore values < −7.00 kcal/mol were taken.
2. **XP** (Extra Precision): a second more accurate screening by using the Extra Precision algorithm. In this case, only MD solutions/poses with GScore values < −6.50 kcal/mol were taken.

After performing both steps of the virtual screening, 94 solutions (14% of the entire database) consistent with all the requirements were found for BACE1_state1 and 115 solutions (34% of the entire database) were found for BACE1_state2 (**Table 4.1**). These results were then filtered by visual inspection of the docking solutions, selecting 18 potential candidates for BACE1_state1 and 70 potential candidates for BACE1_state2.

Table 4.1. Statistics for the virtual screening over the secondary pocket of BACE1.

		HTVS		XP	
Model	Starting Number	N of solutions after docking	N of solutions after filtering*	N of solutions after docking	N of solutions after filtering**
BACE_state1	283130	200886	550 (27%)	687	94 (14%)
BACE_state2	283130	121461	343 (28%)	340	115 (34%)

* only MD solutions/poses with GScore values more negatives than −7.00 kcal/mol.

** only MD solutions/poses with GScore values more negatives than −6.50 kcal/mol.

4.3 Design of huprine–based BACE1 multisite inhibitors

In the light of the results of the virtual screening campaign, the docking solutions for the potential hits were checked, in order to analyse their possible interactions with the secondary pocket of BACE1, and it was found that only few scaffolds might perform additional interactions with the protein structure. These scaffolds were repeated several times within the putative hits, with different substituents that did not play a role for the possible binding at the secondary pocket of BACE1. After analysing the most repeated scaffolds, six structures were selected, taking into account the number of potential additional interactions with BACE1 and their synthetic or commercial accessibility (**Figure 4.4**).

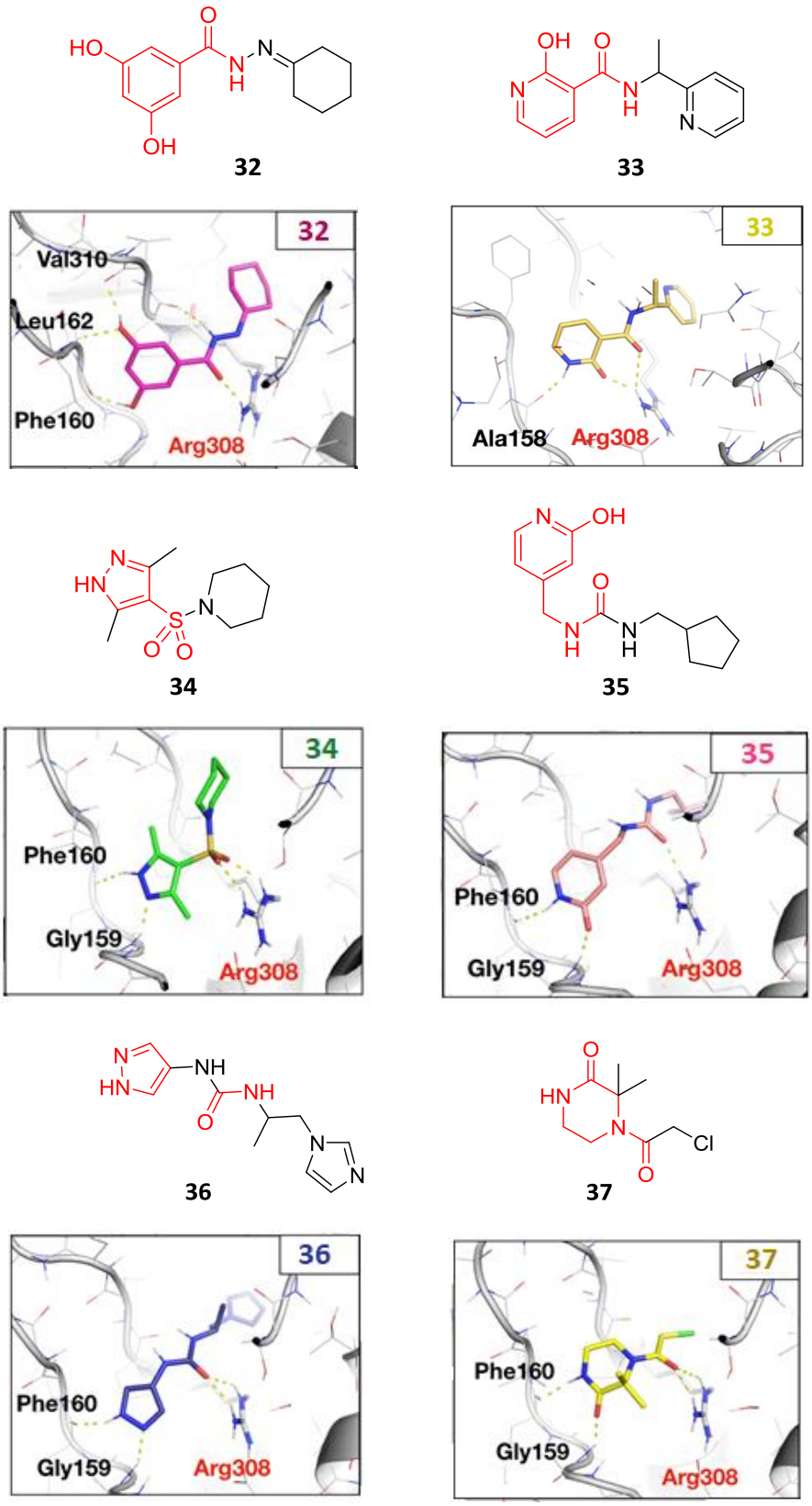

Figure 4.4. Representative solutions of the virtual screening for the six selected compounds and their docking images with the potential interactions with the secondary pocket of BACE1. The relevant scaffolds for each structure are marked in red.

On the basis of these results, we envisaged the synthesis of a new family of huprine-based hybrids that might exhibit a dual site binding within BACE1, using for this purpose the structures of the hits identified by virtual screening. The distance between the catalytic pocket occupied by the huprine moiety and the transient secondary pocket of BACE1 is predicted to be of 10 Å, which is consistent with a tether of 8–9 carbon atoms. As a consequence, the general structures of this new family of hybrids (general structures **II** and **III**, **Figure 4.5**) comprise the huprine connected to the selected structures of the virtual screening hits (VSH) through an octamethylenic or nonamethylenic tether, to enable the desired dual site binding within BACE1.

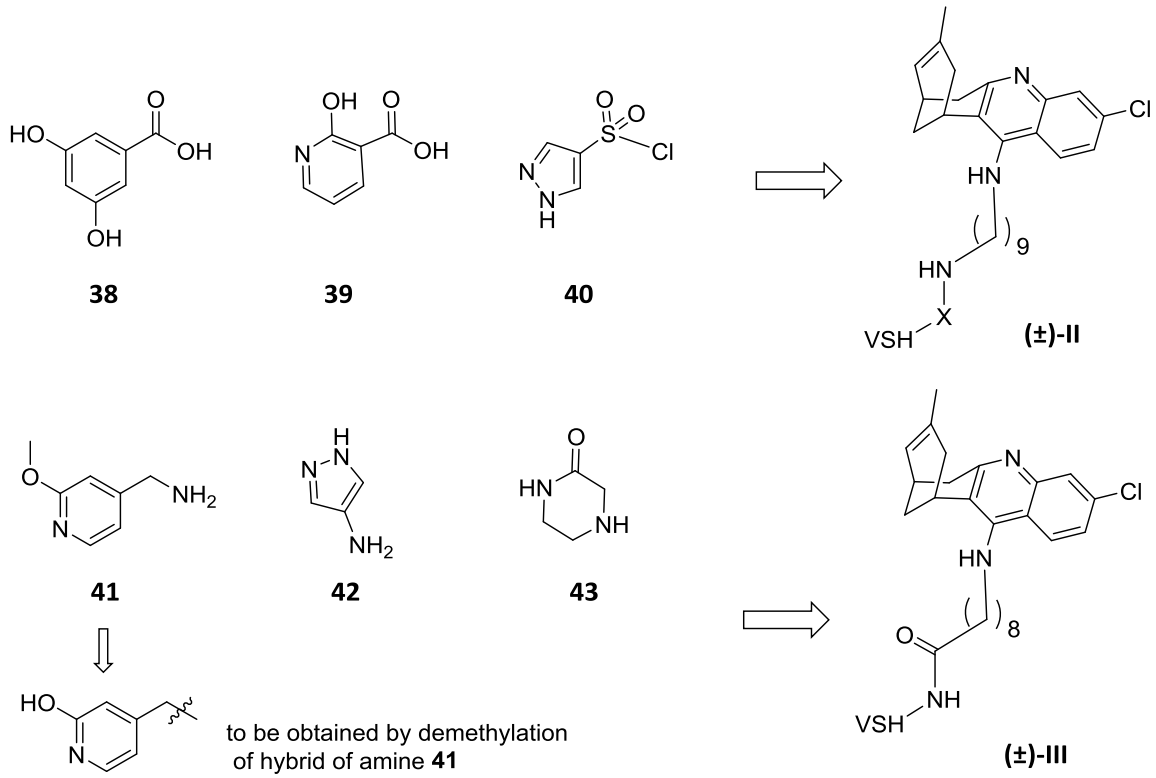

Figure 4.5. Parent compounds with the structures identified from the virtual screening campaign and general structures of the novel family of hybrids.

These novel hybrids were expected to be dual site inhibitors of BACE1, as they were designed specifically for this purpose, thus trying to mimic or even improve the BACE1 inhibitory potency of compound **10.** We expected them to feature a dual site inhibition of AChE, as well, with the huprine moiety being placed at the CAS, at the bottom of the active site gorge, and the VSH scaffolds interacting with the PAS of the enzyme, at the mouth of the gorge. Some of them might also exhibit additionally radical scavenging or metal chelating properties, imparted by the structures of some VSH scaffolds (presence of phenolic groups, metal chelating groups). Finally, these compounds were also expected to display Aβ and tau antiaggregating properties, as found in several classes of huprine-based hybrids developed in our group.

4.4 Synthesis of the huprine-based BACE1 multisite inhibitors

For the synthesis of these compounds, we first prepared the intermediate cyanononylhuprine **28** by alkylation of huprine Y with 9-bromononanenitrile, **27**, in the presence of KOH in DMSO at r. t. overnight (73% yield), as described in section **3.4** (**Scheme 4.1**).

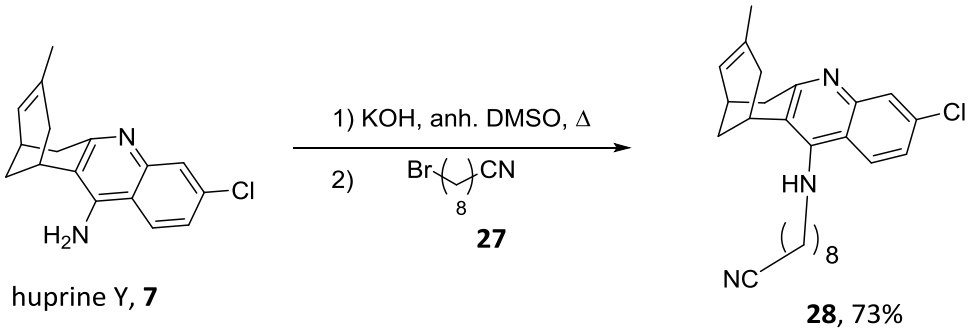

Scheme 4.1

Then, for hybrids with general structure **(±)-II**, nitrile **28** was reduced by treatment with $LiAlH_4$ in Et_2O at r. t. overnight, to afford the corresponding aminononylhuprine, **29**, in a very good yield (96%) without the need of any purification, as described in section **3.4** (**Scheme 4.2**).

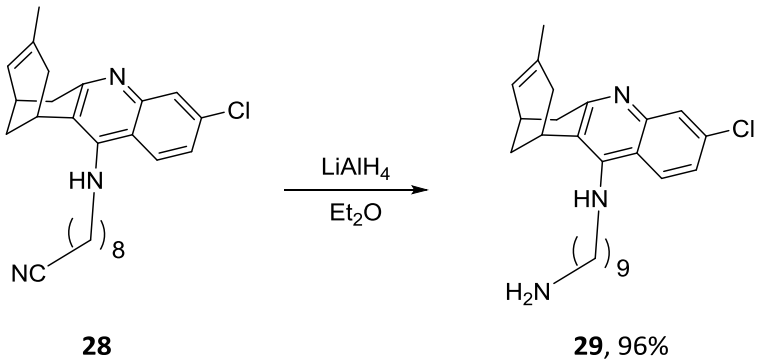

Scheme 4.2

Final amide coupling reaction between carboxylic acids **38** or **39** and the primary amine **29** was performed in the presence of EDC, HOBt, and Et_3N in a mixture of EtOAc / DMF at r. t. overnight, to afford the target hybrids **44** and **45** in moderate yields (63% and 64%, respectively, **Scheme 4.3**), after silica gel column chromatography purification. Compound **45** should be in equilibrium with its tautomeric pyridone form. However, in this case the hydroxypyridine form will very likely be predominant due to stabilization by intramolecular hydrogen bonding with the amide carbonyl group.

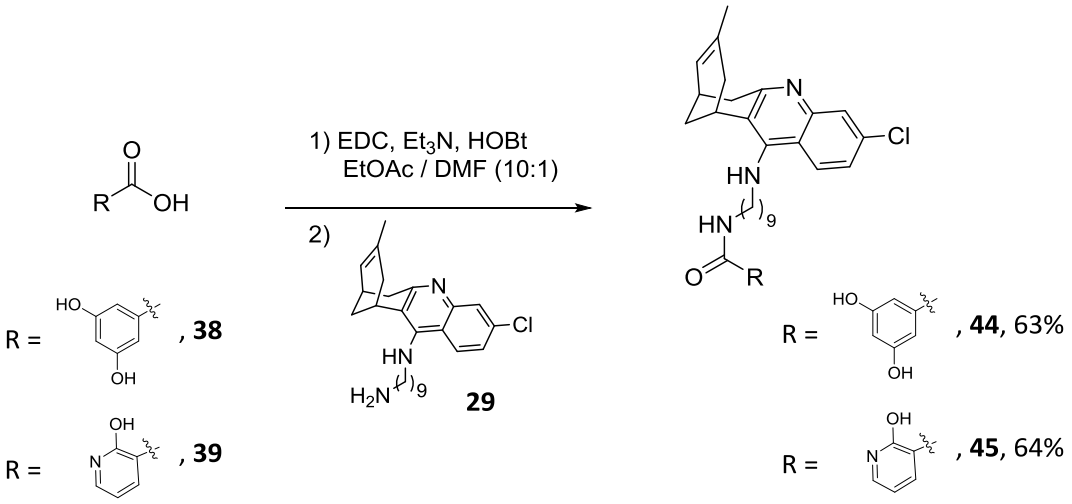

Scheme 4.3

In an analogous way as for compound **25c** (section **3.4**), hybrid **46** was obtained by coupling between the commercially available sulphonyl chloride **40** and the aminononylhuprine **29** in the presence of Et_3N in DMF in excellent yield (96%, **Scheme 4.4**), after silica gel column chromatography purification.

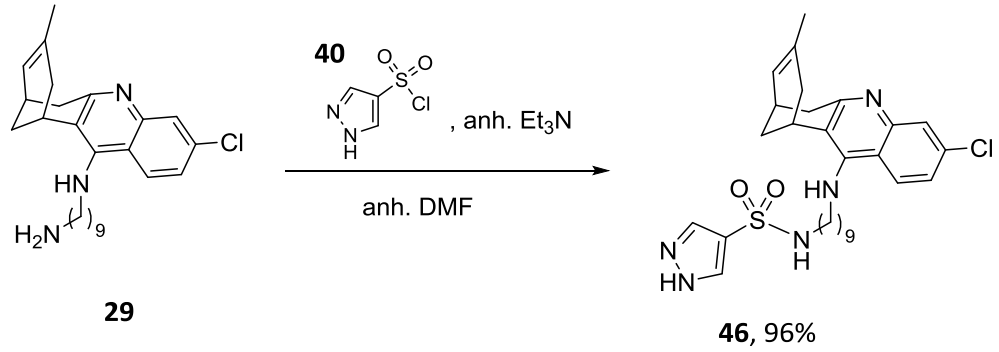

Scheme 4.4

For compounds with general structure **(±)-III**, nitrile intermediate **28** was hydrolysed in basic conditions to the corresponding carboxylic acid, **47**, finally isolated as the corresponding quinoline hydrochloride salt, which was used in the following step without further purification (**Scheme 4.5**).

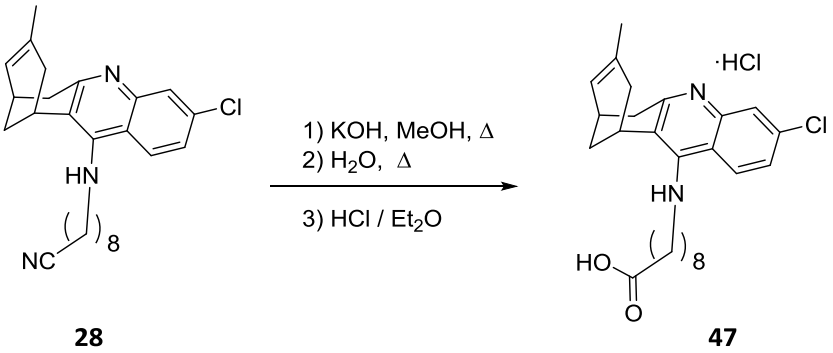

28 **47**

Scheme 4.5

Amide coupling between crude carboxylic acid **47** and amines **41**–**43**, in the presence of EDC, HOBt, and Et_3N in a mixture of EtOAc / DMF at r. t. overnight, led to the target hybrids **48**–**50** in moderate to good yields (47–74%, **Scheme 4.6**), after silica gel column chromatography purification.

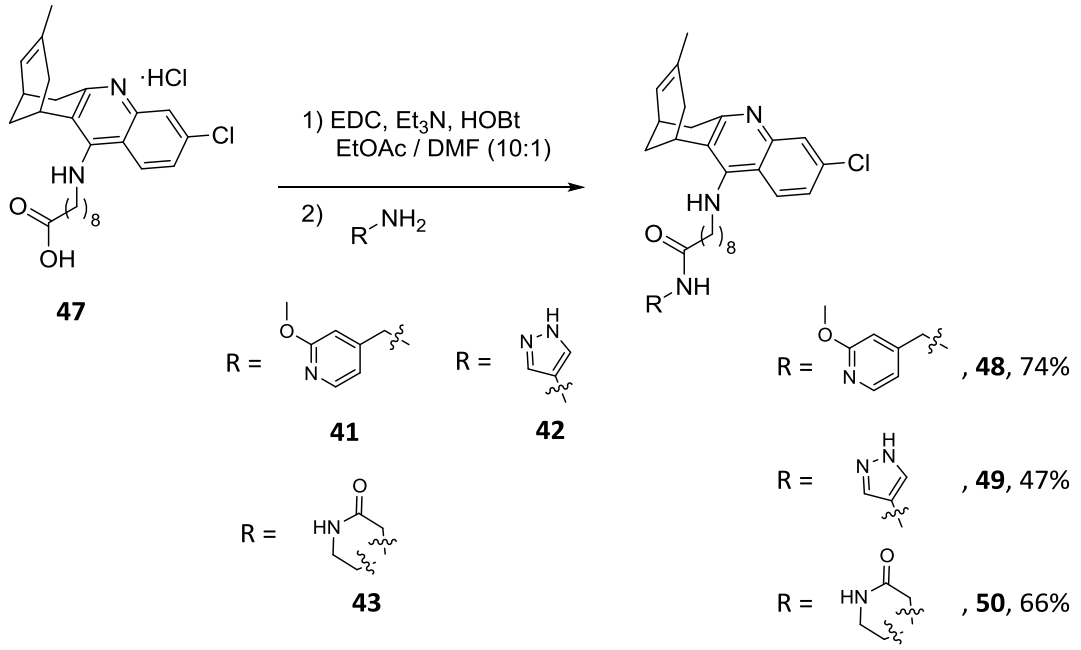

Scheme 4.6

Finally, hybrid **51**, which will be in equilibrium with the corresponding pyridone, being the latter the predominant form, was obtained by demethylation of hybrid **48** upon treatment with LiCl and *p*TSA in DMF at 120 °C for 30 min, in moderate yield (54%, **Scheme 4.7**).

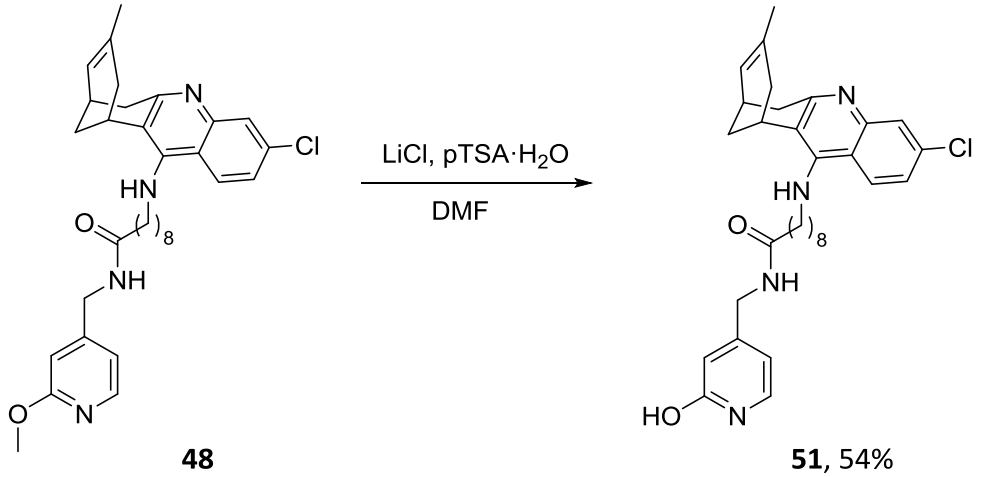

48 **51**, 54%

Scheme 4.7

4.5 Biological characterization of huprine–based BACE1 multisite inhibitors

4.5.1 Cholinesterases inhibitory activity

The anticholinesterase activities were evaluated by Dr. Manuela Bartolini (*Università di Bologna*). The inhibitory activity of the new hybrids, **44–46** and **48–51** against recombinant *h*AChE and serum *h*BChE was evaluated by the method of Ellman *et al.*,[172] and compared with that of the parent racemic huprine Y and the lead rhein–huprine hybrid **10** as a reference huprine-based hybrid compound under the same assay conditions (**Table 4.2**).

These new hybrids resulted to be highly potent inhibitors of *h*AChE, with IC_{50} values in the low nanomolar or subnanomolar range (0.41–2.57 nM, **Table 4.2**). All of them were slightly more potent than the reference compound **10** (IC_{50} ≈ 4 nM), which may indicate that the new scaffolds identified by virtual screening, which are attached to the alkylhuprine moiety, are better accommodated at the PAS of the enzyme than the rhein moiety of compound **10**. Compounds **50** and **51** were the most potent of the series, both displaying IC_{50} values in the subnanomolar range (IC_{50} = 0.41 and 0.62 nM, respectively), and being around 2-fold more potent than the parent huprine Y.

Table 4.2. *h*AChE and *h*BChE inhibitory activities of hybrid **48** (as free base) and the hydrochloride salts of huprine Y, compound **10** and the new hybrids **44–46**, and **49–51**.

Compound	*h*AChE[a] IC_{50} (nM)	*h*BChE[a] IC_{50} (nM)
44	2.57 ± 0.20	43.0 ± 2.7
45	1.82 ± 0.13	31.9 ± 1.4
46	2.40 ± 0.25	50.3 ± 2.6
48	1.25 ± 0.19	88.5 ± 5.4
49	2.39 ± 0.84	64.0 ± 0.9
50	0.412 ± 0.022	74.8 ± 2.5
51	0.625 ± 0.088	75.8 ± 3.2
huprine Y	1.07 ± 0.05[b]	181 ± 15[b]
10	3.60 ± 0.21[b]	620 ± 20[b]

[a] IC_{50} (nM) of human recombinant AChE and human serum BChE. Values are expressed as mean ± SEM of at least three experiments, each one performed in duplicate.
[b] Data from Ref. 158

These compounds turned out to be also potent inhibitors of *h*BChE, with all of them presenting inhibitory potencies in the nanomolar range (32–88 nM, **Table 4.2**), even though they were selective for AChE over BChE (17 to 181-fold). As mentioned in section **3.5.1**, this fact is due to the presence of a chlorine atom at position 3 of the huprine Y moiety, which is crucial for the inhibitory activity against *h*AChE but detrimental for the inhibitory activity against *h*BChE. In every case, all these new compounds are clearly more potent *h*BChE inhibitors than the parent huprine Y and the reference hybrid compound **10**, thus exhibiting a more favourable dual *h*AChE / *h*BChE inhibitory profile than the reference compounds.

4.5.2 BACE1 inhibitory activity

The evaluation of the BACE1 inhibitory activity was performed by the group of Dr. Vincenza Andrisano (*Università di Bologna*). As for the previous family of compounds, the inhibitory activity of hybrids **44**–**46** and **48**–**51** against recombinant *h*BACE1 was evaluated by employing Panvera peptide as the substrate (**Table 4.3**). As mentioned before, huprine Y and the reference huprine-based hybrid compound **10** had been evaluated with M-2420 as the substrate, but due to problems of interference of the compounds in the fluorimetric assay the substrate and assay conditions had to be changed.

These novel hybrids were designed specifically to perform a dual site binding within BACE1, with the huprine moiety being expected to interact with the catalytic pocket of the enzyme, as suggested in previous works of the group,[158,168,171] and the new scaffolds being expected to interact with the transient secondary pocket of BACE1, as predicted by virtual screening. Contrary to our expectations, these compounds turned out to be clearly less potent than the reference compound **10**. In fact, compounds **50** and **51** were found to be inactive, whereas compounds **45**, **48**, and **49** were found to be weak inhibitors of BACE1, with 7%, 26%, and 16% inhibition at 15 μM **(Table 4.3)**, respectively. Compound **46** resulted to be moderately potent, with an IC_{50} = 10.77. Finally, the most potent BACE1 inhibitor of the series was **44**, with an IC_{50} = 2.71 μM, comparable to that of compound **10**, which presented an IC_{50} = 1.67 μM when using the same substrate and assay conditions (Panvera substrate). So, compound **44** was roughly equipotent to the previous lead.

Table 4.3. *h*BACE1 inhibitory activities of hybrid **48** (as free base) and the hydrochloride salts of huprine Y, the reference huprine-based hybrid **10** and the new hybrids **44–46**, and **49–51**.

Compound	*h*BACE1 % inhibition[a] or IC_{50} (μM)[b]
44	2.71 ± 0.21
45	6.92 ± 0.4 %
46	10.77 ± 1.72
48	26.48 ± 2.68 %
49	16.21 ± 0.35 %
50	na[c]
51	na[c]
huprine Y	14%[d,e]
10	0.120 ± 0.90[d,f] 1.67[g]

[a] % inhibition at 15 μM.
[b] IC_{50} (μM) of human recombinant BACE1. Values are expressed as mean ± SEM of at least three experiments, each one performed in duplicate.
[c] Not active
[d] Data from Ref. 158.
[e] 14% inhibition at 5 μM.
[f] IC_{50} value obtained using M-2420 as the substrate.
[g] IC_{50} value obtained using Panvera as the substrate.

4.5.3 Aβ and tau antiaggregating activity

The activity of the novel compounds against spontaneous aggregation of $A\beta_{42}$ and tau was also determined. The inhibitory activity of the novel hybrids against the aggregation of $A\beta_{42}$ peptide and protein tau in intact *E. coli* cells was assessed again by myself under the supervision of Dr. Raimon Sabaté (*Universitat de Bacelona*). This assay, which is based on the overexpression of amyloid-prone proteins in bacteria and the measurement of its aggregation by a fluorimetric assay, will be better elaborated in Chapter **6** of this Thesis.

Overall, the novel series of hybrids presented moderate to good inhibitory potencies of $A\beta_{42}$ and tau self-aggregation (**Table 4.4**). Compounds **50** and **51** displayed weak antiaggregating potencies against both studied proteins (<20% inhibition at 10 μM). As discussed in section **3.5.3**, compounds with aromatic planar moieties can block self-aggregation of $A\beta_{42}$ and tau by interfering in the β-sheets alignment. Compound **50** lacks a planar aromatic moiety linked to the alkylhuprine moiety, which could

account for its lack of antiaggregating activity. This could be also the case for compound **51**, which should be mostly in the nonaromatic pyridone form.

Almost all compounds displayed slightly better antiaggregating capacity against protein tau than against $A\beta_{42}$, except for compound **45**, which is equipotent for both proteins. Nonetheless, they presented the same order of potencies against both proteins, again supporting the notion that common mechanisms rule the aggregation of different amyloidogenic proteins. Overall, the most potent antiaggregating agents of this family were **44**, **45**, and **46**, which were roughly equipotent to the reference compound **10** against $A\beta_{42}$ aggregation but more potent against tau aggregation, with IC_{50} values that must be in the low micromolar range.

Table 4.4. $A\beta_{42}$ and tau antiaggregating activities of hybrid **48** (as free base) and the hydrochloride salts of huprine Y, the reference huprine-based hybrid **10** and the new hybrids **44**–**46**, and **49**–**51**.

Compound	$A\beta_{42}$ aggregation[a] (% inh. at 10 μM)	Tau aggregation[a] (% inh. at 10 μM)
44	49.5 ± 1.6	65.8 ± 1.9
45	42.3 ± 1.9	48.5 ± 2.3
46	35.3 ± 2.8	55.5 ± 2.9
48	29.4 ± 2.1	41.6 ± 2.9
49	32.6 ± 2.5	45.3 ± 4.2
50	9.7 ± 3.5	15.0 ± 3.9
51	19.9 ± 4.2	20.9 ± 2.5
huprine Y	na[b,c]	na[b,c]
10	47.9 ± 14.5[b]	29.6 ± 8.5[b]

[a] % inhibition at 10 μM in intact *E. coli* cells. Values are expressed as mean ± SEM of at least three independent experiments.
[b] Data from Ref. 158.
[c] Not active

4.5.4 Antioxidant properties

Like for the previous family of compounds, to further assess the multitarget profile of this new family of compounds, they were also evaluated for their radical scavenging and metal-chelating properties, in the frame of a collaboration with the group of Prof. Michael Decker (*University of Würzburg*) and Prof. Maria Laura Bolognesi (Università di Bologna).

4.5.4.1 Radical scavenging activity

The evaluation of the radical scavenging properties was performed through a spectrophotometric assay using DPPH as substrate and ascorbic acid as a reference compound. Comparable to the previous family of hybrids, these compounds were generally weak radical scavengers, with a scavenging activity in the range 40–69% at 500 μM, except for two compounds. In this case, compounds **49** and **51** were found to be moderately potent radical scavengers (with IC_{50} = 20 and 91 μM, respectively). Surprisingly, compound **44** displayed only weak scavenging properties (40% scavenging activity at 500 μM), despite having a polyphenolic structure.

Table 4.5. Radical scavenging activities of hybrid **48** (as free base) and the hydrochloride salts of hybrids **44**–**46**, and **49**–**51**.

Compound	% scavenging[a] or EC_{50} (μM)[b]
44	40%
45	50%
46	66%
48	na[c]
49	19.55
50	69%
51	90.63

[a] % DPPH radical scavenging activity at 500 μM.
[b] EC_{50} (μM) of radical scavenging activity. Values are the mean of at least three independent experiments.
[c] na: not active

4.5.4.2 Metal chelating activity

The evaluation of the Cu^{2+} chelating properties of the new hybrids was carried through a spectrophotometric assay using pyrocatechol violet (PV) as the substrate and EDTA as a reference compound. Amongst the compounds evaluated, hybrids **44**, **48**, and **51** presented weak Cu^{2+} chelating activities, as their ability to chelate this ion was below 50% at all compound:Cu^{2+} ratios evaluated, whereas compounds **45** and **50** were moderately potent chelators, with activities of almost 80% and 60% at a 5:1 ratio but lower than 50% at all other ratios evaluated. Finally, pyrazole-based hybrids **46** and **49** were potent Cu^{2+} chelating agents, being able to chelate this ion at any ratio evaluated. Very interestingly, both compounds were more potent chelators than EDTA, as they were able to chelate more than 80% of Cu^{2+} even at 0.5:1 ratio, which may suggest that a single molecule of these hybrids is able to chelate two copper (II) ions.

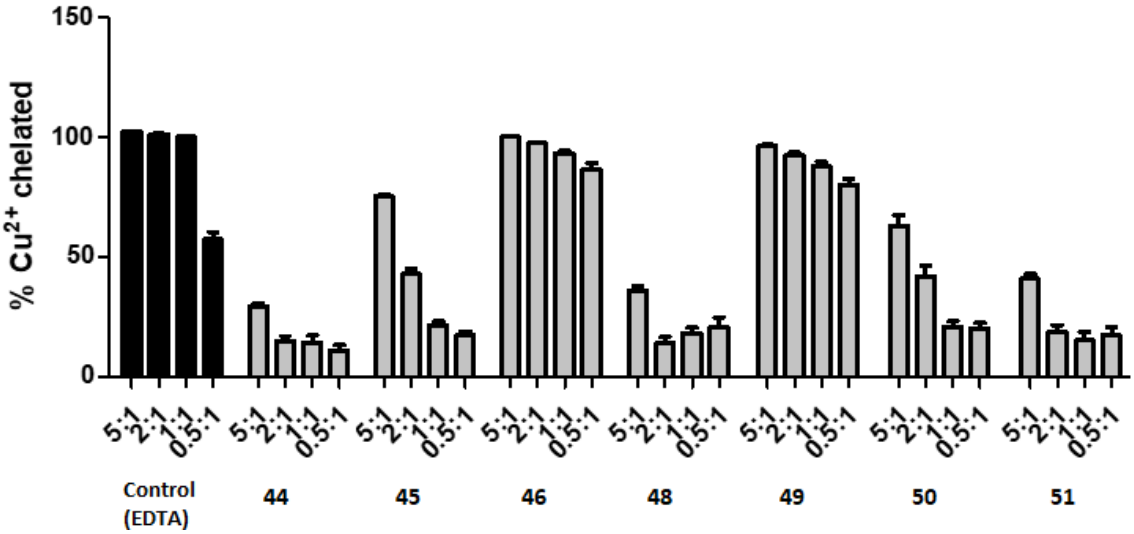

Figure 4.7. Copper (II) chelation properties of hybrid **48** (as free base) and the hydrochloride salts of hybrids **44–46**, and **49–51** at different compound:Cu^{2+} ratios. Values are expressed as means ± SEM of at least three independent assays and referred to control samples with EDTA.

4.5.5 *In vitro* BBB permeation assay

Dr. Belén Pérez (*Universitat Autònoma de Barcelona*) was responsible for assessing the brain permeation of the novel hybrids by the *in vitro* PAMPA-BBB assay.[175] From the correlation obtained by comparing the experimental and reported *in vitro* permeability (P_e) values of fourteen reference drugs and the limits established for BBB permeation,[173] compounds with P_e (10^{-6} cm s^{-1}) > 5.2 would be expected to have high BBB penetration (CNS+), compounds with P_e (10^{-6} cm s^{-1}) < 1.9 should have low BBB penetration (CNS–) and compounds with 5.2 > P_e (10^{-6} cm s^{-1}) > 1.9 would present an uncertain BBB permeation (CNS±).

All these new hybrids had P_e values clearly lower than that of the parent huprine Y and the reference huprine-based hybrid **10** (**Table 4.6**), which might be ascribed to the high polarity conferred by their polyphenolic or heterocyclic VSH moiety. In general, the lower molecular weight and lower lipophilicity of these new hybrids relative to other huprine-based hybrids previously developed in our group should be regarded as favourable properties, provided that these compounds are not too polar to compromise their brain permeation. Indeed, despite the greater polarity of the new hybrids none of them was predicted to suffer from a poor brain permeation. An uncertain BBB penetration was predicted for compounds **44**, **46**, **(±)-50**, and **51**. Gratifyingly, compounds **45**, **48**, and **49** were predicted to have high BBB penetration, which should enable them to reach their multiple CNS targets.

Table 4.6. Permeability results from the PAMPA-BBB assay of hybrid **48** (as free base) and the hydrochloride salts of huprine Y, the reference huprine-based hybrid **10** and the new hybrids **44**–**46**, and **49**–**51**.

Compound	P_e (10^{-6} cm s^{-1})[a]	Prediction
44	3.9 ± 0.2	CNS±
45	6.7 ± 0.4	CNS+
46	4.0 ± 0.4	CNS±
48	8.2 ± 0.1	CNS+
49	5.9 ± 0.4	CNS+
50	4.9 ± 0.6	CNS±
51	3.2 ± 0.3	CNS±
huprine Y	23.8 ± 2.7	CNS+
10	21.5 ± 0.7	CNS+

[a] Permeability values from the PAMPA-BBB assay. Values are expressed as mean ± SEM of three independent experiments.

4.5.6 Toxicological studies

The toxicity of this new family of compounds was evaluated using two different assays, namely a neurotoxicity assay in HT-22 neuronal cells and an acute toxicity assay in a zebra fish model.

4.5.6.1 Neurotoxicity

The evaluation of the potential neurotoxicity of the new hybrids was assessed by the group of Prof. Michael Decker (*University of Würzburg*). The viability of HT-22 neuronal cells in the presence of the new compounds was assessed by the MTT assay. In general, these new hybrids resulted to be non-neurotoxic at 25 μM (**Figure 4.7**), as no significant loss of cell viability was observed. Only hybrid **46** was found to be slightly neurotoxic, leading to a cell viability of 80% at 25 μM.

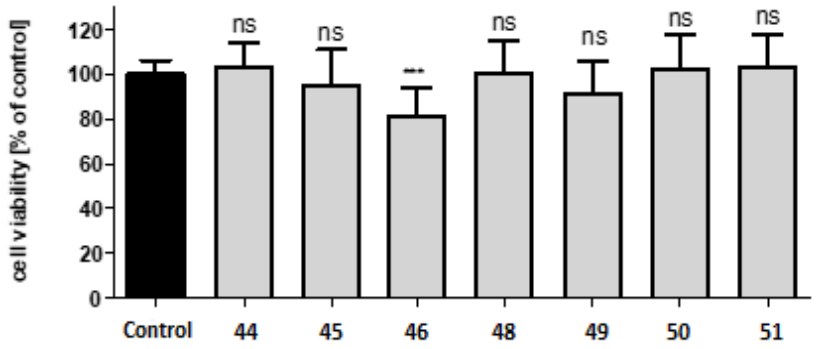

Figure 4.7. Viability of HT-22 neuronal cells in the presence of hybrid **48** (as free base) and the hydrochloride salts of hybrids **44–46**, and **49–51**. Results are presented as means ± SD of three independent experiments, each performed in sextuplicate, and referred to untreated control cells. Levels of significance: **p* < 0.01; ***p* < 0.005; ****p* < 0.001, ns: not significant.

3.5.6.2 Toxicity in a zebra fish model

Like for the previous series, toxicological studies in zebra fish embryos were carried out by the group of Prof. Jesús Gómez and Dr. Marta Barenys (*Universitat de Barcelona*), following the OECD Guideline for Fish Embryo Acute Toxicity (FET) Test. The toxicity of the new hybrids was evaluated and compared with that of the parent huprine Y under the same assay conditions (**Table 3.6**). A calculated LD_{50} was extrapolated from the results obtained at lower concentrations for compounds that crashed out from solution at high doses. For these compounds, the NOAEC (no adverse effect concentration) was the maximum soluble concentration.

Overall, this new family of hybrids was not significantly toxic, with only compound **48** displaying toxicity in the low micromolar range (LD_{50} = 7.1 µM). Hybrids **44**, **46**, **50** and **51** were essentially nontoxic with LD_{50} values of more than 100 µM, whereas hybrids **45** and **49** were found to be toxic at high concentrations, with LD_{50} = 57.8 and 69.1 µM, respectively.

Table 4.7. Toxicology results in zebra fish model of hybrid **48** (as free base) and the hydrochloride salts of hybrids **44**–**46**, and **49**–**51**.

Compound	LC_{50} (μM)[a]	NOAEC (μM)[b]
44	>100[c]	12.5[d]
45	57.8[c]	12.5[d]
46	>100[c]	12.5[d]
48	7.1	5
49	69.1[c]	12.5[d]
50	>100	100
51	>100	25
huprine Y	20.9	12.5

[a] LC_{50} in zebra fish embryos. Values are the result of at least three independent experiments.
[b] No adverse effect concentration.
[c] Calculated LC_{50}
[d] Maximum soluble concentration
[e] nd: not determined

CHAPTER 5

Huprine–TPPU and 6-chlorotacrine–TPPU hybrids

5.1 Soluble epoxide hydrolase (sEH) in AD

Human soluble epoxide hydrolase (sEH) is a 62 kDa enzyme composed of two domains separated by a short proline-rich linker (**Figure 5.1**). In mammals, this enzyme is a homodimer located in the intracellular environment. The N-terminal domain exhibits a phosphatase activity that is involved in lipid phosphates hydrolysis, whereas the C-terminal domain exhibits an epoxide hydrolase activity that converts epoxides into their corresponding diols.[180,181] The enzyme sEH is extensively expressed in the brain, primarily localized in astrocytes, oligodendrocytes and neuronal cell bodies.[182,183] It is thought to regulate blood flow in the brain and it may play a role on the release of neuropeptides.[184]

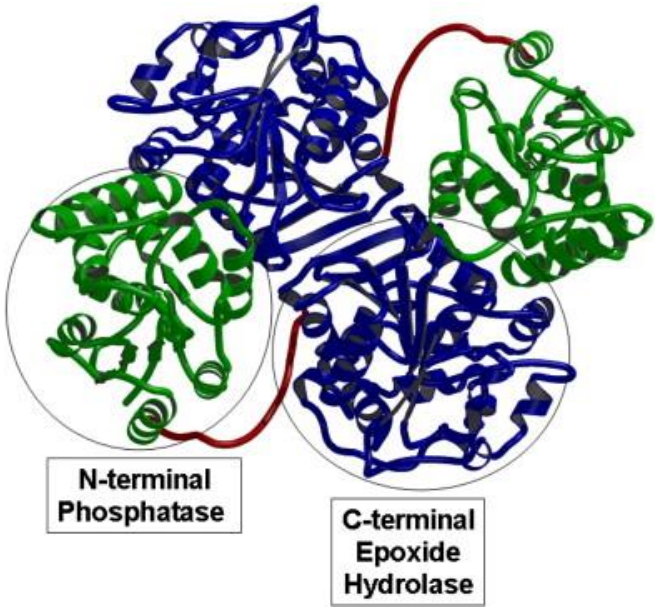

Figure 5.1. Crystal structure of the sEH dimer (PDB ID: 1S80). The sEH monomer is composed of two globular regions displaying α/β fold tertiary structure connected by a short proline-rich linker. The sEH dimer is antiparallel, so that the N-terminal region of one monomer is in contact with the C-terminal region of the other. The catalytic site for epoxide hydrolase activity is located within the C-terminal domain, while the phosphatase activity is located within the N-terminal domain. (Image source: T. R. Harris, B. D. Hammock. *Gene* **2013**, *526*, 61–74).

[180]J. W. Newman, C. Morisseau, B. D. Hammock. *Prog. Lipid Res.* **2005**, *44*, 1–51.
[181]C. Morisseau, B. D. Hammock. *Annu. Rev. Pharmacol. Toxicol.* **2013**, *53*, 37–58.
[182]A. Marowsky, J. Burgener, J. R. Falck, J.-M. Fritschy, M. Arand. *Neuroscience* **2009**, *163*, 646–661.
[183]P. Sura, R. Sura, A. E. Enayetallah, D. F. Grant. *J. Histochem. Cytochem.* **2008**, *56*, 551–559.
[184]C. Brenneis, M. Sisignano, O. Coste, K. Altenrath, M. J. Fischer, C. Angioni, I. Fleming, R. P. Brandes, P. W. Reeh, C. J. Woolf, G. Geisslinger, K. Scholich. *Mol. Pain* **2011**, *7*, 78.

The enzyme sEH is involved in the arachidonic acid (AA) cascade, which is a group of metabolic pathways that degrade AA to several metabolites (**Figure 5.2**). Metabolism via the cyclooxygenase (COX) and lipoxygenase (LOX) pathways gives rise to pro-inflammatory metabolites. As a consequence, both pathways have been extensively studied and pharmacologically targeted. Metabolism of AA through cytochrome P450 (CYP) enzymes leads to hydroxyeicosatetranoic acids (HETEs) by hydroxylation or to epoxyeicosatrienoic acids (EETs) via epoxidation. These EETs have been demonstrated to present potent anti-inflammatory effects, mediate in vasodilatation, attenuate ROS, and block the endoplasmic reticulum (ER) stress response.[185,186] However, they are rapidly subjected to hydrolysis by sEH to their corresponding diols (dihydroeicosatrienoic acids, DHETs), leading to less active anti-inflammatory or even pro-inflammatory metabolites.[187] So, inhibition of sEH will increase the levels of EETs, thus maintaining their beneficial effects.

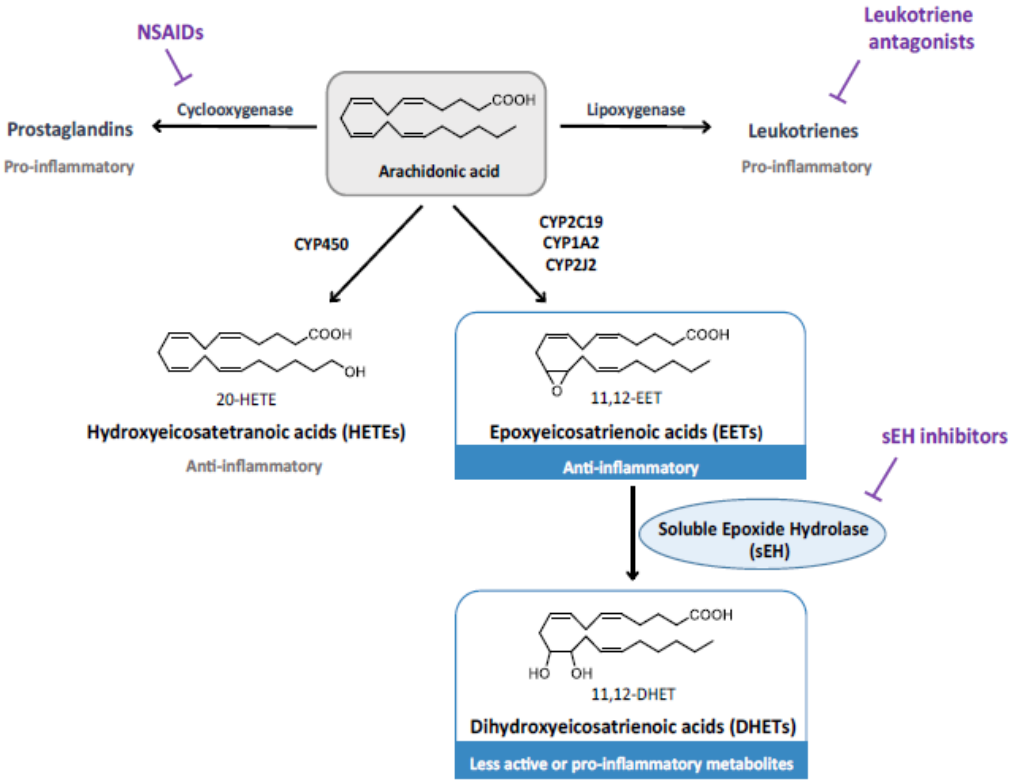

Figure 5.2. The arachidonic acid (AA) cascade. Metabolism of AA by COX and LOX leads to pro-inflammatory metabolites. Metabolism through CYP enzymes leads to HETEs or EETs. EETs are endowed with potent anti-inflammatory properties but are rapidly subjected to hydrolysis by sEH. (Image source: C. Griñán-Ferré, S. Codony, E. Pujol, J. Yang, R. Leiva, C. Escolano, D. Puigoriol-Illamola, J. Companys-Alemany, R. Corpas, C. Sanfeliu, M. I. Loza, J. Brea, C. Morisseau, B. D. Hammock, S. Vázquez, M. Pallàs, C. Galdeano, *BioRxiv* preprint posted online, doi: http://dx.doi.org/10.1101/605055).

[185]B. Inceoglu, A. Bettaieb, F. G. Haj, A. V. Gomes, B. D. Hammock. *Prostaglandins Other Lipid Mediat.* **2017**, *133*, 68–78.
[186]X. Liu, C. M. Davis, N. J. Alkayed. *Antioxid. Redox Signaling* **2018**, *28*, 987–1007.
[187]A. A. Spector, X. Fang, G. D. Snyder, N. L. Weintraub. *Prog. Lipid Res.* **2004**, *43*, 55–90.

In the past few years, the group of Prof. Santiago Vázquez (*Universitat de Barcelona*) has worked in the development of novel small molecule sEH inhibitors for different diseases, such as acute pancreatitis. Recently, in collaboration with the group of Prof. Mercè Pallàs (*Universitat de Barcelona*) they have validated pharmacologically sEH as a novel target for the treatment of AD. Using three potent sEH inhibitors as chemical probes and two murine models of age-related cognitive decline and AD (5xFAD for early onset AD and SAMP8 for late onset AD), they have confirmed the beneficial effects of central sEH inhibition. The treatment of both SAMP8 and 5xFAD mice with the three inhibitors reduced pro-inflammatory, ROS and endoplasmic reticulum stress biomarkers. Furthermore, a reduction in tau hyperphosphorylated species and amyloid burden was also observed, as well as an increase of sAPPα, demonstrating the ability of sEH inhibitors to shift the APP processing towards the non-amyloidogenic pathway. Finally, the three sEH inhibitors reduced cognitive decline, both in short-term and long-term memory tests.

5.2 Design of huprine–TPPU and 6-chlorotacrine–TPPU hybrids

Having into account the promising effect of inhibiting sEH for AD, we considered the potential interest of incorporating a sEH inhibitor pharmacophore as a key element for the design of new MTDLs against AD. Thus, we envisaged the synthesis of a new family of compounds with the potential to be dual inhibitors of sEH and AChE, in collaboration with the group of Prof. Santiago Vázquez. This new family of hybrids was designed formally by assembly of the potent sEH inhibitor TPPU, **15**, with the well-known AChE inhibitors 6-chlorotacrine, **11**, or huprine Y, **7**. The linkage between both units was envisaged through a short tether chain of 2–4 methylenes (general structure **IV** and compounds **(+)-16** and **(–)-16**, **Figure 5.3**)

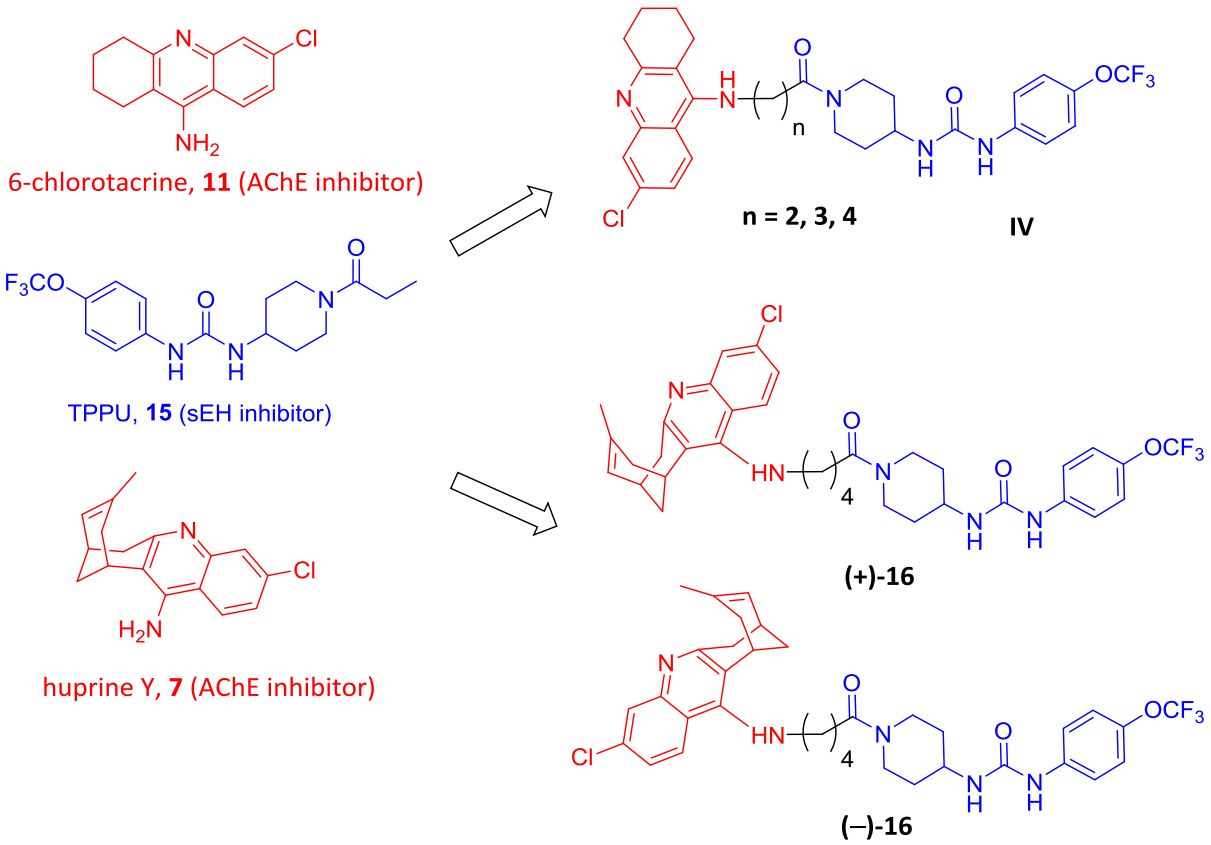

Figure 5.3. Structure of the parent AChEIs huprine Y and 6-chlorotacrine, the parent sEHI TPPU, and structures of the new hybrids (general structure **IV** and compounds **(+)-16** and **(–)-16**).

TPPU, **15** (**Figure 5.3**) is a potent human sEH inhibitor (IC_{50} = 0.7 nM) developed by the group of Prof. Bruce D. Hammock, who has been collaborating with Prof. Santiago Vázquez.[188] The presence of the trifluoromethoxy group at position 4 of the benzene ring slows the metabolic oxidation of the aromatic ring by CYP enzymes. Moreover, this group strengthens hydrogen bonding interaction of the urea hydrogen with Asp334 at the catalytic site of human sEH by inductive withdrawal of the nitrogen lone electron pair, further polarizing the urea N–H bond.[188] A varying degree of polarity, bulkiness, and basicity with regard to the substituent attached to the piperidine nitrogen, away from the urea pharmacophore, is extremely well tolerated by the target enzyme.[188] Therefore, the presence of the AChE inhibitor scaffolds (huprine Y or 6-chlorotacrine) linked by different tethers to the TPPU piperidine ring were not expected to interfere in the sEH inhibitory activity of the TPPU moiety.

[188]T. E. Rose, C. Morisseau, J.-Y. Liu, B. Inceoglu, P. D. Jones, J. R. Sanborn, B. D. Hammock. *J. Med. Chem.* **2010**, *53*, 7067–7075.

As for the AChE inhibitory activity, both huprine Y and 6-chlorotacrine are well-known potent AChE inhibitors. 6-Chlorotacrine, **11**, has been commonly used by our research group as a pharmacophore of several classes of MTDLs due to its synthetic simplicity relative to huprine Y.[189-191] In an analogous way as huprine Y, this compound will be protonated at physiological pH. It tightly binds at the CAS of AChE through cation–π and π–π stacking interactions with the indole ring of Trp86 and the benzene ring of Tyr337, hydrogen bonding between the protonated acridine nitrogen atom and the carbonyl oxygen of His447, and hydrophobic interactions by the chlorine atom, which fills a hydrophobic pocket formed by Pro446, Trp439, and Met443. The same interactions are displayed by huprine Y. Concomitant to the interaction of these moieties at the CAS, we might expect a simultaneous binding of the TPPU moiety of the envisaged hybrids at the PAS, presumably by π–π stacking interactions of the TPPU phenyl ring with the aromatic PAS residues Tyr72 and Trp286. Moreover, the presence of the amide function integrated in the linker might enable further interactions with midgorge residues.

5.3 Synthesis of huprine–TPPU and 6-chlorotacrine–TPPU hybrids

As part of this collaborative project, the TPPU-derived fragment of the target hybrids was synthesised in the frame of the PhD Thesis of Ms. Sandra Codony, following the synthetic methodology previously reported by the group of Prof. Bruce D. Hammock.[188] This methodology involves the reaction of isocyanate **51** with *N*-benzyl-protected aminopiperidine **52**, followed by debenzylation of the resulting urea **53** (**Scheme 5.1**).

[189]I. Sola, E. Aso, D. Frattini, I. López-González, A. Espargaró, R. Sabaté, O. Di Pietro, F. J. Luque, M. V. Clos, I. Ferrer, D. Muñoz-Torrero. *J. Med. Chem.* **2015**, *58*, 6018–6032.

[190]O. Di Pietro, F. J. Pérez-Areales, J. Juárez-Jiménez, A. Espargaró, M. V. Clos, B. Pérez, R. Lavilla, R. Sabaté, F. J. Luque, D. Muñoz-Torrero. *Eur. J. Med. Chem.* **2014**, *84*, 107–117.

[191]P. Camps, X. Formosa, C. Galdeano, T. Gómez, D. Muñoz-Torrero, L. Ramírez, E. Viayna, E. Gómez, N. Isambert, R. Lavilla, A. Badia, M. V. Clos, M. Bartolini, F. Mancini, V. Andrisano, A. Bidon-Chanal, Ó. Huertas, T. Dafni, F. J. Luque. *Chem. Biol. Interact.* **2010**, *187*, 411–415.

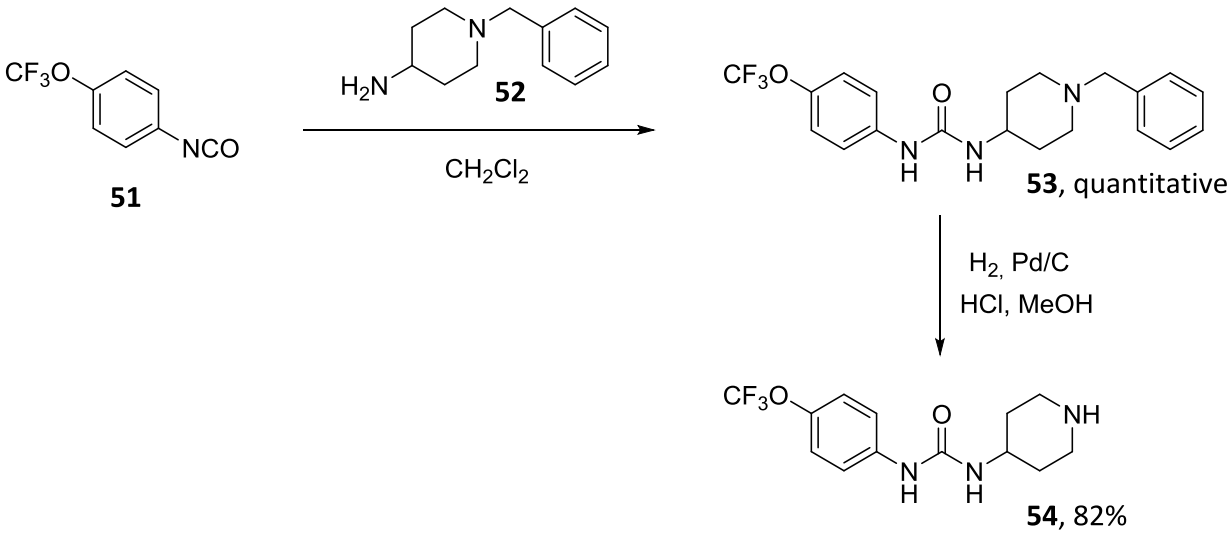

Scheme 5.1

5.3.1 Synthesis of tacrine-derived carboxylic acid intermediates with ethylene or trimethylene linkers (n = 2, 3)

From previous experience in our research group, we knew that direct alkylation of 6-chlorotacrine, **11**, with the appropriate ω-bromoalkanenitrile did not work properly for short linkers. In these cases, likely the α-nitrile position is too acidic due to the closer proximity of the halogen atom, which triggers undesired reactions, so that the desired compounds are not obtained (**Scheme 5.2**).

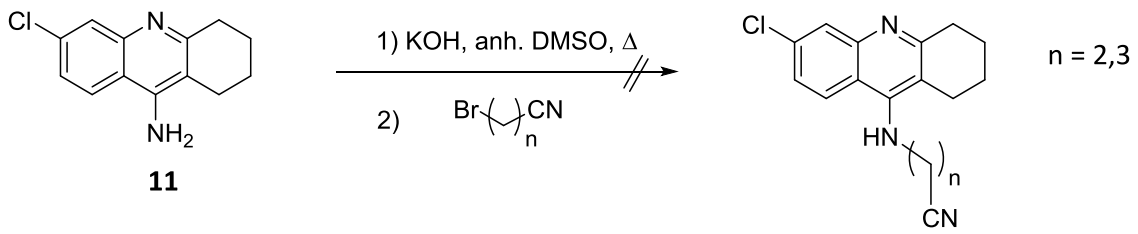

Scheme 5.2

As a consequence, an alternative synthetic route was envisaged, starting with the synthesis of the required 6,9-dichloroacridine **57**, by a procedure widely used in our research group.[189-191] So, this first step involved a Friedländer condensation of cyclohexanone, **56**, with anthranilic acid **55** in the presence of $POCl_3$ under reflux for 2 h, to obtain **57** in good yield (81%, **Scheme 5.3**).

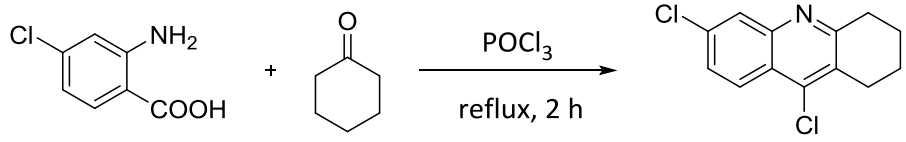

55 **56** **57**, 81%

Scheme 5.3

Afterwards, amination of the 6,9-dichloroacridine **57** with the appropriate ω-aminoalcohols led to the corresponding alcohol derivatives **59a-b** in good yields (93% and 71%, respectively).[192,193] Subsequently, the alcohols were transformed into the corresponding mesylates, **60a-b**, in quantitative yields by treatment with methanesulfonyl chloride in the presence of Et_3N,[194] which were then reacted with NaCN in DMF to afford the desired cyanoalkyltacrines **61a-b**, in moderate or good yields (51% and 91%, respectively, **Scheme 5.4**).

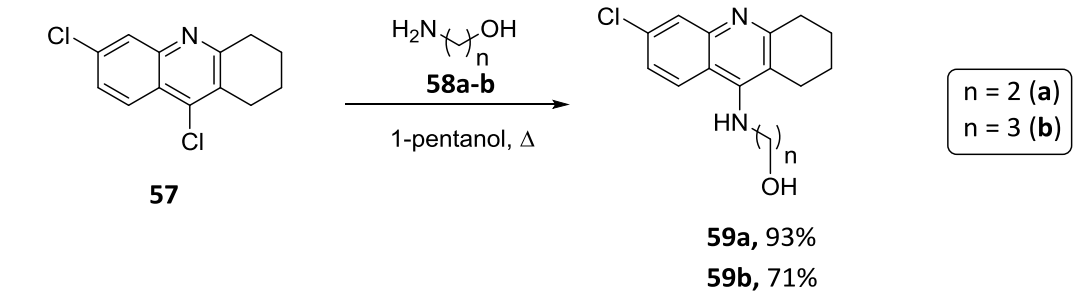

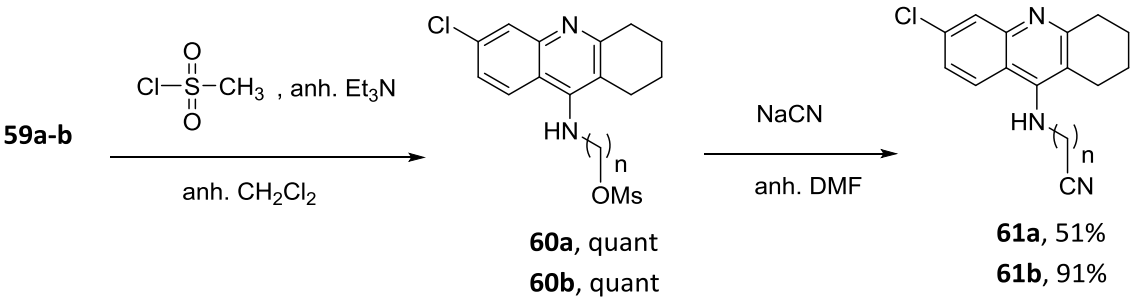

Scheme 5.4

Hydrolysis of nitrile **61a** was first attempted under basic conditions, as described in section **4.4** for compound **47**, but a retro-Michael reaction occurred and only dealkylated tacrine was obtained (**Scheme 5.5**).

[192]P. Camps, X. Formosa, C. Galdeano, T. Gómez, D. Muñoz-Torrero, M. Scarpellini, E. Viayna, A. Badia, M. V. Clos, A. Camins, M. Pallàs, M. Bartolini, F. Mancini, V. Andrisano, J. Estelrich, M. Lizondo, A. Bidon-Chanal, F. J. Luque. *J. Med. Chem.* **2008**, *51*, 3588–3598.

[193]S. J. Burguess, A. Selzer, J. X. Kelly, M. J. Smilkstein, M. K. Riscoe, D. H. Peyton. *J. Med. Chem.* **2006**, *49*, 5623–5625.
[194]M. de Souza, K. Pais, C. Kaiser, M. Peralta, M. Ferreira, M. Lourenço. *Bioorg. Med. Chem.* **2009**, *17*, 1474–1480.

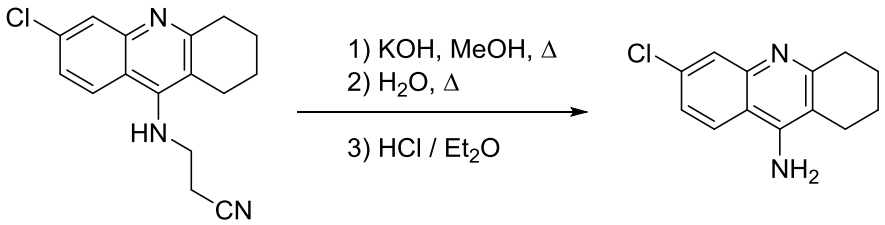

61a **11**

Scheme 5.5

In the light of these results, an alternative acidic hydrolysis of nitrile **61a** was performed, by treatment of the compound with 5N HCl aqueous solution at reflux for 3 h, leading to the corresponding carboxylic acid **62a** in the form of quinoline hydrochloride salt, which was used in the following step without further purification. Nitrile **61b** was hydrolysed under the same acidic conditions, but in this case the ɣ-lactam byproduct **63** was obtained as the major product (64%), while the desired carboxylic acid **62b** was obtained as a minor product (36%) and was used in the following step without further purification (**Scheme 5.6**).

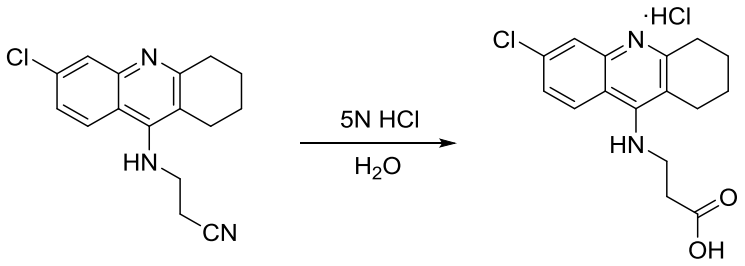

61a **62a**

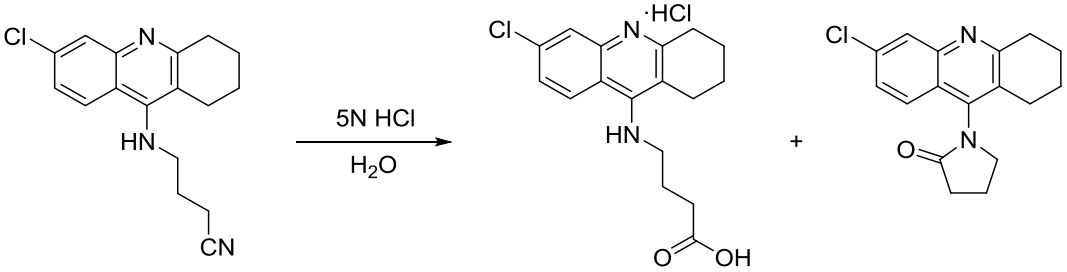

61b **62b,** 36% **63,** 64%

Scheme 5.6

5.3.2 Synthesis of tacrine-derived and huprine-derived carboxylic acid intermediates with a tetramethylene linker (n = 4)

The starting material for the synthesis of the 6-chlorotacrine-derived carboxylic acid intermediate with a tetramethylene linker was 6-chlorotacrine itself, **11**, which was prepared in quantitative yield by a Friedländer condensation of cyclohexanone, **56**, with aminobenzonitrile **64** in the presence of $AlCl_3$ in refluxing 1,2-dichloroethane for 18 h (**Scheme 5.7**).

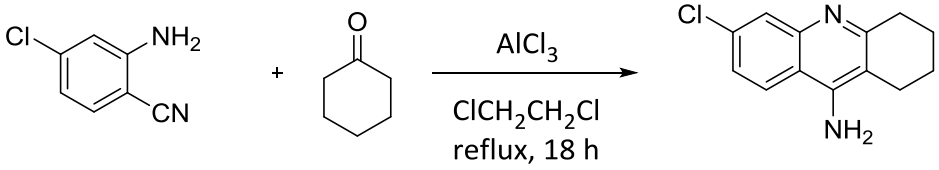

64 **56** **11** (quant)

Scheme 5.7

For the synthesis of the huprine-derived carboxylic acid intermediates with a tetramethylene linker, enantiopure (+)-(7*R*,11*R*)- and (–)-(7*S*,11*S*)-huprine Y previously synthesized in our group were used.

Alkylation of 6-chlorotacrine, **11**, and enantiopure huprines **(+)-7** and **(–)-7**, with 5-bromovaleronitrile, **65**, in the presence of KOH in DMSO at r. t. overnight led to nitriles **61c**, **(+)-66**, and **(–)-66** in moderate to good yields (83%, 62%, and 54%, respectively, **Scheme 5.8**) after silica gel column chromatography purification.

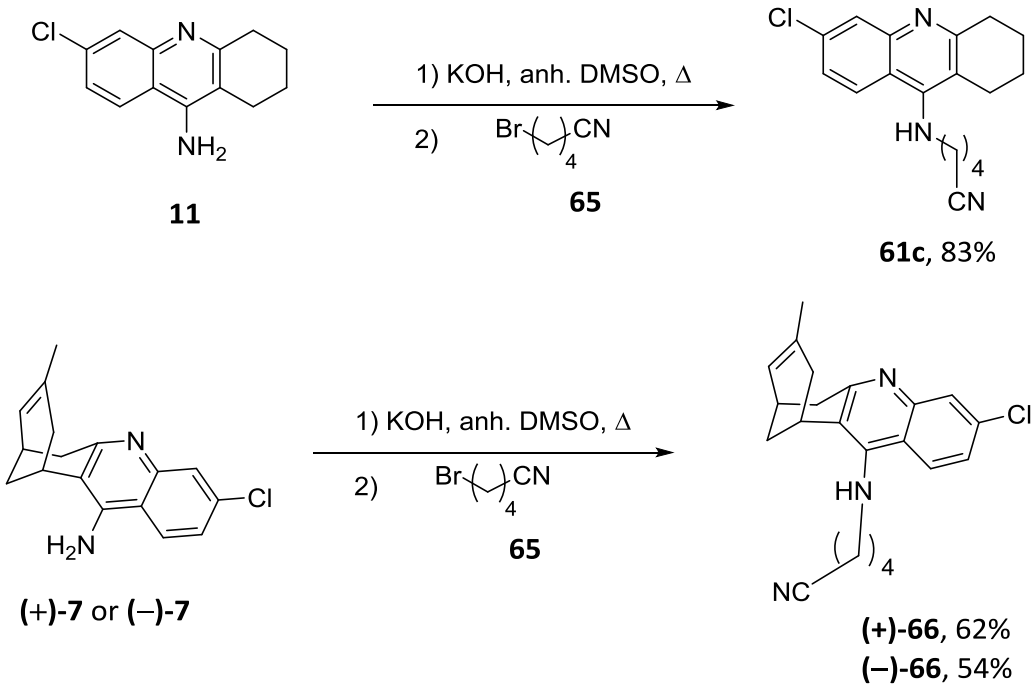

Scheme 5.8

Afterwards, nitrile intermediates **61c**, **(+)-66**, and **(–)-66** were hydrolysed in basic conditions to yield the corresponding carboxylic acids **62c**, **(+)-67**, and **(–)-67** as quinoline hydrochloride salts, which were used in the following step without further purification (**Scheme 5.9**).

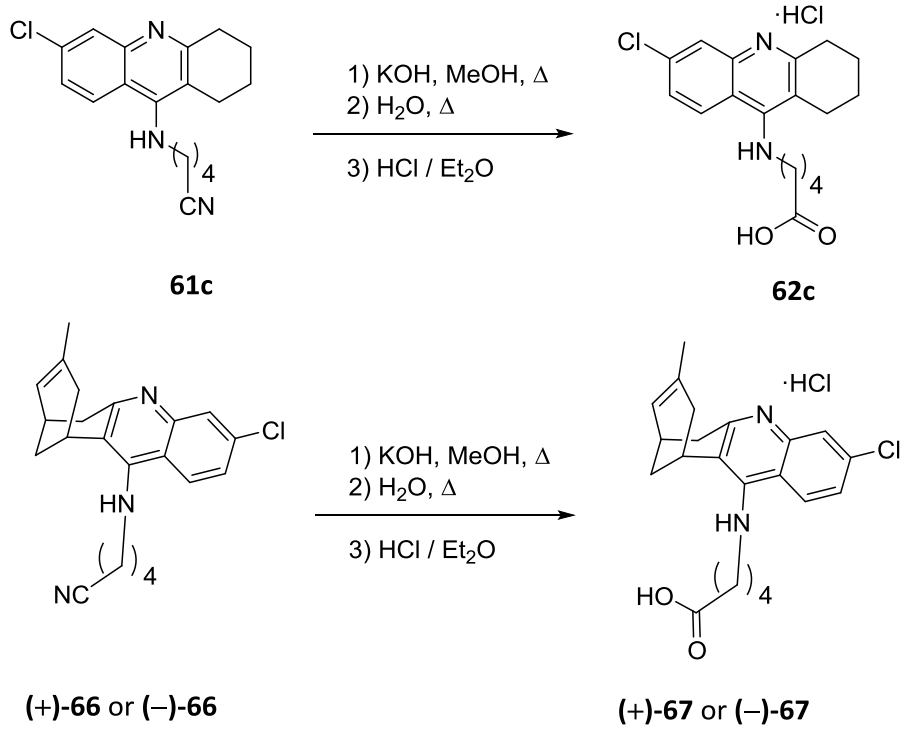

Scheme 5.9

5.3.3 Synthesis of the target hybrids 68a-c, (+)-16, and (–)-16

The final amide coupling of carboxylic acids **62a-c,** **(+)-67**, and **(–)-67**, with the TPPU-derived piperidine **54**, in the presence of EDC, HOBt, and Et_3N in a mixture of EtOAc / DMF at r. t. overnight, led to the target hybrids **68a–c, (+)-16**, and **(–)-16** in moderate to good yields (40–79% overall yield from nitriles, **Scheme 5.10**), after silica gel column chromatography purification.

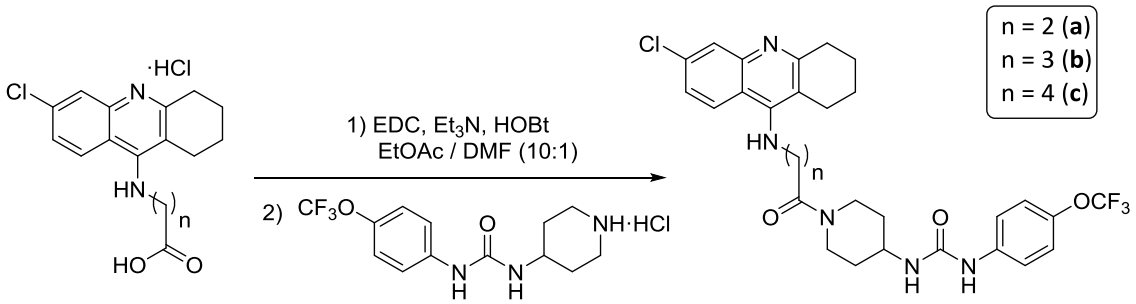

62a-c

68a, 45%
68b, 45%
68c, 79%

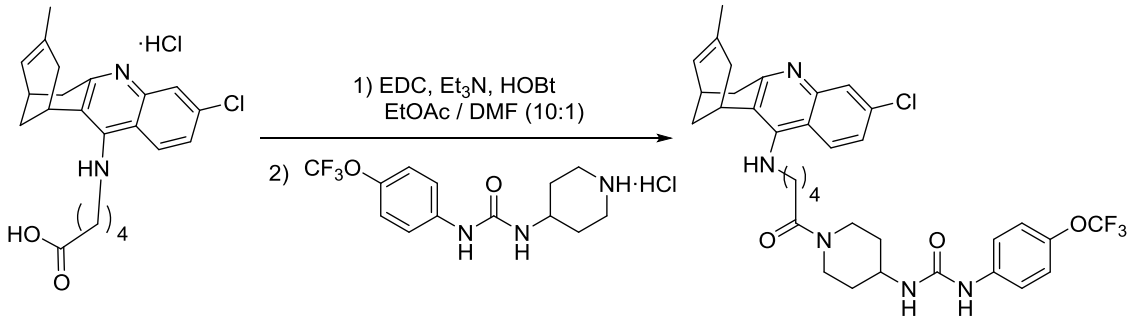

(+)-67 or **(–)-67**

(+)-16, 40%
(–)-16, 76%

Scheme 5.10

5.4 Biological characterization huprine–TPPU and 6-chlorotacrine–TPPU hybrids

5.4.1 Cholinesterases inhibitory activity

The anticholinesterase activities of the new huprine–TPPU and 6-chlorotacrine–TPPU hybrids were evaluated by Dr. Manuela Bartolini (*Università di Bologna*). The inhibitory activity of the new hybrids **68a-c, (+)-16**, and **(–)-16** against recombinant *h*AChE and serum *h*BChE was evaluated by the method of Ellman *et al.*,[172] and compared with that of the parent enantiopure (+)- and (–)-huprine Y and 6-chlorotacrine, under the same assay conditions (**Table 5.1**).

The novel tacrine–TPPU hybrids turned out to be potent inhibitors of *h*AChE, with IC_{50} values in the low nanomolar range (2.71–14.5 nM, **Table 5.1**). Compounds **68a** and **68c** were equipotent to the parent 6-chlorotacrine (IC_{50} = 14.5 nM), whereas the trimethylene-linked hybrid **68b** was 5-fold more potent than the parent 6-chlorotacrine, with IC_{50} = 2.71 nM, which might indicate that this hybrid presents the proper tether length (n = 3) to enable an optimal dual site binding within AChE.

As for the two huprine–TPPU hybrids, the levorotatory hybrid **(–)-16** was also a very potent *h*AChE inhibitor (IC_{50} = 1.94 nM), only slightly less potent than the parent levorotatory huprine Y **(–)-7** (IC_{50} = 0.74 nM). The dextrorotatory huprine-based hybrid **(+)-16** was clearly a less potent inhibitor of *h*AChE, with an inhibitory potency in the low micromolar range. This result is consistent with previous works of our research group, where it has been demonstrated that the levorotatory (7*S*,11*S*)-enantiomer of huprines and huprine-based hybrids binds much more favourably than the dextrorotatory (7*R*,11*R*)-counterpart.[158]

Table 5.1. *h*AChE and *h*BChE inhibitory activities of the hydrochloride salts of (+)-huprine Y, (–)-huprine Y, 6-chlorotacrine and the new hybrids **68a-c, (+)-16**, and **(–)-16**.

Compound	*h*AChE[a] IC_{50} (nM)	*h*BChE[a] IC_{50} (nM)
68a	14.5 ± 0.3	947 ± 6
68b	2.71 ± 0.06	416 ± 35
68c	12.9 ± 1.6	615 ± 34
(+)-16	1660 ± 450	179 ± 26
(–)-16	1.94 ± 0.67	615 ± 34
(+)-huprine Y	321 ± 16[b]	170 ± 17[b]
(–)-huprine Y	0.74 ± 0.06[b]	222 ± 17[b]
6-chlorotacrine	14.5 ± 0.9	505 ± 28

[a] IC_{50} (nM) of human recombinant AChE and human serum BChE. Values are expressed as mean ± SEM of at least three experiments, each one performed in duplicate.
[b] Data from Ref. 158

Like the parent 6-chlorotacrine and (–)-huprine Y, the novel tacrine–TPPU hybrids **68a-c** and the huprine–TPPU hybrid **(–)-16** were clearly selective towards *h*AChE over *h*BChE, with selectivity indices in the range 48–317. As previously discussed, the selectivity is imparted by the chlorine atom at position 3 of huprine or the equivalent position 6 of tacrine, which is crucial for the inhibitory activity against *h*AChE but detrimental for the inhibitory activity against *h*BChE. In contrast, like (+)-huprine Y, hybrid **(+)-16** is more potent towards *h*BChE than towards *h*AChE. In these cases, the (+)-huprine moiety seems to be better accommodate at the CAS of *h*BChE than in *h*AChE.

5.4.2 sEH inhibitory activity

The assessment of the sEH inhibitory activity of these hybrids was carried out by the group of Prof. Bruce D. Hammock (*University of California Davies*). The inhibitory activity of the new hybrids, **68a-c, (+)-16** and **(–)-16** against recombinant murine and human sEH was evaluated using a fluorimetric assay developed in his group,[195] and compared with that of the parent sEH inhibitorTPPU (**Table 5.2**).

[195]N. M. Wolf, C. Morisseau, P. D. Jones, B. Hock, B. D. Hammock. *Anal. Biochem.* **2006**, *355*, 71–80.

In the same way as for AChE inhibitory activity, this novel family of hybrids also retain the inhibitory properties against sEH of the parent TPPU, **15**, which validates the success of the molecular hybridization of both pharmacophores. All the new compounds are potent inhibitors of human and murine sEH, with IC_{50} values in the low nanomolar or even subnanomolar range (0.4-4.6 nM and 12.1-34.3 nM, respectively, **Table 5.2**). The *in vitro* evaluation of the murine sEH inhibitory activity of the compounds can be very interesting with regard to a future *in vivo* assay of a promising lead compound in mice, as the IC_{50} against this enzyme may help to establish the dose of treatment. In this case, the novel hybrids **68a-c, (+)-16** and **(–)-16** turned out to be 2–5-fold less potent mouse sEH inhibitors than the parent TPPU. Regarding the human sEH inhibitory activity, compounds **68a-b** and **(–)-16** displayed the same potency than TPPU, whereas compounds **68c** and **(+)-16** were slightly less potent. As expected, the introduction of the bulky alkyl-6-chlorotacrine or alkylhuprine moieties attached to the piperidine ring of the TPPU scaffold were not detrimental for the activity, as they are far enough from the urea pharmacophore and do not interfere in the binding of the TPPU moiety with the catalytic pocket of sEH.

Table 5.2. Human and mouse sEH inhibitory activities of TPPU and the hydrochloride salts of the new hybrids **68a-c, (+)-16**, and **(–)-16**.

Compound	Human sEH[a] IC_{50} (nM)	Mouse sEH[a] IC_{50} (nM)
68a	0.4	12.1
68b	1.0	15.0
68c	4.6	22.5
(+)-16	3.1	14.5
(–)-16	0.4	34.3
TPPU	0.7	6.5

[a] IC_{50} (nM) of human and murine recombinant sEH. Values are the average of at least three experiments in a linear region of the curve.

5.4.3 *In vitro* BBB permeation assay

The ability to cross the BBB by the new hybrids was assessed *in vitro* by the PAMPA-BBB assay,[175] by Dr. Belén Pérez (*Universitat Autònoma de Barcelona*). From the correlation obtained by comparison of the experimental and reported *in vitro* permeability (P_e) values of fourteen reference drugs and the limits established for BBB permeation,[173] the threshold for high BBB permeation (CNS+) was set at P_e (10^{-6} cm s^{-1}) > 5.2, whereas the threshold for low BBB penetration (CNS–) was set at P_e (10^{-6} cm s^{-1}) < 1.9 and that for uncertain BBB permeation (CNS±) at 5.2 > P_e (10^{-6} cm s^{-1}) > 1.9. All the new tacrine–TPPU and huprine–TPPU hybrids were found to have high BBB penetration, as their P_e values are well over the CNS+ threshold, like in the parent compounds huprine Y and TPPU. Thus, these hybrids should not suffer from any permeability issues to reach their multiple targets in the brain.

Table 4.6. Permeability results from the PAMPA-BBB assay of the hydrochloride salts of **(±)-**huprine Y and the new hybrids **68a-c, (+)-16**, and **(–)-16**.

Compound	P_e (10^{-6} cm s^{-1})[a]	Prediction
68a	9.2 ± 0.25	CNS+
68b	9.1 ± 0.10	CNS+
68c	8.4 ± 0.7	CNS+
(+)-16	12.8 ± 1.1	CNS+
(–)-16	9.9 ± 0.3	CNS+
(±)-huprine Y	23.8 ± 2.7	CNS+
TPPU	11.7 ± 0.2	CNS+

[a] Permeability values from the PAMPA-BBB assay. Values are expressed as mean ± SEM of three independent experiments.

5.4.4 Solubility and microsomal stability evaluation

In the light of the promising multitarget profile of these new hybrids and the novelty, inventive activity, and industrial applicability of the project, a patent was filed (D. Muñoz-Torrero, S. Vázquez, C. Pont, S. Codony, EP19382219.4, priority date 28 March 2019). With the purpose of valorising the project and generating more data to enable the selection of a lead compound for an eventual proof-of-concept in an animal model, some physicochemical and pharmacokinetic properties were determined. Thus, the aqueous solubility and microsomal stability of the huprine–TPPU and 6-chlorotacrine–TPPU hybrids were assessed by the *Unidad de Evaluación de Actividades Farmacológicas de Compuestos Químicos* (USEF, *Universidade de Santiago de Compostela*). Solubility was measured by the method of kinetic solubility, where a previous solution of the compound in DMSO (10 mM) is diluted with increasing volumes of a mixture of PBS (phosphate buffered saline) / DMSO (99:1) until the first precipitate appears. The microsomal stability assay was performed using human, rat and mice recombinant microsomes.

As previously discussed, the evaluation of physicochemical and pharmacokinetic parameters is of great importance in the development of new drugs. Solubility is one of the most important factors, as the first step for a drug to enter the body is dissolution. If a compound presents bad solubility in water, it will not be able to cross body membranes and reach its specific targets to have an effect. In our case, the new hybrids present moderate to poor solubility (6–43 μM), which can likely be ascribed to the high lipophilicity of these compounds. The most soluble compound is **68a**, as expected due to the presence of the shortest linker (n = 2) and the smallest AChEI pharmacophore (6-chlorotacrine). Normally, compounds with solubilities < 50 μM might present problems to solubilize in the aqueous media of the body. So, the solubility of these hybrids should be increased by introduction of polar groups than are not detrimental for the interactions of the compounds with their biological targets.

On the other hand, microsomal stability is another relevant pharmacokinetic parameter, as it helps to have an idea of the metabolism that a compound will suffer within the body. Microsomes contain metabolising enzymes that are bound to endoplasmic reticulum such as CYPs and other phase I metabolic enzymes. As phase I metabolism reactions are normally the most relevant processes that participate in the degradation of a drug, the assessment of the microsomal stability affords a valuable prediction of the metabolism than a compound will suffer *in vivo*. Amongst the novel hybrids, compounds **68a** and **(–)-16** present an extremely fast phase I metabolism in the three species evaluated (human, mouse, and rat), with less than 5% of the compounds remaining after 1 h in all the cases. Compounds **68b-c** present slower metabolism in humans, with 34% and 55% of the compound

remaining after 1 h, but still a fast metabolism in mice. Metabolism in rats is slower but still fast for compound **68c** and very fast for **68b**.

Table 4.4. Solubility and microsomal stability assays of the hydrochloride salts of the new hybrids **68a-c, (+)-16**, and **(**–**)-16**.

Compound	Solubility (µM)	Microsomal stability (h/m/r)[a] (remanent % at 1 h)
68a	43	4 / 1 / 4
68b	14	34 / 1 / 2
68c	7	55 / 2 / 21
(+)-16	nd[b]	nd[b]
(–)-16	6	1 / 0 / 4

[a] h: human, m: mouse, r: rat

[b] nd: not determined

CHAPTER 6

Biological evaluation of amyloidogenic proteins aggregation in E. coli cells

6.1 Amyloidogenic proteins and conformational diseases

Amyloid aggregation is a process where some peptides or proteins undergo conformational changes into misfolded species with high tendency to aggregate. In this process, hydrophobic residues, generally buried in the folded structures, come to the surface of the protein, increasing the intermolecular attractive forces and favouring self-association into increasingly ordered and insoluble fibrils.[196] It has been demonstrated that amyloid aggregation and native folding are processes that compete in the cell. In fact, amyloid-prone proteins are normally poorly expressed in the cell, while proteins with low aggregation propensity are more abundantly expressed. Alterations in the cell environment, such as stress or pathological conditions, can modify cell conditions and may trigger amyloid processes.[197] Although in some cases amyloid aggregates play physiological roles, normally amyloidogenic proteins are the cause of several human diseases, the so-called conformational diseases, amyloidoses, or protein misfolding disorders. These encompass a broad range of different diseases, from neurodegenerative disorders, such as Alzheimer's, Parkinson's or Huntington's diseases to non-neurodegenerative disorders as, for example, type II diabetes and cataracts.[198]

Traditionally, conformational diseases have been investigated separately, in order to find a specific inhibitor for a specific amyloid-prone protein. However, despite having different amino acid composition, length, and *in vivo* distribution, different amyloidogenic proteins aggregate into similar highly ordered structures, displaying a pleated β-sheet structure in a cross-β conformation, in which β-strands are oriented perpendicular to the fibril axis (**Figure 6.1**).[198,199] This fact raises the question of whether common treatments against different amyloidogenic proteins could be found, for example, compounds able to block the formation of β-sheet structures or the elongation of amyloid fibrils, thus becoming generic anti-aggregating agents or amyloid pan-inhibitors.

---

[196] a) A. Aguzzi, T. O'Connor. *Nat. Rev. Drug Discov.* **2010**, *9*, 237–248. b) L. Goldschmidt, P. K. Teng, L. Riek, D. Eisenberg. *Proc. Natl. Acad. Sci. U.S.A.* **2010**, *107*, 3487–3492.

[197] F. Rousseau, L. Serrano, J. W. Schymkowitz. *J. Mol. Biol.* **2006**, *355*, 1037−1047.

[198] F. Chiti, C. M. Dobson. *Annu. Rev. Biochem.* **2006**, *75*, 333−366.

[199] D. Eisenberg, R. Nelson, M. R. Sawaya, M. Balbirnie, S. Sambashivan, M. I. Ivanova, A. O. Madsen, C. Riekel. *Acc. Chem. Res.* **2006**, *39*, 568−575.

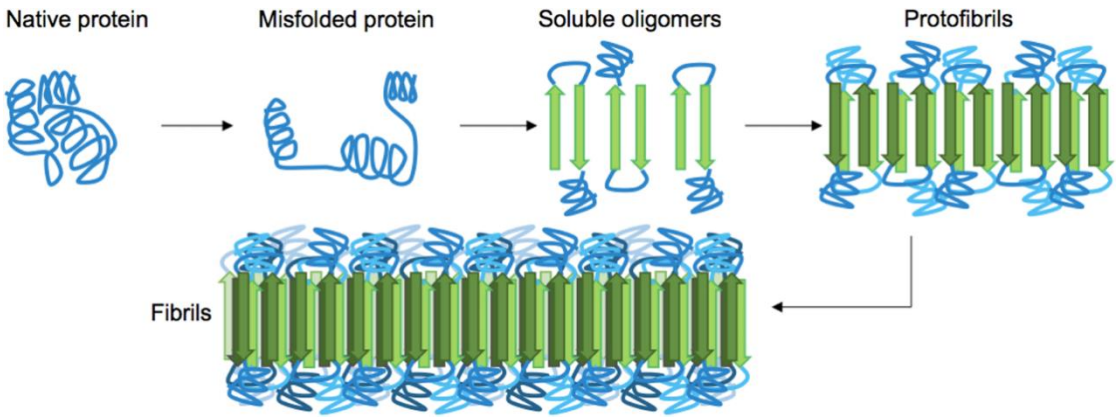

Figure 6.1. Simplified pathway towards amyloid fibril formation. In the misfolded state proteins have an increased propensity to aggregate by association of their metastable β-sheet domains. (Image source: C. F. Kaminski, G. S. Kaminski Schierle. *Neurophotonics* **2016**, *3*, 041807).

6.2 Use of bacterial inclusion bodies (IBs) for the rapid screening of amyloid aggregation inhibitors

Normally, the screening of inhibitors of amyloid aggregation is performed *in vitro*, which requires the use of expensive synthetic peptides and results troublesome due to the high sensitivity of the assay to several factors, such as purity or experimental conditions.[200,201] In addition, aggregation of proteins *in vivo* is dependent on numerous interactions and factors within the cellular environment, which are impossible to mimic *in vitro*, where the protein of study is isolated. As a consequence, aggregation of proteins can proceed through different pathways *in vitro* and *in vivo*, thus leading to differences in the aggregates,[202] which challenges the reliability of *in vitro* experiments.

During the production of proteins in bacteria, aggregation also occurs, leading to insoluble protein aggregates called inclusion bodies (IBs).[203] It has been demonstrated that these IBs present highly ordered amyloid-like structures,[204,205] making bacteria a simple but biologically relevant system to study the mechanisms of amyloid folding and deposition. The amyloid aggregates inside bacteria

[200] I. W. Hamley. *Chem. Rev.* **2012**, *112*, 5147−5192.
[201] a) M. Bartolini, C. Bertucci, M. L. Bolognesi, A. Cavalli, C. Melchiorre, V. Andrisano. *ChemBioChem* **2007**, *8*, 2152−2161. b) T. Akaishi, T. Morimoto, M. Shibao, S. Watanabe, K. Sakai-Kato, N. Utsunomiya-Tate, K. Abe. *Neurosci. Lett*. **2008**, *444*, 280−285.
[202] S. W. Pimplikar. *Int. J. Biochem. Cell Biol.* **2009**, *41*, 1261−1268.
[203] S. Ventura, A. Villaverde. *Trends Biotechnol.* **2006**, *24*, 179−185.
[204] N. S. de Groot, R. Sabate, S. Ventura. *Trends Biochem. Sci.* **2009**, *34*, 408−416.
[205] M. Carrió, N. González-Montalbán, A. Vera, A. Villaverde, S. Ventura. *J. Mol. Biol*. **2005**, *347*, 1025−1037.

can be monitored using conformational-sensitive fluorescent dyes. Thioflavin-S (Th-S) is the most suitable amyloid specific dye for *in vivo* experiments, due to its ability to cross membranes and to penetrate inside cells without interfering with the amyloid processes. When Th-S binds to amyloid deposits, this causes an increment in the intensity and a shift on the maximum of fluorescence in the amyloid band.[206, 207]

In this context, the group of Dr. Raimon Sabaté (*Universitat de Barcelona*) developed a few years ago a rapid, simple, and cost-effective bacterial assay for the screening of amyloid aggregation inhibitors, based on the direct Th-S staining of bacterial IBs in intact *E. coli* cells.[174,206,208] In the presence of an aggregation inhibitor, the Th-S staining fluorescence is significantly decreased, as a consequence of the diminution of amyloid-like structures (**Figure 6.2**). By measuring the differences in fluorescence compared to the adequate controls, the antiaggregating capacity of a compound can be quantified. Moreover, this assay, initially developed only for antiaggregating activity against $A\beta_{42}$, was then extrapolated to tau protein,[174] demonstrating than this methodology can be applied to other amyloidogenic proteins that form IBs when overexpressed in *E. coli* cells.

[206] A. Espargaró, R. Sabate, S. Ventura. *Mol. Biosyst.* **2012**, *8*, 2839–2844.
[207] H. LeVine III. *Methods Enzymol.* **1999**, *309*, 274–284.
[208] A. Espargaro, A. Medina, O. Di Pietro, D. Muñoz-Torrero, R. Sabate. *Sci. Rep.* **2016**, *6*, 23349.

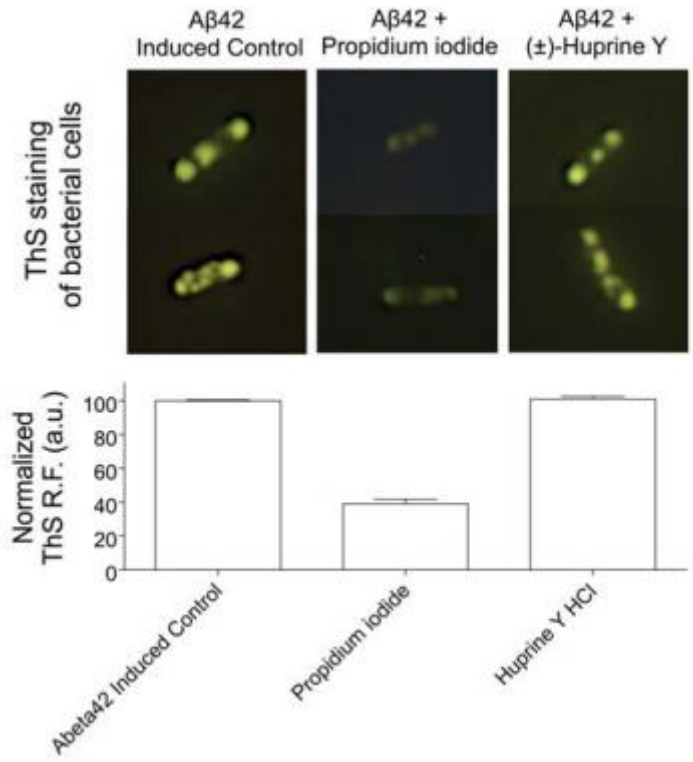

Figure 6.2. Th-S staining of bacterial cells overexpressing $A\beta_{42}$ peptide in the absence and in the presence of an active (propidium iodide) and inactive ((±)-huprine Y) antiaggregating compound. Up: optical fluorescence microscopy images. Down: Th-S relative fluorescence. Excitation and emission wavelengths of 375 and 455 nm have been used, respectively (Image source: S. Pouplana, A. Espargaró, C. Galdeano, E. Viayna, I. Sola, S. Ventura, D. Muñoz-Torrero, R. Sabate. *Curr. Med. Chem*. **2014**, *21*, 1152–1159).

6.3 Biological evaluation of different inhibitors of amyloidogenic proteins aggregation

6.3.1 Evaluation of $A\beta_{42}$ and tau antiaggregating activity

As previously discussed in some chapters of this PhD Thesis, the aggregation of Aβ peptide into senile plaques and the aggregation of hyperphosphorylated protein tau into NFTs are the most prominent pathological hallmarks in the brain of AD patients. For this reason, our group incorporated several years ago the evaluation of antiaggregating properties as a routine assay when evaluating the multitarget biological profile of new compounds. Normally, the anti-Alzheimer multitarget hybrid compounds synthesised by our group are constituted by two aromatic moieties linked by tethers of different lengths and composition, which make them capable of interacting with the β-sheet structures of both proteins and blocking the β-sheet alignment to form fibrils, thus blocking the amyloid

aggregation. Indeed, our compounds are generally endowed with moderate to potent antiaggregating properties against both Aβ and tau.

The assessment of the $A\beta_{42}$ and tau antiaggregating properties of our compounds has been carried out by the group of Dr. Raimon Sabaté (*Universitat de Barcelona*). Since my second year of PhD, I have been responsible for performing this assay for all the new compounds synthesised by our group, under the supervision of Dr. Raimon Sabaté. Thus, apart from the evaluation of the compounds synthesised by myself in the present PhD Thesis (previously discussed in sections **3.5.3** and **4.5.3**), I also have carried out the evaluation of new compounds, belonging to other projects, synthesised by other members of our group.

In particular, I have evaluated six compounds synthesised as part of the PhD Thesis of Dr. F. Javier Pérez Areales, which belonged to two different projects. On the one hand, compounds **69** and **70** (**Figure 6.3**) were developed in a collaborative project between our group and the group of Prof. Santiago Vázquez (*Universitat de Barcelona*) devoted to the synthesis of novel benzohomoadamantane–tacrine hybrids with dual activity against AChE and NMDA receptors, i.e. the targets of the two only types of marketed anti-Alzheimer drugs.[209] On the other hand, compounds **71–74** (**Figure 6.4**) were developed as part of the second generation of rhein–huprine hybrids (mentioned in section **3.2**), with the idea of exploring the effect of the pyridinic ring basicity on the different biological activities.[168]

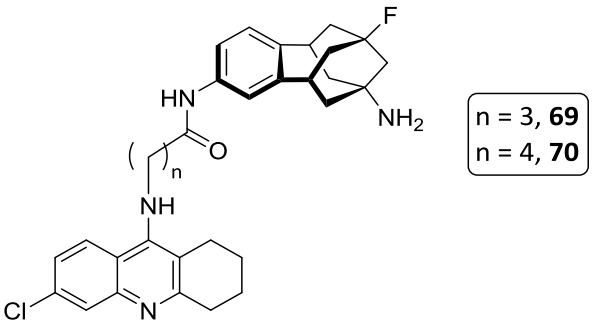

Figure 6.3. Structure of compounds **69** and **70**, evaluated in the $A\beta_{42}$ and tau antiaggregating assay. Hybrids **69** and **70** are part of a project that pursued the synthesis of new dual AChE inhibitors and NMDA receptor antagonists.

[209] F. J. Pérez-Areales, A. L. Turcu, M. Barniol-Xicota, C. Pont, D. Pivetta, A. Espargaró, M. Bartolini, A. De Simone, V. Andrisano, B. Pérez, R. Sabate, F. X. Sureda, S. Vázquez, D. Muñoz-Torrero. *Eur. J. Med. Chem.* **2019**, *180*, 613–626.

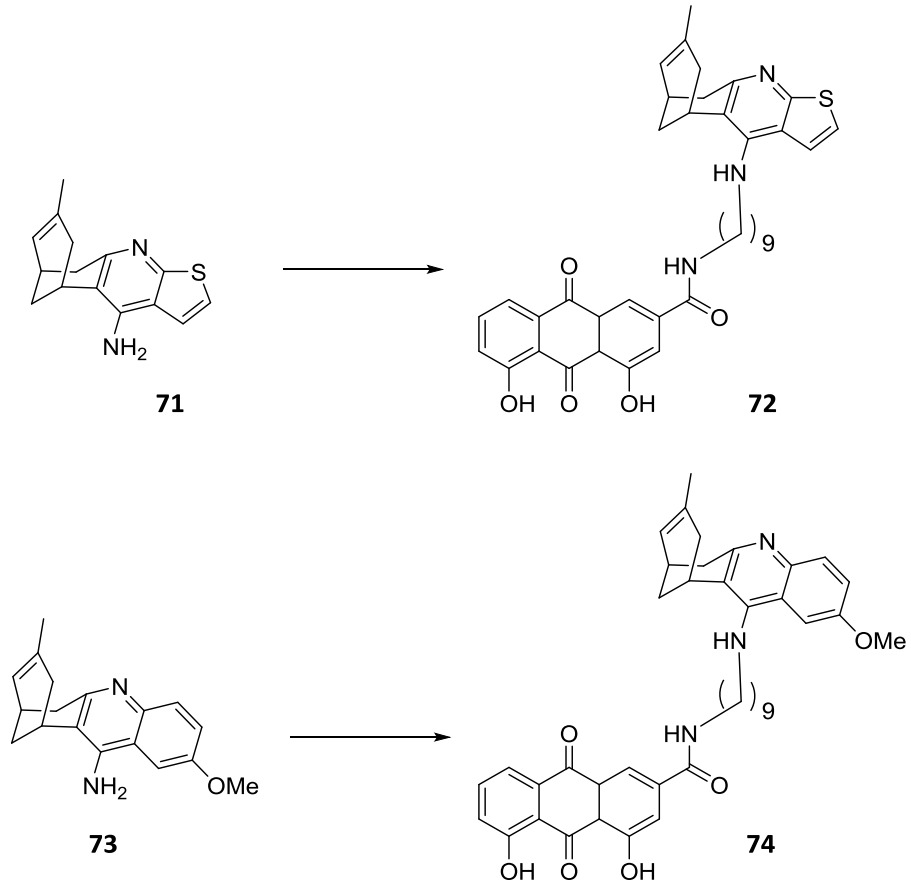

Figure 6.4. Structure of the monomeric modified huprines **71** and **73** and the corresponding second generation rhein–modified huprine hybrids **72** and **74**, evaluated in the $A\beta_{42}$ and tau antiaggregating assay.

The evaluation of these compounds and the target compounds of my PhD Thesis (discussed in sections **3.5.3** and **4.5.3**) against the aggregation of $A\beta_{42}$ and tau was performed following the methodology developed by the group of Dr. Raimon Sabaté,[174,206,208] which is described at the end of **Chapter 8**. The results of the antiaggregating activities of compounds **69–74** are detailed in **Table 6.1**. Compounds **69** and **70** were devoid of activity against the aggregation of $A\beta_{42}$ and were only weakly active against the aggregation of protein tau. This fact is presumably due the lack of a second planar extended π-system in these hybrids, which as previously mentioned seems to be necessary for the antiaggregating activity. The presence of the bicyclic system in the benzohomoadamantane moiety might sterically hamper a proper contribution of the benzene ring to the interaction with the β-sheet structures of the amyloid-prone proteins. In accordance with this fact, monomeric modified huprines **71** and **73** present also no or weak antiaggregating properties, as they lack a second planar aromatic system, whilst hybrids **72** and **74** present moderately potent inhibitory potencies against the aggregation of $A\beta_{42}$ and tau.

Table 6.1. $A\beta_{42}$ and tau antiaggregating activities of the hydrochloride salts of compounds **69–74**.

Compound	$A\beta_{42}$ aggregation[a] (% inh. at 10 μM)	Tau aggregation[a] (% inh. at 10 μM)
69	na[b]	6.9 ± 3.9
70	na[b]	22.9 ± 5.0
71	na[b]	2.6 ± 3.6
72	23.9 ± 1.1	40.7 ± 2.2
73	na[b]	12.8 ± 4.5
74	40.0 ± 2.7	52.4 ± 1.9

[a] % inhibition at 10 μM in intact *E. coli* cells. Values are expressed as mean ± SEM of at least three independent experiments.
[b] na: not active

6.3.2 Screening of $A\beta_{42}$ and tau antiaggregating agents against other amyloidogenic proteins: amyloid pan-inhibitors

Given the fact that different amyloidogenic proteins present similar structure in their aggregates, formed by pleated β-sheet structures, the idea of developing a single compound capable of blocking the aggregation of different amyloids by interfering in the β-sheets alignment seems feasible. In support to this idea, from our experience with different classes of compounds which were tested for their $A\beta_{42}$ and tau antiaggregating activity, we had consistently observed that when they were active against $A\beta_{42}$ aggregation, they were also active against tau aggregation, normally with quite similar potencies. To further explore the feasibility of developing amyloid pan-inhibitors which could afford a potential generic treatment for several conformational diseases, we planned the evaluation of several compounds developed in our group, endowed with $A\beta_{42}$ and tau antiaggregating activity, against a wide range of distinct amyloidogenic proteins.

Thus, we decided to evaluate the broad-spectrum antiaggregating capacity of two tacrine-based hybrids previously described by our group, namely DP128 and HUP7TH, against several amyloid-prone proteins, related and nonrelated with human diseases. Thus, 13 different amyloidogenic proteins were evaluated, which are representative of the range of amyloidogenic proteins, not only those linked to human conformational diseases, but also some present in bacteria, yeast and fungus.[210] In particular, the following proteins and peptides were chosen:

[210] A. Espargaró, C. Pont, P. Gamez, D. Muñoz-Torrero, R. Sabate. *ACS Chem. Neurosci.* **2019**, *10*, 1311–1317.

Peptides and proteins associated with human neurodegenerative diseases:

- $A\beta_{40}$ and $A\beta_{42}$ peptides, both implicated in AD.
- Tau protein and a truncated form of tau containing the aggregation-prone region (htau244-372), which are involved in AD and other tauopathies.
- Synucleins: human and mouse synucleins (synH and synM, respectively), implicated in Parkinson's disease.
- Prion protein (PrP): responsible for spongiform encephalopathies (Creutzfeldt-Jakob in humans or mad cow disease in cattle).

Proteins associated with human non-neurological disorders:

- Transthyretin (TTR), responsible for several transthyretin-related amyloidoses (ATTR).
- Human islet amyloid polypeptide (hIAPP or amylin): a key factor in the progression of type 2 diabetes by aggregation into toxic amyloids, which causes loss of pancreatic β-cells.

Amyloidogenic fungal, yeast, and bacterial proteins:

- PaHET-s, a prion-forming domain (PFD) present in filamentous fungus *Podospora anserina*.
- FgHET-s, a prion-forming domain (PFD) present in filamentous fungus *Fusarium graminium*.
- Sup35NM, an amyloid-prone fragment of a eukaryotic translation release factor, present in *Saccharomyces cerevisiae*.
- The N-terminal domain of *Escherichia coli* carbamoyltransferase HypF (HypF-N).

To validate this hypothesis, two compounds previously developed in our group were chosen: DP128, **75** (**Figure 6.5**), which presents inhibitory activity against Aβ and tau aggregation,[211] and HUP7TH, **76**, which inhibits the aggregation of Aβ and the prion peptide PrP106–126.[212,213] For the latter compound, both enantiomers, **(+)-(7*R*,11*R*)-76** and **(–)-(7*S*,11*S*)-76**, were evaluated. Moreover, the structurally related (±)-huprine Y, **(±)-7**, was used as a negative control due to its poor inhibitory activity against Aβ and tau aggregation.

[211] O. Di Pietro, F. J. Pérez-Areales, J. Juárez-Jiménez, A. Espargaró, M. V. Clos, B. Pérez, R. Lavilla, R. Sabate, F. J. Luque, D. Muñoz- Torrero. *Eur. J. Med. Chem.* **2014**, *84*, 107−117.

[212] D. Muñoz-Torrero, M. Pera, J. Relat, M. Ratia, C. Galdeano, E. Viayna, I. Sola, X. Formosa, P. Camps, A. Badia, M. V. Clos. *Neurodegener. Dis.* **2012**, *10*, 96−99.

[213] C. Galdeano, E. Viayna, I. Sola, X. Formosa, P. Camps, A. Badia, M. V. Clos, J. Relat, M. Ratia, M. Bartolini, F. Mancini, V. Andrisano, M. Salmona, C. Minguillon, G. C. González-Muñoz, M. I. Rodríguez- Franco, A. Bidon-Chanal, F. J. Luque, D. Muñoz-Torrero. *J. Med. Chem.* **2012**, *55*, 661−669.

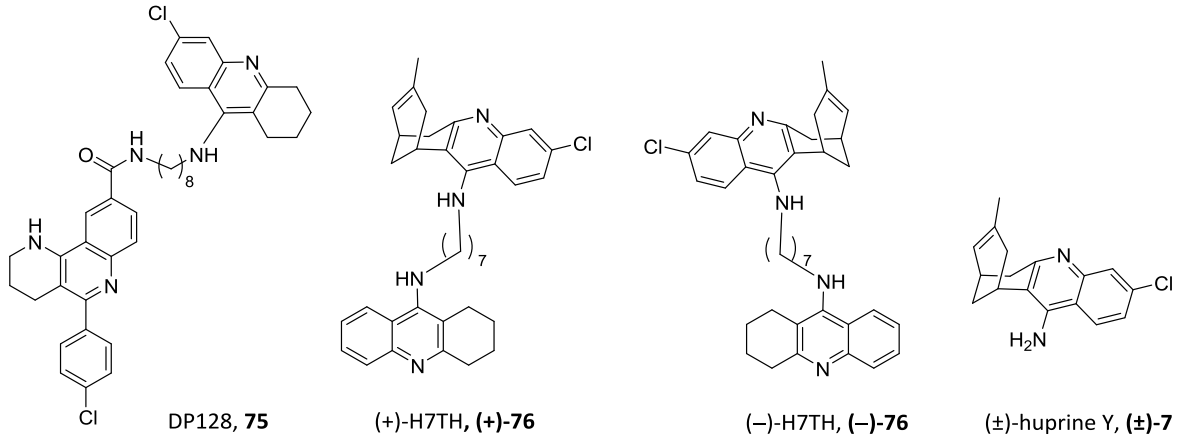

Figure 6.5. Chemical structures of the compounds evaluated against several amyloidogenic proteins. Compounds **75**, **(+)-76**, and **(–)-76** were expected to be inhibitors of aggregation. (±)-huprine Y was used as negative control.

Assay of antiaggregating activity

The evaluation of the four compounds against the 13 amyloidogenic proteins was performed following the method previously discussed.[174,206,208] As we expected, both DP128, **75**, and H7TH, **76**, are able to prevent the aggregation of a wide range of amyloidogenic proteins, from both human and cattle conformational diseases, and from fungus, yeast, and bacteria (**Table 6.2**). At a concentration of 10 μM, **75** was capable of inhibiting the aggregation of the seven amyloidogenic proteins linked to neurodegenerative conformational diseases with an inhibitory potency in the range 64–87% (average of 73%). Moreover, it presented also antiaggregating properties against the two proteins linked to non-neurological amyloidoses, even though with a slightly lower potency than for the previous group, with percentages of inhibition in the range 51–62% (average of 56%). Finally, **75** also acted as an inhibitor of the aggregation of the four fungal, yeast, and bacterial proteins, with an efficacy of 59–83% (average of 70%).

On the other hand, for compound **76**, both enantiomers displayed analogous behaviour against all evaluated proteins, therefore excluding any enantiomeric effect on the aggregation process. Indeed, at a concentration of 10 μM, **(+)-76** and **(–)-76** presented average percentages of inhibition of 58% and 57%, respectively, against amyloidogenic proteins related to neurodegenerative diseases; 78% and 79%, respectively, for amyloidogenic proteins associated with non-neurological conformational diseases; and 70% and 69%, respectively, for fungal, yeast, and bacterial amyloid-prone proteins. When comparing both inhibitors, compound **75** resulted to be a slightly better inhibitor

than compound **76** for neurodegenerative diseases (73% *vs* 57−58% on average), whereas the opposite occurred with non-neurological diseases (56% *vs* 78−79% on average). The two compounds are equally efficient against fungal, yeast, and bacterial amyloidogenic proteins (70 and 69−70%, respectively, on average). As anticipated, (±)-huprine Y did not display remarkable antiaggregating properties. At a concentration of 10 μM, inhibitory potencies of around 10% were observed for most amyloid-prone proteins. Only for tau, PaHET-s PFD and Sup35NM, 20% inhibition was reached, which is clearly below the values obtained for compounds **75** and **76.**

Table 6.2. Antiaggregating activities of the hydrochloride salts of compounds **75**, **(+)-76**, **(–)-76**, and (±)-huprine Y, **(±)-7**.

Protein	75 (% inhibition)[a]	(+)-76 (% inhibition)[a]	(–)-76 (% inhibition)[a]	(±)-huprine Y (% inhibition)[a]
Amyloidogenic proteins associated with neurodegenerative diseases				
$A\beta_{40}$	69.1 ± 0.9	50.4 ± 1.4	53.0 ± 1.1	10.7 ± 1.1
$A\beta_{42}$	69.9 ± 1.1	44.3 ± 1.8	42.8 ± 1.8	1.7 ± 0.6
tau	74.6 ± 4.2	65.7 ± 3.1	62.8 ± 2.8	24.1 ± 4.2
htau(244-372)	78.9 ± 2.8	72.2 ± 3.1	71.8 ± 3.8	13.1 ± 2.2
SynH	66.1 ± 1.4	56.8 ± 1.3	57.7 ± 1.1	7.7 ± 1.8
SynM	65.1 ± 1.2	45.6 ± 2.7	51.2 ± 3.0	1.7 ± 2.1
PrP	86.6 ± 3.3	71.5 ± 3.5	63.2 ± 2.1	11.8 ± 2.0
Amyloidogenic proteins associated with non-neurological diseases				
TTR	50.9 ± 2.6	75.9 ± 1.0	80.7 ± 0.4	4.0 ± 3.0
hIAPP	61.6 ± 3.6	80.4 ± 2.6	77.6 ± 4.8	7.7 ± 1.4
Fungal, yeast, and bacterial amyloidogenic proteins				
PaHET-s PFD	82.6 ± 0.5	75.9 ± 2.1	77.2 ± 1.5	27.9 ± 3.3
FgHET-s PFD	68.7 ± 3.5	71.8 ± 4.9	72.2 ± 4.8	14.3 ± 3.6
Sup35NM	59.2 ± 2.5	67.1 ± 1.9	65.8 ± 1.6	19.9 ± 1.5
HypFN	70.2 ± 1.5	66.9 ± 2.4	61.2 ± 2.4	10.3 ± 2.8

[a] % inhibition at 10 μM in intact *E. coli* cells. Values are expressed as mean ± SEM of at least three independent experiments.

A summary of the inhibitory potencies of each compound against all amyloidogenic proteins can be seen in **Figure 6.6** and **Table 6.3**. As we envisaged, compounds **75**, **(+)-76**, and **(–)-76** showed pan-inhibitory effects (with an average inhibition of >60% for all compounds, **Figure 6.6** and **Table 6.3**) against 13 amyloidogenic proteins encompassing the different types of existing amyloid-prone proteins. The fact that standard errors of the mean (SEMs) < 5% were obtained in all cases, is indicative that a close correlation exists between the inhibitory effects observed for all these unrelated proteins.

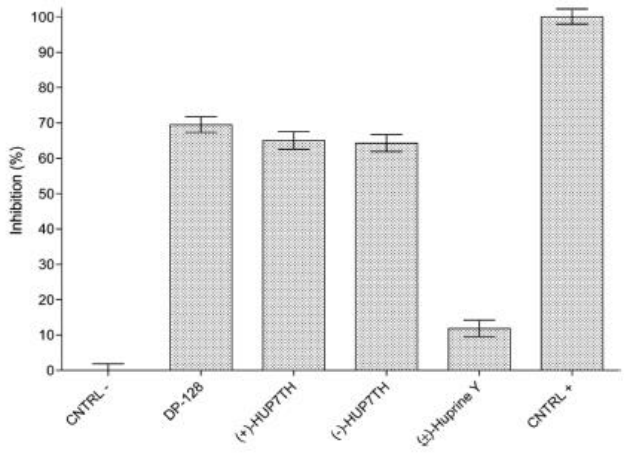

Compound	% inhibition[a]
Control (+)	100 ± 2.8
75	69.5 ± 2.2
(+)-76	65.0 ± 2.5
(–)-76	64.3 ± 2.4
(±)-huprine Y	11.9 ± 2.3
Control (–)	0.0 ± 1.8

Figure 6.6 and Table 6.3. Average antiaggregating activities of the compounds evaluated towards the 13 selected amyloid-prone proteins, at a compound concentration of 10 μM. The results are shown as the mean values of n > 10 independent assays. SEMs are < 5% in all cases. **Control (+)** is a sample not expressing any amyloid-prone protein (minimal amyloid presence), and **Control (–)** is a sample overexpressing the amyloid-prone protein in the absence of an inhibitor (DMSO, maximal amyloid presence).

Accuracy analysis

Although clear differences were observed between inhibitors and non-inhibitors of amyloid aggregation, in order to ensure the statistical significance of the experiment an accurate analysis was performed, using a receiver operating characteristic (ROC) curve and comparing the areas under the curves (AUCs). Thus, the fraction of true positives out of the total true positives (sensitivity) *versus* the fractions of false positives out of the total actual negatives (specificity) is plotted at various thresholds. The resulting AUC estimates the statistical significance of the classification assay, showing the accuracy of the discrimination. As shown in **Figure 6.7**, the ROC plots obtained in this experiment evidenced the total accuracy of the discrimination between active and inactive anti-amyloid agents in all tested amyloidogenic proteins (AUC = 100%), without false positives and negatives, thereby validating the initial hypothesis.

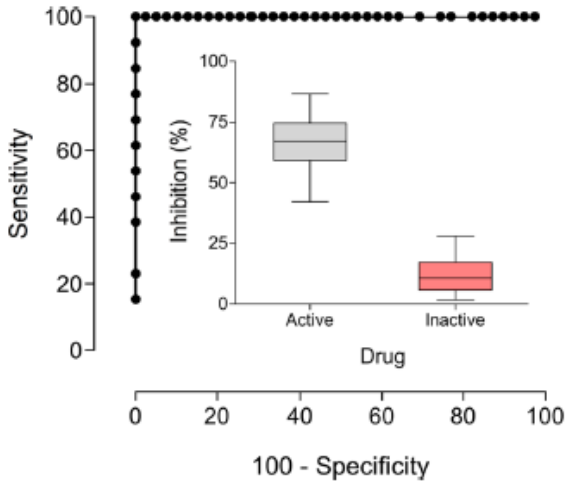

Figure 6.7. Differences between active and inactive anti-amyloid agents for all tested amyloid-prone proteins. ROC plots showing the accuracy in the discrimination between active and inactive antiaggregating agents. The inset shows the performance and box plots showing differences in inhibitory activity between active and inactive molecules.

Evaluation of interferences

Due to the fact that the compounds evaluated in these assays feature flat aromatic moieties, they might establish π-stacking interactions with the aromatic structure of the dye Th-S. In order to make sure that there were not any interferences between the compounds and Th-S, a comparative study with other two conformation-sensitive fluorescent dyes, namely Th-T and Congo Red (CR) was performed. This assay could not be carried out with the *in vivo E. coli* methodology previously used, because CR possesses intrinsic amyloid inhibition capacity,[214] which could interfere with the experiment, and Th-T is a P-glycoprotein substrate, which may cause an inappropriate internalization of the dye into bacterial cells.[215] As a consequence, the *in vitro* inhibitory activities of the four compounds against the aggregation of $A\beta_{40}$ was analysed, using the three different dyes, namely, Th-S, Th-T, and CR (**Table 6.4**). Gratifyingly, similar inhibitory effects were observed using the three specific amyloid dyes. Moreover, they were very close to those obtained in the cell-based assays. So, these results allowed us to discard any interaction between the evaluated compounds and Th-S, ensuring that the antiaggregating effect of these compounds is exclusively due to the direct interaction with the amyloidogenic proteins and not with the dye Th-S.

[214] P. Spólnik, B. Stopa, B. Piekarska, A. Jagusiak, L. Konieczny, J. Rybarska, M. Król, I. Roterman, B. Urbanowicz, J. Zieba-Palus. *Chem. Biol. Drug Des.* **2007**, *70*, 491−501.
[215] N. Darghal, A. Garnier-Suillerot, M. Salerno. *Biochem. Biophys. Res. Commun.* **2006**, *343*, 623−629.

Table 6.4. Comparison of the *in vitro* inhibitory activity of compounds **75**, **(+)-76**, **(–)-76**, and (±)-huprine Y against Aβ40 aggregation using Th-S, Th-T, and CR as dyes.

	% inhibition[a] at 10 μM of drug		
	Th-S	**Th-T**	**CR**
without drug[b]	0.0	0.0	0.0
75	70.0	69.6	62.5
(+)-76	54.8	54.5	44.8
(–)-76	51.7	57.9	45.4
(±)-huprine Y	7.3	7.4	13.4

[a] Values are the result of at least three independent experiments, with standard deviations of < 5% in all cases.

[b] The same amount of DMSO was added in the sample.

CHAPTER 7

Conclusions

7.1 Modified rhein–huprine hybrids

The first objective of this PhD Thesis was the preparation of a third generation of rhein–huprine hybrids. These compounds formally derived from a first series of rhein–huprine hybrids developed in our group 5 years ago, which displayed a very interesting *in vitro* and *in vivo* multitarget anti-Alzheimer profile. In a second step, a second generation of this family was synthesised in our group, with modifications in the huprine aromatic ring of the lead compound of the first family, **10**, in order to explore the influence of the pyridinic ring basicity on the biological activities. In this PhD Thesis, a third generation of these hybrids was designed by replacement of the rhein subunit of the previous generations of hybrids by more simplified analogues, aiming to obtain optimized hybrids with better physicochemical and pharmacokinetic properties and a similar or improved multitarget biological profile. The target hybrids were prepared through a short synthetic sequence involving as the key step the amide coupling of aminononylhuprine, **29**, with the appropriate carboxylic acids or sulfonyl chloride. Hybrids **23a** and **23b** were obtained by demethylation of the methoxypyridine fragment of hybrids **22a** and **22b**. These compounds were found to be potent inhibitors of *h*AChE and *h*BChE, in agreement with the expected dual site binding in both enzymes. Moreover, these compounds presented moderately potent inhibitory potencies against BACE1, with compounds **20b**, **20c**, **25c**, and **25g** being in the same range of potency than the lead **10**, good $A\beta_{42}$ and tau antiaggregating properties and good copper chelation properties, even though they were found to be weak radical scavengers. Of note, in general these compounds should be able to cross the BBB, according to the results of the *in vitro* PAMPA-BBB assay and the majority of them do not elicit significant toxicities or are toxic at high doses in the neurotoxicity and zebra fish model assays, making them interesting lead compounds in the search of new drugs against AD.

7.2 Huprine–based BACE1 multisite inhibitors

Regarding the second objective of this PhD Thesis, a new family of huprine-based hybrids with predicted BACE1 multisite binding was designed, synthesised, fully characterised, and biologically evaluated. The design strategy consisted of the hybridization of huprine Y with new scaffolds identified in a virtual screening campaign over a secondary floppy pocket in BACE1, which was found by computational studies of the lead rhein–huprine hybrid **10** within BACE1. The target hybrids were prepared by alkylation of (±)-huprine Y with 9-bromononanenitrile, followed by either reduction or hydrolysis of the resulting nitrile intermediate **28** to the primary amine **29** or the carboxylic acid **47**, respectively, and a final amide coupling with the adequate acids (carboxylic or sulfonic) or amines. The

synthesis of hybrid **51** needed an additional demethylation step, from hybrid **48**. These compounds were found to be very potent inhibitors of *h*AChE and potent inhibitors of *h*BChE. Contrary to our expectations of a high BACE-1 inhibitory potency arising from a dual site binding within this enzyme, the new hybrids resulted to be inactive or weak inhibitors of BACE1, except for compound **44**, which, with an IC_{50} value of 2.71 μM, displayed a similar potency as the lead rhein–huprine hybrid **10** under equivalent assay conditions. Additionally, these compounds were endowed with moderate to potent antiaggregating activities against $A\beta_{42}$ and tau, and some of them present good antioxidant properties, being able to act as radical scavengers or Cu (II) chelators. They should be able to cross the BBB according to the high permeability values observed in the PAMPA-BBB assay and they were found to be essentially non-toxic or toxic at high doses in a nerutoxicity assay and in a zebra fish toxicity model. Even though this new class of hybrids, in general, does not present the BACE1 inhibitory potency that we expected, they still present an interesting multitarget biological profile. It must be mentioned that the virtual screening over the secondary pocket of BACE1 was performed *in silico* and the binding affinities of the selected scaffolds were only predictions, which not always correspond to what we observe experimentally. The best compound of the family was hybrid **(±)-44**, with potent inhibitory activities against *h*AChE and *h*BChE, moderate activity against BACE1, and potent antiaggregating properties against both $A\beta_{42}$ and tau.

7.3 Huprine–TPPU and 6-chlorotacrine–TPPU hybrids

The third objective of this Thesis was the synthesis of a class of huprine–TPPU and 6-chlorotacrine–TPPU hybrids, designed by combination of a sEH inhibitor pharmacophore with an AChE inhibitor moiety, through oligomethylenic linkers, pursuing a dual inhibitory activity, and, in the case of AChE in a dual site binding mode. The tacrine-based hybrids with shorter methylenic linker (n = 2, 3) were prepared through a synthetic route that involved the amination of a tacrine-derived 4-chloroquinoline intermediate with a suitable amino alcohol, followed by mesylation of the alcohol, and a nucleophilic substitution with sodium cyanide to afford an advanced cyanoalkylhuprine precursor. The synthesis of the tetramethylene-linked 6-chlorotacrine- and huprine-based hybrids involved an initial alkylation of 6-chlorotacrine and (+)-(7*R*,11*R*)- or (–)-(7S,11S)-huprine Y themselves with 5-bromovaleronitrile to yield the advanced cyanoalkyltacrine or cyanoalkylhuprine precursor. Final hydrolysis of the precursor nitriles to the corresponding carboxylic acids and amide coupling with the TPPU-derived piperidine afforded the target hybrids. Overall, these compounds displayed very good inhibitory potencies against both human AChE and sEH, according to what we expected from our design strategy. Regarding *h*BChE, these novel hybrids were found moderately potent, being clearly

selective for *h*AChE over *h*BChE. Finally, these compounds displayed good permeabilities in the PAMPA-BBB assay but they present, in general, only moderate aqueous solubility and poor microsomal stability, which warrants further lead optimization endeavours in order to improve their physicochemical and pharmacokinetic profile. This class of compounds has been protected in a patent with application Number: EP19382219.4, for which the PCT extension will be filed in March 2020.

7.4 Biological evaluation of amyloidogenic proteins aggregation in *E. coli* cells

The last objective of this PhD Thesis consisted of the biological evaluation of the inhibitory properties of new compounds against the aggregation of $A\beta_{42}$ and tau. The methodology followed for this assay involved the overexpression of amyloid-prone proteins in intact *E. coli* cells and the monitoring of the aggregation of these proteins into IBs by Th-S staining and fluorimetric measurement. The antiaggregating capacity of an inhibitor can be measured by the quantification of the reduction in the Th-S fluorescence when it binds to the IBs, as a consequence of the reduction of protein aggregation. On one side, the evaluation of $A\beta_{42}$ and tau antiaggregating properties was performed as a routine assay for the hybrids reported in **Chapters 3** and **4** of this Thesis, as well as for some other inhibitors synthesised by other members of our group. From my participation in the evaluation of the latter compounds, I am co-author in two publications in *Fut. Med. Chem.*[168] and *Eur. J. Med. Chem*.[209]

On the other hand, three compounds, previously developed by our group, were evaluated against 13 amyloidogenic proteins, including all the major types of amyloid-prone proteins, such as those causing neurodegenerative disorders in humans, those causing non-neurological disorders, or fungal, yeast, and bacterial proteins. The objective was to confirm the hypothesis that there may be common mechanisms that drive the aggregation of different amyloidogenic proteins and, therefore, that a common inhibitor for all these proteins could be found. Our results showed that the compounds evaluated presented pan-inhibitory effects (> 60% inhibition in all cases) against the 13 evaluated amyloid proteins, thus confirming the notion that common treatments for conformational diseases, caused by amyloid-prone proteins, can be found. Interestingly, although the tested compounds were able to inhibit all the studied proteins, some inhibition tendencies were observed depending on the nature of the amyloid-prone protein aggregates, therefore suggesting the potential for finding selective treatments against a specific type of amyloidosis. This work has resulted in a publication in *ACS. Chem. Neurosci.*[210]

CHAPTER 8

Experimental part

General Methods.

Melting points were determined in open capillary tubes with an MFB 59510M Gallenkamp melting point apparatus.

NMR spectra were carried out at *Centres Científics I Tecnològics de la Universitat de Barcelona* (CCiTUB). 400 MHz ^{1}H / 100.6 MHz ^{13}C NMR spectra were recorded on a Mercury-400 spectrometer. The chemical shifts are reported in ppm (δ scale) relative to solvent peak, and coupling constants are reported in Hertz (Hz). Assignments given for the NMR spectra of the new compounds have been carried out on the basis of DEPT, COSY ^{1}H / ^{1}H (standard procedures), and COSY ^{1}H / ^{13}C (gHSQC and gHMBC sequences) experiments. Multiplicities are reported as singlet (s), doublet (d), triplet (t), quadruplet (q), multiplet (m), complex signal and combinations thereof.

IR spectra were run on a FTIR Perkin-Elmer Spectrum RX I or Perkin-Elmer Spectrum TWO spectrophotometers, using potassium bromide (KBr) pellets, sodium chloride (NaCl) pellets or attenuated total reflectance (ATR) techniques. Absorption values are expressed as wavenumbers (cm^{-1}); only significant absorption bands are given.

Column chromatography was performed on silica gel 60 Å (Sigma Aldrich, 40 - 63 µm, 230-400 mesh) or with a CombiFlash R_f 150 Teledine ISCO provided with a UV-vis detector, with RediSep® R_f Normal-phase Silica Flash Columns (silica gel 60 Å̊, 35-70 µm, 230-400 mesh). Thin Layer Chromatography (TLC) was performed with aluminium-backed sheets with silica gel 60 F_{254} (Merck, ref 1.05554), and spots were visualized with UV light and / or 1% aqueous solution of $KMnO_4$.

Accurate mass spectra were recorded with ESI techniques on a Hewlett-Packard 5988[a] LC/MSD-TOF instrument at *Unitat d'Espectrometria de Masses dels Centres Científics i Tecnològics de la Universitat de Barcelona* (CCiTUB).

Solvent purification was carried out following the procedures described in: D. D. Perrin, W. L. F. Armarego. *Purification of Laboratory Chemicals*, 4th Edition, Butterworth-Heinemann: Oxford, 1996.

Analytical samples of all the compounds prepared in this PhD Thesis work were dried at 45 °C / 2 Torr for at least 72 h, using phosphorous pentoxide (P2O5, Sigma Aldrich, ref 79609) and Paraffin Wax (mp 53-58 °C, Sigma Aldrich, ref 327204). All the new compounds which were subjected to pharmacological evaluation possessed a purity ≥ 95% as evidenced by their analytical data.

Synthesis of 9-bromononanenitrile, 27.

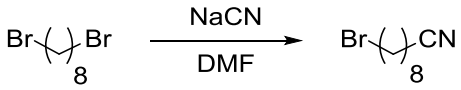

26 **27**

In a triple neck 250 mL round-bottomed flask equipped with a magnetic stirrer and inert atmosphere and connected to a 2N NaOH aq. sol. trap, 1,8-dibromooctane, **26**, (10.2 mL, 55.1 mmol) and NaCN (2.7 g, 55.1 mmol) were dissolved in anhydrous DMF (80 mL). The reaction mixture was heated at 35 °C for 2 h, quenched with water (60 mL), diluted with 1N NaOH (90 mL), and extracted with Et_2O (3 x 10 mL). The combined organic layers were washed with water (3 x 100 mL) and brine (3 x 100 mL), dried over anhydrous Na_2SO_4, filtered, and evaporated to dryness to give a colorless oil (12.3 g), which was split in two equal portions and subjected to purification through column chromatography (silica gel 35–70 μm, CombiFlash, 2 x 100 g, hexane / EtOAc mixtures, gradient elution). On elution with hexane / EtOAc 72:28 to 65:35, pure **27** (#60–90 -first column- and #62-90 -second column-, 5.71 g, 48% yield) was obtained as a colorless oil.

^{1}H NMR (400 MHz, $CDCl_3$) δ: 1.30–1.40 (complex signal, 4H, 5-CH_2, 6-H_2), 1.40–1.50 (complex signal, 4H, 4-H_2, 7-H_2), 1.66 (tt, J = J' = 7.2 Hz, 2H, 3-H_2), 1.86 (tt, J = J' = 7.2 Hz, 2H, 8-H_2), 2.34 (t, J = 7.2 Hz, 2H, 2-H_2), 3.41 (t, J = 7.2 Hz, 2H, 9-H_2).

Synthesis of (±)-9-[(3-chloro-6,7,10,11-tetrahydro-9-methyl-7,11-methanocycloocta[*b*]quinolin-12-yl)amino]nonanenenitrile, 28.

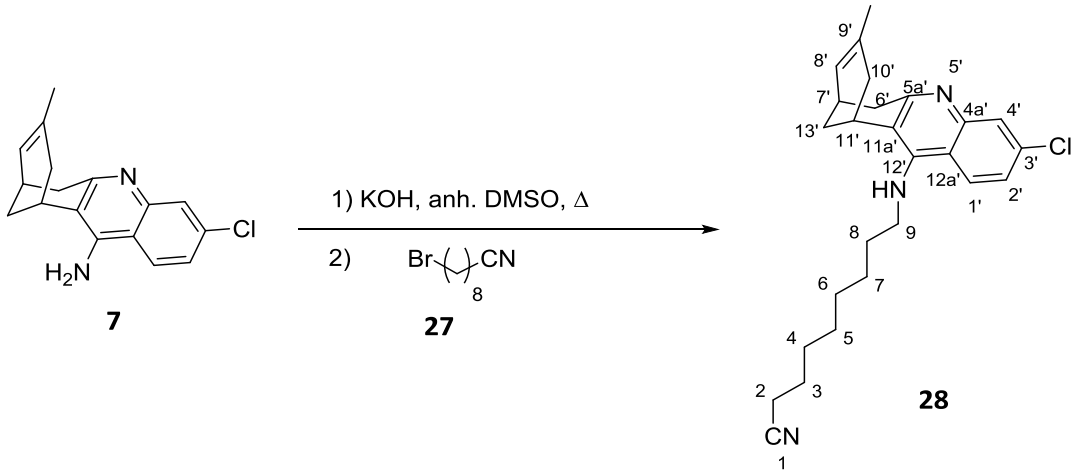

In a triple neck 25 mL round-bottomed flask equipped with magnetic stirrer, inert atmosphere, and 4Å molecular sieves, racemic huprine Y, **7**, (903 mg, 3.17 mmol) and finely powdered KOH (85% purity, 587 mg, 8.89 mmol) were suspended in anhydrous DMSO (13 mL). The resulting suspension was stirred, heating every 10 min with a heat gun for 1 h, and at r. t. for another hour, then treated with a solution of 9-bromononanenitrile, **27**, (761 mg, 3.49 mmol) in anhydrous DMSO (3 mL). The reaction mixture was stirred overnight at r. t., then diluted with 5N NaOH (100 mL) and extracted with EtOAc (3 x 70 mL). The combined organic layers were washed with water (4 x 100 mL) and brine (100 mL), dried over anhydrous Na_2SO_4, filtered and evaporated to dryness to provide a brown oil (2.68 g), which was purified through column chromatography (silica gel 40–63 μm, 65 g, Ø = 4 cm; #1, 300 mL, hexane / Et_3N 100:0.2; #2, 400 mL, hexane / EtOAc / Et_3N 95:5:0.2; #3, 400 mL, hexane / EtOAc / Et_3N 93:7:0.2; #4, 400 mL, hexane / EtOAc / Et_3N 91:9:0.2; #5-6, 900 mL, hexane / EtOAc / Et_3N 90:10:0.2; #7-8, 800 mL, hexane / EtOAc / Et_3N 88:12:0.2; #9-77, 7000 mL, hexane / EtOAc / Et_3N 87:13:0.2), to afford **28** (#17–65, 601 mg, 73% yield) as a yellow oil.

R_f = 0.71 (silica gel, 10 cm, CH_2Cl_2 / MeOH / 50% aq. NH_4OH 9.8:0.2:0.04)

^{1}H NMR (400 MHz, $CDCl_3$) δ: 1.30–1.48 (complex signal, 8H, 4-H_2, 5-H_2, 6-H_2, 7-H_2), 1.52 (s, 3H, 9'-CH_3), superimposed 1.52 (s, NH), 1.60–1.75 (complex signal, 4H, 3-H_2, 8-H_2), 1.81 (br d, *J* = 17.2 Hz, H, 10'-H_{endo}), 1.93 (dm, *J* = 12.4 Hz, 1H, 13'-H_{syn}), 2.05 (dm, *J* = 12.4 Hz, 1H, 13'-H_{anti}), 2.34 (t, *J* = 6.8 Hz, 2H, 2-H_2), 2.53 (dd, *J* = 17.2 Hz, *J'* = 5.2 Hz, 1H, 10'-H_{exo}), 2.74 (m, 1H, 7'-H), 2.99 (dt, *J* = 17.6 Hz, *J'* = 2.0 Hz, 1H, 6'-H_{endo}), 3.14 (dd, *J* = 17.6 Hz, *J'* = 5.6 Hz, 1H, 6'-H_{exo}), 3.29 (m, 1H, 11'-H), 3.46 (m, 2H, 9-H_2), 5.54 (br d, *J* = 5.2 Hz, 1H, 8'-H), 7.27 (dd, *J* = 9.2 Hz, *J'* = 2.0 Hz, 1H, 2'-H), 7.87 (d, *J* = 2.0 Hz, 1H, 4'-H), 9.72 (d, *J* = 9.2 Hz, 1H, 1'-H).

Synthesis of (±)-*N*-(3-chloro-6,7,10,11-tetrahydro-9-methyl-7,11-methanocycloocta[*b*]quinolin-12-yl)-1,9-diaminononane, 29.

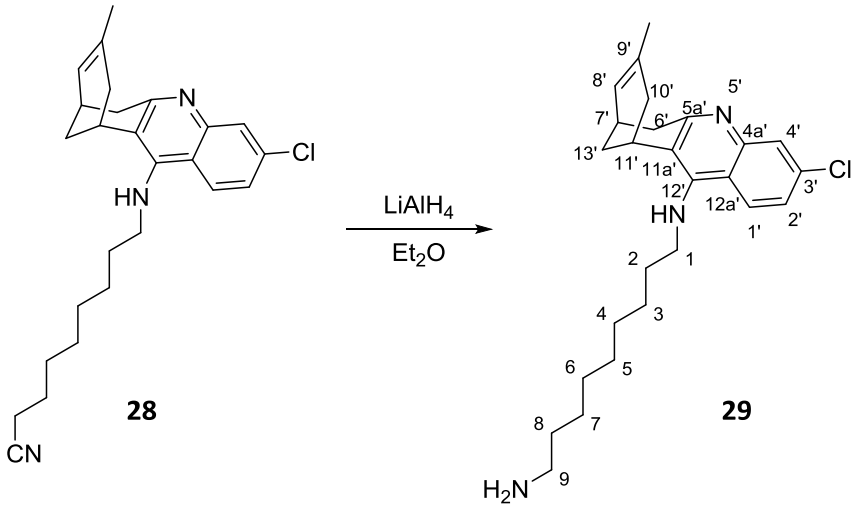

In a 100 mL round-bottomed flask provided with magnetic stirrer and inert atmosphere, nitrile **28** (1.36 g, 3.22 mmol) was dissolved in anhydrous Et_2O (48 mL), cooled down to 0 °C in an ice bath and treated dropwise with $LiAlH_4$ (4 M in Et_2O, 2.40 mL, 9.67 mmol). The resulting yellow suspension was stirred at r. t. overnight, diluted dropwise with 1N NaOH (60 mL) and water (120 mL), and extracted with EtOAc (3 x 120 mL). The combined organic extracts were dried over anhydrous Na_2SO_4, filtered, and evaporated to dryness to afford **29** (1.30 g, 96% yield) as a yellow oil.

R_f = 0.53 (silica gel, 10 cm, CH_2Cl_2 / MeOH / 50% aq. NH_4OH 9.8:0.2:0.07)

^{1}H NMR (400 MHz, $CDCl_3$) δ: 1.27–1.35 (complex signal, 10H, 3-H_2, 4-H_2, 5-H_2, 6-H_2, 7-H_2), 1.41 (tt, *J* = *J'* = 7.2 Hz, 2H, 8-H_2), 1.51 (s, 3H, 9'-CH_3), 1.70 (tt, *J* = *J'* = 7.2 Hz, 2H, 2-H_2), 1.81 (br d, *J* = 16.8 Hz, 1H, 10'-H_{endo}), 1.92 (dm, *J* = 12.4 Hz, 1H, 13'-H_{syn}), 2.04 (dm, *J* = 12.4 Hz, 1H, 13'-H_{anti}), 2.53 (dd, *J* = 16.8 Hz, *J'* = 5.6 Hz, 1H, 10'-H_{exo}), 2.68 (t, *J* = 7.2 Hz, 2H, 9-H_2), 2.73 (m, 1H, 7'-H), 2.99 (dt, *J* = 17.6 Hz, *J'* = 2.0 Hz, 1H, 6'-H_{endo}), 3.14 (dd, *J* = 17.6 Hz, *J'* = 5.6 Hz, 1H, 6'-H_{exo}), 3.30 (m, 1H, 11'-H), 3.46 (m, 2H, 1-H_2), 3.96 (br t, *J* = 17.6 Hz, NH), 5.54 (br d, *J* = 4.4 Hz, 1H, 8'-H), 7.26 (dd, *J* = 9.2 Hz, *J'* = 2.4 Hz, 1H, 2'-H), 7.87 (d, *J* = 2.4 Hz, 1H, 4'-H), 7.93 (d, *J* = 9.2 Hz, 1H, 1'-H).

Synthesis of (±)-*N*-{9-[(3-chloro-6,7,10,11-tetrahydro-9-methyl-7,11-methanocycloocta[*b*]quinolin-12-yl)amino]nonyl}anthraquinone-2-carboxamide, 20a.

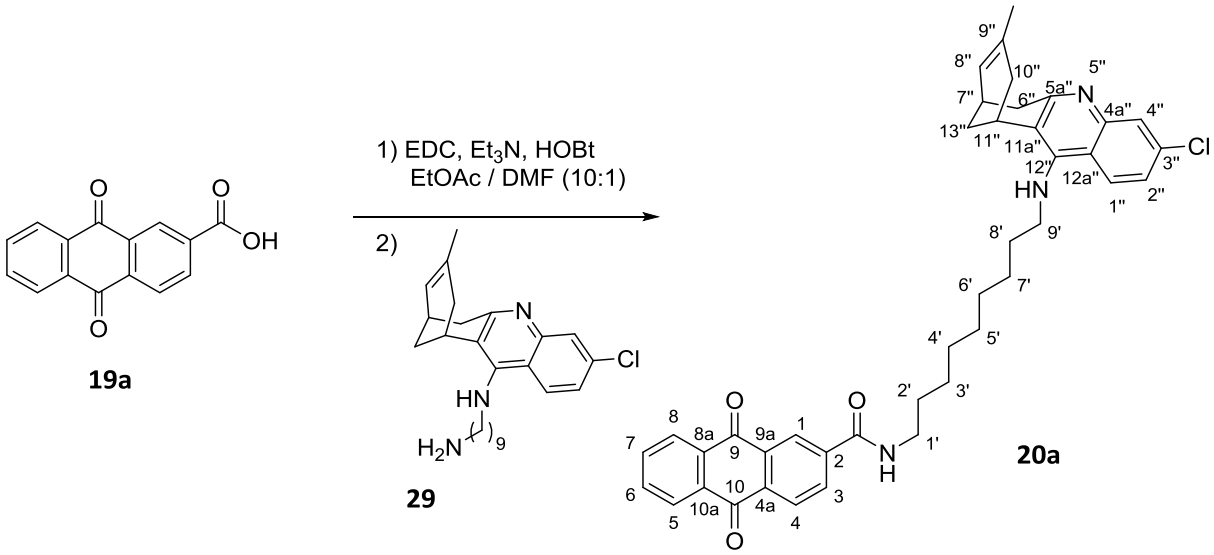

In a 25 mL round-bottomed flask provided with magnetic stirrer, anthraquinone-2-carboxylic acid, **19a**, (56 mg, 0.22 mmol) was suspended in a mixture of EtOAc / DMF (4.4 mL, 10:1), and treated subsequently with EDC·HCl (58 mg, 0.30 mmol), Et_3N (0.07 mL, 0.50 mmol), and HOBt (41 mg, 0.30 mmol). After stirring for 10 min at r. t., a solution of amine **(±)-29** (85 mg, 0.20 mmol) in EtOAc / DMF (2.2 mL, 10:1) was added and the reaction mixture was stirred at r. t. overnight, and then evaporated to dryness. The resulting yellow oil (307 mg) was purified through column chromatography (silica gel 40–63 µm, 14 g, Ø = 2 cm; #1, 100 mL, hexane / Et_3N 100:0.2; #2, 150 mL, hexane / EtOAc / Et_3N 90:10:0.2; #3, 150 mL, hexane / EtOAc / Et_3N 85:15:0.2, #4, 700 mL, hexane / EtOAc / Et_3N 82:18:0.2; #5-189, 3100 mL, hexane / EtOAc / Et_3N 80:20:0.2, #190-194, 100 mL, hexane / EtOAc / Et_3N 75:25:0.5), to afford **(±)-20a** (#5–192, 187 mg, quantitative yield) as a yellow oil.

R_f = 0.22 (silica gel, 10 cm, hexane / EtOAc / Et_3N 6:4:0.02)

Analytical sample of 20a·HCl

In a vial, **20a** (187 mg that could contain a maximum of 132 mg of product) was dissolved in CH_2Cl_2 (2 mL), filtered through a 0.2 µm PTFE filter, treated with excess of a solution of HCl in Et_2O (1 mL, 1.17 M) and evaporated to dryness. The resulting solid was washed with hexane (2 x 2 mL) and pentane (2 x 2 mL), evaporated to dryness, and dried at 45 °C/2 Torr for 5 days, to provide **20a·HCl** (94 mg) as a yellowish solid.

Melting Point: 123–125 °C

IR (ATR) ν: 3600–2200 (max at 3249, 3064, 2926, 2855, N–H, $^{+}$N–H, C–H st), 1674, 1633, 1584, (C=O, Ar–C–C, Ar–C–N st) cm^{-1}.

^{1}H NMR (400 MHz, CD_3OD) δ: 1.37–1.50 (complex signal, 10H, 3'-H_2, 4'-H_2, 5'-H_2, 6'-H_2, 7'-H_2), 1.59 (s, 3H, 9''-CH_3), 1.68 (tt, *J* = *J'* = 7.2 Hz, 2H, 2'-H_2), 1.85 (m, 2H, 8'-H_2) superimposed in part 1.89–1.96 (complex signal, 2H, 10''-H_{endo}, 13''-H_{syn}), 2.07 (dm, *J* = 11.2 Hz, 1H, 13''-H_{anti}), 2.53 (dd, *J* = 18.0 Hz, *J'* = 5.2 Hz, 1H, 10''-H_{exo}), 2.75 (m, 1H, 7''-H) superimposed in part 2.80 (dt, *J* = 18.0 Hz, *J'* = 2.0 Hz, 1H, 6''-H_{endo}), 3.15 (dd, *J* = 18.0 Hz, *J'* = 5.2 Hz, 1H, 6''-H_{exo}), 3.38 (m, 1H, 11''-H), 3.44 (td, *J* = 7.2 Hz, *J'* = 2.4 Hz, 2H, 1'-H_2), 3.89 (m, 2H, 9'-H_2), 4.85 (s, NH, $^{+}$NH), 5.58 (br d, *J* = 5.6 Hz, 1H, 8''-H), 7.43 (dd, *J* = 9.2 Hz, *J'* = 2.4 Hz, 1H, 2''-H), 7.59 (d, *J* = 2.4 Hz, 1H, 4''-H), 7.88 (m, 2H, 6(7)-H), 8.19–8.28 (complex signal, 4H, 3-H, 4-H, 5-H, 8-H), 8.31 (d, *J* = 9.2 Hz, 1H, 1''-H), 8.63 (d, *J* = 2.0 Hz, 1H, 1-H).

^{13}C NMR (100.6 MHz, CD_3OD) δ: 23.47 (CH_3, 9''-CH_3), 27.25 (CH, C11''), 27.65 ($2CH_2$, C6', C7'), 27.83 (CH, C7''), 29.27 (CH_2, C13''), 29.85 ($2CH_2$), 30.15 (CH_2), 30.20 (CH_2) (C2', C3', C4', C5'), 31.23 (CH_2, C8'), 35.98 ($2CH_2$, C6'', C10''), 41.04 (CH_2, C1'), 49.59 (CH_2, C9'), 115.42 (C, C12a''), 117.47 (C, C11a''), 119.09 (CH, C4''), 125.13 (CH, C8''), 126.60 (CH, C2''), 126.82 (CH, C1), 128.02 (CH), 128.10 (CH), 128.45 (CH) (C4, C5, C8), 129.29 (CH, C1''), 133.63 (CH, C3), 134.55 (C), 134.56 (C), 134.59 (C), 134.72 (C) (C4a, C8a, C10a, C9''), 135.59 (CH), 135.64 (CH) (C6, C7), 136.20 (C, C9a), 140.20 (C, C3''), 140.81 (C, C4a''), 141.09 (C, C2), 151.03 (C, C5a''), 156.66 (C, C12''), 168.13 (C, CONH), 183.36 (C), 183.38 (C) (C9, C10).

HRMS ESI:

Calculated for $[C_{41}H_{42}{}^{35}ClN_3O_3 + H]^{+}$:	660.2987
Found:	660.2983

Synthesis of (±)-*N*-{9-[(3-chloro-6,7,10,11-tetrahydro-9-methyl-7,11-methanocycloocta[*b*]quinolin-12-yl)amino]nonyl}-9-fluorenone-2-carboxamide, 20b.

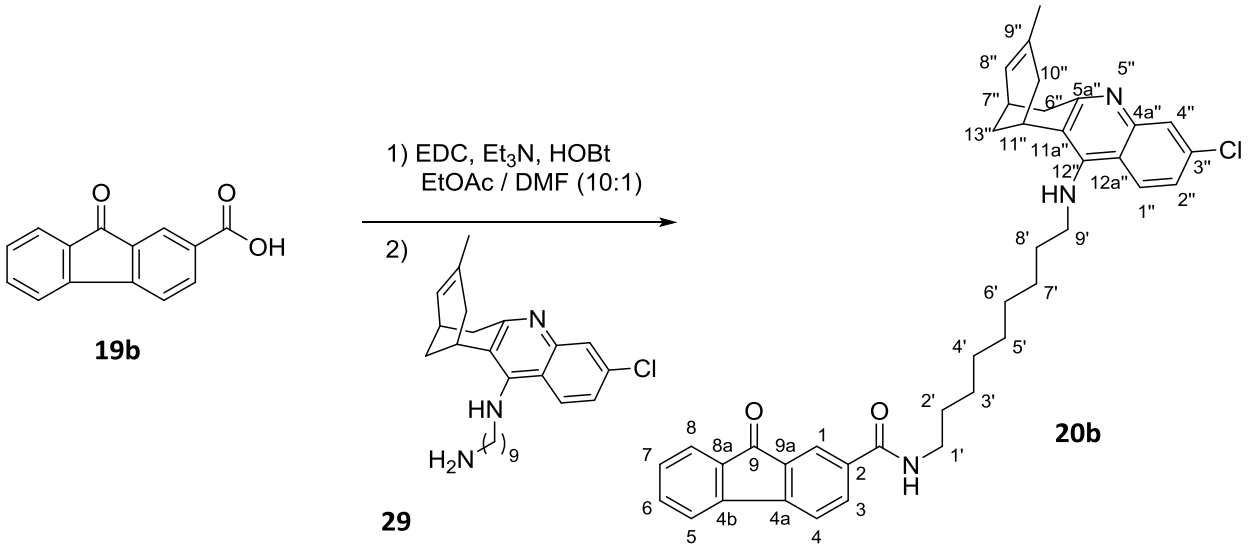

In a 25 mL round-bottomed flask equipped with magnetic stirrer, 9-fluorenone-2-carboxylic acid, **19b**, (70 mg, 0.31 mmol) was suspended in a mixture of EtOAc / DMF (3.8 mL, 10:1), and treated subsequently with EDC·HCl (66 mg, 0.42 mmol), Et_3N (0.08 mL, 0.56 mmol), and HOBt (58 mg, 0.42 mmol). After 10 min stirring at r. t., a solution of the amine **29** (120 mg, 0.28 mmol) in EtOAc / DMF (5.5 mL, 10:1) was added and the mixture was stirred at r. t. overnight, then evaporated to dryness. The resulting yellow oil (449 mg) was purified through column chromatography (silica gel 40–63 µm, 35 g, Ø = 3.5 cm; #1-5, 400 mL, CH_2Cl_2 / 50% aq. NH_4OH 100:0.4; #6-16, 600 mL, CH_2Cl_2 / MeOH / 50% aq. NH_4OH 99.9:0.1:0.4), to obtain **20b** (#3-13, 124 mg, 70% yield) as a yellow oil.

R_f = 0.83 (silica gel, 10 cm, CH_2Cl_2 / MeOH / 50% aq. NH_4OH 9:1:0.1)

Analytical sample of 20b·HCl

In a 25 mL round-bottomed flask, **20b** (124 mg) was dissolved in CH_2Cl_2 (4 mL), filtered through a 0.2 µm PTFE filter, treated with excess of a solution of HCl in Et_2O (2 mL, 1.17 M), and evaporated to dryness. The solid was washed with pentane (3 x 4 mL), and dried under *vacuum*, and the resulting brown solid was finally purified by dissolution with a few drops of MeOH, followed by dropwise addition of EtOAc to allow precipitation (88 mg). The resulting brown solid was dried at 45 °C/2 Torr for 3 days.

Melting Point: 218 °C

IR (ATR) ν: 3600–2300 (max at 3261, 3056, 2926, 2854, N–H, $^{+}$N–H, C–H st), 1715, 1630, 1582, 1511, 1456 (C=O, Ar–C–C, Ar–C–N st) cm^{-1}.

^{1}H NMR (400 MHz, CD_3OD) δ: 1.35–1.50 (complex signal, 10H, 3'-H_2, 4'-H_2, 5'-H_2, 6'-H_2, 7'-CH_2) 1.59 (s, 3H, 9''-CH_3), 1.64 (tt, *J* = *J'* = 6.8 Hz, 2H, 2'-H_2), 1.84 (tt, *J* = *J'* = 7.2 Hz, 2H, 8'-H_2) superimposed in part 1.90–1.98 (complex signal, 2H, 10''-H_{endo}, 13''-H_{syn}), 2.06 (dm, *J* = 12.4 Hz, 1H, 13''-H_{anti}), 2.53 (dd, *J* = 18.0 Hz, *J'* = 5.2 Hz, 1H, 10''-H_{exo}), 2.75 (m, 1H, 7''-H), 2.82 (br d, *J* = 17.2 Hz, 1H, 6''-H_{endo}), 3.16 (dd, *J* = 17.2 Hz, *J'* = 5.6 Hz, 1H, 6''-H_{exo}), 3.35–3.45 (complex signal, 2H, 11''-H, 1'-H_2), 3.89 (m, 2H, 9'-H_2), 4.85 (s, NH, $^{+}$NH), 5.58 (br d, *J* = 5.6 Hz, 1H, 8''-H), 7.38 (ddd, *J* = *J'* = 7.2 Hz, *J''* = 1.2 Hz, 1H, 6-H), 7.45 (dd, *J* = 9.2 Hz, *J'* = 2.0 Hz, 1H, 2''-H), 7.56 (br d, *J* = 7.2 Hz, 1H, 3-H) superimposed in part 7.58 (ddd, *J* = *J'* = 7.2 Hz, *J''* = 1.2 Hz, 1H, 7-H), 7.63 (d, *J* = 2.0 Hz, 1H, 4''-H), 7.67 (ddd, *J* = 7.2 Hz, *J'* = *J''* = 1.2 Hz, 1H, 5-H), 7.70 (d, *J* = 7.6 Hz, 1H, 4-H), 7.97 (d, *J* = 2.0 Hz, 1H, 1-H), 8.01 (ddd, *J* = 7.2 Hz, *J'* = *J''* = 1.6 Hz, 1H, 8-H), 8.26 (d, *J* = 9.2 Hz, 1H, 1''-H).

^{13}C NMR (100.6 MHz, CD_3OD) δ: 23.47 (CH_3, 9''-CH_3), 27.25 (CH, C11''), 27.65 ($2CH_2$, C6', C7'), 27.84 (CH, C7''), 29.29 (CH_2, C13''), 29.86 ($2CH_2$), 30.18 ($2CH_2$), (C2', C3', C4', C5'), 31.22 (CH_2, C8'), 36.00 ($2CH_2$, C6'', C10''), 40.91 (CH_2, C1'), 49.60 (CH_2, C9'), 115.49 (C, C12a''), 117.51 (C, C11a''), 119.15 (CH, C4''), 121.80 (CH), 122.45 (CH) (C4, C5), 123.51 (CH, C1), 125.10 (CH, C3), 125.14 (CH, C8''), 126.60 (CH, C2''), 129.32 (CH, C1''), 131.11 (CH, C6), 134.62 (C, C9''), 135.31 (C, C2), 135.38 (CH, C8), 136.54 (CH, C7), 135.53 (C), 136.85 (C) (C8a, C9a), 140.19 (C, C3''), 140.92 (C, C4a''), 144.75 (C), 148.26 (C) (C4a, C4b), 151.07 (C, C5a''), 156.73 (C, C12''), 168.67 (C, CONH), 185.05 (C, C9).

HRMS ESI:

Calculated for $[C_{40}H_{42}{}^{35}ClN_3O_2 + H]^+$: 632.3038

Found: 632.3034

Synthesis of (±)-3-benzoyl-*N*-{9-[(3-chloro-6,7,10,11-tetrahydro-9-methyl-7,11-methanocycloocta[*b*]quinolin-12-yl)amino]nonyl}benzamide, 20c

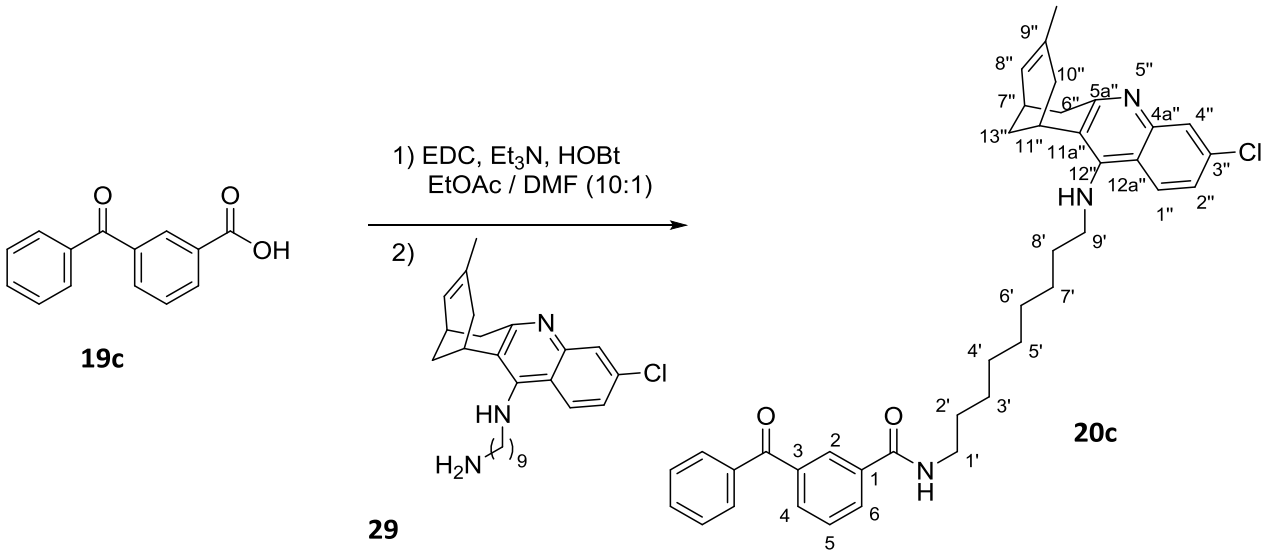

In a 25 mL round-bottomed flask equipped with magnetic stirrer, 3-benzoylbenzoic acid, **19c**, (88 mg, 0.39 mmol) was suspended in a mixture of EtOAc / DMF (4.5 mL, 10:1), and treated subsequently with EDC·HCl (82 mg, 0.53 mmol), Et_3N (0.1 mL, 0.72 mmol) and HOBt (72 mg, 0.53 mmol). After 10 min stirring at r. t., a solution of the amine **(±)-29** (150 mg, 0.35 mmol) in EtOAc / DMF (7.6 mL, 10:1) was added and the mixture was stirred at r. t. overnight, then evaporated to dryness. The resulting yellow oil (629 mg) was purified through column chromatography (silica gel 40–63 µm, 45 g, Ø = 4.5 cm; #1-4, 400 mL, CH_2Cl_2 / 50% aq. NH_4OH 100:0.4; #5-12, 400 mL, CH_2Cl_2 / MeOH / 50% aq. NH_4OH 99.9:0.1:0.4; #13-18, 200 mL, CH_2Cl_2 / 50% aq. NH_4OH 99.8:0.2:0.4; #19-25, 200 mL, CH_2Cl_2 / MeOH / 50% aq. NH_4OH 99.6:0.4:0.4; #26-31, 400 mL, CH_2Cl_2 / 50% aq. NH_4OH 99.5:0.5:0.4), to afford **(±)-20c** (#2-26, 216 mg, 96% yield) as a yellow oil.

R_f = 0.84 (silica gel, 10 cm, CH_2Cl_2 / MeOH / 50% aq. NH_4OH 9:1:0.1)

Analytical sample of (±)-20c·HCl

In a 25 mL round-bottomed flask, **(±)-20c** (216 mg) was dissolved in CH_2Cl_2 (5 mL), filtered through a 0.2 µm PTFE filter, treated with excess of a solution of HCl in Et_2O (2 mL, 1.17 M), and evaporated to dryness. The resulting solid was washed with pentane (3 x 4 mL) and evaporated to dryness, to provide a brown solid (112 mg). A portion of this solid (100 mg) was purified by dissolution with a few drops of MeOH, followed by dropwise addition of EtOAc to allow precipitation (95 mg). The resulting brown solid was dried at 45 °C/2 Torr for 3 days.

Melting Point: 125 °C

IR (ATR) ν: 3600–2400 (max at 3239, 3060, 2926, 2856, N–H, $^{+}$N–H, C–H st), 1657, 1632, 1582, 1568, 1525 (C=O, Ar–C–C, Ar–C–N st) cm^{-1}.

^{1}H NMR (400 MHz, CD_3OD) δ: 1.34–1.45 (complex signal, 10H, 3'-H_2, 4'-H_2, 5'-H_2, 6'-H_2, 7'-H_2), 1.57 (s, 3H, 9''-CH_3) superimposed in part 1.60 (m, 2H, 2'-H_2), 1.84 (tt, *J* = *J'* = 7.2 Hz, 2H, 8'-H_2), 1.92 (dm, *J* = 11.2 Hz, 1H, 13''-H_{syn}) superimposed in part 1.93 (br d, *J* = 17.2 Hz, 1H, 10''-H_{endo}) 2.06 (dm, *J* = 13.6 Hz, 1H, 13''-H_{anti}), 2.53 (dd, *J* = 17.6 Hz, *J'* = 5.6 Hz, 1H, 10''-H_{exo}), 2.75 (m, 1H, 7''-H), 2.87 (ddd, *J* = 18.0 Hz, *J'* = *J''* = 1.6 Hz, 1H, 6''-H_{endo}), 3.19 (dd, *J* = 18.0 Hz, *J'* = 5.6 Hz, 1H, 6''-H_{exo}), 3.73 (t, *J'* = 7.2 Hz, 2H, 1'-H_2), 3.43 (m, 1H, 11''-H), 3.96 (td, *J* = 7.2 Hz, *J'* = 2.8 Hz, 2H, 9'-H_2), 4.85 (s, NH, $^{+}$NH), 5.57 (br d, *J* = 5.2 Hz, 1H, 8''-H), 7.50–7.57 (complex signal, 3H, 2''-H, benzoyl H_{meta}), 7.60–7.68 (complex signal, 2H, 5-H, benzoyl H_{para}), 7.74–7.77 (complex signal, 3H, 4''-H, benzoyl H_{ortho}), 7.88 (dt, *J* = 7.6 Hz, *J'* = 1.6 Hz, 1H), 8.07 (dt, *J* = 8.0 Hz, *J'* = 1.6 Hz, 1H) (4-H, 6-H), 8.20 (t, *J* = 1.6 Hz, 1H, 2-H), 8.39 (d, *J* = 9.2 Hz, 1H, 1''-H).

^{13}C NMR (100.6 MHz, CD_3OD) δ: 23.47 (CH_3, 9''-CH_3), 27.27 (CH, C11''), 27.72, 27.84, 27.88 ($2CH_2$ + CH) (C6', C7', C7''), 29.30 (CH_2, C13''), 30.05 (CH_2), 30.09 (CH_2), 30.33 (CH_2), 30.38 (CH_2) (C2', C3', C4', C5'), 31.20 (CH_2, C8'), 36.03 (CH_2), 36.07 (CH_2) (C6'', C10''), 41.00 (CH_2, C1'), 49.67 (CH_2, C9'), 115.62 (C, C12a''), 117.56 (C, C11a''), 119.18 (CH, C4''), 125.15 (CH, C8''), 126.61 (CH, C2''), 129.43 (CH, C1''), 129.56 (CH, C5), 129.64 (2CH, benzoyl C_{meta}), 129.80 (CH, benzoyl C_{para}), 131.02 (2CH, benzoyl C_{ortho}), 132.10 (CH), 133.67 (CH), 134.08 (CH) (C2, C4, C6), 134.52 (C, C9''), 136.29 (C), 138.36 (C), 139.16 (C) (C1, C3, benzoyl C_{ipso}), 140.20 (C, C3''), 140.97 (C, C4a''), 151.21 (C, C5a''), 156.90 (C, C12''), 169.02 (C, CONH), 197.56 (C, benzoyl CO).

HRMS ESI:

Calculated for $[C_{40}H_{44}{}^{35}ClN_3O_2 + H]^{+}$:	634.3195
Found:	634.3187

Synthesis of (±)-3-acetyl-*N*-{9-[(3-chloro-6,7,10,11-tetrahydro-9-methyl-7,11-methanocycloocta[*b*]quinolin-12-yl)amino]nonyl}benzamide, 20d

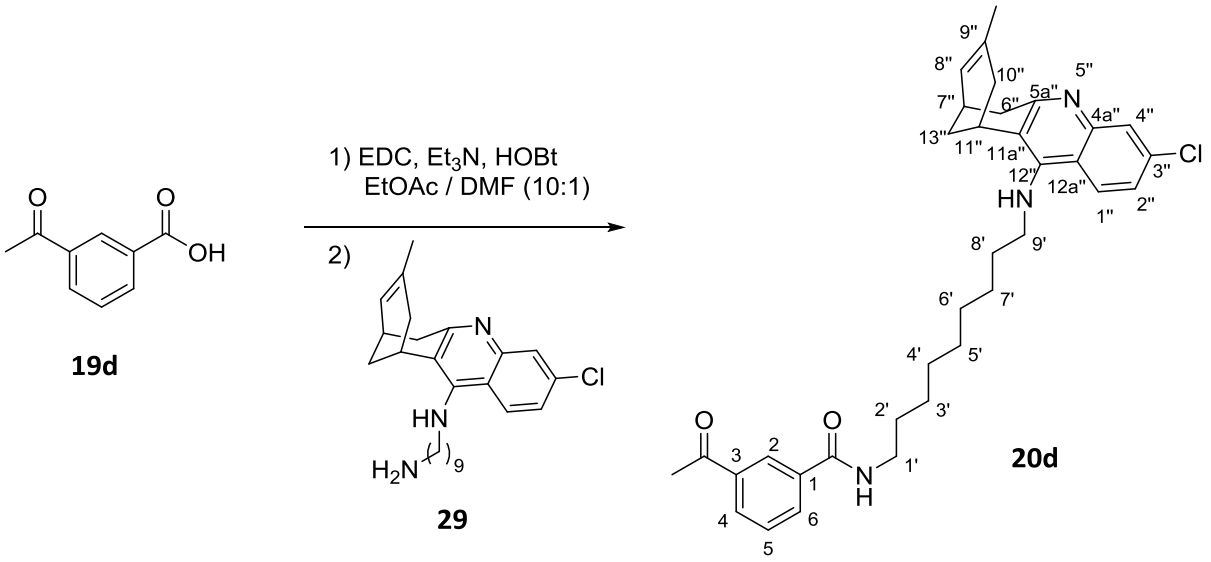

In a 25 mL round-bottomed flask equipped with magnetic stirrer, 3-acetylbenzoic acid, **19d**, (36 mg, 0.22 mmol) was suspended in a mixture of EtOAc / DMF (4.4 mL, 10:1), and treated subsequently with EDC·HCl (58 mg, 0.30 mmol), Et_3N (0.07 mL, 0.50 mmol) and HOBt (41 mg, 0.30 mmol). After 15 min stirring at r. t., a solution of the amine **29** (85 mg, 0.20 mmol) in EtOAc / DMF (2.2 mL, 10:1) was added and the mixture was stirred at r. t. overnight, then evaporated to dryness. The resulting brown oil (272 mg) was purified through column chromatography (silica gel 40–63 µm, 27 g, Ø = 3 cm; #1, 200 mL, hexane / Et_3N 100:0.2; #2, 250 mL, hexane / EtOAc / Et_3N 95:5:0.2; #3, 500 mL, hexane / EtOAc / Et_3N 90:10:0.2; #4, 1750 mL, hexane / EtOAc / Et_3N 85:15:0.2; #5, 900 mL, hexane / EtOAc / Et_3N 80:20:0.2; #6, 750 mL, hexane / EtOAc / Et_3N 72:28:0.2; #7-116, 1500 mL, hexane / EtOAc / Et_3N 70:30:0.2; #117-126, 250mL, hexane / EtOAc / Et_3N 60:40:0.5), to afford **20d** (#7-116, 146 mg, quantitative yield) as a yellow oil.

R_f = 0.13 (silica gel, 10 cm, hexane / EtOAc / Et_3N 6:4:0.02)

Analytical sample of 20d·HCl

In a vial, **(±)-20d** (146 mg that could contain a maximum of 114 mg of product) was dissolved in CH_2Cl_2 (2 mL), filtered through a 0.2 µm PTFE filter, treated with excess of a solution of HCl in Et_2O (1 mL, 1.17 M) and evaporated to dryness. The resulting solid was washed with hexane (2 x 2 mL) and pentane (2 x 2 mL), evaporated to dryness and dried at 45 °C/2 Torr for 5 days, to provide **20d·HCl** (92 mg) as a yellowish solid.

Melting Point: 85–87 °C

IR (ATR) ν: 3600–2300 (max at 3251, 3056, 2926, 2854, N–H, $^{+}$N–H, C–H st), 1684, 1632, 1582, 1568, 1541 (C=O, Ar–C–C, Ar–C–N st) cm^{-1}.

^{1}H NMR (400 MHz, CD_3OD) δ: 1.33–1.47 (complex signal, 10H, 3'-H_2, 4'-H_2, 5'-H_2, 6'-H_2, 7'-H_2), 1.58 (s, 3H, 9''-CH_3) superimposed in part 1.63 (m, 2H, 2'-H_2), 1.85 (tt, *J* = *J'* = 7.2 Hz, 2H, 8'-H_2), superimposed in part 1.89–1.96 (complex signal, 2H, 10''-H_{endo}, 13''-H_{syn}), 2.08 (dm, *J* = 12.8 Hz, 1H, 13''-H_{anti}), 2.54 (dd, *J* = 17.6 Hz, *J'* = 5.2 Hz, 1H, 10''-H_{exo}), 2.64 (s, 3H, CH_3CO), 2.77 (m, 1H, 7''-H), 2.85 (ddd, *J* = 18.0 Hz, *J'* = *J''* = 2.0 Hz, 1H, 6''-H_{endo}), 3.20 (dd, *J* = 18.0 Hz, *J'* = 5.6 Hz, 1H, 6''-H_{exo}), 3.39 (t, *J'* = 7.2 Hz, 2H, 1'-H_2) superimposed in part 3.43 (m, 1H, 11''-H), 3.97 (td, *J* = 7.6 Hz, *J'* = 3.2 Hz, 2H, 9'-H_2), 4.85 (s, NH, $^{+}$NH), 5.58 (br d, *J* = 5.6 Hz, 1H, 8''-H), 7.55 (dd, *J* = 9.2 Hz, *J'* = 2.4 Hz, 1H, 2''-H), 7.60 (ddd, *J* = *J'* = 8.0 Hz, *J''* = 0.8 Hz, 1H, 5-H), 7.74 (d, *J* = 2.4 Hz, 1H, 4''-H), 8.04 (ddd, *J* = 7.6 Hz, *J'* = 1.6 Hz, *J''* = 1.2 Hz, 1H), 8.14 (ddd, *J* = 7.6 Hz, *J'* = 1.6 Hz, *J''* = 1.2 Hz, 1H) (4-H, 6-H), 8.39 (d, *J* = 9.6 Hz, 1H, 1''-H) superimposed in part 8.41 (td, *J* = 1.6 Hz, *J'* = 0.8 Hz, 1H, 2-H).

^{13}C NMR (100.6 MHz, CD_3OD) δ: 23.47 (CH_3, 9''-CH_3), 26.81 (CH_3, *C*H_3CO), 27.27 (CH, C11''), 27.74, 27.85, 27.95 (2CH_2 + CH) (C6', C7', C7''), 29.30 (CH_2, C13''), 30.10 (CH_2), 30.17 (CH_2), 30.40 (CH_2), 30.43 (CH_2) (C2', C3', C4', C5'), 31.21 (CH_2, C8'), 36.03 (CH_2), 36.08 (CH_2) (C6'', C10''), 41.04 (CH_2, C1'), 49.67 (CH_2, C9'), 115.63 (C, C12a''), 117.57 (C, C11a''), 119.11 (CH, C4''), 125.12 (CH, C8''), 126.63 (CH, C2''), 128.06 (CH, C5), 129.46 (CH, C1''), 130.05 (CH), 132.16 (CH), 132.77 (CH) (C2, C4, C6), 134.53 (C, C9''), 136.42 (C), 138.55 (C) (C1, C3), 140.23 (C, C3''), 140.96 (C, C4a''), 151.17 (C, C5a''), 156.92 (C, C12''), 169.10 (C, CONH), 199.48 (C, CH_3*C*O).

HRMS ESI:

Calculated for $[C_{35}H_{42}{}^{35}ClN_3O_2 + H]^+$: 572.3038

Found: 572.3039

Synthesis of (±)-*N*-{9-[(3-chloro-6,7,10,11-tetrahydro-9-methyl-7,11-methanocycloocta[*b*]quinolin-12-yl)amino]nonyl}-6-methoxypyridine-2-carboxamide, 22a

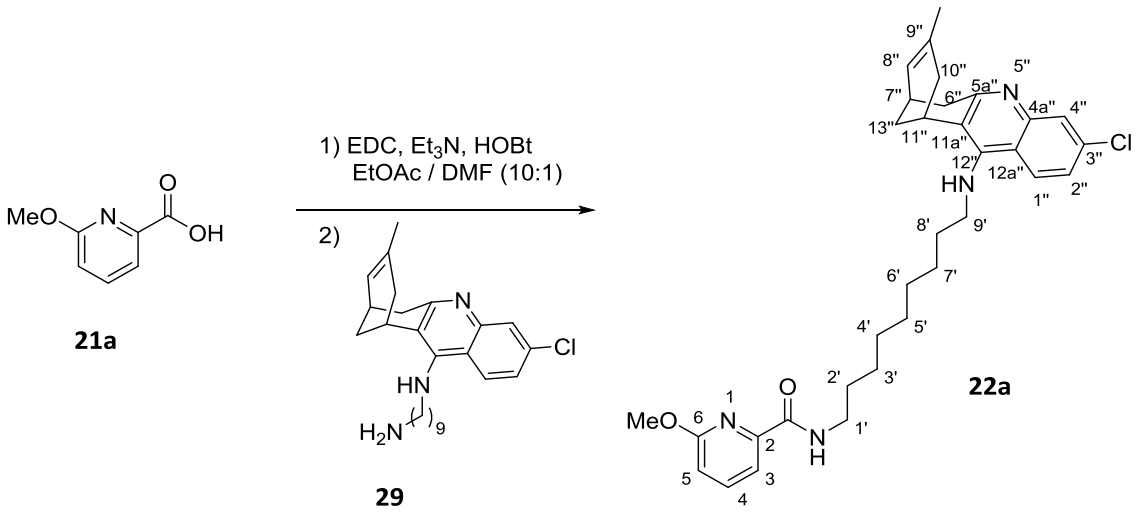

In a 50 mL round-bottomed flask equipped with magnetic stirrer, 6-methoxypyridine-2-carboxylic acid, **21a**, (113 mg, 0.74 mmol) was suspended in a mixture of EtOAc / DMF (13.2 mL, 10:1), and treated subsequently with EDC·HCl (192 mg, 1 mmol), Et_3N (0.17 mL, 1.67 mmol) and HOBt (136 mg, 1 mmol). After 10 min stirring at r. t., a solution of the amine **29** (285 mg, 0.67 mmol) in EtOAc / DMF (11 mL, 10:1) was added and the mixture was stirred at r. t. overnight, then evaporated to dryness. The resulting brown oil (946 mg) was purified through column chromatography (silica gel 40–63 µm, 47 g, Ø = 3 cm; #1, 300 mL hexane / EtOAc / Et_3N 95:5:0.2 #2, 300 mL, hexane / EtOAc / Et_3N 90:10:0.2, #3, 300 mL, hexane / EtOAc / Et_3N 85:15:0.2, #4, 300 mL, hexane / EtOAc / Et_3N 80:20:0.2, #5-221, 2400 mL, hexane / EtOAc / Et_3N 75:25:0.2), to afford **22a** (#44-209, 220 mg, 59% yield) as a brown oil.

R_f = 0.28 (silica gel, 10 cm, hexane / EtOAc / Et_3N 5:5:0.02)

Analytical sample of 22a·HCl

In a vial, **22a** (220 mg) was dissolved in CH_2Cl_2 (2 mL), filtered through a 0.2 µm PTFE filter, treated with excess of a methanolic solution of HCl (1 mL, 1.25 M) and evaporated to dryness. The resulting solid was washed with pentane (5 x 2 mL), evaporated to dryness and dried at 45 °C/2 Torr for 3 days, to provide **22a·HCl** (113 mg) as a yellowish solid.

Melting Point: 84–86 °C

IR (ATR) ν: 3500–2400 (max at 3253, 3056, 2926, 2854, N–H, $^{+}$N–H, C–H st), 1661, 1631, 1575, 1521, 1465 (C=O, Ar–C–C, Ar–C–N st) cm^{-1}.

^{1}H NMR (400 MHz, CD_3OD) δ: 1.32–1.47 (complex signal, 10H, 3'-H_2, 4'-H_2, 5'-H_2, 6'-H_2, 7'-H_2), 1.58 (s, 3H, 9''-CH_3) superimposed in part 1.62 (tt, *J* = *J'* = 6.8 Hz, 2H, 2'-H_2), 1.84 (tt, *J* = *J'* = 7.2 Hz, 2H, 8'-H_2) superimposed in part 1.90 (m, 1H, 13''-H_{syn}) superimposed in part 1.93 (br d, *J* = 16.4 Hz, 1H, 10''-H_{endo}), 2.08 (dm, *J* = 12.4 Hz, 1H, 13''-H_{anti}), 2.54 (dd, *J* = 17.6 Hz, *J* = 4.4 Hz, 1H, 10''-H_{exo}), 2.76 (m, 1H, 7''-H), 2.86 (dt, *J* = 18.0 Hz, *J'* = 1.6 Hz, 1H, 6''-H_{endo}), 3.20 (dd, *J* = 18.0 Hz, *J'* = 5.6 Hz, 1H, 6''-H_{exo}), 3.40 (t, *J* = 6.8 Hz, 2H, 1'-H_2) superimposed in part 3.43 (m, 1H, 11''-H), 3.96 (m, 2H, 9'-H_2), 3.98 (s, 3H, 6-OCH_3), 4.85 (s, NH, $^{+}$NH), 5.58 (br d, *J* = 4.8 Hz, 1H, 8''-H), 6.94 (d, *J* = 8.4 Hz, 1H, 5-H), 7.54 (dd, *J* = 9.2 Hz, *J'* = 2.4 Hz, 1H, 2''-H), 7.64 (d, *J* = 7.2 Hz, 1H, 3-H), 7.75 (d, *J* = 2.4 Hz, 1H, 4''-H) superimposed in part 7.78 (dd, *J* = 8.4 Hz, *J'* = 7.2 Hz, 1H, 4-H), 8.38 (d, *J* = 9.2 Hz, 1H, 1''-H).

^{13}C NMR (100.6 MHz, CD_3OD) δ: 23.46 (CH_3, 9''-CH_3), 27.27 (CH, C11''), 27.73 (CH_2), 27.85 (CH_2) (C6', C7'), 27.93 (CH, C7''), 29.30 (CH_2, C13''), 30.09 (CH_2), 30.18 (CH_2), 30.42 (CH_2), 30.60 (CH_2) (C2', C3', C4', C5'), 31.19 (CH_2, C8'), 36.03 (CH_2), 36.07 (CH_2) (C6'', C10''), 40.45 (CH_2, C1'), 49.56 (CH_2, C9'), 54.12 (CH_3, 6-OCH_3), 115.45 (CH, C5), 115.63 (C, C12a''), 116.26 (CH, C3), 117.57 (C, C11a''), 119.11 (CH, C4''), 125.12 (CH, C8''), 126.63 (CH, C2''), 129.46 (CH, C1''), 134.53 (C, C9''), 140.23 (C, C3''), 140.96 (C, C4a''), 141.03 (CH, C4), 148.61 (C, C2), 151.17 (C, C5a''), 156.93 (C, C12''), 164.64 (C, C6), 166.54 (C, CONH).

HRMS ESI:

Calculated for $[C_{33}H_{41}{}^{35}ClN_4O_2 + H]^+$: 561.2991

Found: 561.2983

Synthesis of (±)-*N*-{9-[(3-chloro-6,7,10,11-tetrahydro-9-methyl-7,11-methanocycloocta[*b*]quinolin-12-yl)amino]nonyl}-4-methoxypyridine-2-carboxamide, 22b

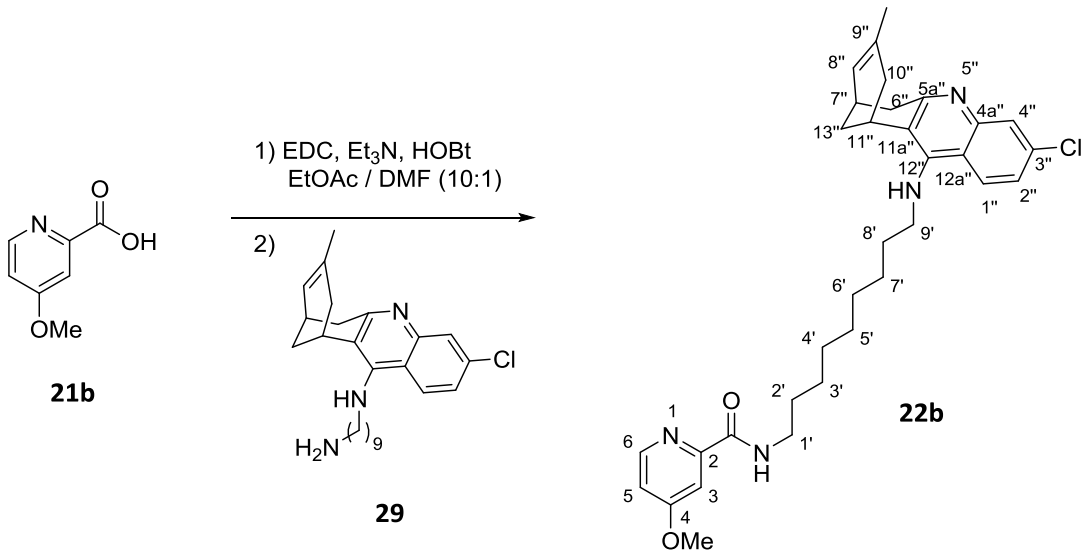

In a 25 mL round-bottomed flask equipped with magnetic stirrer, 4-methoxypyridine-2-carboxylic acid, **21b**, (51 mg, 0.33 mmol) was suspended in a mixture of EtOAc / DMF (5.5 mL, 10:1), and treated subsequently with EDC·HCl (86 mg, 0.45 mmol), Et_3N (0.21 mL, 1.5 mmol) and HOBt (61 mg, 0.45 mmol). After 10 min stirring at r. t., a solution of the amine **29** (150 mg, 0.30 mmol) in EtOAc / DMF (4.4 mL, 10:1) was added and the mixture was stirred at r. t. overnight, then evaporated to dryness. The resulting dark yellow oil (570 mg) was purified through column chromatography (silica gel 40–63 µm, 30 g, Ø = 3 cm; #1, 300 mL hexane / EtOAc / Et_3N 95:5:0.2 #2, 300 mL, hexane / EtOAc / Et_3N 90:10:0.2, #3, 300 mL, hexane / EtOAc / Et_3N 85:15:0.2, #4-21, 2600 mL, hexane / EtOAc / Et_3N 80:20:0.2, #22-26, 500 mL, hexane / EtOAc / Et_3N 75:25:0.2; #27-45, 1600 mL, hexane / EtOAc / Et_3N 70:30:0.2, #46-52, 500 mL, hexane / EtOAc / Et_3N 70:30:0.5; #53-58, 500 mL, hexane / EtOAc / Et_3N 65:35:1), to afford **22b** (#28-53, 146 mg, 87% yield) as a yellow oil.

Analytical sample of 22b

In an initial attempt of formation of the hydrochloride salt of **22b** the product was partially demethylated upon reaction with HCl. As a consequence, **22b** was characterized and tested as a base. **22b** (146 mg) was dissolved in MeOH (15 mL) and washed with hexane (2 x 10 mL) and pentane (10 mL) in a separatory funnel. The methanolic layer was evaporated to dryness and dried at 45 °C/2 Torr for 3 days, to provide **22b** (81 mg) as a brown sticky solid.

R_f = 0.14 (silica gel, 10 cm, hexane / EtOAc / Et_3N 5:5:0.02).

IR (ATR) ν: 3377, 2925, 2855 (N–H, C–H st), 1671, 1599, 1555, 1524 (C=O, Ar–C–C, Ar–C–N st) cm^{-1}.

^1H NMR (400 MHz, CD_3OD) δ: 1.25–1.40 (complex signal, 10H, 3'-H_2, 4'-H_2, 5'-H_2, 6'-H_2, 7'-H_2), 1.51 (s, 3H, 9''-CH_3), 1.59 (tt, *J* = *J'* = 7.2 Hz, 2'-H_2), 1.69 (tt, *J* = *J'* = 7.2 Hz, 2H, 8'-H_2), 1.86 (br d, *J* = 17.6 Hz, 1H, 10''-H_{endo}) superimposed in part 1.90 (dm, *J* = 12.0 Hz, 1H, 13''-H_{syn}), 2.03 (dm, *J* = 12.0 Hz, 1H, 13''-H_{anti}), 2.52 (dd, *J* = 17.6 Hz, *J'* = 5.6 Hz, 1H, 10''-H_{exo}), 2.68 (m, 1H, 7''-H), 2.88 (dt, *J* = 17.2 Hz, *J'* = 2.0 Hz, 1H, 6''-H_{endo}), 3.07 (dd, *J* = 17.2 Hz, *J'* = 5.2 Hz, 1H, 6''-H_{exo}), 3.38 (t, *J'* = 7.2 Hz, 2H, 1'-H_2) superimposed in part 3.42 (m, 1H, 11''-H), 3.56 (t, *J* = 7.2 Hz, 2H, 9'-H_2), 3.90 (s, 3H, 4-OCH_3), 4.85 (s, NH), 5.52 (br d, *J* = 5.6 Hz, 1H, 8''-H), 7.03 (dd, *J* = 5.6 Hz, *J'* = 2.4 Hz, 1H, 5-H), 7.29 (dd, *J* = 9.2 Hz, *J'* = 2.4 Hz, 1H, 2''-H), 7.61 (d, *J* = 2.4 Hz, 1H, 3-H), 7.71 (d, *J* = 2.4 Hz, 1H, 4''-H), 8.06 (d, *J* = 9.2 Hz, 1H, 1''-H), 8.57 (d, *J* = 5.6 Hz, 1H, 6-H).

^{13}C NMR (100.6 MHz, CD_3OD) δ: 23.60 (CH_3, 9''-CH_3), 27.88 (CH_2), 27.94 (CH_2) (C6', C7'), 28.38 (CH, C11''), 29.44 (CH, C7''), 30.11 (CH_2, C13''), 30.20 (CH_2), 30.22 (CH_2), 30.44 (CH_2), 30.50 (CH_2) (C2', C3', C4', C5'), 32.21 (CH_2, C8'), 37.82 (CH_2, C10'), 40.35 (CH_2, C6'), 40.47 (CH_2, C1'), 50.74 (CH_2, C9'), 56.16 (CH_3, 4-OCH_3), 109.17 (CH, C3), 113.22 (CH, C5), 119.69 (C, C12a''), 121.57 (C, C11a''), 124.88 (CH, C2''), 126.10 (CH, C8''), 126.40 (CH, C4''), 127.52 (CH, C1''), 133.64 (C), 135.68 (C) (C9'', C4a''), 148.82 (C, C3''), 151.06 (CH, C6), 152.95 (C), 153.01 (C) (C5a'', C12''), 159.00 (C, C2), 166.47 (C, C4), 168.62 (C, CONH).

HRMS ESI:

Calculated for $[C_{33}H_{41}{}^{35}ClN_4O_2 + H]^+$:	561.2991
Found:	561.2985

Synthesis of (±)-*N*-{9-[(3-chloro-6,7,10,11-tetrahydro-9-methyl-7,11-methanocycloocta[*b*]quinolin-12-yl)amino]nonyl}-6-(hydroxymethyl)pyridine-2-carboxamide, 22c

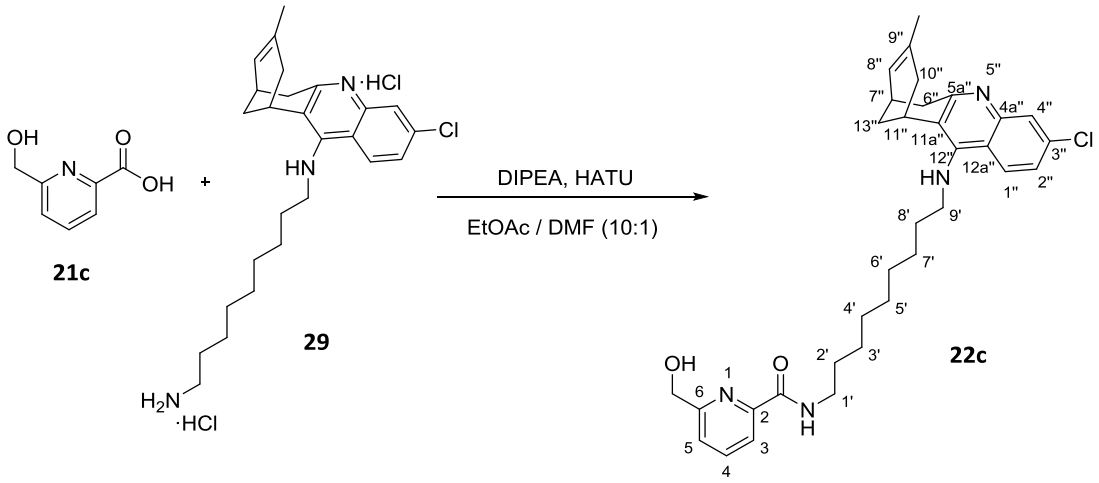

In a 25 mL round-bottomed flask equipped with magnetic stirrer, 6-(hydroxymethyl)picolinic acid, **21c**, (40 mg, 0.26 mmol) and amine **29** (83 mg, 0.19 mmol) were suspended in a mixture of EtOAc / DMF (1.73 mL, 10:1) and the mixture was treated with DIPEA (0.20 mL, 1.18 mmol). After 5 min stirring, HATU (149 mg, 0.39 mmol) was added to the mixture. Finally, after 2 min stirring, more DMF (0.16 mL) was added and the mixture was stirred at r. t. for 2 h, diluted with EtOAc (60 mL), washed with 2M Na_2CO_3 (3 x 15 mL) and brine (15 mL), dried over Na_2SO_4, filtered and evaporated to dryness. The resulting brown oil (208 mg) was purified through column chromatography (silica gel 40–63 µm, 30 g, Ø = 3 cm; #1, 250 mL hexane / Et_3N 100:0.2 #2, 250 mL, hexane / EtOAc / Et_3N 75:25:0.2, #3, 250 mL, hexane / EtOAc / Et_3N 50:50:0.2, #4, 250 mL, hexane / EtOAc / Et_3N 40:60:0.2, #5, 2300 mL, hexane / EtOAc / Et_3N 30:70:0.2; #6-17, 1250 mL, hexane / EtOAc / Et_3N 20:80:0.2), to afford **22c** (#6-8, 78 mg, 53% yield) as a yellow solid.

R_f = 0.36 (silica gel, 10 cm, CH_2Cl_2 / MeOH / 50% aq. NH_4OH 9.6:0.4:0.04)

Analytical sample of 22c·HCl

In a 25 mL round-bottomed flask, **22c** (78 mg) was dissolved in CH_2Cl_2 (5 mL), filtered through a 0.2 µm PTFE filter, treated with excess of a methanolic solution of HCl (2 mL, 1.25 M) and evaporated to dryness. The resulting solid was washed with pentane (3 x 2 mL), evaporated to dryness and dried at 45 °C/2 Torr for 3 days, to provide **22c·HCl** (73 mg) as a yellowish solid.

Melting Point: 96–98 °C

IR (ATR) ν: 3600–2300 (max at 3255, 2926, 2854, N–H, $^{+}$N–H, O–H, C–H st), 1661, 1630, 1583, 1524 (C=O, Ar–C–C, Ar–C–N st) cm^{-1}.

^{1}H NMR (400 MHz, CD_3OD) δ: 1.32–1.47 (complex signal, 10H, 3'-H_2, 4'-H_2, 5'-H_2, 6'-H_2, 7'-H_2), 1.58 (s, 3H, 9''-CH_3) superimposed in part 1.63 (tt, *J* = *J'* = 7.2 Hz, 2H, 2'-H_2), 1.85 (tt, *J* = *J'* = 7.2 Hz, 2H, 8'-H_2) superimposed in part 1.90 (m, 1H, 13''-H_{syn}) superimposed in part 1.93 (br d, *J* = 18.8 Hz, 1H, 10''-H_{endo}), 2.08 (dm, *J* = 12.8 Hz, 1H, 13''-H_{anti}), 2.54 (dd, *J* = 18.8 Hz, *J* = 5.6 Hz, 1H, 10''-H_{exo}), 2.76 (m, 1H, 7''-H), 2.85 (br d, *J* = 17.6 Hz, 1H, 6''-H_{endo}), 3.20 (dd, *J* = 17.6 Hz, *J'* = 5.6 Hz, 1H, 6''-H_{exo}), 3.40 (t, *J* = 7.2 Hz, 2H, 1'-H_2) superimposed 3.42 (m, 1H, 11''-H), 3.97 (td, *J* = 7.2 Hz, *J'* = 3.2 Hz, 2H, 9'-H_2), 4.76 (s, 2H, 6-CH_2OH), 4.85 (s, NH, $^{+}$NH, OH), 5.58 (br d, *J* = 5.6 Hz, 1H, 8''-H), 7.55 (dd, *J* = 9.6 Hz, *J'* = 2.0 Hz, 1H, 2''-H), 7.61 (br d, *J* = 7.2 Hz, 1H, 5-H), 7.74 (d, *J* = 2.0 Hz, 1H, 4''-H), 7.92–8.00 (complex signal, 2H, 3-H, 4-H), 8.39 (d, *J* = 9.6 Hz, 1H, 1''-H).

^{13}C NMR (100.6 MHz, CD_3OD) δ: 23.46 (CH_3, 9''-CH_3), 27.27 (CH, C11''), 27.73 (CH_2), 27.85 (CH_2) (C6', C7'), 27.96 (CH, C7''), 29.31 (CH_2, C13''), 30.11 (CH_2), 30.20 (CH_2), 30.43 (CH_2), 30.53 (CH_2) (C2', C3', C4', C5'), 31.19 (CH_2, C8'), 36.03 (CH_2), 36.08 (CH_2) (C6'', C10''), 40.48 (CH_2, C1'), 49.59 (CH_2, C9'), 65.36 (CH_2, 6-CH_2OH), 115.65 (C, C12a''), 117.60 (C, C11a''), 119.14 (CH, C4''), 121.54 (CH, C3), 124.57 (CH, C5), 125.14 (CH, C8''), 126.66 (CH, C2''), 129.50 (CH, C1''), 134.56 (C, C9''), 139.61 (CH, C4), 140.27 (C, C3''), 140.99 (C, C4a''), 149.92 (C, C6), 151.20 (C, C5a''), 156.97 (C, C12''), 161.45 (C, C2), 166.57 (C, CONH).

HRMS ESI:

Calculated for $[C_{33}H_{41}{}^{35}ClN_4O_2 + H]^+$:	561.2991
Found:	561.2989

Synthesis of (±)-*N*-{9-[(3-chloro-6,7,10,11-tetrahydro-9-methyl-7,11-methanocycloocta[*b*]quinolin-12-yl)amino]nonyl}-5-methylisoxazole-3-carboxamide, 22d

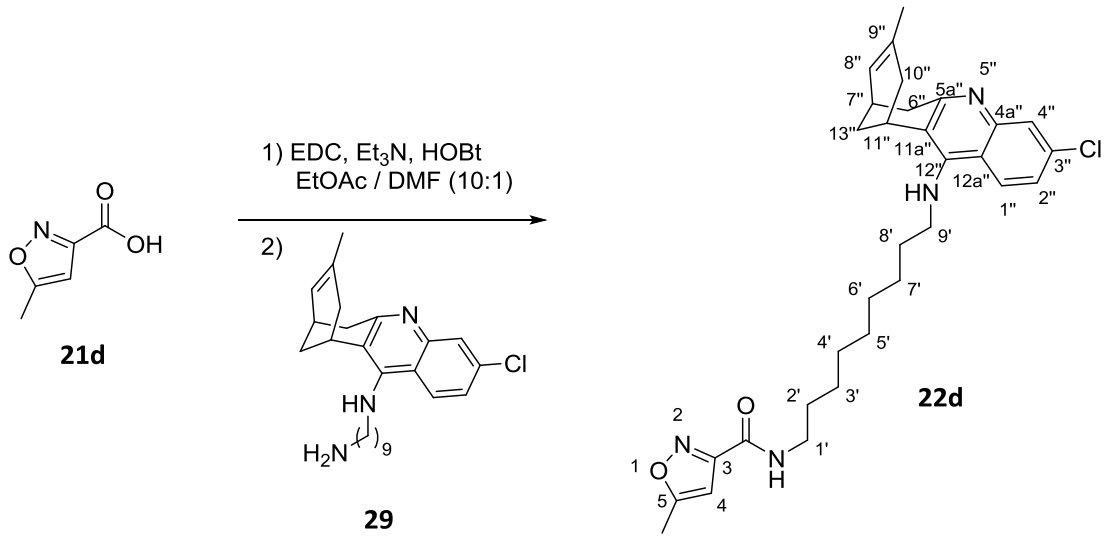

In a 25 mL round-bottomed flask equipped with magnetic stirrer, 5-methylisoxazole-3-carboxylic acid, **21d**, (27 mg, 0.21 mmol) was suspended in a mixture of EtOAc / DMF (4.4 mL, 10:1), and treated subsequently with EDC·HCl (55 mg, 0.29 mmol), Et_3N (0.07 mL, 0.48 mmol) and HOBt (39 mg, 0.29 mmol). After stirring for 15 min at r. t., a solution of the amine **29** (83 mg, 0.19 mmol) in EtOAc / DMF (2.2 mL, 10:1) was added and the reaction mixture was stirred at r. t. overnight, then evaporated to dryness. The resulting brown oil (296 mg) was purified through column chromatography (silica gel 40–63 µm, 30 g, Ø = 3 cm; #1, 200 mL, hexanee / Et_3N 100:0.2, #2, 250 mL, hexane / EtOAc / Et_3N 95:5:0.2, #3, 500 mL, hexane / EtOAc / Et_3N 90:10:0.2, #4, 250 mL, hexane / EtOAc / Et_3N 87:13:0.2, #5, 250 mL, hexane / EtOAc / Et_3N 84:16:0.2, #6, 250 mL, hexane / EtOAc / Et_3N 81:19:0.2, #7, 250 mL, hexane / EtOAc / Et_3N 78:22:0.2, #8-131, 2250 mL, 75:25:0.2), to afford **22d** (#9-104, 73 mg, 72% yield) as a yellow oil.

R_f = 0.17 (silica gel, 10 cm, hexane / EtOAc / Et_3N 6:4:0.02)

Analytical sample of 22d·HCl

In a vial, **22d** (73 mg) was dissolved in CH_2Cl_2 (2 mL), filtered through a 0.2 µm PTFE filter, treated with excess of a solution of HCl in Et_2O (1 mL, 1.17 M), and evaporated to dryness. The resulting solid was washed with hexane (2 x 2 mL) and pentane (2 x 2 mL), evaporated to dryness and dried at 45 °C/2 Torr for 3 days, to provide **22d·HCl** (56 mg) as an off-white solid.

Melting Point: 78–80 °C

IR (ATR) ν: 3500–2400 (max at 3237, 3062, 2927, 2854, 2780, N–H, $^{+}$N–H, C–H st), 1667, 1632, 1584, 1566 (C=O, Ar–C–C, Ar–C–N st) cm^{-1}.

^{1}H NMR (400 MHz, CD_3OD) δ: 1.25–1.50 (complex signal, 10H, 3'-H_2, 4'-H_2, 5'-H_2, 6'-H_2, 7'-H_2), 1.58 (s, 3H, 9''-CH_3), superimposed 1.58 (m, 2H, 2'-H_2), 1.85 (tt, *J* = *J'* = 7.2 Hz, 2H, 8'-H_2), 1.90–1.97 (complex signal, 2H, 10''-H_{endo}, 13''-H_{syn}), 2.09 (dm, *J* = 12.8 Hz, 1H, 13''-H_{anti}), 2.46 (s, 3H, 5-CH_3), 2.55 (dd, *J* = 18.0 Hz, *J'* = 5.6 Hz, 1H, 10''-H_{exo}), 2.77 (m, 1H, 7''-H), 2.85 (ddd, *J* = 17.6 Hz, *J'* = *J''* = 1.6 Hz, 1H, 6''-H_{endo}), 3.20 (dd, *J* = 17.6 Hz, *J'* = 5.6 Hz, 1H, 6''-H_{exo}), 3.33 (t, *J'* = 7.2 Hz, 2H, 1'-H_2), 3.43 (m, 1H, 11''-H), 3.98 (td, *J* = 7.2 Hz, *J'* = 3.2 Hz, 2H, 9'-H_2), 4.85 (s, NH, $^{+}$NH), 5.59 (br d, *J* = 5.6 Hz, 1H, 8''-H), 6.42 (s, 1H, 4-H), 7.56 (dd, *J* = 9.2 Hz, *J'* = 2.4 Hz, 1H, 2''-H), 7.75 (d, *J* = 2.4 Hz, 1H, 4''-H), 8.40 (d, *J* = 9.2 Hz, 1H, 1''-H).

^{13}C NMR (100.6 MHz, CD_3OD) δ: 12.04 (CH_3, 5-CH_3), 23.47 (CH_3, 9''-CH_3), 27.28 (CH, C11''), 27.74 (CH_2), 27.85 (CH_2) (C6', C7') superimposed 27.85 (CH, C7''), 29.31 (CH_2, C13''), 30.10 (CH_2), 30.14 (CH_2), 30.30 (CH_2), 30.42 (CH_2) (C2', C3', C4', C5'), 31.20 (CH_2, C8'), 36.04 (CH_2), 36.09 (CH_2) (C6'', C10''), 40.40 (CH_2, C1'), 49.79 (CH_2, C9'), 101.83 (CH, C4), 115.64 (C, C12a''), 117.58 (C, C11a''), 119.11 (CH, C4''), 125.12 (CH, C8''), 126.64 (CH, C2''), 129.47 (CH, C1''), 134.53 (C, C9''), 140.23 (C, C3''), 140.97 (C, C4a''), 151.19 (C, C5a''), 156.94 (C, C12''), 160.14 (C), 161.53 (C) (C3, C5), 172.88 (C, CONH).

HRMS ESI:

Calculated for $[C_{31}H_{39}{}^{35}ClN_4O_2 + H]^+$: 535.2834

Found: 535.2834

Synthesis of (±)-*N*-{9-[(3-chloro-6,7,10,11-tetrahydro-9-methyl-7,11-methanocycloocta[*b*]quinolin-12-yl)amino]nonyl}-5-methylpyrazine-2-carboxamide, 22e

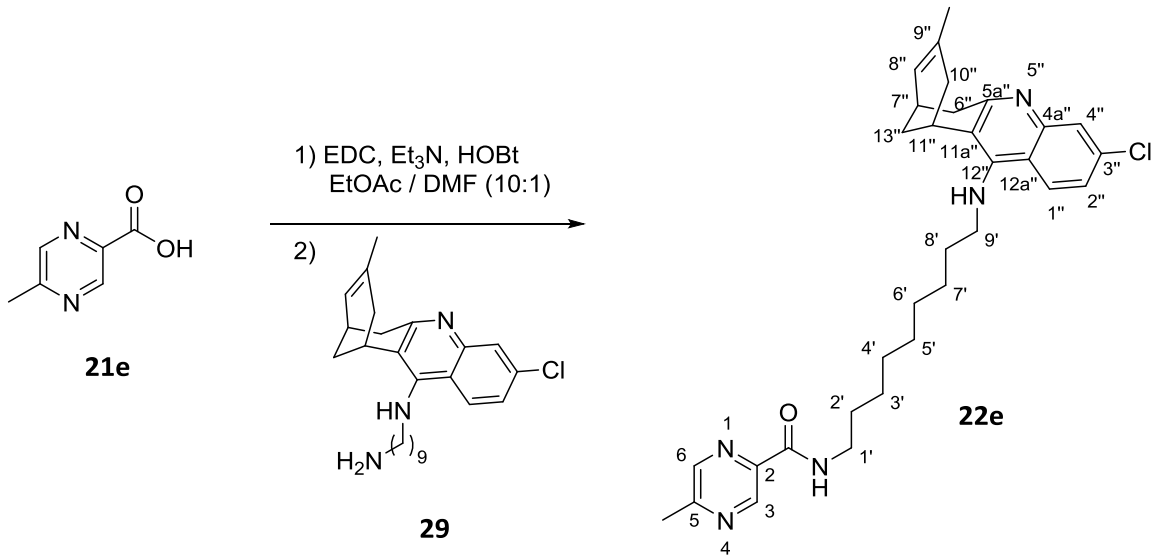

In a 25 mL round-bottomed flask equipped with magnetic stirrer, 5-methylpyrazine-2-carboxylic acid, **21e**, (29 mg, 0.21 mmol) was suspended in a mixture of EtOAc / DMF (4.4 mL, 10:1), and treated subsequently with EDC·HCl (55 mg, 0.29 mmol), Et_3N (0.07 mL, 0.48 mmol) and HOBt (39 mg, 0.29 mmol). After stirring for 15 min at r. t., a solution of the amine **29** (83 mg, 0.19 mmol) in EtOAc / DMF (2.2 mL, 10:1) was added and the reaction mixture was stirred at r. t. overnight, then evaporated to dryness. The resulting brown oil (240 mg) was purified through column chromatography (silica gel 40–63 µm, 24 g, Ø = 2 cm; #1, 250 mL hexane / EtOAc / Et_3N 95:5:0.2 #2, 250 mL, hexane / EtOAc / Et_3N 90:10:0.2, #3, 250 mL, hexane / EtOAc / Et_3N 85:15:0.2, #4, 250 mL, hexane / EtOAc / Et_3N 70:30:0.2, #5-144, 2300 mL, hexane / EtOAc / Et_3N 68:32:0.5), to afford **22e** (#5-129, 102 mg, 98% yield) as a yellow oil.

R_f = 0.24 (silica gel, 10 cm, hexane / EtOAc / Et_3N 6:4:0.02)

Analytical sample of 22e·HCl

In a vial, **22e** (102 mg) was dissolved in CH_2Cl_2 (2 mL), filtered through a 0.2 µm PTFE filter, treated with excess of a solution of HCl in Et_2O (1 mL, 1.17 M), and evaporated to dryness. The resulting solid was washed with hexane (2 x 2 mL) and pentane (2 x 2 mL), evaporated to dryness and dried at 45 °C/2 Torr for 3 days, to provide **22e·HCl** (72 mg) as a yellowish solid.

Melting Point: 73–75 °C

IR (ATR) ν: 3600–2400 (max at 3266, 3052, 2927, 2855, N–H, $^{+}$N–H, C–H st), 1677, 1632, 1583, 1525 (C=O, Ar–C–C, Ar–C–N st) cm^{-1}.

^{1}H NMR (400 MHz, CD_3OD) δ: 1.30–1.46 (complex signal, 10H, 3'-H_2, 4'-H_2, 5'-H_2, 6'-H_2, 7'-H_2), 1.58 (s, 3H, 9''-CH_3) superimposed in part 1.61 (tt, *J* = *J'* = 7.2 Hz, 2H, 2'-H_2), 1.85 (tt, *J* = *J'* = 7.2 Hz, 2H, 8'-H_2), superimposed in part 1.90–1.97 (complex signal, 2H, 10''-H_{endo}, 13''-H_{syn}), 2.08 (dm, *J* = 12.8 Hz, 1H, 13''-H_{anti}), 2.54 (dd, *J* = 17.2 Hz, *J'* = 5.6 Hz, 1H, 10''-H_{exo}), 2.63 (s, 3H, 5-CH_3), 2.77 (m, 1H, 7''-H), 2.85 (ddd, *J* = 17.6 Hz, *J'* = *J''* = 2.0 Hz, 1H, 6''-H_{endo}), 3.20 (dd, *J* = 17.6 Hz, *J'* = 5.6 Hz, 1H, 6''-H_{exo}), 3.40 (t, *J'* = 7.2 Hz, 2H, 1'-H_2) superimposed in part 3.43 (m, 1H, 11''-H), 3.97 (td, *J* = 7.2 Hz, *J'* = 3.2 Hz, 2H, 9'-H_2), 4.85 (s, NH, $^{+}$NH), 5.58 (br d, *J* = 5.6 Hz, 1H, 8''-H), 7.55 (dd, *J* = 9.2 Hz, *J'* = 2.0 Hz, 1H, 2''-H), 7.74 (d, *J* = 2.0 Hz, 1H, 4''-H), 8.39 (d, *J* = 9.2 Hz, 1H, 1''-H), 8.56 (br s, 1H, 6-H), 9.05 (br s, 1H, 3-H).

^{13}C NMR (100.6 MHz, CD_3OD) δ: 21.51 (CH_3, 5-CH_3), 23.45 (CH_3, 9''-CH_3), 27.27 (CH, C11''), 27.73, 27.85, 27.91 (2CH_2 + CH, C6', C7', C7''), 29.30 (CH_2, C13''), 30.10 (CH_2), 30.17 (CH_2), 30.43 (CH_2), 30.51 (CH_2) (C2', C3', C4', C5'), 31.20 (CH_2, C8'), 36.03 (CH_2), 36.08 (CH_2) (C6'', C10''), 40.40 (CH_2, C1'), 49.68 (CH_2, C9'), 143.48 (2CH, C3, C6), 115.64 (C, C12a''), 117.58 (C, C11a''), 119.11 (CH, C4''), 125.12 (CH, C8''), 126.64 (CH, C2''), 129.48 (CH, C1''), 134.53 (C, C9''), 140.24 (C, C3''), 140.97 (C, C4a''), 151.18 (C, C5a''), 156.95 (C, C12''), 158.58 (2C, C2, C5), 167.24 (C, CONH).

HRMS ESI:

Calculated for $[C_{32}H_{40}{}^{35}ClN_5O + H]^{+}$:	546.2994
Found:	546.2998

Synthesis of (±)-*N*-{9-[(3-chloro-6,7,10,11-tetrahydro-9-methyl-7,11-methanocycloocta[*b*]quinolin-12-yl)amino]nonyl}-6-oxo-1,6-dihydropyridine-2-carboxamide, 23a

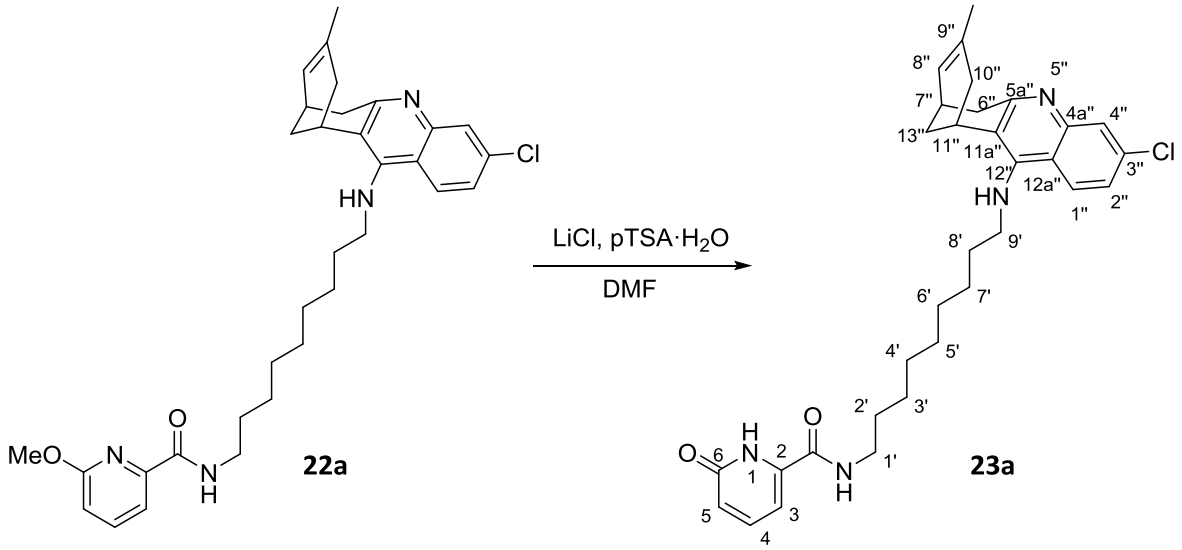

In a double neck 25 mL round-bottomed flask equipped with magnetic stirrer and reflux condenser, **22a** (190 mg, 0.34 mmol) was dissolved in DMF (1 mL) and treated with LiCl (72 mg, 1.69 mmol) and *p*-toluenesulfonic acid monohydrate (322 mg, 1.69 mmol). The resulting orange suspension was stirred at 120 °C for 3.5 h. Then, more LiCl (72 mg, 1.69 mmol) and *p*-toluenesulfonic acid monohydrate (322 mg, 1.69 mmol) were added and the mixture was stirred at 120 °C for 2 h, cooled down to r. t. and quenched with H_2O (2 mL), diluted with sat. aq. $NaHCO_3$ (10 mL), and extracted with EtOAc (3 x 10 mL). The combined organic extracts were washed with water (3 x 10 mL) and brine (2 x 10 mL), dried over anhydrous Na_2SO_4, filtered and evaporated to dryness to provide **23a** (62 mg, 33% yield) as a brown oil.

R_f = 0.78 (silica gel, 10 cm, CH_2Cl_2 / MeOH / 50% aq. NH_4OH 9:1:0.04)

Analytical sample of 23a·HCl

In a 10 mL round-bottomed flask, **23a** (62 mg) was dissolved in analytical MeOH (2 mL), filtered through a 0.2 µm PTFE filter, treated with excess of a methanolic solution of HCl, and evaporated to dryness. The resulting solid was washed with analytical EtOAc (2 x 5 mL), analytical hexane (2 x 5 mL) and analytical pentane (2 x 5 mL), evaporated to dryness and dried at 45 ºC/2 Torr for 3 days, to provide **23a·HCl** (33 mg) as a pale brown solid.

Melting Point: 134–136 °C

IR (ATR) v: 3600–2500 (max at 3241, 3062, 2926, 2854, N–H, $^{+}$N–H, C–H st), 1633, 1583, 1526, 1455 (C=O, Ar–C–C, Ar–C–N st) cm^{-1}.

^{1}H NMR (400 MHz, CD_3OD) δ: 1.30–1.47 (complex signal, 10H, 3'-H_2, 4'-H_2, 5'-H_2, 6'-H_2, 7'-H_2), 1.58 (s, 3H, 9''-CH_3) superimposed in part 1.60 (m, 2H, 2'-H_2), 1.85 (tt, *J* = *J'* = 7.2 Hz, 2H, 8'-H_2) superimposed in part 1.90 (m, 1H, 13''-H_{syn}) superimposed in part 1.93 (br d, *J* = 17.2 Hz, 1H, 10''-H_{endo}), 2.09 (dm, *J* = 12.8 Hz, 1H, 13''-H_{anti}), 2.54 (dd, *J* = 17.2 Hz, *J* = 5.6 Hz, 1H, 10''-H_{exo}), 2.77 (m, 1H, 7''-H), 2.84 (ddd, *J* = 17.6 Hz, *J'* = *J''* = 1.6 Hz, 1H, 6''-H_{endo}), 3.20 (dd, *J* = 17.6 Hz, *J'* = 5.6 Hz, 1H, 6''-H_{exo}), 3.56 (t, *J* = 7.2 Hz, 2H, 1'-H_2), 3.42 (m, 1H, 11''-H), 3.97 (td, *J* = 7.2 Hz, *J'* = 3.2 Hz, 2H, 9'-H_2), 4.85 (s, NH, $^{+}$NH), 5.59 (br d, *J* = 5.6 Hz, 1H, 8''-H), 6.74 (br d, *J* = 8.8 Hz, 1H, 5-H), 7.15 (m, 1H, 3-H), 7.56 (dd, *J* = 9.2 Hz, *J'* = 2.0 Hz, 1H, 2''-H), 7.68 (dd, *J* = 8.8 Hz, *J'* = 7.6 Hz, 1H, 4-H), 7.73 (d, *J* = 2.0 Hz, 1H, 4''-H), 8.39 (d, *J* = 9.2 Hz, 1H, 1''-H).

^{13}C NMR (100.6 MHz, CD_3OD) δ: 23.43 (CH_3, 9''-CH_3), 27.25 (CH, C11''), 27.71 (CH_2), 27.82 (CH_2) (C6', C7'), 27.88 (CH, C7''), 29.28 (CH_2, C13''), 30.08 (CH_2), 30.14 (CH_2), 30.39 ($2CH_2$) (C2', C3', C4', C5'), 31.18 (CH_2, C8'), 36.01 (CH_2), 36.06 (CH_2) (C6'', C10''), 40.82 (CH_2, C1'), 49.65 (CH_2, C9'), 112.27 (CH, C5), 115.61 (C, C12a''), 115.90 (CH, C3), 117.55 (C, C11a''), 119.10 (CH, C4''), 125.10 (CH, C8''), 126.62 (CH, C2''), 129.46 (CH, C1''), 134.50 (C, C9''), 140.01 (CH, C4), 140.21 (C, C3''), 140.94 (C, C4a''), 150.54 (C, C2), 151.16 (C, C5a''), 156.90 (C, C12''), 163.87 (C, C6), 166.97 (C, CONH).

HRMS ESI:

Calculated for $[C_{32}H_{39}{}^{35}ClN_4O_2 + H]^+$: 547.2834

Found: 547.2832

Synthesis of (±)-*N*-{9-[(3-chloro-6,7,10,11-tetrahydro-9-methyl-7,11-methanocycloocta[*b*]quinolin-12-yl)amino]nonyl}-4-oxo-1,4-dihydropyridine-2-carboxamide, 23b

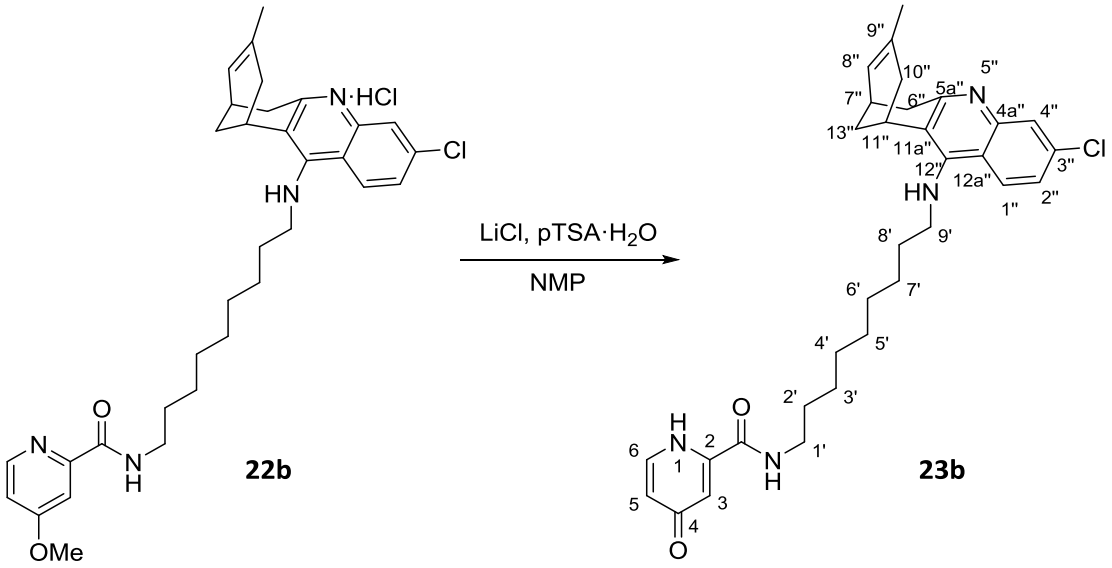

In a double neck 10 mL round-bottomed flask equipped with magnetic stirrer and reflux condenser, **(±)-22b·HCl** (116 mg of a sample that was partially demethylated, maximum of 0.18 mmol) was dissolved in *N*-methyl-2-pyrrolidone, NMP (1 mL) and treated with LiCl (78 mg, 1.83 mmol) and *p*-toluenesulfonic acid monohydrate (348 mg, 1.83 mmol). The resulting orange suspension was stirred at 180 °C for 2 h, cooled down to r. t. and quenched with H_2O (2 mL), diluted with sat. aq. $NaHCO_3$ (10 mL) and extracted with EtOAc (3 x 5 mL). The combined organic extracts were washed with water (3 x 10 mL) and brine (2 x 10 mL), dried over anhydrous Na_2SO_4, filtered and evaporated to dryness to provide **23b** (64 mg, 64% yield) as a brown oil.

R_f = 0.53 (silica gel, 10 cm, CH_2Cl_2 / MeOH / 50% aq. NH_4OH 9:1:0.04)

Analytical sample of 23b·HCl

In a 10 mL round-bottomed flask, **23b** (64 mg) was dissolved in MeOH (2 mL), filtered through a 0.2 µm PTFE filter, treated with excess of a methanolic solution of HCl (2 mL, 1.25 M), and evaporated to dryness. The resulting solid was washed with EtOAc (2 x 5 mL), hexane (2 x 5 mL), and pentane (2 x 5 mL), evaporated to dryness and dried at 45 °C/2 Torr for 3 days, to provide **23b·HCl** (52 mg) as a pale brown solid.

Melting Point: 135–136 °C

IR (ATR) ν: 3600–2500 (max at 3239, 3066, 2955, 2926, N–H, $^{+}$N–H, C–H st), 1674, 1618, 1585, 1504, 1452 (C=O, Ar–C–C, Ar–C–N st) cm^{-1}.

^{1}H NMR (400 MHz, CD_3OD) δ: 1.30–1.50 (complex signal, 10H, 3'-H_2, 4'-H_2, 5'-H_2, 6'-H_2, 7'-H_2), 1.58 (s, 3H, 9''-CH_3) superimposed in part 1.64 (m, 2H, 2'-H_2), 1.84 (m, 2H, 8'-H_2) superimposed in part 1.90 (m, 1H, 13''-H_{syn}) superimposed in part 1.93 (br d, *J* = 17.6 Hz, 1H, 10''-H_{endo}), 2.08 (dm, *J* = 12.4 Hz, 1H, 13''-H_{anti}), 2.55 (dm, *J* = 17.6 Hz, 1H, 10''-H_{exo}), 2.77 (m, 1H, 7''-H), 2.86 (br d, *J* = 17.6 Hz, 1H, 6''-H_{endo}), 3.20 (dd, *J* = 17.6 Hz, *J'* = 5.6 Hz, 1H, 6''-H_{exo}), 3.36–3.50 (complex signal, 3H, 1'-H_2, 11''-H), 3.98 (br t, *J* = 7.2 Hz, 2H, 9'-H_2), 4.85 (s, NH, $^{+}$NH, OH), 5.58 (br d, *J* = 5.2 Hz, 1H, 8''-H), 7.16 (m, 1H, 5-H), 7.55 (dd, *J* = 9.2 Hz, *J'* = 2.0 Hz, 1H, 2''-H), 7.62 (m, 1H, 3-H), 7.76 (d, *J* = 2.0 Hz, 1H, 4''-H), 8.39 (d, *J* = 9.2 Hz, 1H, 1''-H) superimposed 8.39 (m, 1H, 6-H).

^{13}C NMR (100.6 MHz, CD_3OD) δ: 23.45 (CH_3, 9''-CH_3), 27.27 (CH, C11''), 27.78 (CH_2), 27.84 (CH_2) (C6', C7'), 27.98 (CH, C7''), 29.30 (CH_2, C13''), 30.19 ($2CH_2$), 30.24 (CH_2), 30.50 (CH_2) (C2', C3', C4', C5'), 31.24 (CH_2, C8'), 36.03 (CH_2), 36.08 (CH_2), (C6'', C10''), 41.27 (CH_2, C1'), 49.68 (CH_2, C9'), 113.30 (CH, C3), 115.64 (C, C12a''), 117.58 (C, C11a''), 119.12 (CH, C4''), 125.12 (CH, C8''), 126.64 (CH, C2''), 129.48 (CH, C1''), 134.52 (C, C9''), 136.58 (CH, C5), 140.23 (C, C3''), 140.97 (C, C4a''), 146.67 (CH, C6), 151.19 (C, C5a''), 156.93 (C, C12''), 159.96 (C), 161.54 (C) (C2, C4), 168.03 (C, CONH).

HRMS ESI:

Calculated for $[C_{32}H_{39}{}^{35}ClN_4O_2 + H]^{+}$:	547.2834
Found:	547.2835

Synthesis of (±)-*N*-{9-[(3-chloro-6,7,10,11-tetrahydro-9-methyl-7,11-methanocycloocta[*b*]quinolin-12-yl)amino]nonyl}-2-(4-pyridyl)thiazole-4-carboxamide, 25a

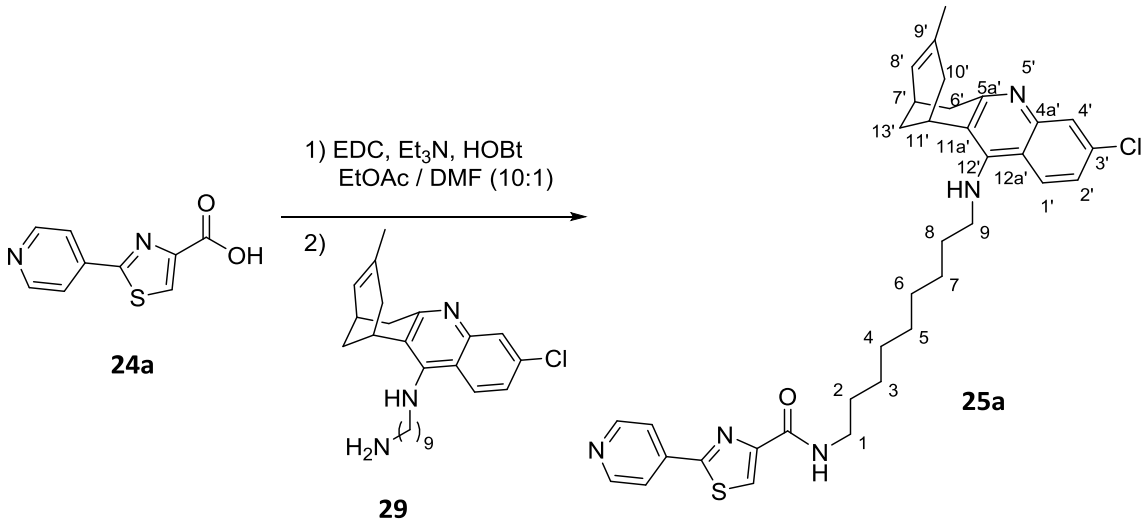

In a 50 mL round-bottomed flask provided with magnetic stirrer, 2-(4-pyridyl)thiazole-4-carboxylic acid, **24a**, (95 mg, 0.46 mmol) was suspended in a mixture of EtOAc / DMF (8.8 mL, 10:1), and treated subsequently with EDC·HCl (120 mg, 0.62 mmol), Et_3N (0.14 mL, 1.04 mmol) and HOBt (85 mg, 0.62 mmol). After stirring for 10 min at r. t., a solution of the amine **29** (177 mg, 0.42 mmol) in EtOAc / DMF (5.5 mL, 10:1) was added and the reaction mixture was stirred at r. t. overnight, then evaporated to dryness. The resulting yellow oil (550 mg) was purified through column chromatography (silica gel 40–63 μm, 55 g, Ø = 4 cm; #1, 250 mL, CH_2Cl_2 / 50% aq. NH_4OH 100:0.4; #2-63, 1800 mL, CH_2Cl_2 / MeOH / 50% aq. NH_4OH 99:1:0.4), to provide **25a** (#30-36, 131 mg, 53% yield) as an orange oil.

R_f = 0.44 (silica gel, 10 cm, CH_2Cl_2 / MeOH / 50% aq. NH_4OH 9.5:0.5:0.04)

Analytical sample of (±)-25a·HCl

In a 10 mL round-bottomed flask, **(±)-25a** (131 mg) was dissolved in CH_2Cl_2 (5 mL), filtered through a 0.2 μm PTFE filter, treated with excess of a methanolic solution of HCl (2 mL, 1.25 M), and evaporated to dryness. The resulting solid was washed with EtOAc (2 x 5 mL), hexane (2 x 5 mL), and pentane (2 x 5 mL), evaporated to dryness and dried at 45 °C/2 Torr for 5 days, to provide **25a·HCl** (134 mg) as a pale orange solid.

Melting Point: 79–81 °C

IR (ATR) ν: 3600–2300 (max at 3257, 3057, 2925, 2854, N–H, $^{+}$N–H, C–H st), 1662, 1631, 1583, 1566, 1515 (C=O, Ar–C–C, Ar–C–N, Ar–C–S st) cm^{-1}.

^{1}H NMR (400 MHz, CD_3OD) δ: 1.34–1.47 (complex signal, 10H, 3-H_2, 4-H_2, 5-H_2, 6-H_2, 7-H_2), 1.57 (s, 3H, 9'-CH_3), 1.65 (tt, *J* = *J'* = 6.8 Hz, 2H, 2-H_2), 1.84 (tt, *J* = *J'* = 6.8 Hz, 2H, 8-H_2) superimposed in part 1.91 (m, 1H, 13'-H_{syn}) superimposed in part 1.92 (br d, *J* = 17.6 Hz, 1H, 10'-H_{endo}), 2.07 (dm, *J* = 12.8 Hz, 1H, 13'-H_{anti}), 2.53 (dd, *J* = 17.6 Hz, *J'* = 5.6 Hz, 1H, 10'-H_{exo}), 2.75 (m, 1H, 7'-H), 2.84 (ddd, *J* = 17.6 Hz, *J'* = *J"* = 2.0 Hz, 1H, 6'-H_{endo}), 3.19 (dd, *J* = 17.6 Hz, *J'* = 5.6 Hz, 1H, 6'-H_{exo}), 3.42 (m, 1H, 11'-H) superimposed 3.42 (t, *J* = 6.8 Hz, 2H, 1-H_2), 3.96 (td, *J* = 6.8 Hz, *J'* = 3.2 Hz, 2H, 9-H_2), 4.85 (s, NH, $^{+}$NH), 5.57 (br d, *J* = 5.2 Hz, 1H, 8'-H), 7.54 (m, 1H, 2'-H), 7.74 (d, *J* = 2.4 Hz, 1H, 4'-H), 8.38 (d, *J* = 9.2 Hz, 1H, 1'-H), 8.44 [br d, *J* = 6.4 Hz, 2H, pyridine 3(5)-H], 8.49 (s, 1H, thiazole 5-H), 8.86 [d, *J* = 6.4 Hz, 2H, pyridine 2(6)-H].

^{13}C NMR (100.6 MHz, CD_3OD) δ: 23.47 (CH_3, 9'-CH_3), 27.27 (CH, C11'), 27.75 (CH_2), 27.84 (CH_2) (C6, C7), 27.97 (CH, C7'), 29.30 (CH_2, C13'), 30.13 (CH_2), 30.22 (CH_2), 30.46 (CH_2), 30.62 (CH_2) (C2, C3, C4, C5), 31.20 (CH_2, C8), 36.03 (CH_2), 36.08 (CH_2) (C6', C10'), 40.56 (CH_2, C1), 49.56 (CH_2, C9), 115.62 (C, C12a'), 117.57 (C, C11a'), 119.12 (CH, C4'), 123.82 [2CH, pyridine C3(5)], 125.13 (CH, C8'), 126.63 (CH, C2'), 128.68 (CH, thiazole C5), 129.46 (CH, C1'), 134.52 (C, C9'), 140.21 (C, C3'), 140.96 (C, C4a'), 146.43 (C, thiazole C2), 146.90 [2CH, pyridine C2(6)], 151.19 (C, C5a'), 153.33 (C, pyridine C4), 156.90 (C, C12'), 162.65 (C), 164.19 (C) (thiazole C4, CONH).

HRMS ESI:

Calculated for $[C_{35}H_{40}{}^{35}ClN_5OS + H]^{+}$: 614.2715

Found: 614.2706

Synthesis of (±)-*N*-{9-[(3-chloro-6,7,10,11-tetrahydro-9-methyl-7,11-methanocycloocta[*b*]quinolin-12-yl)amino]nonyl}-5-(2-pyridyl)thiophene-2-carboxamide, 25b

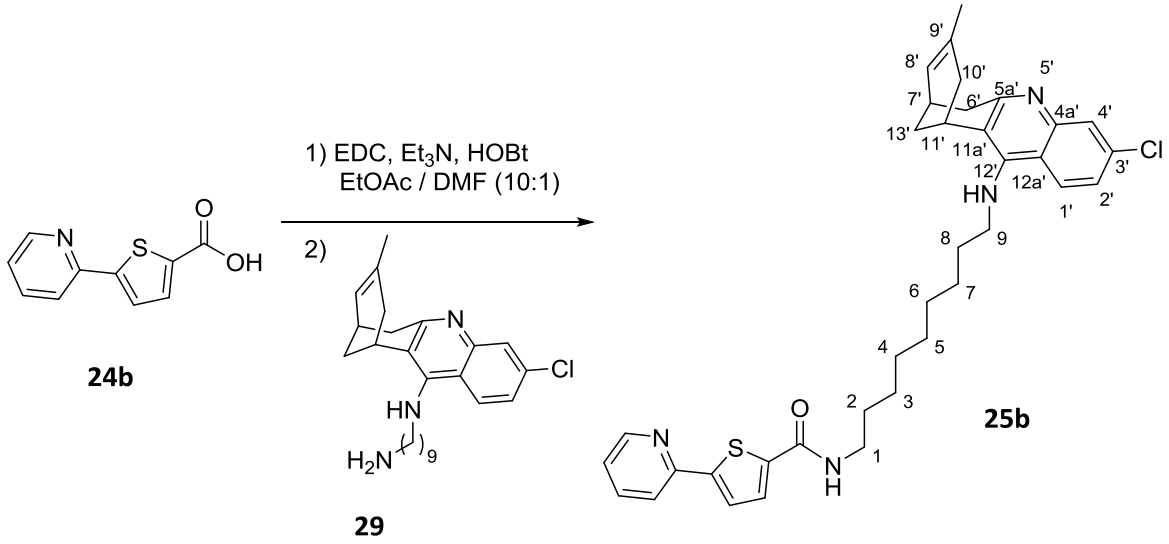

In a 50 mL round-bottomed flask equipped with magnetic stirrer, 5-(2-pyridyl)thiophene-2-carboxylic acid, **24b**, (133 mg, 0.64 mmol) was suspended in a mixture of EtOAc / DMF (11 mL, 10:1), and treated subsequently with EDC·HCl (169 mg, 0.88 mmol), Et_3N (0.24 mL, 1.76 mmol) and HOBt (120 mg, 0.88 mmol). After stirring for 10 min at r. t., a solution of the amine **(±)-29** (250 mg, 0.59 mmol) in EtOAc / DMF (8.8 mL, 10:1) was added and the reaction mixture was stirred at r. t. overnight, then evaporated to dryness. The resulting yellow oil (788 mg) was purified through column chromatography (silica gel 40–63 µm, 63 g, Ø = 4 cm; #1-2, 800 mL, CH_2Cl_2 / 50% aq. NH_4OH 100:0.4; #3-11, 1200 mL, CH_2Cl_2 / MeOH / 50% aq. NH_4OH 99.5:0.5:0.4), to afford **(±)-25b** (#3-6, 272 mg, 76% yield) as a yellow oil.

R_f = 0.69 (silica gel, 10 cm, CH_2Cl_2 / MeOH / 50% aq. NH_4OH 9.6:0.4:0.04)

Analytical sample of (±)-25b·HCl

In a 10 mL round-bottomed flask, **(±)-25b** (272 mg) was dissolved in CH_2Cl_2 (2 mL), filtered through a 0.2 µm PTFE filter, treated with excess of a methanolic solution of HCl (2 mL, 1.25 M), and evaporated to dryness. The resulting solid was washed with EtOAc (2 x 5 mL) and pentane (2 x 5 mL), evaporated to dryness and dried at 45 °C/2 Torr for 5 days, to provide **(±)-25b·HCl** (229 mg) as a yellow solid.

Melting Point: 144–146 °C

IR (ATR) v: 3600–2400 (max at 3247, 3060, 2926, 2854, N–H, $^{+}$N–H, C–H st), 1631, 1583, 1565, 1515 (C=O, Ar–C–C, Ar–C–N st) cm^{-1}.

^{1}H NMR (400 MHz, CD_3OD) δ: 1.33–1.47 (complex signal, 10H, 3-H_2, 4-H_2, 5-H_2, 6-H_2, 7-H_2), 1.58 (s, 3H, 9'-CH_3), 1.62 (m, 2H, 2-H_2), 1.85 (tt, *J* = *J'* = 7.2 Hz, 2H, 8-H_2) superimposed in part 1.92 (m, 1H, 13'-H_{syn}) superimposed in part 1.93 (br d, *J* = 17.2 Hz, 1H, 10'-H_{endo}), 2.08 (dm, *J* = 12.8 Hz, 1H, 13'-H_{anti}), 2.54 (dd, *J* = 17.2 Hz, *J'* = 4.8 Hz, 1H, 10'-H_{exo}), 2.76 (m, 1H, 7'-H), 2.86 (ddd, *J* = 18.0 Hz, *J'* = *J''* = 2.0 Hz, 1H, 6'-H_{endo}), 3.19 (dd, *J* = 18.0 Hz, *J'* = 5.6 Hz, 1H, 6'-H_{exo}), 3.36 (t, *J* = 7.2 Hz, 2H, 1-H_2), 3.44 (m, 1H, 11'-H), 3.97 (td, *J* = 7.2 Hz, *J'* = 2.4 Hz, 2H, 9-H_2), 4.85 (s, NH, $^{+}$NH), 5.58 (br d, *J* = 5.6 Hz, 1H, 8'-H), 7.54 (dd, *J* = 9.2 Hz, *J'* = 2.4 Hz, 1H, 2'-H), 7.70 (ddd, *J* = 7.6 Hz, *J'* = 5.6 Hz, *J''* = 1.2 Hz, 1H, pyridine 5-H), 7.75 (d, *J* = 2.4 Hz, 1H, 4'-H), 7.78 (d, *J* = 4.4 Hz, 1H), 7.88 (d, *J* = 4.4 Hz, 1H) (thiophene 3-H, thiophene 4-H), 8.15 (ddd, *J* = 8.0 Hz, *J'* = *J''* = 1.2 Hz, 1H, pyridine 3-H), 8.29 (ddd, *J* = 8.0 Hz, *J'* = 7.6 Hz, *J''* = 1.6 Hz, 1H, pyridine 4-H), 8.38 (d, *J* = 9.2 Hz, 1H, 1'-H), 8.66 (ddd, *J* = 5.6 Hz, *J'* = 1.6 Hz, *J''* = 1.2 Hz, 1H, pyridine 6-H).

^{13}C NMR (100.6 MHz, CD_3OD) δ: 23.47 (CH_3, 9'-CH_3), 27.27 (CH, C11'), 27.73 (CH_2), 27.85 (CH_2) (C6, C7), 27.91 (CH, C7'), 29.30 (CH_2, C13'), 30.09 (CH_2), 30.14 (CH_2), 30.41 ($2CH_2$) (C2, C3, C4, C5), 31.20 (CH_2, C8), 36.03 (CH_2), 36.08 (CH_2) (C6', C10'), 41.00 (CH_2, C1), 48.79 (CH_2, C9), 115.63 (C, C12a'), 117.57 (C, C11a'), 119.12 (CH, C4'), 124.03 (CH, pyridine C3), 125.13 (CH, C8'), 125.71 (CH, pyridine C5), 126.63 (CH, C2'), 129.47 (CH, C1'), 130.10 (CH), 130.30 (CH) (thiophene C3, thiophene C4), 134.55 (C, C9'), 140.22 (C, C3'), 140.96 (C, C4a'), 142.52 (C), 145.08 (C) (thiophene C2, thiophene C5), 144.36 (CH, pyridine C4), 146.21 (CH, pyridine C6), 149.60 (C, pyridine C2), 151.17 (C, C5a'), 156.90 (C, C12'), 163.24 (C, CONH).

HRMS ESI:

Calculated for $[C_{36}H_{41}{}^{35}ClN_4OS + H]^{+}$:	613.2800
Found:	613.2800

Synthesis of (±)-*N*-{9-[(3-chloro-6,7,10,11-tetrahydro-9-methyl-7,11-methanocycloocta[*b*]quinolin-12-yl)amino]nonyl}-5-(2-pyridyl)thiophene-2-sulfonamide, 25c

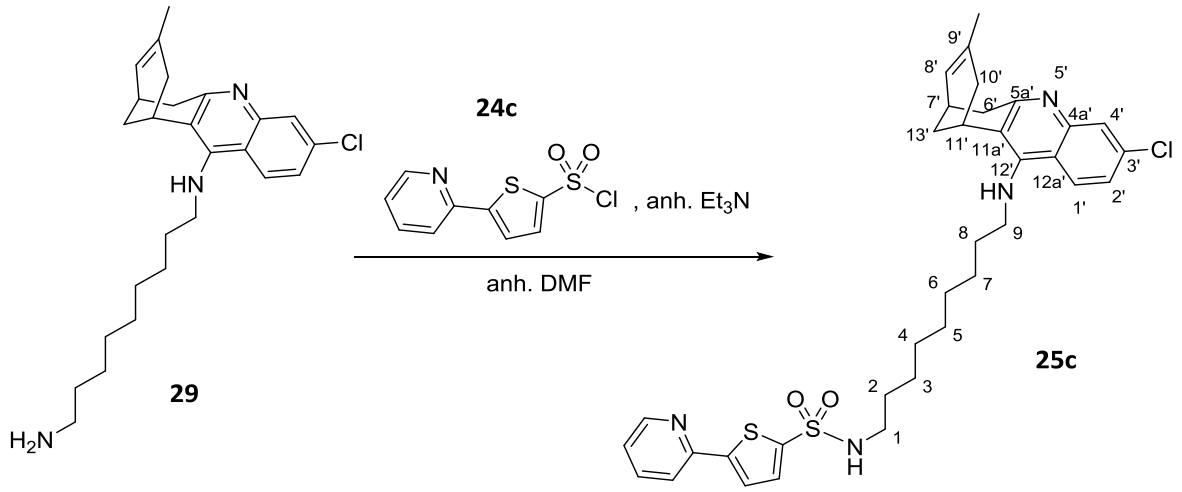

In a 10 mL round-bottomed flask equipped with magnetic stirrer and inert atmosphere, **29** (250 mg, 0.59 mmol) and anhydrous Et_3N (0.12 mL, 0.88 mmol) were dissolved in anhydrous DMF (3.8 mL). The mixture was cooled down to 0 °C in an ice / water bath, treated with 5-(2-pyridyl)thiophene-2-sulfonyl chloride, **24c**, (181 mg, 0.65 mmol) and stirred at r. t. overnight. The resulting dark yellow solution was evaporated to dryness and the crude (597 mg) was purified through column chromatography (silica gel 40–63 µm, 48 g; Ø = 3.5 cm; #1-2, 600 mL, CH_2Cl_2 / 50% aq. NH_4OH 100:0.4; #3-4, 600 mL, CH_2Cl_2 / MeOH / 50% aq. NH_4OH 99.75:0.25:0.4; #5-26, 3100 mL, CH_2Cl_2 / MeOH / 50% aq. NH_4OH 99.5:0.5:0.4; #27-39, 1000 mL, CH_2Cl_2 / MeOH / 50% aq. NH_4OH 99:1:0.4), to obtain **25c** (#9-26, 325 mg, 85% yield) as a yellow solid.

R_f = 0.81 (silica gel, 10 cm, CH_2Cl_2 / MeOH / 50% aq. NH_4OH 9.6:0.4:0.04)

Analytical sample of 25c·HCl

In a 10 mL round-bottomed flask, **25c** (325 mg) was dissolved in CH_2Cl_2 (2 mL), filtered through a 0.2 µm PTFE filter, treated with excess of a methanolic solution of HCl (2 mL, 1.25 M), and evaporated to dryness. The resulting solid was washed with EtOAc (2 x 5 mL) and pentane (2 x 5 mL), evaporated to dryness and dried at 45 °C/2 Torr for 5 days, to afford **25c·HCl** (264 mg) as a yellow solid.

Melting Point: 103–105 °C

IR (ATR) v: 3600–2400 (max at 3259, 3050, 2925, 2854, N–H, $^{+}$N–H, C–H st), 1631, 1582, 1570, 1515 (Ar–C–C, Ar–C–N, Ar–C–S st) cm^{-1}.

^{1}H NMR (400 MHz, CD_3OD) δ: 1.25–1.43 (complex signal, 10H, 3-H_2, 4-H_2, 5-H_2, 6-H_2, 7-H_2), 1.50 (tt, *J* = *J'* = 7.2 Hz 2H, 2-H_2), 1.58 (s, 3H, 9'-CH_3), 1.84 (tt, *J* = *J'* = 7.2 Hz, 2H, 8-H_2), 1.93 (br d, *J* = 17.6 Hz, 1H, 10'-H_{endo}), superimposed in part 1.94 (m, 1H, 13'-H_{syn}), 2.08 (dm, *J* = 12.4 Hz, 1H, 13'-H_{anti}), 2.54 (dd, *J* = 17.6 Hz, *J'* = 5.6 Hz, 1H, 10'-H_{exo}), 2.77 (m, 1H, 7'-H), 2.85 (dm, *J* = 18.0 Hz, 1H, 6'-H_{endo}), 2.98 (t, *J* = 7.2 Hz, 2H, 1-H_2), 3.20 (dd, *J* = 18.0 Hz, *J'* = 5.6 Hz, 1H, 6'-H_{exo}), 3.43 (m, 1H, 11'-H), 3.96 (td, *J* = 7.2 Hz, *J'* = 2.8 Hz, 2H, 9-H_2), 4.85 (s, NH, $^{+}$NH), 5.58 (br d, *J* = 5.6 Hz, 1H, 8'-H), 7.52–7.57 (complex signal, 2H, 2'-H, pyridine 5-H), 7.60 (d, *J* = 3.6 Hz, 1H), 7.78 (d, *J* = 3.6 Hz, 1H) (thiophene 3-H, thiophene 4-H), 7.73 (d, *J* = 2.0 Hz, 1H, 4'-H), 8.04 (d, *J* = 8.0 Hz, 1H, pyridine 3-H), 8.10 (ddd, *J* = 8.0 Hz, *J'* = 7.6 Hz, *J''* = 1.6 Hz, 1H, pyridine 4-H), 8.38 (d, *J* = 9.2 Hz, 1H, 1'-H), 8.61 (ddd, *J* = 5.6 Hz, *J'* = 1.6 Hz, *J''* = 0.8 Hz, 1H, pyridine 6-H).

^{13}C NMR (100.6 MHz, CD_3OD) δ: 23.51 (CH_3, 9'-CH_3), 27.27 (CH, C11'), 27.48 (CH_2), 27.71 (CH_2) (C6, C7), 27.85 (CH, C7'), 29.33 (CH_2, C13'), 29.88 (CH_2), 30.06 (CH_2), 30.32 (CH_2), 30.47 (CH_2) (C2, C3, C4, C5), 31.24 (CH_2, C8), 36.05 (CH_2), 36.11 (CH_2) (C6', C10'), 44.28 (CH_2, C1), 49.00 (CH_2, C9), 115.64 (C, C12a'), 117.58 (C, C11a'), 119.12 (CH, C4'), 123.32 (CH, pyridine C3), 125.14 (CH, C8'), 125.84 (CH), 128.54 (CH) (thiophene C3, thiophene C4), 126.64 (CH, C2'), 129.51 (CH, C1'), 133.27 (CH, pyridine C5), 134.53 (C, C9'), 140.16 (C, C3'), 140.93 (C, C4a'), 142.99 (CH, pyridine C4), 145.89 (C), 146.50 (C) (thiophene C2, thiophene C5), 147.58 (CH, pyridine C6), 149.84 (C, pyridine C2), 151.16 (C, C5a'), 156.88 (C, C12').

HRMS ESI:

Calculated for $[C_{35}H_{41}{}^{35}ClN_4O_2S_2 + H]^{+}$: 649.2432

Found: 649.2427

Synthesis of (±)-*N*-{9-[(3-chloro-6,7,10,11-tetrahydro-9-methyl-7,11-methanocycloocta[*b*]quinolin-12-yl)amino]nonyl}-6-(2-furyl)pyridine-2-carboxamide, 25d

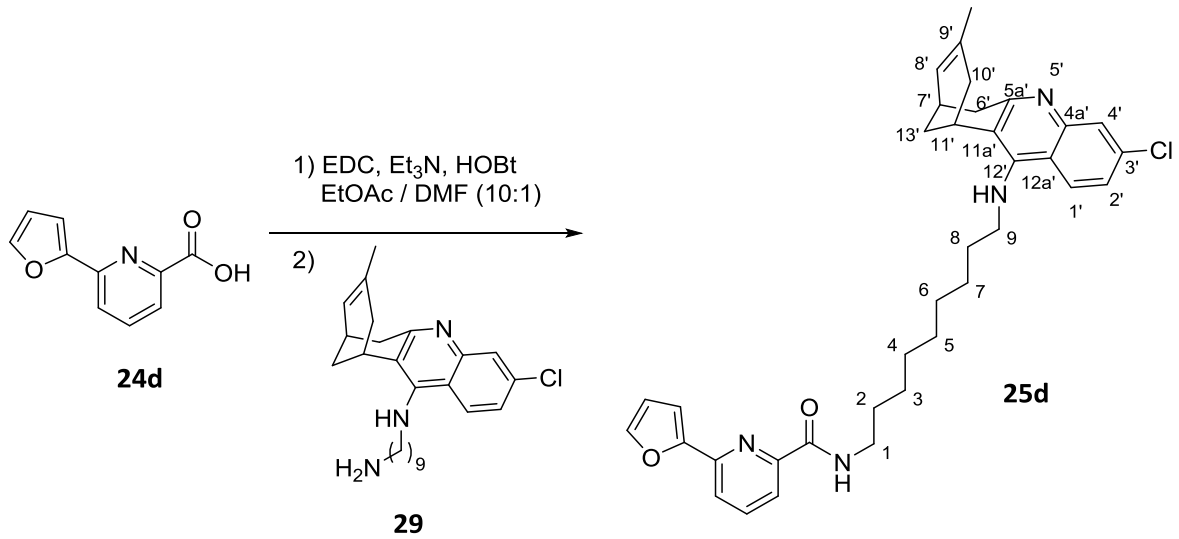

In a 50 mL round-bottomed flask equipped with magnetic stirrer, 6-(2-furyl)pyridine-2-carboxylic acid, **24d**, (95 mg, 0.50 mmol) was suspended in a mixture of EtOAc / DMF (8.8 mL, 10:1), and treated subsequently with EDC·HCl (132 mg, 0.69 mmol), Et_3N (0.19 mL, 1.37 mmol) and HOBt (93 mg, 0.69 mmol). After stirring for 10 min at r. t., a solution of the amine **29** (195 mg, 0.46 mmol) in EtOAc / DMF (6.6 mL, 10:1) was added and the reaction mixture was stirred at r. t. overnight, then evaporated to dryness. The resulting brown oil (671 mg) was purified through column chromatography (silica gel 40–63 µm, 67 g, Ø = 4 cm; #1-2, 800 mL, CH_2Cl_2 / 30% aq. NH_4OH 100:0.7; #3-42, 3600 mL, CH_2Cl_2 / MeOH / 30% aq. NH_4OH 99.5:0.5:0.7), to obtain **25d** (#12-24, 160 mg, 58% yield) as a yellow oil.

R_f = 0.48 (silica gel, 10 cm, CH_2Cl_2 / MeOH / 50% aq. NH_4OH 9.6:0.4:0.04)

Analytical sample of 25d·HCl

In a 10 mL round-bottomed flask, **25d** (160 mg) was dissolved in CH_2Cl_2 (2 mL), filtered through a 0.2 µm PTFE filter, treated with excess of a methanolic solution of HCl (2 mL, 1.25 M), and evaporated to dryness. The resulting solid was washed with EtOAc (2 x 5 mL) and pentane (2 x 5 mL), evaporated to dryness and dried at 45 °C/2 Torr for 5 days, to provide **25d·HCl** (97 mg) as a beige solid.

Melting Point: 125–127 °C

IR (ATR) ν: 3600–2400 (max at 3237, 3056, 2926, 2854, N–H, $^{+}$N–H, C–H st), 1667, 1631, 1582, 1570, 1521 (C=O, Ar–C–C, Ar–C–N st) cm^{-1}.

^{1}H NMR (400 MHz, CD_3OD) δ: 1.30–1.47 (complex signal, 10H, 3-H_2, 4-H_2, 5-H_2, 6-H_2, 7-H_2), 1.57 (s, 3H, 9'-CH_3), 1.65 (tt, *J* = *J'* = 6.8 Hz, 2H, 2-H_2), 1.84 (tt, *J* = *J'* = 6.8 Hz, 2H, 8-H_2), superimposed in part 1.90 (m, 1H, 13'-H_{syn}), superimposed in part 1.92 (br d, *J* = 17.2 Hz, 1H, 10'-H_{endo}), 2.07 (dm, *J* = 12.8 Hz, 1H, 13'-H_{anti}), 2.53 (dm, *J* = 17.2 Hz, 1H, 10'-H_{exo}), 2.76 (m, 1H, 7'-H), 2.84 (br d, *J* = 18.0 Hz, 1H, 6'-H_{endo}), 3.19 (dd, *J* = 18.0 Hz, *J'* = 5.6 Hz, 1H, 6'-H_{exo}), 3.42 (m, 1H, 11'-H), superimposed 3.44 (t, *J* = 6.8 Hz, 2H, 1-H_2), 3.95 (br t, *J* = 6.8 Hz, 2H, 9-H_2), 4.85 (s, NH, $^{+}$NH), 5.57 (br d, *J* = 5.6 Hz, 1H, 8'-H), 6.60 (dd, *J* = 3.6 Hz, *J'* = 1.6 Hz, 1H, furan 4-H), 7.31 (d, *J* = 3.6 Hz, 1H, furan 3-H), 7.52 (dd, *J* = 9.2 Hz, *J'* = 2.0 Hz, 1H, 2'-H), 7.66 (d, *J* = 1.6 Hz, 1H, furan 5-H), 7.78 (d, *J* = 2.4 Hz, 1H, 4'-H), 7.86 (dd, *J* = 7.6 Hz, *J'* = 1.2 Hz, 1H), 7.92 (dd, *J* = 7.6 Hz, *J'* = 1.6 Hz, 1H) (pyridine 3-H, pyridine 5-H), superimposed in part 7.96 (dd, *J* = *J'* = 7.6 Hz, 1H, pyridine 4-H), 8.36 (d, *J* = 9.2 Hz, 1H, 1'-H).

^{13}C NMR (100.6 MHz, CD_3OD) δ: 23.48 (CH_3, 9'-CH_3), 27.26 (CH, C11'), 27.71 (CH_2), 27.82 (CH_2) (C6, C7), 27.91 (CH, C7'), 29.32 (CH_2, C13'), 30.03 (CH_2), 30.13 (CH_2), 30.37 (CH_2), 30.54 (CH_2) (C2, C3, C4, C5), 31.20 (CH_2, C8), 36.05 (CH_2), 36.09 (CH_2) (C6', C10'), 40.49 (CH_2, C1), 49.68 (CH_2, C9), 110.96 (CH, furan C3), 113.28 (CH, furan C4), 115.58 (C, C12a'), 117.54 (C, C11a'), 119.11 (CH, C4'), 121.01 (CH), 121.83 (CH) (pyridine C3, pyridine C5), 125.13 (CH, C8'), 126.64 (CH, C2'), 129.45 (CH, C1'), 134.50 (C, C9'), 139.53 (CH, pyridine C4), 140.19 (C, C3'), 140.92 (C, C4a'), 145.29 (CH, furan C5), 149.62 (C), 150.83 (C) (pyridine C6, furan C2), 151.12 (C, C5a'), 154.15 (C, pyridine C2), 156.85 (C, C12'), 166.34 (C, CONH).

HRMS ESI:

Calculated for $[C_{36}H_{41}{}^{35}ClN_4O_2 + H]^+$:	597.2991
Found:	597.2993

Synthesis of (±)-*N*-{9-[(3-chloro-6,7,10,11-tetrahydro-9-methyl-7,11-methanocycloocta[*b*]quinolin-12-yl)amino]nonyl}-4-(morpholin-4-yl)pyridine-2-carboxamide, 25e

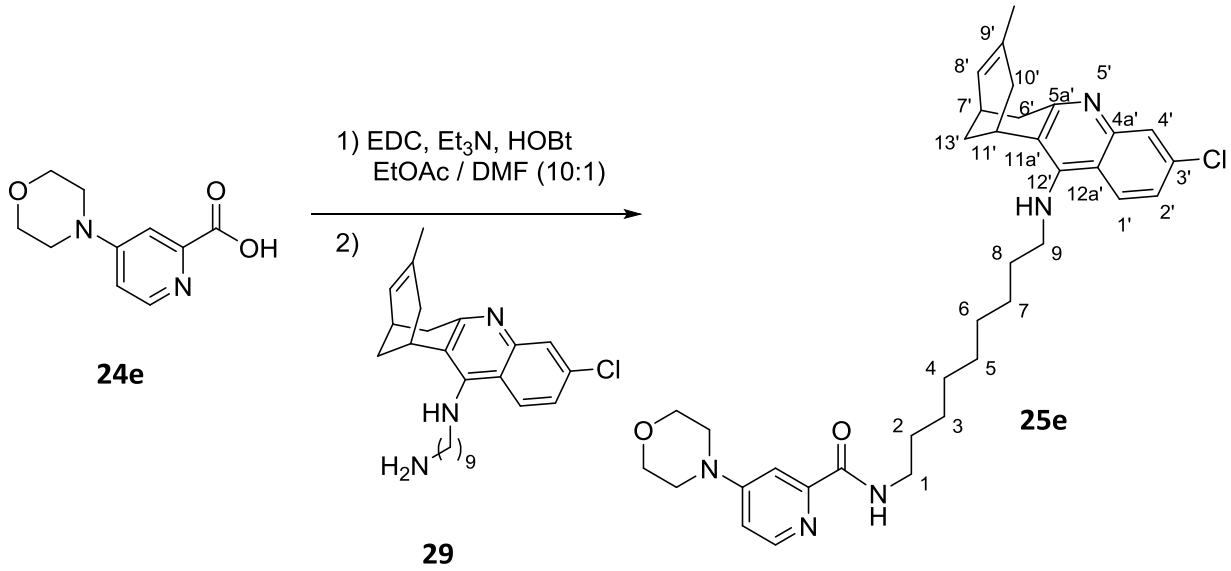

In a 50 mL round-bottomed flask equipped with magnetic stirrer, 4-(morpholine-4-yl)pyridine-2-carboxylic acid, **24e**, (92 mg, 0.44 mmol) was suspended in a mixture of EtOAc / DMF (9.9 mL, 10:1), and treated subsequently with EDC·HCl (115 mg, 0.6 mmol), Et_3N (0.14 mL, 1 mmol) and HOBt (82 mg, 0.6 mmol). After stirring for 15 min at r. t., a solution of the amine **29** (171 mg, 0.4 mmol) in EtOAc / DMF (3.3 mL, 10:1) was added and the reaction mixture was stirred at r. t. overnight, then evaporated to dryness. The resulting brown oil (579 mg) was purified through column chromatography (silica gel 40–63 µm, 58 g, Ø = 4 cm; #1, 400 mL, CH_2Cl_2 / 50% aq. NH_4OH 100:0.4; #2-251, 4800 mL, CH_2Cl_2 / MeOH / 50% aq. NH_4OH 99:1:0.4), to afford **25e** (#65-135, 131 mg, 53% yield) as a yellow oil.

R_f = 0.52 (silica gel, 10 cm, CH_2Cl_2 / MeOH / 50% aq. NH_4OH 9.6:0.4:0.04)

Analytical sample of 25e·HCl

In a 10 mL round-bottomed flask, **25e** (131 mg) was dissolved in CH_2Cl_2 (2 mL), filtered through a 0.2 µm PTFE filter, treated with excess of a methanolic solution of HCl (2 mL, 1.25 M), and evaporated to dryness. The resulting solid was washed with EtOAc (3 x 3 mL), hexane (3 x 3 mL), and pentane (3 x 3 mL), evaporated to dryness and dried at 45 °C/2 Torr for 5 days, to provide **25e·HCl** (61 mg) as a pale brown solid.

Melting Point: 162 °C (dec).

IR (ATR) ν: 3600–2400 (max at 3226, 3050, 2998, 2924, 2854, N–H, $^{+}$N–H, C–H st), 1770, 1760, 1677, 1628, 1586, 1554, 1534 (C=O, Ar–C–C, Ar–C–N st) cm^{-1}.

^{1}H NMR (400 MHz, CD_3OD) δ: 1.34–1.48 (complex signal, 10H, 3-H_2, 4-H_2, 5-H_2, 6-H_2, 7-H_2), 1.58 (s, 3H, 9'-CH_3), 1.65 (tt, *J* = *J'* = 7.2 Hz, 2H, 2-H_2), 1.86 (tt, *J* = *J'* = 7.2 Hz, 2H, 8-H_2) superimposed in part 1.90 (m, 1H, 13'-H_{syn}) superimposed in part 1.93 (br d, *J* = 17.6 Hz, 1H, 10'-H_{endo}), 2.08 (dm, *J* = 12.0 Hz, 1H, 13'-H_{anti}), 2.55 (dm, *J* = 17.6 Hz, 1H, 10'-H_{exo}), 2.77 (m, 1H, 7'-H), 2.87 (br d, *J* = 18.0 Hz, 1H, 6'-H_{endo}), 3.21 (dd, *J* = 18.0 Hz, *J'* = 5.6 Hz, 1H, 6'-H_{exo}), 3.42 (t, *J* = 7.2 Hz, 2H, 1-H_2) superimposed in part 3.44 (m, 1H, 11'-H), 3.77–3.87 (complex signal, 8H, morpholine CH_2), 3.98 (t, *J* = 7.2 Hz, 2H, 9-H_2), 4.85 (s, NH, $^{+}$NH), 5.58 (br d, *J* = 4.8 Hz, 1H, 8'-H), 7.24 (br d, *J* = 6.8 Hz, 1H, pyridine 5-H), 7.55 (br d, *J* = 9.2 Hz, 1H, 2'-H), 7.78 (d, *J* = 1.6 Hz, 1H, 4'-H), 7.83 (s, 1H, pyridine 3-H), 8.16 (d, *J* = 6.8 Hz, 1H, pyridine 6-H), 8.40 (d, *J* = 9.2 Hz, 1H, 1'-H).

^{13}C NMR (100.6 MHz, CD_3OD) δ: 23.47 (CH_3, 9'-CH_3), 27.28 (CH, C11'), 27.79 (CH_2), 27.85 (CH_2) (C6, C7), 28.03 (CH, C7'), 29.32 (CH_2, C13'), 30.16 (CH_2), 30.21 (CH_2), 30.26 (CH_2), 30.51 (CH_2) (C2, C3, C4, C5), 31.24 (CH_2, C8), 36.05 (CH_2), 36.10 (CH_2) (C6', C10'), 41.47 (CH_2, C1), 48.16 (CH_2, C9), 67.17 (4CH_2, morpholine C2, C3, C5, C6), 107.04 (CH, pyridine C3), 109.35 (CH, pyridine C5), 115.64 (C, C12a'), 117.59 (C, C11a'), 119.12 (CH, C4'), 125.14 (CH, C8'), 126.64 (CH, C2'), 129.50 (CH, C1'), 134.52 (C, C9'), 140.21 (C, C3'), 140.97 (C, C4a'), 141.10 (CH, pyridine C6), 143.18 (C, pyridine C4), 151.20 (C, C5a'), 156.92 (C, C12'), 159.44 (C, pyridine C2), 160.78 (C, CONH).

HRMS ESI:

Calculated for $[C_{36}H_{46}{}^{35}ClN_5O_2 + H]^+$: 616.3413

Found: 616.3414

Synthesis of (±)-*N*-{9-[(3-chloro-6,7,10,11-tetrahydro-9-methyl-7,11-methanocycloocta[*b*]quinolin-12-yl)amino]nonyl}imidazo[1,2-*a*]pyridine-2-carboxamide, 25f

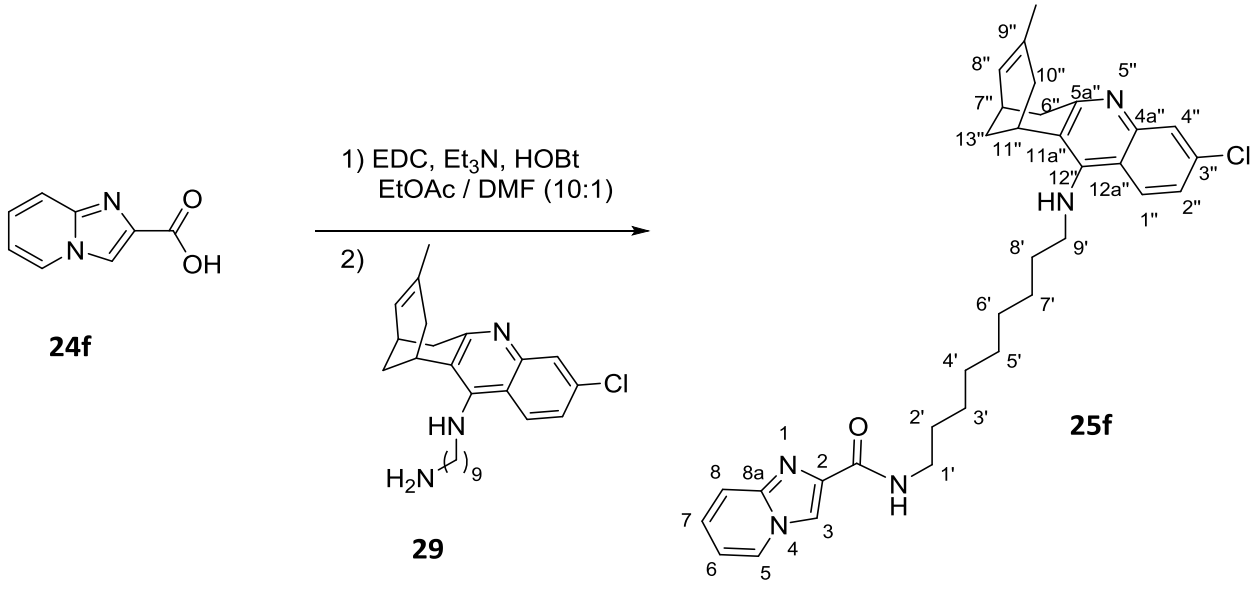

In a 50 mL round-bottomed flask equipped with magnetic stirrer, imidazo[1,2-*a*]pyridine-2-carboxylic acid, **24f**, (78 mg, 0.48 mmol) was suspended in a mixture of EtOAc / DMF (7.7 mL, 10:1), and treated subsequently with EDC·HCl (127 mg, 0.66 mmol), Et_3N (0.15 mL, 1.1 mmol) and HOBt (90 mg, 0.66 mmol). After stirring for 15 min at r. t., a solution of the amine **29** (187 mg, 0.44 mmol) in EtOAc / DMF (6.6 mL, 10:1) was added and the reaction mixture was stirred at r. t. overnight, then evaporated to dryness. The resulting brown oil (596 mg) was purified through column chromatography (silica gel 40–63 µm, 60 g, Ø = 4 cm; #1, 400 mL, CH_2Cl_2 / 50% aq. NH_4OH 100:0.4; #2-21, 600 mL, CH_2Cl_2 / MeOH / 50% aq. NH_4OH 99:1:0.4; #22-159, 1600 mL, CH_2Cl_2 / MeOH / 50% aq. NH_4OH 98:2:0.4), to afford **25f** (#44-81, 162 mg, 65% yield) as a yellow oil.

R_f = 0.38 (silica gel, 10 cm, CH_2Cl_2 / MeOH / 50% aq. NH_4OH 9.6:0.4:0.04)

Analytical sample of 25f·HCl

In a vial, **25f** (162 mg) was dissolved in CH_2Cl_2 (2 mL), filtered through a 0.2 µm PTFE filter, treated with excess of a methanolic solution of HCl (1 mL, 1.25 M), and evaporated to dryness. The resulting solid was washed with pentane (5 x 2 mL), evaporated to dryness, and dried at 45 °C/2 Torr for 5 days, to provide **25f·HCl** (105 mg) as a pale brown solid.

Melting Point: 152 °C (dec).

IR (ATR) ν: 3600–2400 (max at 3235, 3054, 2925, 2854, 2790, N–H, $^{+}$N–H, C–H st), 1770, 1757, 1668, 1630, 1583, 1564 (C=O, Ar–C–C, Ar–C–N st) cm^{-1}.

^{1}H NMR (400 MHz, CD_3OD) δ: 1.30–1.48 (complex signal, 10H, 3'-H_2, 4'-H_2, 5'-H_2, 6'-H_2, 7'-CH_2), 1.58 (s, 3H, 9''-CH_3), 1.65 (m, 2H, 2'-H_2), 1.86 (m, 2H, 8'-H_2) superimposed in part 1.90 (m, 1H, 13''-H_{syn}) superimposed in part 1.93 (br d, *J* = 18.0 Hz, 1H, 10''-H_{endo}), 2.08 (dm, *J* = 12.4 Hz, 1H, 13''-H_{anti}), 2.55 (dd, *J* = 18.0 Hz, *J* = 3.2 Hz, 1H, 10''-H_{exo}), 2.77 (m, 1H, 7''-H), 2.86 (dm, *J* = 17.6 Hz, 1H, 6''-H_{endo}), 3.20 (dd, *J* = 17.6 Hz, *J'* = 5.6 Hz, 1H, 6''-H_{exo}), 3.38–3.50 (complex signal, 3H, 1'-H_2, 11''-H), 3.98 (t, *J* = 6.8 Hz, 2H, 9'-H_2), 4.85 (s, NH, $^{+}$NH), 5.58 (br d, *J* = 4.4 Hz, 1H, 8''-H), 7.48 (br dd, *J* = *J'* = 7.2 Hz, 1H, 7-H), 7.55 (dd, *J* = 9.2 Hz, *J'* = 1.2 Hz, 1H, 2''-H), 7.76 (d, *J* = 1.2 Hz, 1H, 4''-H), 7.88 (m, 1H), 7.97 (m, 1H) (6-H, 8-H), 8.40 (d, *J* = 9.2 Hz, 1H, 1''-H), 8.65 (m, 1H, 3-H), 8.84 (m, 1H, 5-H).

^{13}C NMR (100.6 MHz, CD_3OD) δ: 23.46 (CH_3, 9''-CH_3), 27.27 (CH, C11''), 27.78 (CH_2), 27.83 (CH_2) (C6', C7'), 27.99 (CH, C7''), 29.31 (CH_2, C13''), 30.18 (CH_2), 30.24 (CH_2), 30.49 ($2CH_2$) (C2', C3', C4', C5'), 31.24 (CH_2, C8'), 36.05 (CH_2), 36.11 (CH_2) (C6'', C10''), 40.93 (CH_2, C1'), 49.69 (CH_2, C9'), 113.82 (CH, C6 or C8), 115.61 (CH, C12a''), 117.56 (C, C11a''), 118.72 (CH, C7), 119.12 (CH, C4''), 125.12 (CH, C8''), 126.65 (CH, C2''), 129.51 (CH, C1''), 134.50 (C, C9''), 135.73 (CH, C8 or C6), 140.17 (C, C3''), 140.94 (C, C4a''), 150.22 (C, C2 or C8a), 151.18 (C, C5a''), 155.90 (C, C8a or C2), 156.88 (C, C12''), 177.83 (C, CONH).

HRMS ESI:

Calculated for $[C_{34}H_{40}{}^{35}ClN_5O + H]^{+}$:	570.2994
Found:	570.2994

Synthesis of (±)-*N*-{9-[(3-chloro-6,7,10,11-tetrahydro-9-methyl-7,11-methanocycloocta[*b*]quinolin-12-yl)amino]nonyl}-8-hydroxyquinoline-2-carboxamide, 25g

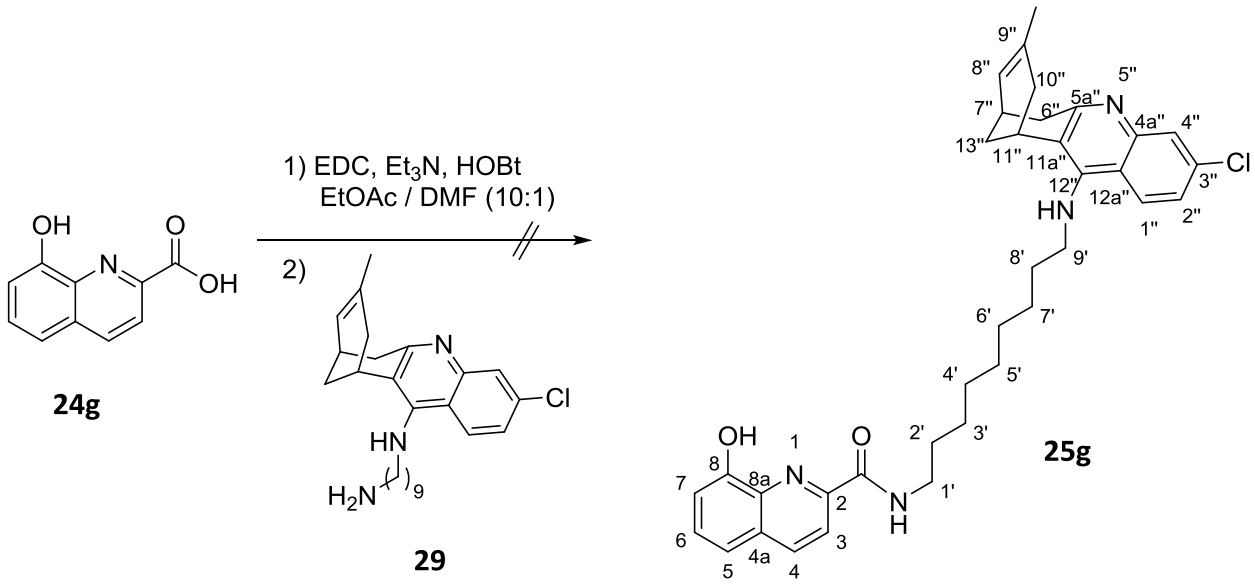

In a 50 mL round-bottomed flask equipped with magnetic stirrer, 8-hydroxyquinoline-2-carboxylic acid, **25g**, (73 mg, 0.39 mmol) was suspended in a mixture of EtOAc / DMF (7.7 mL, 10:1), and treated subsequently with EDC·HCl (100mg, 0.53 mmol), Et_3N (0.12 mL, 0.88 mmol) and HOBt (72 mg, 0.93 mmol). After stirring for 10 min at r. t., a solution of the amine **29** (150 mg, 0.38 mmol) in EtOAc / DMF (5.5 mL, 10:1) was added and the reaction mixture was stirred at r. t. overnight, then evaporated to dryness. The resulting brown oil (230 mg) was subjected to column chromatography (silica gel 40–63 µm, 12 g, Ø = 2 cm; #1, 150 mL, CH_2Cl_2 / 50% aq. NH_4OH 100:0.4; #2-72, 1400 mL, CH_2Cl_2 / MeOH / 50% aq. NH_4OH 99.5:0.5:0.4; #73-242, 1500 mL, CH_2Cl_2 / MeOH / 50% aq. NH_4OH 99:1:0.4). After analysing all fractions by ^{1}H-NMR, the expected compound was not found.

Synthesis of 8-acetoxyquinoline-2-carboxylic acid, 30

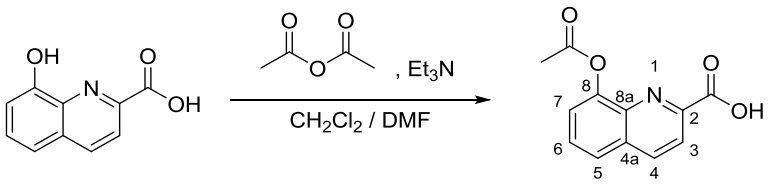

24g **30**

In a 25 mL round-bottomed flask equipped with magnetic stirrer, 8-hydroxyquinoline-2-carboxylic acid, **24g**, (200 mg, 1.06 mmol), Et_3N (0.36 mL, 2.64 mmol) and acetic anhydride (0.5 mL, 5.35 mmol) were dissolved in a mixture of CH_2Cl_2 (4.5 mL) and DMF (1 mL) and stirred at reflux for 2 h. The resulting solution was acidified with 5 N HCl until pH = 2, diluted with CH_2Cl_2 (5 mL) and washed with H_2O (3 x 10 mL), then evaporated to dryness, to provide **30** (218 mg, 89% yield) as a white solid.

R_f = 0.14 (silica gel, 10 cm, CH_2Cl_2 / MeOH / 50% aq. NH_4OH 9:1:0.4)

^{1}H NMR (400 MHz, $CDCl_3$) δ: 1.50 (s, 3H, $COCH_3$), 7.59 (dd, *J* = 7.6 Hz, *J'* = 1.6 Hz, 1H, 5-H), 7.72 (dd, *J* = 8.4 Hz, *J'* = 7.6 Hz, 1H, 6-H), 7.86 (dd, *J* = 8.4 Hz, *J'* = 1.6 Hz, 1H, 7-H), 8.32 (d, *J* = 8.4 Hz, 1H, 4-H), 8.47 (d, *J* = 8.4 Hz, 1H, 3-H).

Synthesis of (±)-8-acetoxy-*N*-{9-[(3-chloro-6,7,10,11-tetrahydro-9-methyl-7,11-methanocycloocta[*b*]quinolin-12-yl)amino]nonyl}quinoline-2-carboxamide, 31

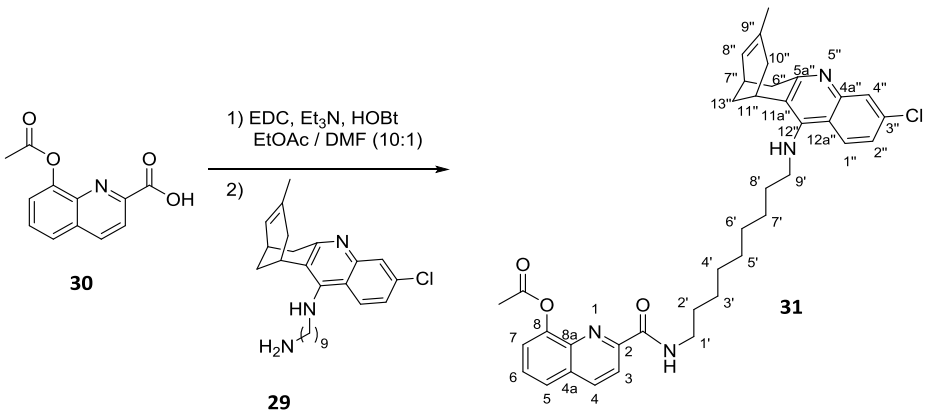

In a 50 mL round-bottomed flask equipped with magnetic stirrer, 8-acetoxyquinoline-2-carboxylic acid, **30**, (125 mg, 0.54 mmol) was suspended in a mixture of EtOAc / DMF (9.9 mL, 10:1), and treated subsequently with EDC·HCl (142mg, 0.74 mmol), Et_3N (0.17 mL, 1.23 mmol) and HOBt (100 mg, 0.74 mmol). After stirring for 10 min at r. t., a solution of the amine **29** (125 mg, 0.54 mmol) in EtOAc / DMF (8.8 mL, 10:1) was added and the reaction mixture was stirred at r. t. overnight, then evaporated to dryness. The resulting brown oil (597 mg) was purified through column chromatography (silica gel 40–63 µm, 30 g, Ø = 2 cm; #1, 600 mL, CH_2Cl_2 / 50% aq. NH_4OH 100:0.4; #2-221, 3500 mL, CH_2Cl_2 / MeOH / 50% aq. NH_4OH 99:1:0.4), to afford impure **31** (#30-88, 131 mg). The impure product was subjected to a second purification through column chromatography (silica gel 40–63 µm, 6.5 g, Ø = 1 cm; #1, 400 mL hexane / Et_3N 100:0.2 #2, 400 mL, hexane / EtOAc / Et_3N 90:10:0.2, #3, 400 mL, hexane / EtOAc / Et_3N 80:20:0.2, #4-28, 400 mL, hexane / EtOAc / Et_3N 70:30:0.2), to provide pure **31** (98 mg, 31% yield) as a yellow oil.

^{1}H NMR (400 MHz, $CDCl_3$) δ: 1.20–1.32 (complex signal, 10H, 3'-H_2, 4'-H_2, 5'-H_2, 6'-H_2, 7'-CH_2), 1.40 (m, 2H, 2'-H_2), 1.52 (s, 3H, 9''-CH_3), superimposed 1.62 (s, NH), 1.70 (tt, *J* = *J'* = 7.2 Hz, 2H, 8'-H_2), 1.84 (br d, *J* = 17.6 Hz, 1H, 10''-H_{endo}), 1.90 (dm, *J* = 12.8 Hz, 1H, 13''-H_{syn}), 2.03 (m, 1H, 13''-H_{anti}), superimposed in part 2.04 (s, 3H, $COCH_3$), 2.52 (dm, *J* = 17.6 Hz, 1H, 10''-H_{exo}), 2.68 (m, 1H, 7''-H), 3.00 (dm, *J* = 17.6 Hz, 1H, 6''-H_{endo}), 3.12 (dd, *J* = 17.6 Hz, *J'* = 5.2 Hz, 1H, 6''-H_{exo}), 3.29 (m, 2H, 1'-H_2), 3.37–3.65 (complex signal, 3H, 11''-H, 9'-H_2), 5.51 (br d, *J* = 5.6 Hz, 1H, 8''-H), 7.23 (dd, *J* = 7.6 Hz, *J'* = 1.2 Hz, 1H, 5-H) superimposed in part 7.27 (m, 1H, 2''-H), 7.41 (dd, *J* = 8.4 Hz, *J'* = 1.2 Hz, 1H, 7-H), 7.54 (dd, *J* = 8.4 Hz, *J'* = 7.6 Hz, 1H, 6-H), 7.96 (d, *J* = 9.2 Hz, 1H, 1''-H), 8.29 (br t, *J* = 5.6 Hz, CONH), 8.33 (d, *J* = 8.4 Hz, 1H), superimposed in part 8.35 (d, *J* = 8.4 Hz, 1H) (3-H, 4-H), superimposed in part 8.34 (d, *J* = 2.0 Hz, 1H, 4''-H).

.

Synthesis of (±)-*N*-{9-[(3-chloro-6,7,10,11-tetrahydro-9-methyl-7,11-methanocycloocta[*b*]quinolin-12-yl)amino]nonyl}-8-hydroxyquinoline-2-carboxamide, (±)-25g

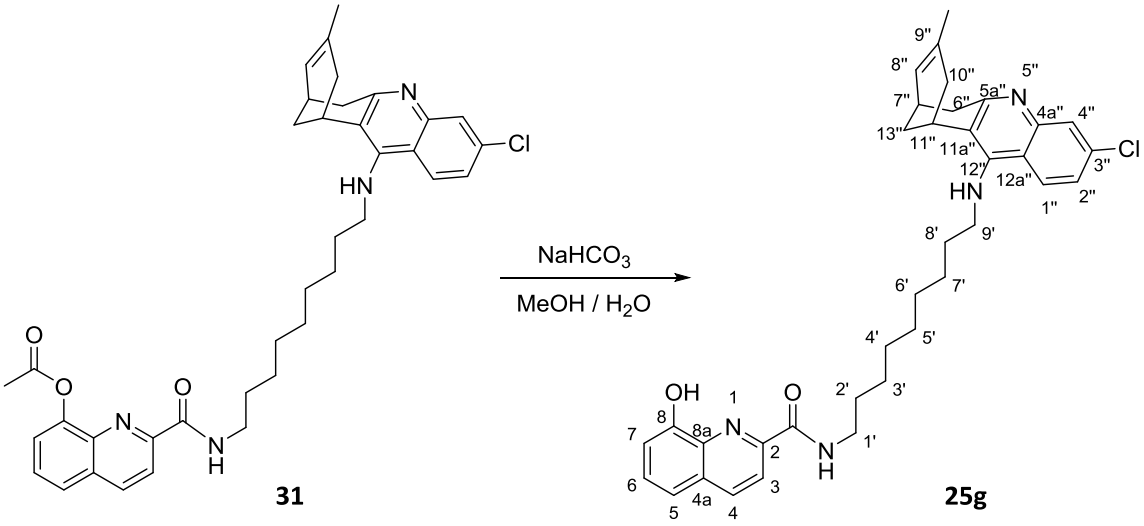

In a 50 mL round-bottomed flask equipped with magnetic stirrer, **31** (90 mg, 0.15 mmol) was dissolved in MeOH (3.2 mL) and H_2O (1.75 mL) and treated with sat. aq. $NaHCO_3$ (2.4 mL). The resulting suspension was stirred at r. t. overnight. The mixture was concentrated under reduced pressure, taken up in H_2O (2 mL), and extracted with CH_2Cl_2 (3 x 3 mL). The combined organic extracts were washed with H_2O (3 x 5 mL), dried over anhydrous Na_2SO_4, filtered, and evaporated under reduced pressure to provide **25g** (86 mg, 93% yield).

R_f = 0.72 (silica gel, 10 cm, CH_2Cl_2 / MeOH / 50% aq. NH_4OH 9.5:0.5:0.04)

Analytical sample of 25g·HCl

In a 10 mL round-bottomed flask, **25g** (86 mg) was dissolved in CH_2Cl_2 (2 mL), filtered through a 0.2 µm PTFE filter, treated with excess of a methanolic solution of HCl (2 mL, 1.25 M), and evaporated to dryness. The resulting solid was washed with EtOAc (3 x 5 mL), hexane (3 x 5 mL), and pentane (3 x 5 mL), evaporated to dryness, and dried at 45 °C/2 Torr for 3 days, to provide **25g·HCl** (97 mg) as a pale brown solid.

Melting Point: 147–149 °C

IR (ATR) ν: 3600–2300 (max at 3241, 3054, 2926, 2854, N–H, $^+$N–H, O–H, C–H st), 1721, 1651, 1631, 1583, 1567, 1502 (C=O, Ar–C–C, Ar–C–N st) cm^{-1}.

^{1}H NMR (400 MHz, CD_3OD) δ: 1.33–1.45 (complex signal, 10H, 3'-H_2, 4'-H_2, 5'-H_2, 6'-H_2, 7'-H_2), 1.56 (s, 3H, 9''-CH_3), 1.69 (tt, *J* = *J'* = 6.8 Hz, 2H, 2'-H_2), 1.82 (tt, *J* = *J'* = 6.8 Hz, 2H, 8'-H_2) superimposed in part 1.90 (m, 1H, 13''-H_{syn}), superimposed in part 1.91 (br d, *J* = 17.6 Hz, 1H, 10''-H_{endo}), 2.06 (dm, *J* = 12.8 Hz, 1H, 13''-H_{anti}), 2.52 (dd, *J* = 17.6 Hz, *J'* = 4.4 Hz, 1H, 10''-H_{exo}), 2.74 (m, 1H, 7''-H), 2.85 (br d, *J* = 17.6 Hz, 1H, 6''-H_{endo}), 3.17 (dd, *J* = 17.6 Hz, *J'* = 5.6 Hz, 1H, 6''-H_{exo}), 3.40 (m, 1H, 11''-H), 3.47 (t, *J* = 6.8 Hz, 2H, 1'-H_2), 3.92 (br t, *J* = 6.8 Hz, 2H, 9'-H_2), 4.85 (s, NH, $^{+}$NH, OH), 5.56 (br d, *J* = 5.2 Hz, 1H, 8''-H), 7.12 (dd, *J* = 7.6 Hz, *J'* = 0.8 Hz, 1H, 5-H), 7.38 (br d, *J* = 8.0 Hz, 1H, 7-H), 7.48 (br d, *J* = 9.2 Hz, 1H, 2''-H), superimposed 7.49 (dd, *J* = 8.0 Hz, *J'* = 7.6 Hz, 1H, 6-H), 7.70 (d, *J* = 2.0 Hz, 1H, 4''-H), 8.15 (d, *J* = 8.4 Hz, 1H, 3-H or 4-H), 8.32 (d, *J* = 9.2 Hz, 1H, 1''-H), 8.36 (d, *J* = 8.4 Hz, 1H, 4-H or 3-H).

^{13}C NMR (100.6 MHz, CD_3OD) δ: 23.46 (CH_3, 9''-CH_3), 27.25 (CH, C11''), 27.68 (CH_2), 27.83 (CH_2) (C6', C7'), 27.94 (CH, C7''), 29.29 (CH_2, C13''), 29.98 (CH_2), 30.10 (CH_2), 30.33 (CH_2), 30.47 (CH_2) (C2', C3', C4', C5'), 31.16 (CH_2, C8'), 36.00 (CH_2), 36.04 (CH_2) (C6'', C10''), 40.59 (CH_2, C1'), 49.59 (CH_2, C9'), 112.79 (CH, C5), 115.52 (C, C12a''), 117.50 (C, C11a''), 118.91 (CH, C7), 119.08 (CH, C4''), 119.87 (CH, C3 or C4), 125.11 (CH, C8''), 126.56 (CH, C2''), 129.31 (CH, C1''), 130.48 (CH, C6), 134.52 (C, C9''), 138.34 (C, C4a), 138.78 (CH, C4 or C3), 140.17 (C, C3''), 140.87 (C, C4a''), 148.80 (C), 154.03 (C) (C8, C8a), 151.07 (C, C5a''), 156.80 (C, C12''), 166.12 (C), 166.49 (C) (C2, CONH).

HRMS ESI:

Calculated for $[C_{36}H_{41}{}^{35}ClN_4O_2 + H]^+$: 597.2991

Found: 597.2984

Synthesis of (±)-*N*-{9-[(3-chloro-6,7,10,11-tetrahydro-9-methyl-7,11-methanocycloocta[*b*]quinolin-12-yl)amino]nonyl}-3,5-hydroxybenzamide, 44

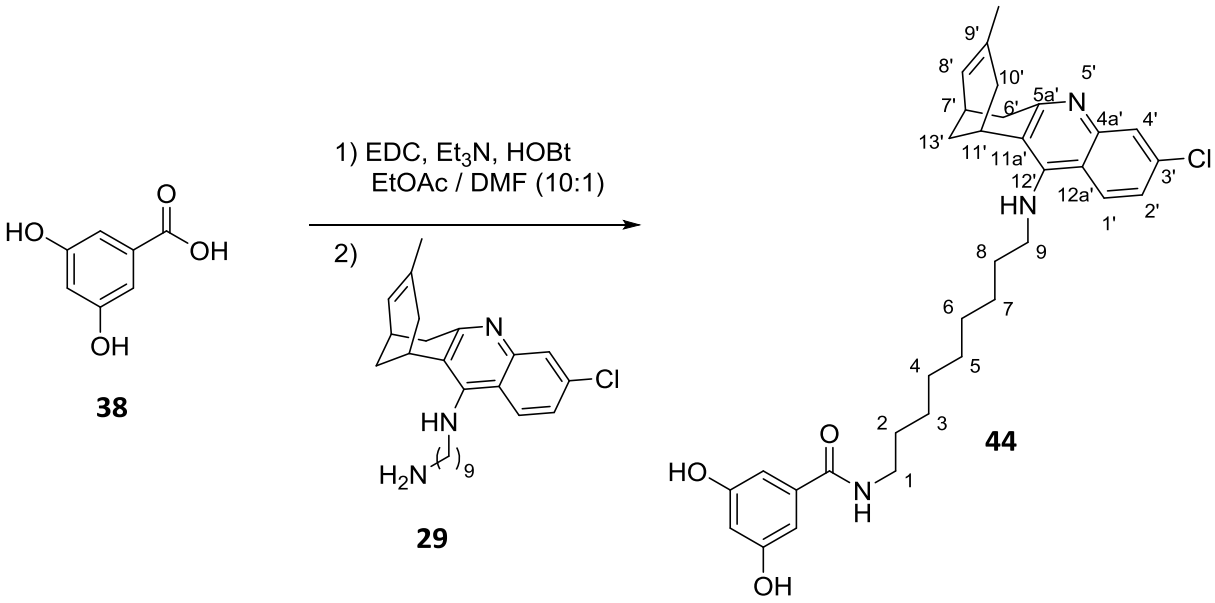

In a 50 mL round-bottomed flask equipped with magnetic stirrer, 3,5-dihydroxybenzoic acid, **38**, (90 mg, 0.59 mmol) was suspended in a mixture of EtOAc / DMF (11 mL, 10:1), and treated subsequently with EDC·HCl (157 mg, 0.80 mmol), Et_3N (0.18 mL, 1.33 mmol) and HOBt (108 mg, 0.80 mmol). After stirring for 10 min at r. t., a solution of the amine **29** (227 mg, 0.53 mmol) in EtOAc / DMF (6.6 mL, 10:1) was added and the reaction mixture was stirred at r. t. overnight, then evaporated to dryness. The resulting yellow oil (759 mg) was purified through column chromatography (silica gel 40–63 µm, 61 g, Ø = 4 cm; #1, 400 mL, CH_2Cl_2 / 50% aq. NH_4OH 100:0.4; #2, 400 mL, CH_2Cl_2 / MeOH / 50% aq. NH_4OH 99:1:0.4; #3-11, 1200 mL, CH_2Cl_2 / MeOH / 50% aq. NH_4OH 98:2:0.4; #12-15, 400 mL, CH_2Cl_2 / MeOH / 50% aq. NH_4OH 97:3:0.4; #16-19, 400 mL, CH_2Cl_2 / MeOH / 50% aq. NH_4OH 96:4:0.4; #20-35, 1600 mL, CH_2Cl_2 / MeOH / 50% aq. NH_4OH 95:5:0.4; #36-38, 400 mL, CH_2Cl_2 / MeOH / 50% aq. NH_4OH 93:7:0.4), to afford **44** (#24-30, 188 mg, 63% yield) as a yellowish solid.

R_f = 0.47 (silica gel, 10 cm, CH_2Cl_2 / MeOH / 50% aq. NH_4OH 9:1:0.04)

Analytical sample of 44·HCl

In a 25 mL round-bottomed flask, **44** (188 mg) was dissolved in CH_2Cl_2 (5 mL), filtered through a 0.2 µm PTFE filter, treated with excess of a methanolic solution of HCl (2 mL, 1.25 M), and evaporated to dryness. The resulting solid was washed with EtOAc (2 x 5 mL), hexane (2 x 5 mL), and pentane (2 x

5 mL), evaporated to dryness and dried at 45 °C/2 Torr for 3 days, to provide **44·HCl** (116 mg) as a pale brown solid.

Melting Point: 159–160 °C

IR (ATR) ν: 3600–2400 (max at 3243, 3076, 2926, 2854, N–H, $^{+}$N–H, O–H, C–H st), 1631, 1584, 1512 (C=O, Ar–C–C, Ar–C–N st) cm^{-1}.

^{1}H NMR (400 MHz, CD_3OD) δ: 1.33–1.48 (complex signal, 10H, 3-H_2, 4-H_2, 5-H_2, 6-H_2, 7-H_2), 1.58 (s, 3H, 9'-CH_3), superimposed 1.58 (m, 2H, 2-H_2), 1.84 (tt, *J* = *J'* = 7.2 Hz, 2H, 8-H_2), superimposed in part 1.93 (br d, *J* = 17.6 Hz, 1H, 10'-H_{endo}), superimposed in part 1.94 (m, 1H, 13'-H_{syn}), 2.08 (dm, *J* = 12.8 Hz, 1H, 13'-H_{anti}), 2.54 (dd, *J* = 17.6 Hz, *J'* = 5.6 Hz, 1H, 10'-H_{exo}), 2.76 (m, 1H, 7'-H), 2.84 (ddd, *J* = 17.6 Hz, *J'* = *J''* = 2.0 Hz, 1H, 6'-H_{endo}), 3.19 (dd, *J* = 17.6 Hz, *J'* = 5.6 Hz, 1H, 6'-H_{exo}), 3.31 (m, 2H, 1-H_2), 3.42 (m, 1H, 11'-H), 3.96 (td, *J* = 7.2 Hz, *J'* = 3.6 Hz, 2H, 9-H_2), 4.85 (s, NH, $^{+}$NH, OH), 5.58 (br d, *J* = 5.6 Hz, 1H, 8'-H), 6.38 (dd, *J* = *J'* = 2.4 Hz, 1H, phenyl 4-H), 6.67 [d, *J* = 2.4 Hz, 2H, phenyl 2(6)-H], 7.55 (dd, *J* = 9.2 Hz, *J'* = 2.0 Hz, 1H, 2'-H), 7.74 (d, *J* = 2.0 Hz, 1H, 4'-H), 8.38 (d, *J* = 9.2 Hz, 1H, 1'-H).

^{13}C NMR (100.6 MHz, CD_3OD) δ: 23.46 (CH_3, 9'-CH_3), 27.27 (CH, C11'), 27.70 (CH_2), 27.84 (CH_2) (C6, C7), 27.88 (CH, C7'), 29.29 (CH_2, C13'), 30.04 (CH_2), 30.10 (CH_2), 30.37 ($2CH_2$) (C2, C3, C4, C5), 31.19 (CH_2, C8), 36.02 (CH_2), 36.07 (CH_2) (C6', C10'), 40.82 (CH_2, C1), 49.00 (CH_2, C9), 106.40 (CH, phenyl C4), 106.66 [2CH, phenyl C2(6)], 115.63 (C, C12a'), 117.56 (C, C11a'), 119.10 (CH, C4'), 125.10 (CH, C8'), 126.63 (CH, C2'), 129.45 (CH, C1'), 134.53 (C, C9'), 138.05 (C, phenyl C1), 140.22 (C, C3'), 140.95 (C, C4a'), 151.15 (C, C5a'), 156.91 (C, C12'), 159.79 [2C, phenyl C3(5)], 170.46 (C, CONH).

HRMS ESI:

Calculated for $[C_{33}H_{40}{}^{35}ClN_3O_3 + H]^+$: 562.2831

Found: 562.2825

Synthesis of (±)-*N*-{9-[(3-chloro-6,7,10,11-tetrahydro-9-methyl-7,11-methanocycloocta[*b*]quinolin-12-yl)amino]nonyl}-2-hydroxypyridine-3-carboxamide, 45

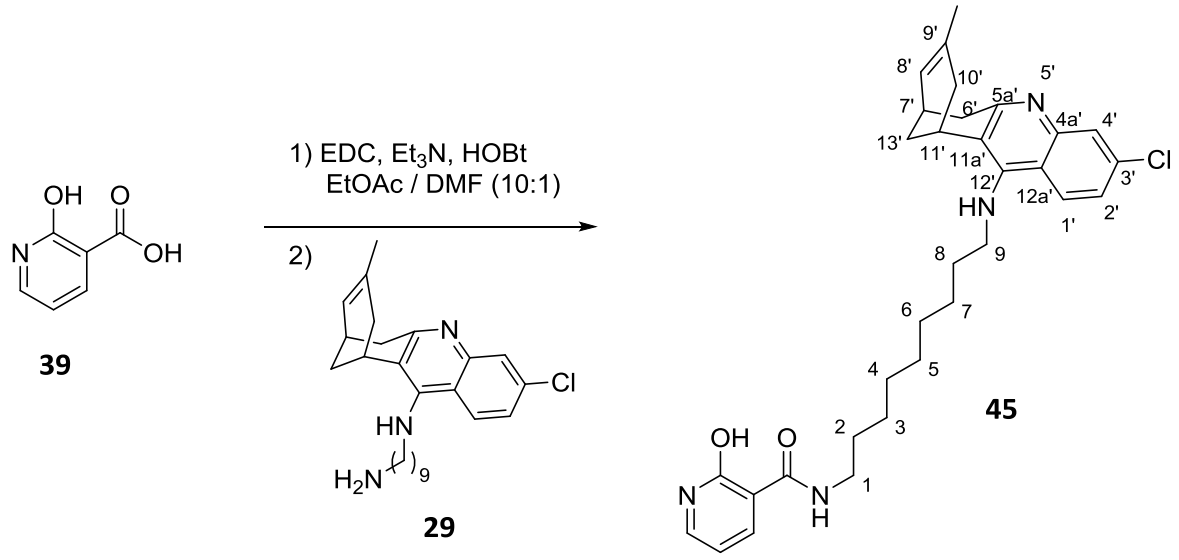

In a 25 mL round-bottomed flask equipped with magnetic stirrer, 2-hydroxynicotinic acid, **39**, (51 mg, 0.37 mmol) was suspended in a mixture of EtOAc / DMF (6.6 mL, 10:1), and treated subsequently with EDC·HCl (99 mg, 0.50 mmol), Et_3N (0.14 mL, 1.01 mmol) and HOBt (69 mg, 0.51 mmol). After stirring for 10 min at r. t., a solution of the amine **29** (143 mg, 0.34 mmol) in EtOAc / DMF (4.4 mL, 10:1) was added and the reaction mixture was stirred at r. t. overnight, then evaporated to dryness. The resulting red oil (423 mg) was purified through column chromatography (silica gel 40–63 µm, 42 g, Ø = 3.5 cm; #1-2, 600 mL, CH_2Cl_2 / 50% aq. NH_4OH 100:0.4; #3, 300 mL, CH_2Cl_2 / MeOH / 50% aq. NH_4OH 99:1:0.4; #4-26, 2400 mL, CH_2Cl_2 / MeOH / 50% aq. NH_4OH 98:2:0.4), to afford **45** (#9-18, 177 mg, 64% yield) as a yellow solid.

R_f = 0.24 (silica gel, 10 cm, CH_2Cl_2 / MeOH / 50% aq. NH_4OH 9.5:0.5:0.04)

Analytical sample of 45·HCl

In a 25 mL round-bottomed flask, **45** (117 mg) was dissolved in CH_2Cl_2 (5 mL), filtered through a 0.2 µm PTFE filter, treated with excess of a methanolic solution of HCl (2 mL, 1.25 M), and evaporated to dryness. The resulting solid was washed with EtOAc (2 x 5 mL), hexane (2 x 5 mL), and pentane (2 x 5 mL), evaporated to dryness and dried at 45 °C/2 Torr for 3 days, to provide **45·HCl** (88 mg) as a pale brown solid.

Melting Point: 135–136 °C

IR (ATR) v: 3600–2400 (max at 3247, 3064, 2925, 2854, N–H, $^{+}$N–H, O–H, C–H st), 1665, 1630, 1599, 1583, 1553 (C=O, Ar–C–C, Ar–C–N st) cm^{-1}.

^{1}H NMR (400 MHz, CD_3OD) δ: 1.32–1.48 (complex signal, 10H, 3-H_2, 4-H_2, 5-H_2, 6-H_2, 7-H_2), 1.58 (s, 3H, 9'-CH_3), superimposed 1.58 (m, 2H, 2-H_2), 1.85 (tt, *J* = *J'* = 7.2 Hz, 2H, 8-H_2), superimposed in part 1.93 (br d, *J* = 17.2 Hz, 1H, 10'-H_{endo}), superimposed in part 1.94 (m, 1H, 13'-H_{syn}), 2.08 (dm, *J* = 12.8 Hz, 1H, 13'-H_{anti}), 2.54 (dd, *J* = 17.2 Hz, *J'* = 4.4 Hz, 1H, 10'-H_{exo}), 2.76 (m, 1H, 7'-H), 2.86 (ddd, *J* = 18.0 Hz, *J'* = *J''* = 2.0 Hz, 1H, 6'-H_{endo}), 3.20 (dd, *J* = 18.0 Hz, *J'* = 5.6 Hz, 1H, 6'-H_{exo}), 3.38 (t, *J* = 7.2 Hz, 2H, 1-H_2), 3.44 (m, 1H, 11'-H), 3.98 (td, *J* = 7.2 Hz, *J'* = 2.8 Hz, 2H, 9-H_2), 4.85 (s, NH, $^{+}$NH, OH), 5.58 (br d, *J* = 5.2 Hz, 1H, 8'-H), 6.56 (dd, *J* = 7.2 Hz, *J'* = 6.0 Hz, 1H, pyridine 5-H), 7.54 (dd, *J* = 9.2 Hz, *J'* = 2.0 Hz, 1H, 2'-H), 7.66 (dd, *J* = 6.0 Hz, *J'* = 2.0 Hz, 1H, pyridine 4-H), 7.76 (d, *J* = 2.0 Hz, 1H, 4'-H), 8.39 (d, *J* = 9.2 Hz, 1H, 1'-H), 8.46 (dd, *J* = 7.2 Hz, *J'* = 2.0 Hz, 1H, pyridine 6-H).

^{13}C NMR (100.6 MHz, CD_3OD) δ: 23.47 (CH_3, 9'-CH_3), 27.28 (CH, C11'), 27.70 (CH_2), 27.85 (CH_2) (C6, C7), 27.97 (CH, C7'), 29.31 (CH_2, C13'), 30.05 (CH_2), 30.10 (CH_2), 30.37 (CH_2), 30.40 (CH_2) (C2, C3, C4, C5), 31.16 (CH_2, C8), 36.04 (CH_2), 36.10 (CH_2) (C6', C10'), 40.24 (CH_2, C1), 49.00 (CH_2, C9), 108.26 (CH, pyridine C5), 115.64 (C, C12a'), 117.58 (C, C11a'), 119.13 (CH, C4'), 121.75 (C, pyridine C3), 125.12 (CH, C8'), 126.65 (CH, C2'), 129.49 (CH, C1'), 134.53 (C, C9'), 140.11 (CH, pyridine C4), 140.23 (C, C3'), 140.97 (C, C4a'), 145.85 (CH, pyridine C2), 151.18 (C, C5a'), 156.95 (C, C12'), 164.36 (C, pyridine C2), 166.00 (C, CONH).

HRMS ESI:

Calculated for $[C_{32}H_{39}{}^{35}ClN_4O_2 + H]^{+}$:	547.2834
Found:	547.2829

Synthesis of (±)-*N*-{9-[(3-chloro-6,7,10,11-tetrahydro-9-methyl-7,11-methanocycloocta[*b*]quinolin-12-yl)amino]nonyl}-1*H*-pyrazole-4-sulfonamide, 46

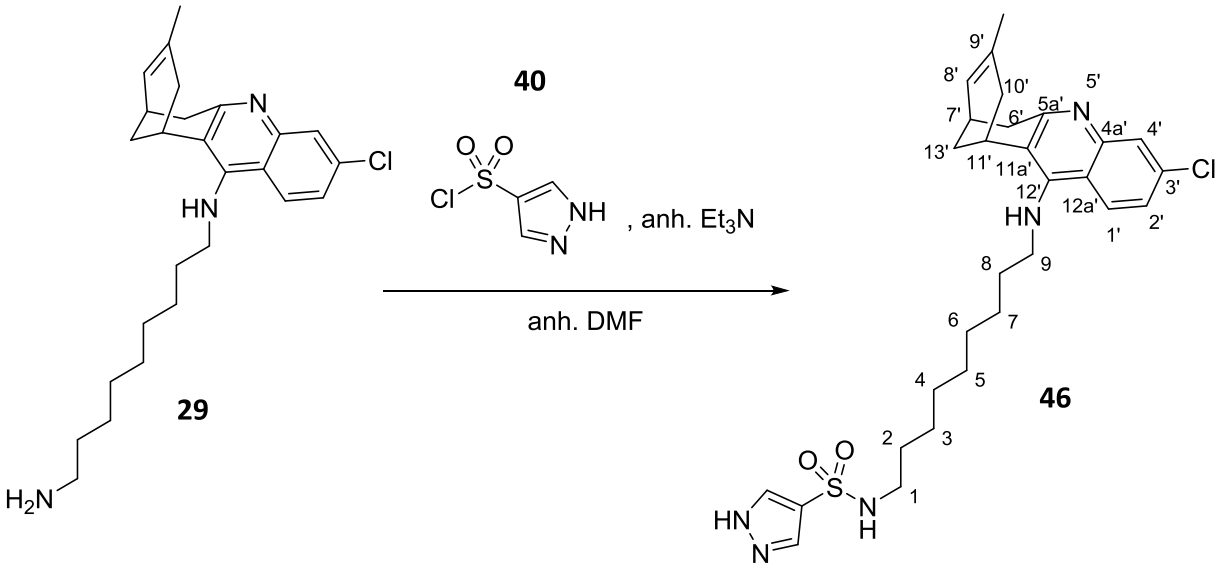

In a 10 mL round-bottomed flask equipped with magnetic stirrer and inert atmosphere, **29** (151 mg, 0.35 mmol) and anhydrous Et_3N (0.07 mL, 0.53 mmol) were dissolved in anhydrous DMF (2.3 mL). The mixture was cooled down to 0 °C in an ice /water bath, treated with 1*H*-pyrazole-4-sulfonyl chloride, **40**, (65 mg, 0.39 mmol) and stirred at r. t. overnight. Because analysis of the reaction mixture by TLC showed the presence of starting material, an additional amount of 1*H*-pyrazole-4-sulfonyl chloride, **40**, (65 mg, 0.39 mmol) was added and the mixture was stirred at r. t. overnight. The resulting dark yellow solution was evaporated to dryness and the residue purified through column chromatography (silica gel 40–63 μm, 45 g; Ø = 3.5 cm; #1, 300 mL, CH_2Cl_2 / 50% aq. NH_4OH 100:0.4; #2, 300 mL, CH_2Cl_2 / MeOH / 50% aq. NH_4OH 99:1:0.4; #3-11, 1000 mL, CH_2Cl_2 / MeOH / 50% aq. NH_4OH 98:2:0.4; #12-24, 1400 mL, CH_2Cl_2 / MeOH / 50% aq. NH_4OH 97:3:0.4; #25-29, 500 mL, CH_2Cl_2 / MeOH / 50% aq. NH_4OH 95:5:0.4), to obtain **46** (#12-18, 190 mg, 96% yield) as a yellow oil.

R_f = 0.53 (silica gel, 10 cm, CH_2Cl_2 / MeOH / 50% aq. NH_4OH 9:1:0.04)

Analytical sample of 46·HCl

In a 10 mL round-bottomed flask, **46** (190 mg) was dissolved in CH_2Cl_2 (5 mL), filtered through a 0.2 μm PTFE filter, treated with excess of a methanolic solution of HCl (2 mL, 1.25 M), and evaporated to dryness. The resulting solid was washed with EtOAc (5 mL) and pentane (5 x 5 mL), evaporated to dryness and dried at 45 °C/2 Torr for 3 days, to provide **46·HCl** (75 mg) as a pale brown solid.

Melting Point: 131–133 °C

IR (ATR) ν: 3500–2500 (max at 3259, 3119, 2926, 2855, N–H, $^{+}$N–H, C–H st), 1631, 1584, 1570, 1513 (Ar–C–C, Ar–C–N st) cm^{-1}.

^{1}H NMR (400 MHz, CD_3OD) δ: 1.25–1.40 (complex signal, 10H, 3-H_2, 4-H_2, 5-H_2, 6-H_2, 7-H_2), superimposed in part 1.45 (tt, *J* = *J'* = 7.2 Hz, 2H, 2-H_2), 1.58 (s, 3H, 9'-CH_3), 1.85 (tt, *J* = *J'* = 6.8 Hz, 2H, 8-H_2), superimposed in part 1.93 (br d, *J* = 17.6 Hz, 1H, 10'-H_{endo}), superimposed in part 1.94 (m, 1H, 13'-H_{syn}), 2.08 (dm, *J* = 12.4 Hz, 1H, 13'-H_{anti}), 2.54 (dm, *J* = 17.6 Hz, 1H, 10'-H_{exo}), 2.77 (m, 1H, 7'-H), 2.84 (m, 1H, 6'-H_{endo}), superimposed 2.86 (t, *J* = 7.2 Hz, 2H, 1-H_2), 3.20 (m, 1H, 6'-H_{exo}), 3.43 (m, 1H, 11'-H), 3.98 (t, *J* = 6.8 Hz, 2H, 9-H_2), 4.85 (s, NH, $^{+}$NH), 5.58 (br d, *J* = 5.6 Hz, 1H, 8'-H), 7.55 (dd, *J* = 9.2 Hz, *J'* = 2.0 Hz, 1H, 2'-H), 7.74 (d, *J* = 2.0 Hz, 1H, 4'-H), 7.97 (br s, 2H, pyrazole 3-H, pyrazole 5-H), 8.40 (d, *J* = 9.2 Hz, 1H, 1'-H).

^{13}C NMR (100.6 MHz, CD_3OD) δ: 23.52 (CH_3, 9'-CH_3), 27.30 (CH, C11'), 27.54 (CH_2), 27.76 (CH_2) (C6, C7), 27.84 (CH, C7'), 29.38 (CH_2, C13'), 29.95 (CH_2), 30.08 (CH_2), 30.34 (CH_2), 30.44 (CH_2) (C2, C3, C4, C5), 31.29 (CH_2, C8), 36.11 (CH_2), 36.15 (CH_2) (C6', C10'), 43.98 (CH_2, C1), 49.84 (CH_2, C9), 115.66 (C, C12a'), 117.59 (C, C11a'), 119.15 (CH, C4'), 125.15 (CH, C8'), 126.70 (CH, C2'), 129.03 (CH), 129.04 (CH) (pyrazole C3, pyrazole C5), 129.57 (CH, C1'), 134.52 (C, C9'), 140.18 (C, C3'), 140.95 (C, C4a'), 151.17 (C, C5a'), 151.22 (C, pyrazole C4), 156.92 (C, C12').

HRMS ESI:

Calculated for $[C_{29}H_{38}{}^{35}ClN_5O_2S + H]^{+}$: 556.2508

Found: 556.2511

Synthesis of (±)-9-[(3-chloro-6,7,10,11-tetrahydro-9-methyl-7,11-methanocycloocta[*b*]quinolin-12-yl)amino]nonanoic acid, 47

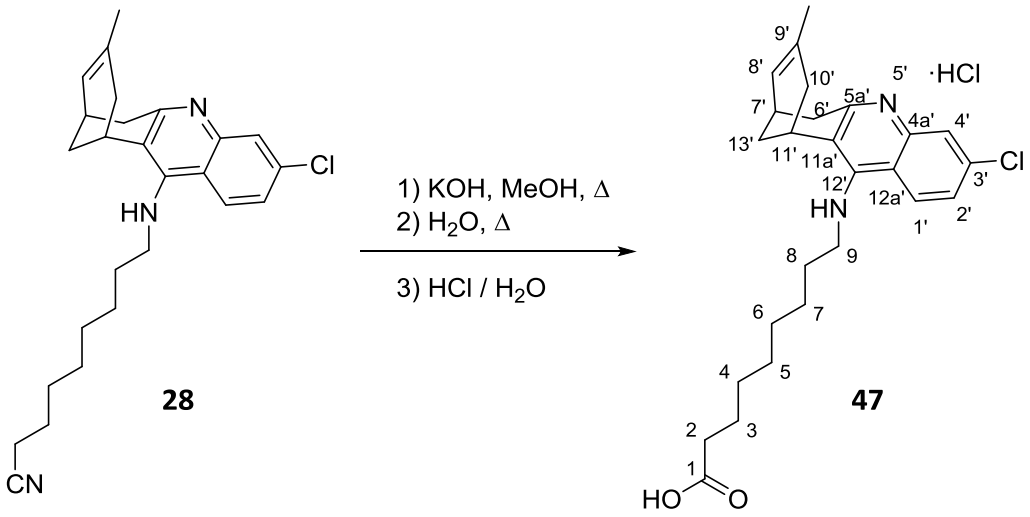

In a 25 mL round-bottomed flask equipped with magnetic stirrer and reflux condenser, **28** (232 mg, 0.55 mmol) was dissolved in MeOH (2.8 mL), treated with a solution of KOH (40% in MeOH, 1.5 mL). The resulting suspension was stirred under reflux overnight. Because analysis of the reaction mixture by TLC showed the presence of starting material, an additional amount of KOH solution (40% in MeOH, 1 mL) was added and the mixture was stirred at reflux for 5 h. Still an additional amount KOH solution (40% in MeOH, 1 mL) was added and the mixture was stirred at reflux overnight, treated with water (2 mL) and stirred at reflux overnight. The resulting yellow solution was cooled down to r. t., evaporated under reduced pressure, treated with excess of 5 N HCl (10 mL), and evaporated to dryness, to afford a brilliant yellow solid, whose ^{1}H-NMR spectra was consistent with the presence of the desired acid, in the form of the quinoline hydrochloride salt **47·HCl** (1.99 g of crude product containing a maximum of 263 mg of acid), and was used in the following step without further purification.

Synthesis of (±)-9-[(3-chloro-6,7,10,11-tetrahydro-9-methyl-7,11-methanocycloocta[*b*]quinolin-12-yl)amino]-*N*-[(2-methoxy-4-pyridyl)methyl]nonanamide, 48

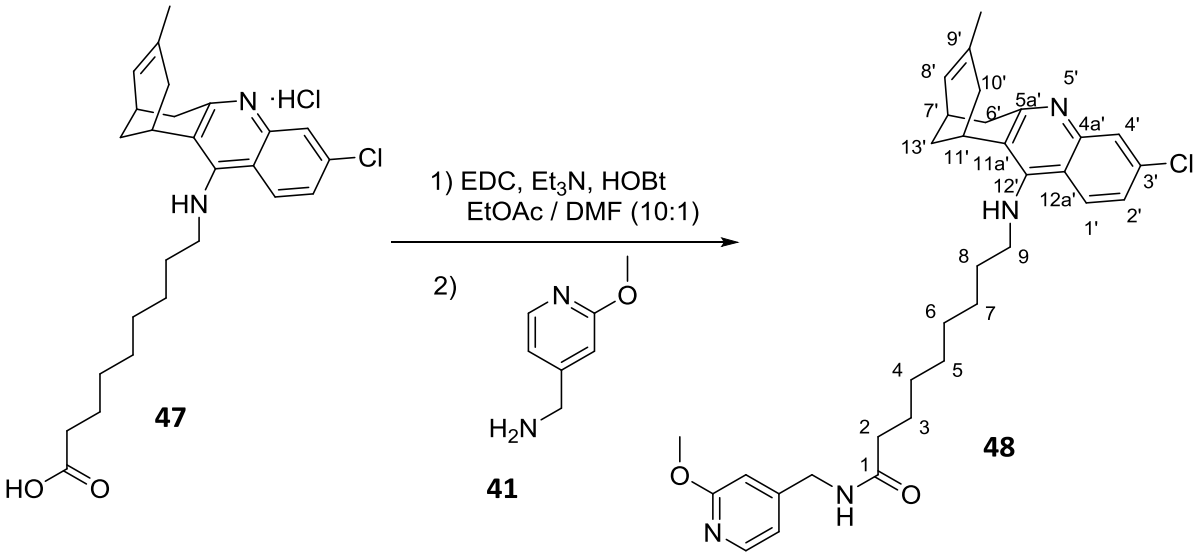

In a 50 mL round-bottomed flask equipped with magnetic stirrer, **47·HCl** (2.03 g of a crude that could contain a maximum of 350 mg of acid) was suspended in a mixture of EtOAc / DMF (13.2 mL, 10:1), and treated subsequently with EDC·HCl (210 mg, 1.09 mmol), Et_3N (0.4 mL, 2.92 mmol) and HOBt (149 mg, 1.09 mmol). After stirring for 10 min at r. t., a solution of (2-methoxy-4-pyridyl)methanamine, **41**, (112 mg, 0.81 mmol) in EtOAc / DMF (11 mL, 10:1) was added and the reaction mixture was stirred at r. t. overnight. The resulting mixture was diluted with more EtOAc (18 mL) and washed with water (3 x 45 mL) and brine (45 mL). The organic phase was dried over anhydrous Na_2SO_4, filtered, and evaporated to dryness to afford a brown oil (396 mg), which was purified through column chromatography (silica gel 40–63 µm, 36 g, Ø = 3 cm; #1-2, 450 mL, CH_2Cl_2 / 30% aq. NH_4OH 100:0.7; #3, 250 mL, CH_2Cl_2 / MeOH / 30% aq. NH_4OH 99:1:0.7; #4-35, 800 mL, CH_2Cl_2 / MeOH / 30% aq. NH_4OH 98:2:0.7), to provide **48** (#12-27, 246 mg, 74% yield) as a dark yellow oil.

Analytical sample of 48

In a 10 mL round-bottomed flask, **48** (137 mg) was dissolved in CH_2Cl_2 (2 mL), filtered through a 0.2 µm PTFE filter, treated with excess of a methanolic solution of HCl (2 mL, 1.25 M), and evaporated to dryness. The resulting solid was washed with EtOAc (2 x 5 mL) and pentane (2 x 5 mL), evaporated to dryness and dried at 45 °C/2 Torr for 7 days. Analysis by ^{1}H-NMR showed that the product was partially demethylated.

The rest of **48** (141 mg) was dissolved in MeOH (15 mL) and washed with hexane (2 x 10 mL) and pentane (10 mL) in a separatory funnel. The methanolic fraction was evaporated to dryness and dried at 45 °C/2 Torr for 3 days, to provide **48** (103 mg) as a brown oil.

R_f = 0.45 (silica gel, 10 cm, CH_2Cl_2 / MeOH / 50% aq. NH_4OH 9.5:0.5:0.04)

IR (ATR) ν: 3283, 3061 (N–H st), 1655, 1611, 1557 (C=O, Ar–C–C, Ar–C–N st) cm^{-1}.

^1H NMR (400 MHz, CD_3OD) δ: 1.28–1.40 (complex signal, 8H, 4-H_2, 5-H_2, 6-H_2, 7-H_2), 1.52 (s, 3H, 9'-CH_3), 1.61 (tt, *J* = *J'* = 7.2 Hz, 2H, 3-H_2), 1.71 (tt, *J* = *J'* = 7.2 Hz, 2H, 8-H_2), 1.86 (br d, *J* = 17.6 Hz, 1H, 10'-H_{endo}), superimposed in part 1.91 (dm, *J* = 12.4 Hz, 1H, 13'-H_{syn}), 2.05 (dm, *J* = 12.4 Hz, 1H, 13'-H_{anti}), 2.24 (t, *J* = 7.2 Hz, 2H, 2-H_2), 2.53 (dd, *J* = 17.6 Hz, *J'* = 5.6 Hz, 1H, 10'-H_{exo}), 2.69 (m, 1H, 7'-H), 2.89 (ddd, *J* = 17.6 Hz, *J'* = *J''* = 1.6 Hz, 1H, 6'-H_{endo}), 3.09 (dd, *J* = 17.6 Hz, *J'* = 5.6 Hz, 1H, 6'-H_{exo}), 3.43 (m, 1H, 11'-H), 3.57 (td, *J* = 7.2 Hz, *J'* = 2.0 Hz, 2H, 9-H_2), 3.86 (s, 3H, OCH_3), 4.33 (s, 2H, pyridine-CH_2-CONH), 4.85 (s, NH), 5.54 (br d, *J* = 5.2 Hz, 1H, 8'-H), 6.66 (dd, *J* = 1.6 Hz, *J'* = 0.8 Hz, 1H, pyridine 3-H), 6.84 (dd, *J* = 5.2 Hz, *J'* = 1.6 Hz, 1H, pyridine 5-H), 7.31 (dd, *J* = 9.2 Hz, *J'* = 2.0 Hz, 1H, 2'-H), 7.72 (d, *J* = 2.0 Hz, 1H, 4'-H), 8.02 (dd, *J* = 5.2 Hz, *J'* = 0.8 Hz, 1H, pyridine 6-H), 8.08 (d, *J* = 9.2 Hz, 1H, 1'-H).

^{13}C NMR (100.6 MHz, CD_3OD) δ: 23.59 (CH_3, 9'-CH_3), 26.91 (CH_2, C3), 27.88 (CH_2, C7), 28.39 (CH, C11'), 29.45 (CH, C7'), 30.11 (2CH_2, C13', C6), 30.20 (CH_2), 30.25 (CH_2) (C4, C5), 32.23 (CH_2, C8), 36.92 (CH_2, C2), 37.85 (CH_2, C10'), 40.36 (CH_2, C6'), 42.80 (CH_2, pyridine-*C*H_2-CONH), 50.77 (CH_2, C9), 54.07 (CH_3, OCH_3), 109.62 (CH, pyridine C3), 116.93 (CH, pyridine C5), 119.73 (C, C12a'), 121.64 (C, C11a'), 124.92 (CH, C2'), 126.11 (CH, C8'), 126.40 (CH, C4'), 127.52 (CH, C1'), 133.66 (C, pyridine C4) superimposed 133.66 (C), 135.70 (C) (C4a', C9'), 147.73 (CH, pyridine C6), 148.82 (C, C3'), 152.98 (C), 153.06 (C) (C5a', C12'), 159.03 (C, pyridine C2), 176.38 (C, CONH).

HRMS ESI:

Calculated for $[C_{33}H_{41}{}^{35}ClN_4O_2 + H]^+$: 561.2991

Found: 561.2985

Synthesis of (±)-9-[(3-chloro-6,7,10,11-tetrahydro-9-methyl-7,11-methanocycloocta[*b*]quinolin-12-yl)amino]-*N*-(1*H*-pyrazol-4-yl)nonanamide, 49

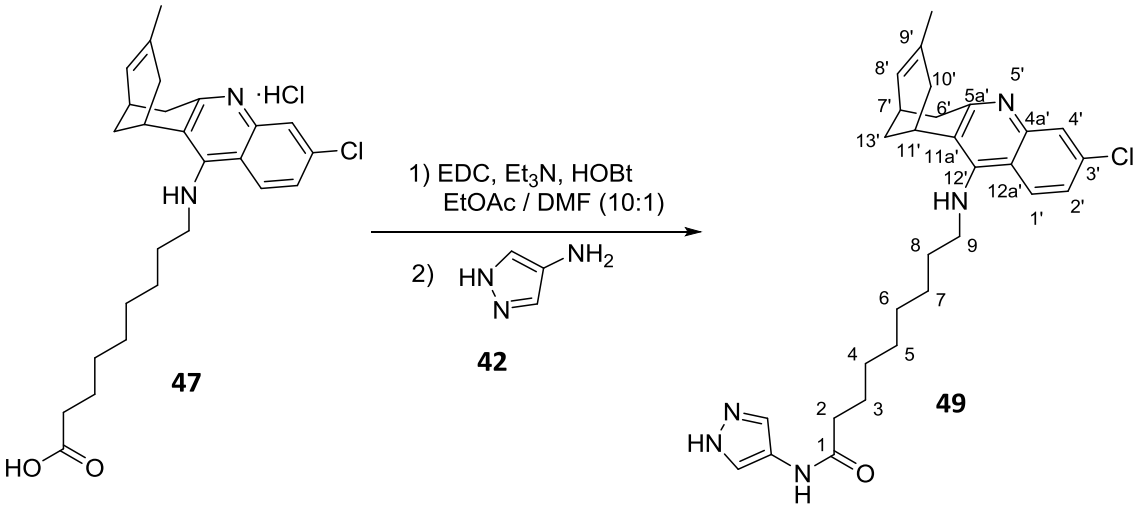

In a 50 mL round-bottomed flask equipped with magnetic stirrer, **47·HCl** (2.03 g of a crude that could contain a maximum of 350 mg of acid) was suspended in a mixture of EtOAc / DMF (13.2 mL, 10:1), and treated subsequently with EDC·HCl (210 mg, 1.09 mmol), Et_3N (0.4 mL, 2.92 mmol) and HOBt (149 mg, 1.09 mmol). After stirring for 10 min at r. t., a solution of 4-amino-1*H*-pyrazole, **42**, (67 mg, 0.81 mmol) in EtOAc / DMF (11 mL, 10:1) was added and the reaction mixture was stirred at r. t. overnight. The resulting mixture was diluted with EtOAc (18 mL) and washed with water (3 x 45 mL) and brine (45 mL). The organic phase was dried over anhydrous Na_2SO_4, filtered, and evaporated to dryness to afford a brown oil (212 mg), which was purified through column chromatography (silica gel 40–63 µm, 30 g, Ø = 3 cm; #1, 300 mL, CH_2Cl_2 / 50% aq. NH_4OH 100:0.4; #2-7, 900 mL, CH_2Cl_2 / MeOH / 50% aq. NH_4OH 99.5:0.5:0.4; #8-18, 900 mL, CH_2Cl_2 / MeOH / 50% aq. NH_4OH 99:1:0.4; #19-23, 600 mL, CH_2Cl_2 / MeOH / 50% aq. NH_4OH 98:2:0.4; #24-36, 1100 mL, CH_2Cl_2 / MeOH / 50% aq. NH_4OH 97:3:0.4; #37-39, 300 mL, CH_2Cl_2 / MeOH / 50% aq. NH_4OH 96:4:0.4; #40-42, 300 mL, CH_2Cl_2 / MeOH / 50% aq. NH_4OH 95:5:0.4; #43-45, 300 mL, CH_2Cl_2 / MeOH / 50% aq. NH_4OH 94:6:0.4), to provide **49** (#25-37, 175 mg, 47% yield) as a dark yellow oil.

R_f = 0.14 (silica gel, 10 cm, CH_2Cl_2 / MeOH / 50% aq. NH_4OH 9.5:0.5:0.04)

Analytical sample of 49·HCl

In a 10 mL round-bottomed flask, **49** (175 mg) was dissolved in CH_2Cl_2 (2 mL), filtered through a 0.2 µm PTFE filter, treated with excess of a methanolic solution of HCl (2 mL, 1.25 M), and evaporated to dryness. The resulting solid was washed with EtOAc (2 x 5 mL) and pentane (2 x 5 mL), evaporated to dryness and dried at 45 °C/2 Torr for 7 days, to provide **49·HCl** (149 mg) as a pale brown solid.

Melting Point: 141–142 °C

IR (ATR) ν: 3600–2300 (max at 3237, 3058, 2926, 2854, N–H, $^{+}$N–H, C–H st), 1733, 1671, 1630, 1582, 1511 (C=O, Ar–C–C, Ar–C–N st) cm^{-1}.

^{1}H NMR (400 MHz, CD_3OD) δ: 1.30–1.48 (complex signal, 8H, 4-H_2, 5-H_2, 6-H_2, 7-H_2), 1.58 (s, 3H, 9'-CH_3), 1.68 (m, 2H, 3-H_2), 1.86 (m, 2H, 8-H_2), superimposed in part 1.93 (br d, *J* = 17.6 Hz, 1H, 10'-H_{endo}), superimposed in part 1.94 (m, 1H, 13'-H_{syn}), 2.08 (dm, *J* = 12.4 Hz, 1H, 13'-H_{anti}), 2.36 (t, *J* = 7.2 Hz, 2H, 2-H_2), 2.55 (dm, *J* = 17.6 Hz, 1H, 10'-H_{exo}), 2.77 (m, 1H, 7'-H), 2.85 (br d, *J* = 17.6 Hz, 1H, 6'-H_{endo}), 3.20 (dd, *J* = 17.6 Hz, *J'* = 5.6 Hz, 1H, 6'-H_{exo}), 3.44 (m, 1H, 11'-H), 3.98 (t, *J* = 7.2 Hz, 2H, 9-H_2), 4.85 (s, NH, $^{+}$NH), 5.59 (br d, *J* = 5.2 Hz, 1H, 8'-H), 7.56 (dd, *J* = 9.2 Hz, *J'* = 1.6 Hz, 1H, 2'-H), 7.75 (d, *J* = 1.6 Hz, 1H, 4'-H), 8.12 (br s, 2H, pyrazole 3-H, pyrazole 5-H), 8.40 (d, *J* = 9.2 Hz, 1H, 1'-H).

^{13}C NMR (100.6 MHz, CD_3OD) δ: 23.54 (CH_3, 9'-CH_3), 25.91 (CH_2, C3), 26.35 (CH, C11'), 27.32 (CH_2, C6 or C7), 27.83 (CH, C7'), 29.41 (CH_2, C13'), 30.11 (CH_2), 30.14 (CH_2), 30.29 (CH_2) (C4, C5, C7 or C6), 31.33 (CH_2, C8), 36.14 (CH_2), 36.20 (CH_2) (C6', C10'), 37.05 (CH_2, C2), 49.81 (CH_2, C9), 115.66 (C, C12a'), 117.60 (C, C11a'), 119.16 (CH, C4'), 120.13 (CH), 120.16 (CH) (pyrazole C3, pyrazole C5), 125.16 (CH, C8'), 126.72 (CH, C2'), 129.57 (CH, C1'), 134.51 (C, C9'), 140.15 (C, C3'), 140.94 (C, C4a'), 151.19 (C, C5a'), 152.87 (C, pyrazole C4), 156.87 (C, C12'), 173.79 (C, CONH).

HRMS ESI:

Calculated for $[C_{29}H_{36}{}^{35}ClN_5O + H]^+$:	506.2681
Found:	506.2681

Synthesis of (±)-4-{9-[(3-chloro-6,7,10,11-tetrahydro-9-methyl-7,11-methanocycloocta[*b*]quinolin-12-yl)amino]nonanoyl}piperazin-2-one, 50

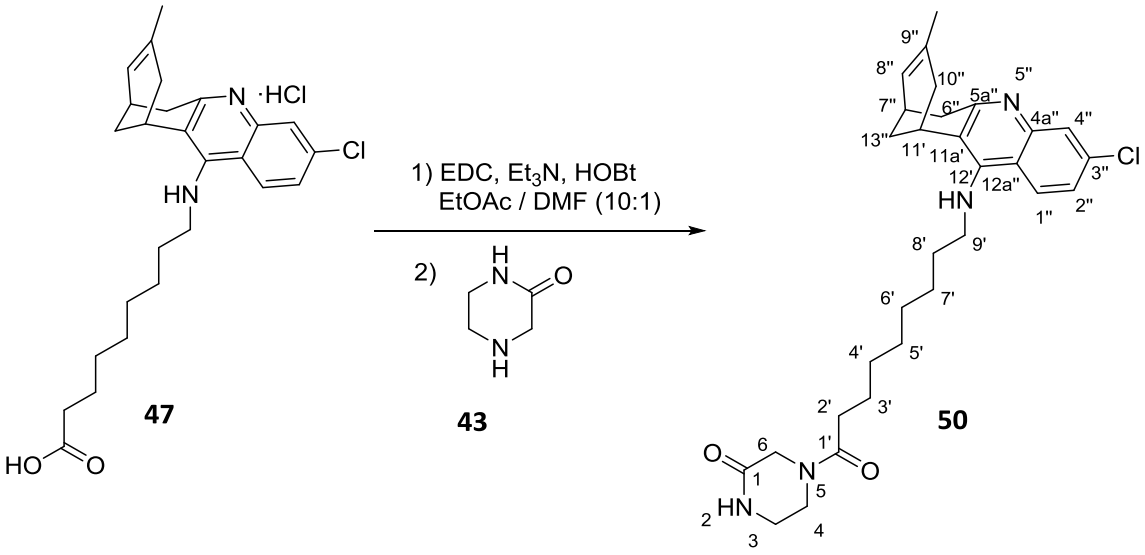

In a 50 mL round-bottomed flask equipped with magnetic stirrer, **47·HCl** (1.99 g of a crude that could contain a maximum of 260 mg of acid) was suspended in a mixture of EtOAc / DMF (11 mL, 10:1), and treated subsequently with EDC·HCl (156 mg, 0.82 mmol), Et_3N (0.3 mL, 2.18 mmol) and HOBt (111 mg, 0.82 mmol). After stirring for 10 min at r. t., a solution of piperazin-2-one, **43**, (60 mg, 0.60 mmol) in EtOAc / DMF (6.6 mL, 10:1) was added and the reaction mixture was stirred at r. t. overnight, then evaporated to dryness to give a brown oil (2.64 g), which was purified through column chromatography (silica gel 40–63 µm, 60 g, Ø = 4 cm; #1-3, 1200 mL, CH_2Cl_2 / 50% aq. NH_4OH 100:0.4; #4-9, 1200 mL, CH_2Cl_2 / MeOH / 50% aq. NH_4OH 99.5:0.5:0.4; #10-20, 1200 mL, CH_2Cl_2 / MeOH / 50% aq. NH_4OH 99:1:0.4; #21-42, 1600 mL, CH_2Cl_2 / MeOH / 50% aq. NH_4OH 98:2:0.4; #43-46, 400 mL, CH_2Cl_2 / MeOH / 50% aq. NH_4OH 95:5:0.4), to provide **50** (#27-42, 187 mg, 66% yield) as a yellow oil.

R_f = 0.25 (silica gel, 10 cm, CH_2Cl_2 / MeOH / 50% aq. NH_4OH 9.6:0.4:0.04)

Analytical sample of 50·HCl

In a 10 mL round-bottomed flask, **50** (187 mg) was dissolved in CH_2Cl_2 (2 mL), filtered through a 0.2 µm PTFE filter, treated with excess of a methanolic solution of HCl (2 mL, 1.25 M), and evaporated to dryness. The resulting solid was washed with EtOAc (2 x 5 mL) and pentane (2 x 5 mL), evaporated to dryness and dried at 45 °C/2 Torr for 7 days, to provide **50·HCl** (147 mg) as a pale brown solid.

Melting Point: 92–95 °C

IR (ATR) ν: 3600–2400 (max at 3245, 3054, 2926, 2854, N–H, $^{+}$N–H, C–H st), 1743, 1630, 1582, 1513 (C=O, Ar–C–C, Ar–C–N st) cm^{-1}.

^{1}H NMR (400 MHz, CD_3OD) δ: 1.30–1.48 (complex signal, 8H, 4'-H_2, 5'-H_2, 6'-H_2, 7'-H_2), 1.59 (s, 3H, 9''-CH_3), superimposed 1.59 (m, 2H, 3'-H_2), 1.86 (tt, *J* = *J'* = 7.2 Hz, 2H, 8'-H_2), superimposed in part 1.93 (br d, *J* = 18.0 Hz, 1H, 10''-H_{endo}), superimposed in part 1.94 (m, 1H, 13''-H_{syn}), 2.09 (dm, *J* = 12.8 Hz, 1H, 13''-H_{anti}), 2.29 (t, *J* = 7.2 Hz, 2H, 2'-H_2), 2.55 (dd, *J* = 18.0 Hz, *J'* = 5.2 Hz, 1H, 10''-H_{exo}), 2.77 (m, 1H, 7''-H), 2.87 (dd, *J* = 18.0 Hz, *J'* = 2.0 Hz, 1H, 6''-H_{endo}), 3.14 (t, *J* = 6.0 Hz, 2H, 5-H_2 or 6-H_2), 3.21 (dd, *J* = 18.0 Hz, *J'* = 5.6 Hz, 1H, 6''-H_{exo}), 3.46 (m, 1H, 11''-H), 3.67 (t, *J* = 6.0 Hz, 2H, 6-H_2 or 5-H_2), 3.79 (s, 2H, 3-H_2), 3.98 (t, *J* = 7.2 Hz, 2H, 9'-H_2), 4.85 (s, NH, $^{+}$NH), 5.59 (br d, *J* = 5.6 Hz, 1H, 8''-H), 7.56 (dd, *J* = 9.2 Hz, *J'* = 2.0 Hz, 1H, 2''-H), 7.79 (d, *J* = 2.0 Hz, 1H, 4''-H), 8.40 (d, *J* = 9.2 Hz, 1H, 1''-H).

^{13}C NMR (100.6 MHz, CD_3OD) δ: 23.46 (CH_3, 9''-CH_3), 25.77 (CH_2, C3'), 27.27 (CH, C11''), 27.74, 27.82, 27.86 (CH + 2CH_2, C7'', C6', C7'), 29.31 (CH_2, C13''), 30.15 (CH_2), 30.45 (CH_2) (C4', C5'), 31.26 (CH_2, C8'), 33.82 (CH_2, C2'), 36.04 (CH_2), 36.10 (CH_2) (C6'', C10''), 39.44 (CH_2), 46.78 (CH_2) (C5, C6), 49.68 (CH_2, C9'), 53.17 (CH_2, C3), 115.65 (C, C12a''), 117.59 (C, C11a''), 125.14 (CH, C8''), 126.65 (CH, C2''), 129.48 (CH, C1''), 134.54 (C, C9''), 140.22 (C, C3''), 140.99 (C, C4a''), 151.22 (C, C5a''), 156.92 (C, C12''), 172.21 (C), 173.79 (C) (C2, CON).

HRMS ESI:

Calculated for $[C_{39}H_{39}{}^{35}ClN_4O_2 + H]^{+}$: 541.2940

Found: 541.2934

Synthesis of (±)-9-[(3-chloro-6,7,10,11-tetrahydro-9-methyl-7,11-methanocycloocta[*b*]quinolin-12-yl)amino]-*N*-[(2-oxo-1,2-dihydro-4-pyridyl)methyl]nonanamide, 51

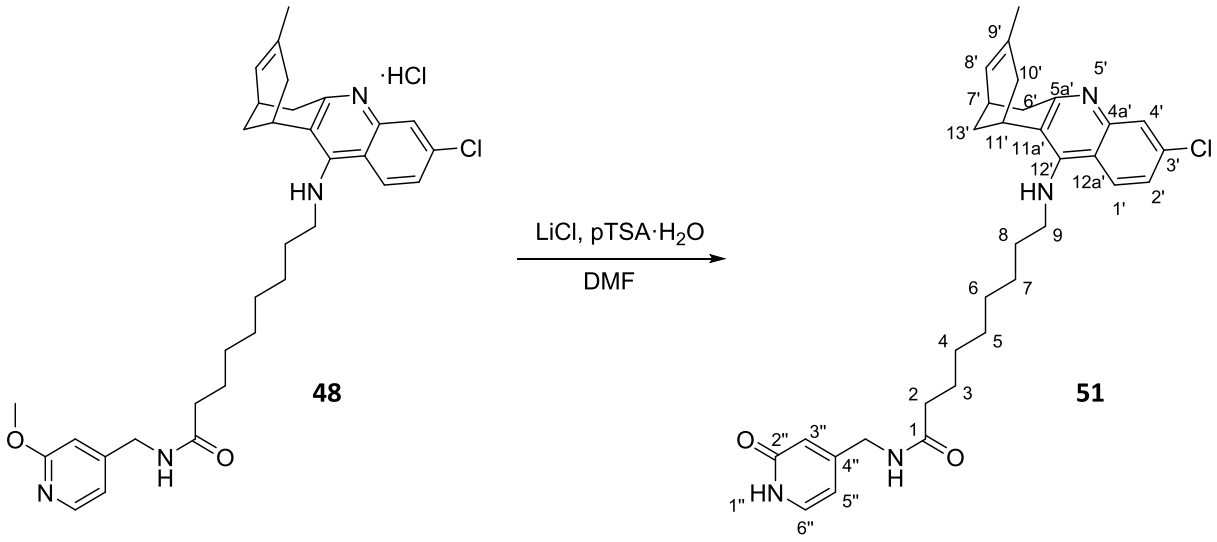

In a double neck 10 mL round-bottomed flask equipped with magnetic stirrer and reflux condenser, **48·HCl** (95 mg of a sample that was partially demethylated, maximum of 0.15 mmol) was dissolved in DMF (1 mL) and treated with LiCl (32 mg, 0.75 mmol) and *p*-toluenesulfonic acid monohydrate (144 mg, 0.75 mmol). The resulting yellow solution was stirred at 120 °C for 35 min, cooled down to r. t., quenched with H_2O (2 mL) and sat. aq. $NaHCO_3$ (5 mL), and extracted with EtOAc (3 x 5 mL). The combined organic extracts were washed with water (3 x 7 mL), dried over anhydrous Na_2SO_4, filtered, and evaporated to dryness to afford **51** (44 mg, 54% yield) as a brown oil.

R_f = 0.41 (silica gel, 10 cm, CH_2Cl_2 / MeOH / 50% aq. NH_4OH 9:1:0.04)

Analytical sample of 51·HCl

In a 10 mL round-bottomed flask, **51** (44 mg) was dissolved in MeOH (2 mL), filtered through a 0.2 µm PTFE filter, treated with excess of a methanolic solution of HCl (2 mL, 1.25 M), and evaporated to dryness. The resulting solid was washed with EtOAc (2 x 5 mL), hexane (2 x 5 mL), and pentane (2 x 5 mL), evaporated to dryness and dried at 45 °C/2 Torr for 3 days, to provide **51·HCl** (45 mg) as an off-white solid.

Melting Point: 132–134 °C

IR (ATR) ν: 3500–2300 (max at 3245, 3058, 2926, 2854, N–H, $^{+}$N–H, , C–H st), 1650, 1632, 1582, 1598, 1516 (C=O, Ar–C–C, Ar–C–N st) cm^{-1}.

^{1}H NMR (400 MHz, CD_3OD) δ: 1.33–1.48 (complex signal, 8H, 4-H_2, 5-H_2, 6-H_2, 7-H_2), 1.58 (s, 3H, 9'-CH_3), 1.64 (m, 2H, 3-H_2), 1.86 (m, 2H, 8-H_2), superimposed in part 1.93 (br d, *J* = 18.0 Hz, 1H, 10'-H_{endo}), superimposed in part 1.94 (m, 1H, 13'-H_{syn}), 2.08 (dm, *J* = 12.4 Hz, 1H, 13'-H_{anti}), 2.28 (t, *J* = 7.2 Hz, 2H, 2-H_2), 2.54 (dm, *J* = 18.0 Hz, 1H, 10'-H_{exo}), 2.77 (m, 1H, 7'-H), 2.86 (br d, *J* = 17.6 Hz, 1H, 6'-H_{endo}), 3.20 (dd, *J* = 17.6 Hz, *J'* = 5.6 Hz, 1H, 6'-H_{exo}), 3.45 (m, 1H, 11'-H), 3.98 (t, *J* = 7.2 Hz, 2H, 9-H_2), 4.31 (s, 2H, 4"-C*H*$_2$-NHCO), 4.85 (s, NH, $^{+}$NH), 5.58 (br d, *J* = 5.6 Hz, 1H, 8'-H), 6.55 (m, 2H, 3"-H, 5"-H), 7.55 (dd, *J* = 9.2 Hz, *J'* = 2.0 Hz, 1H, 2'-H), superimposed in part 7.58 (br s, 1H, 6"-H), 7.76 (d, *J* = 2.0 Hz, 1H, 4'-H), 8.40 (d, *J* = 9.2 Hz, 1H, 1'-H).

^{13}C NMR (100.6 MHz, CD_3OD) δ: 23.47 (CH_3, 9'-CH_3), 26.84 (CH_2, C3), 27.27 (CH, C11'), 27.75, 27.85 (CH + CH_2, C7', C6 or C7), 29.32 (CH_2, C13'), 30.06 (CH_2), 30.16 (CH_2), 30.24 (CH_2) (C4, C5, C7 or C6), 31.24 (CH_2, C8), 36.04 (CH_2), 36.11 (CH_2) (C6', C10'), 36.87 (CH_2, C2), 43.09 (CH_2, 4"-*C*H_2-NHCO), 49.68 (CH_2, C9), 110.44 (2CH, C3", C5"), 115.65 (C, C12a'), 117.59 (C, C11a'), 119.12 (CH, C4'), 123.25 (C, C4"), 125.12 (CH, C8'), 126.67 (CH, C2'), 129.50 (CH, C1'), 134.55 (C, C9'), 136.34 (CH, C6"), 140.23 (C, C3'), 140.97 (C, C4a'), 151.18 (C, C5a'), 156.92 (C, C12'), 158.46 (C, CONH), superimposed 158.46 (C, C2").

HRMS ESI:

Calculated for $[C_{32}H_{39}{}^{35}ClN_4O_2 + H]^+$: 547.2834

Found: 547.2830

Synthesis of 6,9-dichloro-1,2,3,4-tetrahydroacridine, 57

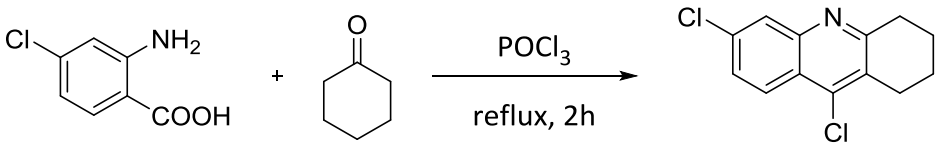

55 **56** **57**

In a triple neck 250 mL round-bottomed flask equipped with magnetic stirrer, reflux condenser and an ice bath, a mixture of 4-chloroanthranilic acid, **55**, (10.0 g, 58.3 mmol), cyclohexanone, **56**, (5.73 mL, 55.3 mmol), and $POCl_3$ (50 mL, 0.55 mmol) was heated under reflux for 2 h. The resulting suspension was cooled down to r. t. and evaporated to dryness. The resulting residue was dissolved in CH_2Cl_2 (150 mL) and treated dropwise with 5 N NaOH until basic pH, while cooling with an ice bath. The aqueous layer was extracted with CH_2Cl_2 (3 x 200 mL) and the combined organic extracts were washed with 5 N NaOH (3 x 200 mL), dried over anhydrous Na_2SO_4, filtered, and evaporated to dryness to afford **57** (11.3 g, 81% yield) as a brown solid.

R_f = 0.92 (silica gel, 10 cm, CH_2Cl_2 / MeOH / 50% aq. NH_4OH 9:1:0.1).

Analytical sample of 57·HCl

In a 25 mL round-bottomed flask, **57** (240 mg) was dissolved in MeOH (10 mL), filtered through a 0.2 µm PTFE filter, treated with excess of a methanolic solution of HCl (2 mL, 1.25 M), and evaporated to dryness. The resulting solid was crystallized from a mixture of MeOH / EtOAc 1:2 (3 mL) and dried at 45 °C/2 Torr for 3 days, to provide **57·HCl** (254 mg) as a beige solid.

^{1}H NMR (300 MHz, CD_3OD) δ: 2.03–2.09 (complex signal, 4H, 2-H_2, 3-H_2), 3.15 (m, 2H), 3.37 (m, 2H,) (1-H_2, 4-H_2), 4.87 (s, $^+$NH), 7.97 (dd, *J* = 9.0 Hz, *J'* = 2.0 Hz, 1H, 7-H), 8.10 (d, *J* = 2.0 Hz, 1H, 5-H), 8.52 (d, *J* = 9.0 Hz, 1H, 8-H).

Synthesis of 2-[(6-chloro-1,2,3,4-tetrahydroacridin-9-yl)amino]ethanol, 59a

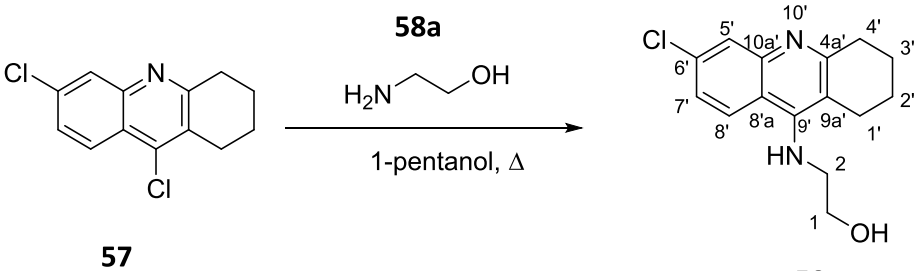

57 **59a**

In a 25 mL round-bottomed flask equipped with magnetic stirrer and reflux condenser, 6,9-dichloro-1,2,3,4-tetrahydroacridine, **57** (1.00 g, 3.97 mmol) and 2-aminoethanol, **58a**, (0.72 mL, 11.9 mmol) were dissolved in 1-pentanol (4 mL), and the reaction mixture was heated under reflux overnight. The resulting dark brown solution was cooled down to r. t. until a precipitate was formed, was diluted with EtOAc (25 mL) and was extracted with 1 N HCl (4 x 15 mL). The combined aqueous layers were washed with EtOAc (3 x 20 mL), alkalinized with NaOH pellets (8–10 pellets, until pH = 12), and extracted with CH_2Cl_2 (3 x 25 mL). The combined organic extracts were dried over anhydrous Na_2SO_4, filtered, and evaporated to dryness to provide **59a** (1.03 g, 93% yield) as an ochre solid.

^{1}H NMR (400 MHz, CD_3OD) δ: 1.90–1.98 (complex signal, 4H, 2'-H_2, 3'-H_2), 2.78 (m, 2H, 1'-H_2), 2.98 (m, 2H, 4'-H_2), 3.64 (t, *J* = 5.2 Hz, 2H, 2-H_2), 3.72 (t, *J* = 5.2 Hz, 2H, 1-H_2), 4.85 (s, NH, OH), 7.34 (dd, *J* = 9.2 Hz, *J'* = 2.4 Hz, 1H, 7'-H), 7.75 (d, *J* = 2.4 Hz, 1H, 5'-H), 8.13 (d, *J* = 9.2 Hz, 1H, 8'-H).

Synthesis of 3-[(6-chloro-1,2,3,4-tetrahydroacridin-9-yl)amino]propanol, 59b

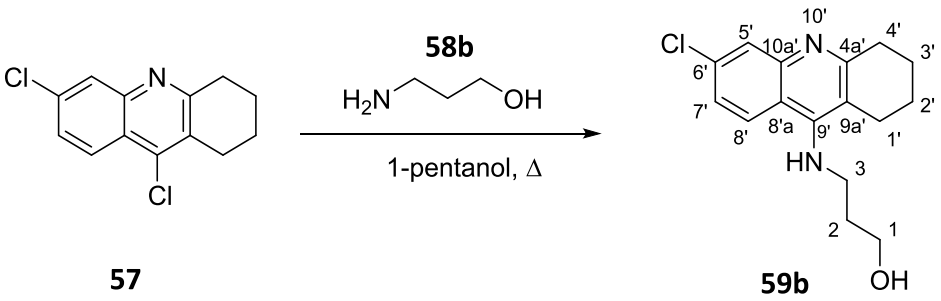

57 **59b**

In a 25 mL round-bottomed flask equipped with magnetic stirrer and reflux condenser, 6,9-dichloro-1,2,3,4-tetrahydroacridine, **57**, (1.00 g, 3.97 mmol) and 3-amino-1-propanol, **58b**, (0.91 mL, 11.9 mmol) were dissolved in 1-pentanol (4 mL), and the reaction mixture was heated under reflux overnight. The resulting dark brown solution was cooled down to r. t. until a precipitate was formed, was diluted with EtOAC (25 mL) and was extracted with 1 N HCl (4 x 15 mL). The combined aqueous layers were washed with EtOAc (4x 10 mL), alkalinized with NaOH pellets (20 pellets, until pH = 12), and extracted with EtOAc (3 x 25 mL). The combined organic extracts were dried over anhydrous Na_2SO_4, filtered, and evaporated to dryness to provide **59b** (817 mg, 71% yield) as a pale yellow solid.

^{1}H NMR (400 MHz, $CDCl_3$) δ: 1.83–1.88 (complex signal, 4H, 2'-H_2, 3'-H_2), 1.92 (tt, $J = J' = 6.0$ Hz, 2H, 2-H_2), 2.65 (m, 2H, 1'-H_2), 2.96 (m, 2H, 4'-H_2), 3.67 (dt, $J = J' = 6.0$ Hz, 2H, 3-H_2), 3.89 (t, $J = 6.0$ Hz, 2H, 1-H_2), 4.64 (br t, $J = 6.0$ Hz, 1H, NH), 7.21 (dd, $J = 8.8$ Hz, $J' = 2.0$ Hz, 1H, 7'-H), 7.83 (d, $J = 2.0$ Hz, 1H, 5'-H), 7.90 (d, $J = 8.8$ Hz, 1H, 8'-H).

Synthesis of 2-[(6-chloro-1,2,3,4-tetrahydroacridin-9-yl)amino]ethyl methanesulfonate, 60a

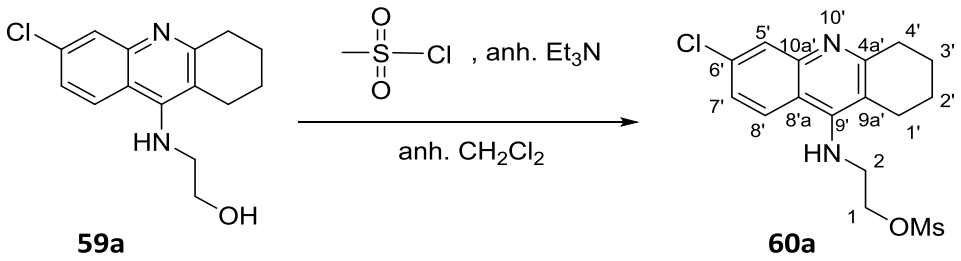

59a **60a**

In a 25 mL round-bottomed flask equipped with magnetic stirrer and inert atmosphere, **59a** (300 mg, 1.08 mmol) and anhydrous Et_3N (0.26 mL, 1.84 mL) were suspended in anh. CH_2Cl_2 (6 mL), cooled down to −10 °C in an ice / NaCl bath and methanesulfonyl chloride (0.13 mL, 1.62 mmol) was added dropwise. The mixture was stirred at −10 °C for 30 min, concentrated *in vacuo*, redissolved in CH_2Cl_2 (6 mL), and washed with 2 N NaOH until the waters remained basic (2 x 5 mL). The organic layer was dried over anhydrous Na_2SO_4, filtered, and evaporated to dryness to provide **60a** (422 mg, quantitative yield), as a dark brown oil.

^{1}H NMR (400 MHz, $CDCl_3$) δ: 1.90–1.98 (complex signal, 4H, 2'-H_2, 3'-H_2), 2.76 (m, 2H, 1'-H_2), 3.03 (s, 3H, CH_3SO_3), 3.06 (m, 2H, 4'-H_2), 3.80 (dt, J = J' = 5.2 Hz, 2H, 2-H_2), 4.29 (m, 1H, NH), 4.33 (t, J = 5.2 Hz, 2H, 1-H_2), 7.34 (dd, J = 8.8 Hz, J' = 2.0 Hz, 1H, 7'-H), 7.84 (d, J = 8.8 Hz, 1H, 8'-H), 7.92 (d, J = 2.0 Hz, 1H, 5'-H).

Synthesis of 3-[(6-chloro-1,2,3,4-tetrahydroacridin-9-yl)amino]propyl methanesulfonate, 60b

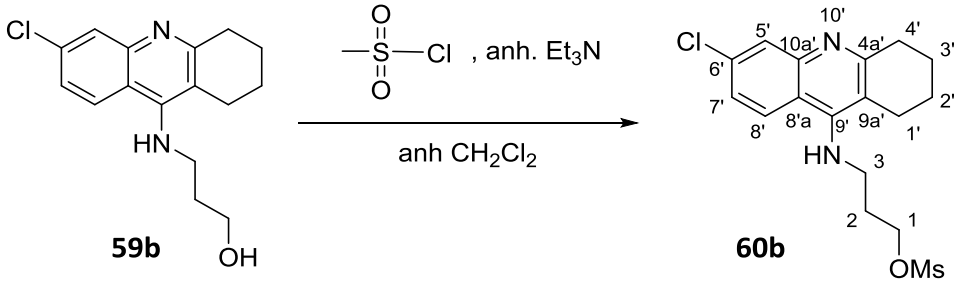

In a 50 mL round-bottomed flask equipped with magnetic stirrer and inert atmosphere, **59b** (426 mg, 1.46 mmol) and anhydrous Et_3N (0.35 mL, 2.49 mL) were suspended in anh. CH_2Cl_2 (8.5 mL), cooled down to −10 °C in an ice / NaCl bath and methanesulfonyl chloride (0.17 mL, 2.2 mmol) was added dropwise. The mixture was stirred at −10 °C for 30 min, concentrated *in vacuo*, redissolved in CH_2Cl_2 (8 mL) and washed with 2 N NaOH until the waters remained basic (2 x 8 mL). The organic layer was dried over anhydrous Na_2SO_4, filtered, and evaporated to dryness to provide **60b** (582 mg, quantitative yield), as a dark brown oil.

^{1}H NMR (400 MHz, $CDCl_3$) δ: 1.90–1.98 (complex signal, 4H, 2'-H_2, 3'-H_2), 2.11 (m, 2H, 2-H_2), 2.71 (m, 2H, 1'-H_2), 3.01 (s, 3H, CH_3SO_3), 3.05 (m, 2H, 4'-H_2), 3.63 (m, 2H, 3-H_2), 3.66 (t, *J* = 6.0 Hz, 2H, 1-H_2), 4.38 (m, 1H, NH), 7.31 (dd, *J* = 9.2 Hz, *J'* = 2.4 Hz, 1H, 7'-H), 7.86 (d, *J* = 9.2 Hz, 1H, 8'-H), 7.90 (d, *J* = 2.4 Hz, 1H, 5'-H).

Synthesis of 3-[(6-chloro-1,2,3,4-tetrahydroacridin-9-yl)amino]propanenitrile, 61a

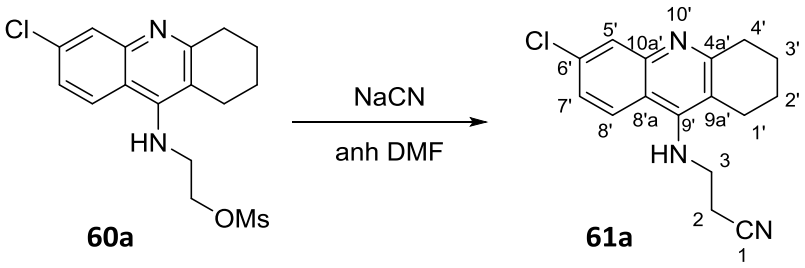

60a **61a**

In a double neck 25 mL round-bottomed flask equipped with a 2 N NaOH trap, magnetic stirrer and inert atmosphere, **60a** (383 mg, 1.08 mmol) and NaCN (53 mg, 1.08 mmol) were dissolved in anhydrous DMF (3 mL). The reaction mixture was heated at 35 °C for 2 h, quenched with water (4 mL) and 1 N NaOH (6 mL), and extracted with EtOAc (3 x 5 mL). The combined organic extracts were washed with water (3 x 5 mL) and brine (5 mL), dried over anhydrous Na_2SO_4, filtered, and evaporated to dryness. The resulting residue was purified through column chromatography (silica gel 40–63 μm, 18 g, Ø = 2 cm; #1, 100 mL, hexane / Et_3N 100:0.1; #2, 150 mL, hexane / EtOAc / Et_3N 95:5:0.1; #3-33, 700 mL, hexane / EtOAc / Et_3N 90:10:0.2; #34-106, 700 mL, hexane / EtOAc / Et_3N 88:12:0.2; #107-122, 150 mL, hexane / EtOAc / Et_3N 87:13:0.2; #123-198, 750 mL, hexane / EtOAc / Et_3N 86:14:0.2; #199-212, 250 mL, hexane / EtOAc / Et_3N 82.2:17.8:0.24, #213-228, 300 mL, hexane / EtOAc / Et_3N 82:18:0.2, #229-233, 100 mL, hexane / EtOAc / Et_3N 80:20:0.2, #234-238, 100 mL, hexane / EtOAc / Et_3N 75:25:0.5, #239-244, 100 mL, hexane / EtOAc / Et_3N 70:30:1), to afford **61a** (#137-237, 157 mg, 51% yield), as a yellow oil.

R_f = 0.3 (silica gel, 10 cm, hexane / EtOAc / 50% aq. NH_4OH 6:4:0.02).

Analytical sample of 61a·HCl

In a vial, **61a** (28 mg) was dissolved in CH_2Cl_2 (2 mL), filtered through a 0.2 μm PTFE filter, treated with excess of a solution of HCl in Et_2O (1 mL, 1.17 M), and evaporated to dryness. The resulting solid was washed with hexane (2 x 2 mL) and pentane (2 x 2 mL), evaporated to dryness, and dried at 45 °C/2 Torr for 3 days, to provide **61a·HCl** (29 mg) as a pale toasted solid.

Melting Point: 278 °C (dec).

IR (ATR) ν: 3300–2500 (max at 3226, 2943, 2727, N–H, $^+$N–H, C–H st), 2246 (C≡N st), 1639, 1610, 1568, 1534 (Ar–C–C, Ar–C–N st) cm^{-1}.

^{1}H NMR (400 MHz, CD_3OD) δ: 1.96–2.04 (complex signal, 4H, 2'-H_2, 3'-H_2), 2.78 (m, 2H, 1'-H_2), 3.00 (t, *J* = 6.4 Hz, 2H, 2-H_2), 3.06 (m, 2H, 4'-H_2), 4.21 (t, *J* = 6.4 Hz, 2H, 3-H_2), 4.85 (s, NH, $^{+}$NH), 7.63 (dd, *J* = 9.2 Hz, *J'* = 2.4 Hz, 1H, 7'-H), 7.84 (d, *J* = 2.4 Hz, 1H, 5'-H), 8.37 (d, *J* = 9.2 Hz, 1H, 8'-H).

^{13}C NMR (100.6 MHz, CD_3OD) δ: 19.62 (CH_2, C2), 21.66 (CH_2, C3'), 22.81 (CH_2, C2'), 25.18 (CH_2, C1'), 29.51 (CH_2, C4'), 44.82 (CH_2, C3), 114.89 (C), 116.11 (C) (C8a', C9a'), 118.83 (C, C1), 119.41 (CH, C5'), 127.52 (CH, C7'), 128.17 (CH, C8'), 140.24 (C, C6'), 140.37 (C, C10a'), 153.63 (C, C4a'), 158.19 (C, C9').

HRMS ESI:

Calculated for $[C_{16}H_{16}{}^{35}ClN_3 + H]^+$:	286.1106
Found:	286.1101

Synthesis of 4-[(6-chloro-1,2,3,4-tetrahydroacridin-9-yl)amino]butanenitrile, 61b

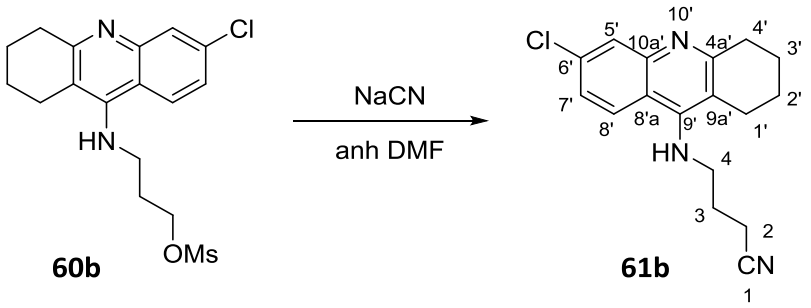

In a triple neck 25 mL round-bottomed flask equipped with a 2 N NaOH trap, magnetic stirrer and inert atmosphere, **60b** (539 mg, 1.46 mmol) and NaCN (358 mg, 7.3 mmol) were dissolved in anhydrous DMF (4.5 mL). The reaction mixture was heated at 35 °C for 2 h, quenched with 2 N NaOH (8 mL), and extracted with EtOAc (3 x 10 mL). The combined organic extracts were washed with water (3 x 15 mL) and brine (15 mL), dried over anhydrous Na_2SO_4, filtered, and evaporated to dryness to afford **61b** (400 mg, 91% yield), as a dark brown oil.

R_f = 0.3 (silica gel, 10 cm, hexane / EtOAc / 50% aq. NH_4OH 6:4:0.02).

Analytical sample of 61b·HCl

In a vial, **61b** (39 mg) was dissolved in CH_2Cl_2 (2 mL), filtered through a 0.2 µm PTFE filter, treated with excess of a solution of HCl in Et_2O (1 mL, 1.17 M), and evaporated to dryness. The resulting solid was washed with hexane (2 x 3 mL) and pentane (2 x 3 mL), evaporated to dryness, and dried at 45 °C/2 Torr for 5 days, to provide **61b·HCl** (41 mg) as a foamy yellow solid.

Melting Point: 201 °C (dec)

IR (ATR) ν: 3500–2400 (max at 3343, 3245, 2945, 2743, N–H, $^+$N–H, C–H st), 2247 (C≡N st), 1633, 1602, 1571, 1520 (Ar–C–C and Ar–C–N st) cm^{-1}.

^{1}H NMR (400 MHz, CD_3OD) δ: 1.90–2.00 (complex signal, 4H, 2'-H_2, 3'-H_2), 2.18 (tt, J = J' = 7.2 Hz, 2H, 3-H_2), 2.63 (t, J = 7.2 Hz, 2H, 2-H_2), 2.72 (m, 2H, 1'-H_2), 3.03 (m, 2H, 4'-H_2), 4.08 (t, J = 7.2 Hz, 2H, 4-H_2), 4.85 (s, NH, $^+$NH), 7.57 (dd, J = 9.2 Hz, J' = 2.0 Hz, 1H, 7'-H), 7.81 (d, J = 2.0 Hz, 1H, 5'-H), 8.38 (d, J = 9.2 Hz, 1H, 8'-H).

^{13}C NMR (100.6 MHz, CD_3OD) δ: 14.99 (CH_2, C2), 21.68 (CH_2, C3'), 22.83 (CH_2, C2'), 24.93 (CH_2, C1'), 27.04 (CH_2, C3), 29.39 (CH_2, C4'), 47.72 (CH_2, C4), 113.89 (C), 115.51 (C) (C8a', C9a'), 119.23 (CH, C5'), 120.52 (C, C1), 127.03 (CH, C7'), 128.50 (CH, C8'), 140.13 (C, C6'), 140.40 (C, C10a'), 152.62 (C, C4a'), 157.89 (C, C9').

HRMS ESI:

Calculated for $[C_{17}H_{18}{}^{35}ClN_3 + H)]^+$: 300.1262

Found: 300.1260

Synthesis of 6-chloro-1,2,3,4-tetrahydroacridin-9-amine, 11

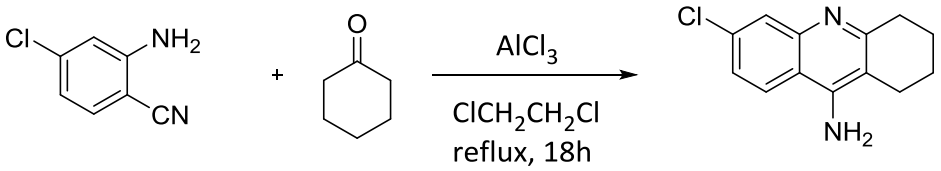

64 **56** **11**

In a triple neck 2 L round-bottomed flask equipped with magnetic stirrer, reflux condenser and inert atmosphere, a suspension of $AlCl_3$ (16.2 g, 121.5 mmol) and 2-amino-4-chlorobenzonitrile, **64**, (14 g, 91.78 mmol) in anhydrous 1,2-dichloroethane (140 mL) was treated with a solution of cyclohexanone, **56**, (8.4 mL, 85.4 mmol) in 1,2-dichloroethane (600 mL). The resulting mixture was stirred under reflux for 18 h, then cooled down to r. t., diluted with THF (500 mL) and water (400 mL), and stirred at r. t. for 30 min. The organic solvents were evaporated under reduced pressure and the resulting residue was filtered under vacuum. The resulting yellow solid was crystallized from EtOAc (300 mL) to obtain the desired compound **11** (18.9 g, quantitative yield), as a yellow solid.

R_f = 0.29 (silica gel, 10 cm, CH_2Cl_2 / MeOH / 50% aq. NH_4OH 9.5:0.5:0.1).

Synthesis of (+)-(7*R*,11*R*)-5-[(3-chloro-6,7,10,11-tetrahydro-9-methyl-7,11-methanocycloocta[*b*]quinolin-12-yl)amino]pentanenenitrile, (+)-66

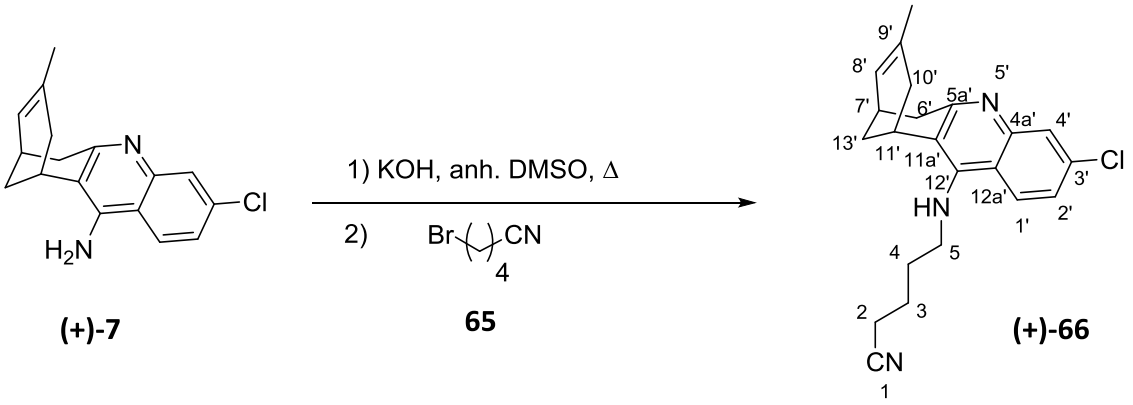

In a double neck 25 mL round-bottomed flask equipped with magnetic stirrer, inert atmosphere and 4Å molecular sieves, (+)-huprine Y, **(+)-7**, (250 mg, 0.88 mmol) and finely powdered KOH (85% purity, 191 mg, 2.90 mmol) were suspended in anhydrous DMSO (4 mL). The resulting suspension was stirred, heating every 10 min with a heat gun for 1 h, and at r. t. for another hour, then treated with a solution of 5-bromovaleronitrile, **65**, (0.11 mL, 0.96 mmol) in anhydrous DMSO (1 mL). The reaction mixture was stirred overnight at r. t., then diluted with 5 N NaOH (30 mL) and extracted with EtOAc (3 x 20 mL). The combined organic layers were washed with water (3 x 30 mL) and brine (30 mL), dried over anhydrous Na_2SO_4, filtered, and evaporated to dryness to provide a brown oil (309 mg), which was purified through column chromatography (silica gel 40–63 μm, 16 g, Ø = 2 cm; #1, 100 mL, hexane / Et_3N 100:0.4; #2, 150 mL, hexane / CH_2Cl_2 / Et_3N 98:2:0.4; #3-13, 300 mL, hexane / CH_2Cl_2 / Et_3N 96:4:0.4; #14-41, 600 mL, hexane / CH_2Cl_2 / Et_3N 85:15:0.4; #42-49, 150 mL, hexane / CH_2Cl_2 / Et_3N 75:25:0.4; #50-53, 100 mL, hexane / CH_2Cl_2 / Et_3N 50:50:1) to afford a first fraction of **(+)-66** (#3, 145 mg) impurified with 5-bromovaleronitrile and second pure fraction of **(+)-66** (#4-9, 97 mg). The impure product was taken up in 5 N HCl (15 mL) and washed with Et_2O (3 x 10 mL). The acidic aqueous phase was alkalinized with NaOH pellets until pH = 10 and extracted with CH_2Cl_2 (3 x 10 mL). The combined organic extracts were dried over anhydrous Na_2SO_4, filtered, and evaporated at reduced pressure, to afford an additional crop of **(+)-66** (102 mg) as a yellowish oil (62% total yield).

R_f = 0.62 (silica gel, 10 cm, hexane / CH_2Cl_2 / 50% aq. NH_4OH 6:4:0.04).

$[\alpha]^{20}_D$ = +95 (*c* 0.13, CH_2Cl_2)

IR (ATR) ν: 3377 (N–H st), 2243 (C≡N st), 1654, 1606, 1577, 1556 (Ar–C–C, Ar–C–N st) cm^{-1}.

^{1}H NMR (400 MHz, CD_3OD) δ: 1.52 (s, 3H, 9'-CH_3), 1.75–1.98 (complex signal, 6H, 3-H_2, 4-H_2, 10'-H_{endo}, 13'-H_{syn}), 2.06 (dm, *J* = 12.4 Hz, 1H, 13'-H_{anti}), 2.43 (t, *J* = 7.2 Hz, 2H, 2-H_2), 2.56 (dd, *J* = 17.2 Hz, *J'* = 4.8 Hz, 1H, 10'-H_{exo}), 2.75 (m, 1H, 7'-H), 3.02 (ddd, *J* = 17.6 Hz, *J'* = *J''* = 2.0 Hz, 1H, 6'-H_{endo}), 3.16 (dd, *J* = 17.6 Hz, *J'* = 5.6 Hz, 1H, 6'-H_{exo}), 3.31 (m, 1H, 11'-H), 3.48 (m, 2H, 5-H_2), 3.98 (br s, 1H, NH), 5.54 (br d, *J* = 5.2 Hz, 1H, 8'-H), 7.29 (dd, *J* = 9.2 Hz, *J'* = 2.0 Hz, 1H, 2'-H), 7.88 (d, *J* = 9.2 Hz, 1H, 1'-H), superimposed in part 7.91 (d, *J* = 2.0 Hz, 1H, 4'-H).

HRMS ESI:

Calculated for $[C_{22}H_{24}{}^{35}ClN_3 + H]^+$:	366.1732
Found:	366.1731

Synthesis of (–)-(7*S*,11*S*)-5-[(3-chloro-6,7,10,11-tetrahydro-9-methyl-7,11-methanocycloocta[*b*]quinolin-12-yl)amino]pentanenenitrile, (–)-66

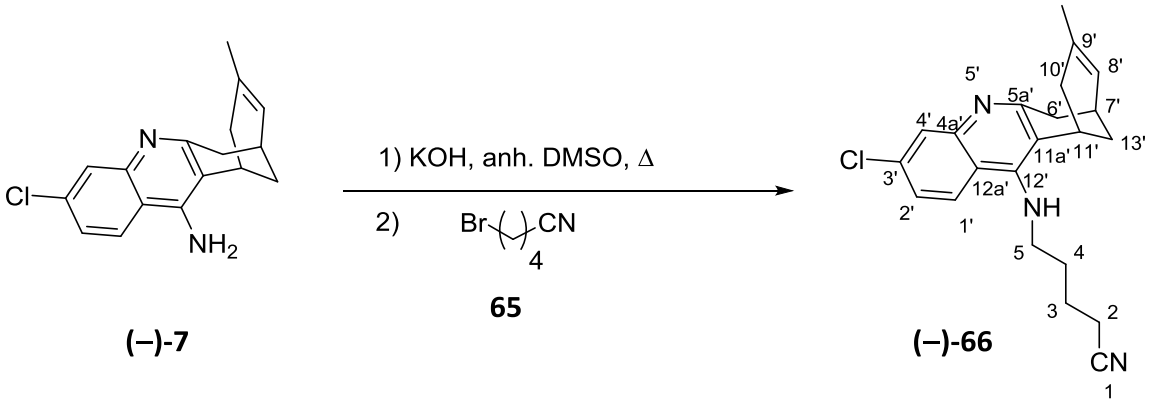

In a double neck 25 mL round-bottomed flask equipped with magnetic stirrer, inert atmosphere and 4Å molecular sieves, (–)-huprine Y, **(–)-7**, (297 mg, 1.04 mmol) and finely powdered KOH (85% purity, 279 mg, 4.22 mmol) were suspended in anhydrous DMSO (5 mL). The resulting suspension was stirred, heating every 10 min with a heat gun for 1 h, and at r. t. for another hour, then treated with a solution of 5-bromovaleronitrile, **65**, (0.16 mL, 1.40 mmol) in anhydrous DMSO (1 mL). The reaction mixture was stirred overnight at r. t., then diluted with 5 N NaOH (30 mL) and extracted with EtOAc (3 x 20 mL). The combined organic layers were washed with water (3 x 30 mL) and brine (30 mL), dried over anhydrous Na_2SO_4, filtered, and evaporated to dryness to provide a brown oil (349 mg), which was purified through column chromatography (silica gel 40–63 μm, 17 g, Ø = 2 cm; #1, 150 mL, hexane / Et_3N 100:0.4; #2, 150 mL, hexane / CH_2Cl_2 / Et_3N 98:2:0.4; #3, 150 mL, hexane / CH_2Cl_2 / Et_3N 96:4:0.4; #4, 150 mL, hexane / CH_2Cl_2 / Et_3N 94:6:0.4; #5, 300 mL, hexane / CH_2Cl_2 / Et_3N 90:10:0.4; #6-40, 1050 mL, hexane / CH_2Cl_2 / Et_3N 88:12:0.4; #41-146, 2250 mL, hexane / CH_2Cl_2 / Et_3N 86:14:0.4, #147-160, 300 mL, hexane / CH_2Cl_2 / Et_3N 75:25:1) to afford impure **(–)-66** (#55-149, 250 mg). The product was recrystallized from EtOAc (2 mL) to afford a white solid consisting of unreacted (–)-huprine Y, with the mother liquors being enriched in the desired nitrile. After evaporation of the mother liquors at reduced pressure, this recrystallization process was repeated (EtOAc, 1 mL). Evaporation of the final mother liquors afforded pure **(–)-66** (206 mg, 54% yield) as a yellowish oil.

R_f = 0.62 (silica gel, 10 cm, hexane / CH_2Cl_2 / 50% aq. NH_4OH 6:4:0.04).

$[\alpha]^{20}_D$ = –95 (*c* 0.48, CH_2Cl_2)

IR (ATR) ν: 3377 (N–H st), 2243 (C≡N st), 1654, 1606, 1577, 1556 (Ar–C–C, Ar–C–N st) cm^{-1}.

^{1}H NMR (400 MHz, CD_3OD) δ: 1.52 (s, 3H, 9'-CH_3), 1.75–1.98 (complex signal, 6H, 3-H_2, 4-H_2, 10'-H_{endo}, 13'-H_{syn}), 2.06 (dm, *J* = 12.4 Hz, 1H, 13'-H_{anti}), 2.44 (t, *J* = 6.8 Hz, 2H, 2-H_2), 2.57 (dd, *J* = 16.8 Hz, *J'* = 5.6 Hz, 1H, 10'-H_{exo}), 2.75 (m, 1H, 7'-H), 3.01 (ddd, *J* = 17.6 Hz, *J'* = *J''* = 2.0 Hz, 1H, 6'-H_{endo}), 3.16 (dd, *J* = 17.6 Hz, *J'* = 5.6 Hz, 1H, 6'-H_{exo}), 3.31 (m, 1H, 11'-H), 3.48 (m, 2H, 5-H_2), 3.90 (br s, 1H, NH), 5.54 (br d, *J* = 5.6 Hz, 1H, 8'-H), 7.30 (dd, *J* = 9.2 Hz, *J'* = 2.4 Hz, 1H, 2'-H), 7.88 (d, *J* = 9.2 Hz, 1H, 1'-H), superimposed in part 7.89 (d, *J* = 2.4 Hz, 1H, 4'-H).

HRMS ESI:

Calculated for $[C_{22}H_{24}{}^{35}ClN_3 + H]^+$:	366.1732
Found:	366.1734

Synthesis of 5-[(6-chloro-1,2,3,4-tetrahydroacridin-9-yl)amino]pentanenitrile, 61c

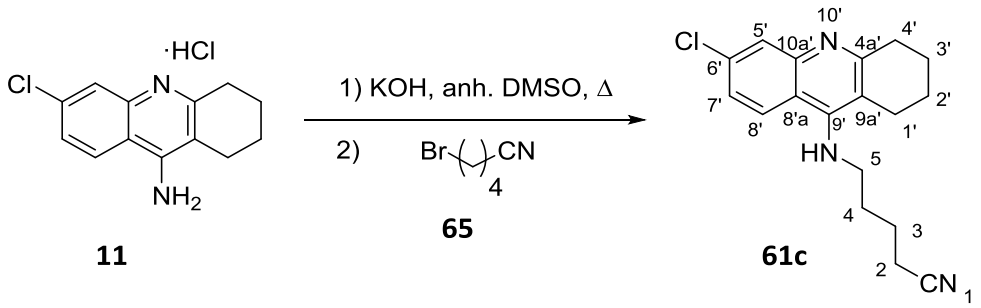

11 **65** **61c**

In a double neck 25 mL round-bottomed flask equipped with magnetic stirrer, inert atmosphere and 4Å molecular sieves, 6-chlorotacrine hydrochloride, **11·HCl**, (300 mg, 1.11 mmol) and finely powdered KOH (85% purity, 281 mg, 4.26 mmol) were suspended in anhydrous DMSO (4 mL). The resulting suspension was stirred, heating every 10 min with a heat gun for 1 h, and at r. t. for another hour, then treated with a solution of 5-bromovaleronitrile, **65**, (0.17 mL, 1.42 mmol) in anhydrous DMSO (1 mL). The reaction mixture was stirred overnight at r. t., then diluted with 5 N NaOH (30 mL) and extracted with EtOAc (3 x 20 mL). The combined organic layers were washed with water (3 x 30 mL) and brine (30 mL), dried over anhydrous Na_2SO_4, filtered, and evaporated to dryness to provide a brown oil (419 mg). After a failed attempt of purification by column chromatography (silica gel, hexane / CH_2Cl_2 / Et_3N mixtures), the crude product was recrystallized from EtOAc (2.5 mL), to afford a white solid consisting of unreacted 6-chlorotacrine, with the mother liquors being enriched in the desired nitrile. After evaporation of the mother liquors at reduced pressure, this recrystallization process was repeated twice (EtOAc, 2 x 1 mL). Evaporation of the final mother liquors afforded pure **61c** (289 mg, 83% yield), as a dark yellow oil.

R_f = 0.73 (silica gel, 10 cm, CH_2Cl_2 / MeOH / 50% aq. NH_4OH 9.5:0.5:0.02).

^{1}H NMR (400 MHz, $CDCl_3$) δ: 1.56 (s, NH), 1.74–1.88 (complex signal, 4H, 3-H_2, 4-H_2), 1.90–1.98 (complex signal, 4H, 2'-H_2, 3'-H_2), 2.40 (t, *J* = 7.2 Hz, 2H, 2-H_2), 2.69 (m, 2H, 1'-H_2), 3.04 (m, 2H, 4'-H_2), 3.50 (t, *J* = 7.2 Hz, 2H, 5-H_2), 7.29 (dd, *J* = 9.2 Hz, *J'* = 2.4 Hz, 1H, 7'-H), 7.84 (d, *J* = 9.2 Hz, 1H, 8'-H), 7.90 (d, *J* = 2.4 Hz, 1H, 5'-H).

Synthesis of 1-{1-{3-[(6-chloro-1,2,3,4-tetrahydroacridin-9-yl)amino]propanoyl}piperidin-4-yl}-3-[4-(trifluoromethoxy)phenyl]urea, 68a

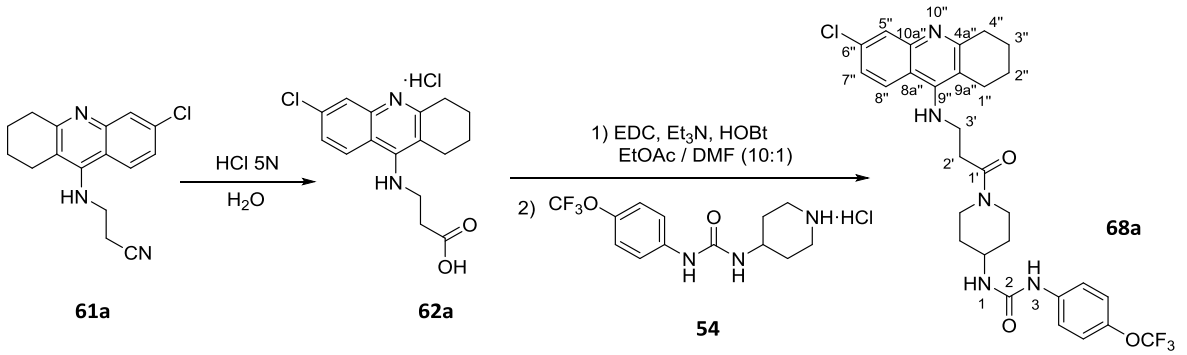

In a 25 mL round-bottomed flask provided with magnetic stirrer and reflux condenser, **61** (150 mg, 0.53 mmol) was suspended in 5 N HCl (13 mL) and heated at reflux for 4.5 h. The resulting yellow solution was evaporated to dryness, helping with drops of MeOH to remove the water. Analysis by ^{1}H-NMR showed that the mixture contained a small portion of the methyl ester. The mixture was treated again with 5 N HCl (13 mL) and heated at reflux for 3.5 h. The resulting yellow solution was evaporated to dryness, to provide a pale yellow solid (171 mg), whose ^{1}H-NMR spectra was consistent with the desired acid, in the form of the quinoline hydrochloride salt, **62a·HCl**, that was used in the following step without further purification.

In a 25 mL round-bottomed flask equipped with magnetic stirrer, crude **62a·HCl** (144 mg) was suspended in a mixture of EtOAc / DMF (7.7 mL, 10:1), and treated subsequently with EDC·HCl (121 mg, 0.63 mmol), Et_3N (0.27 mL, 1.94 mmol) and HOBt (86 mg, 0.63 mmol). After stirring for 10 min at r. t., a solution of the amine **54·HCl** (158 mg, 0.46 mg) in EtOAc / DMF (8.8 mL, 10:1) was added and the reaction mixture was stirred at r. t. overnight, then evaporated to dryness to give a brown oil (708 mg), which was purified through column chromatography (silica gel 40–63 μm, 35 g, Ø = 3 cm; #1, 250 mL, CH_2Cl_2 / 50% aq. NH_4OH 100:0.4; #2-82, 2000 mL, CH_2Cl_2 / MeOH / 50% aq. NH_4OH 99:1:0.4; #83, 100 mL, CH_2Cl_2 / MeOH / 50% aq. NH_4OH 98:2:0.4), to provide a slightly impure fraction of **68a** (#30-31 and #45-47, 44 mg) and a pure fraction of **68a** (#32-44, 69 mg), as a yellowish solid (45% overall yield).

R_f = 0.7 (silica gel, 10 cm, CH_2Cl_2 / MeOH / 50% aq. NH_4OH 9.5:0.5:0.02)

Analytical sample of 68a·HCl

In a vial, **68a** (69 mg) was dissolved in CH_2Cl_2 (2 mL), filtered through a 0.2 µm PTFE filter, treated with excess of a solution of HCl in Et_2O (1 mL, 1.17 M), and evaporated to dryness. The resulting solid was washed with EtOAc (2 x 2 mL), hexane (2 x 2 mL), and pentane (2 x 2 mL), evaporated to dryness and dried at 45 °C/2 Torr for 5 days, to provide **68a·HCl** (65 mg) as a yellowish solid.

Melting Point: 191–192 °C

IR (ATR) ν: 3500–2500 (max at 3279, 3056, 2939, 2864, N–H, $^+$N–H, C–H st), 1683, 1634, 1558, 1509 (C=O, Ar–C–C, Ar–C–N st) cm^{-1}.

^{1}H NMR (400 MHz, CD_3OD) δ: 1.30–1.51 [m, 2H, piperidine 3(5)-H_a], 1.91–2.08 [complex signal, 6H, 2''-H_2, 3''-H_2, piperidine 3(5)-H_b], 2.67 (m, 2H, 1''-H_2), 2.90–3.34 (complex signal, 4H, 4''-H_2, 2'-H_2), superimposed 2.90–3.34 (m, 1H), 3.27 (ddd, *J* = 14.0 Hz, *J'* = 11.2 Hz, *J''* = 2.8 Hz, 1H), 3.93 (dm, *J* = 14.0 Hz, 1H), 4.37 (dm, *J* = 13.6 Hz, 1H) [piperidine 2(6)-H_a, piperidine 2(6)-H_b], 3.83 (m, 1H, piperidine 4-H), 4.23 (t, *J* = 6.4 Hz, 2H, 3'-H_2), 4.85 (s, NH, $^+$NH), 7.15 [d, *J* = 9.2 Hz, 2H, phenyl 3(5)-H], 7.44 [d, *J* = 9.2 Hz, 2H, phenyl 2(6)-H], 7.57 (dd, *J* = 9.2 Hz, *J'* = 2.0 Hz, 1H, 7''-H), 7.78 (d, *J* = 2.0 Hz, 1H, 5''-H), 8.39 (d, *J* = 9.2 Hz, 1H, 8''-H).

^{13}C NMR (100.6 MHz, CD_3OD) δ: 21.76 (CH_2, C3''), 22.81 (CH_2, C2''), 24.62 (CH_2, C1''), 29.31 (CH_2, C4''), 32.96 (CH_2), 33.75 (CH_2) [piperidine C3(5)], 33.58 (CH_2, C2'), 41.74 (CH_2), 45.47 (CH_2) [piperidine C2(6)], piperidine C6), 45.66 (CH_2, C3'), 48.02 (CH, piperidine C4), 113.66 (C), 115.56 (C) (C8a'', C9a''), 119.61 (CH, C5''), 120.86 [2CH, phenyl C2(6)], 121.98 (C, q, $J_{C\text{-}F}$ = 254.8 Hz, CF_3), 122.63 [2CH, phenyl C3(5)], 126.82 (CH, C7''), 128.77 (CH, C8''), 140.11 (C, C6''), 140.15 (C, C10a''), 140.53 (C, phenyl C1), 145.02 (C, q, $J_{C\text{-}F}$ = 1.9 Hz, phenyl C4), 153.63 (C, C4a''), 157.98 (C, C9''), 157.98 (C), 171.11 (C) (C2, C1').

HRMS ESI:

Calculated for $[C_{29}H_{31}{}^{35}ClF_3N_5O_3 + H]^+$: 590.2140

Found: 590.2137

Synthesis of 1-{1-{4-[(6-chloro-1,2,3,4-tetrahydroacridin-9-yl)amino]butanoyl}piperidin-4-yl}-3-[4-(trifluoromethoxy)phenyl]urea, 68b

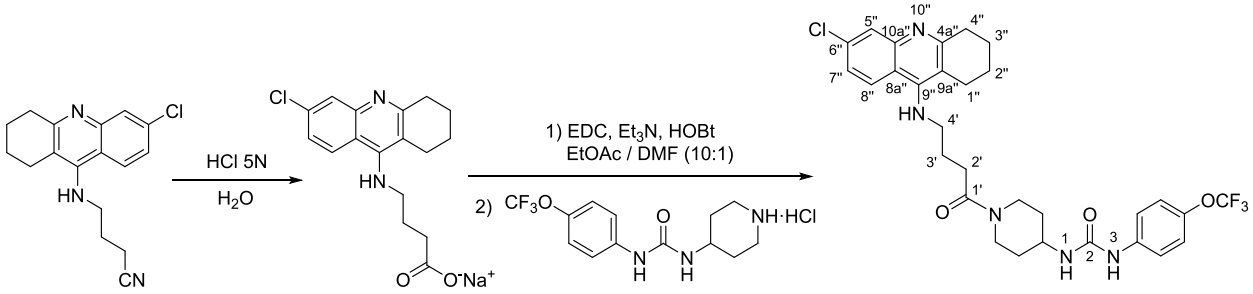

61b **62b** **54** **68b**

In a 25 mL round-bottomed flask equipped with magnetic stirrer and reflux condenser, **61b** (109 mg, 0.53 mmol) was suspended in 5 N HCl (9 mL) and heated at reflux for 3 h. The resulting yellow solution was evaporated to dryness and the resulting orange residue was taken up in H_2O (15 mL), alkalinized with 10 N NaOH (few drops, until pH = 12), and extracted with EtOAc (3 x 10 mL). The combined organic extracts were dried over anhydrous Na_2SO_4, filtered, and evaporated at reduced pressure, to afford 1-(6-chloro-1,2,3,4-tetrahydroacridin-9-yl)pyrrolidin-2-one (254 mg, 64% yield) as a byproduct. The alkaline aqueous layer was evaporated to dryness, to provide a pale yellow solid (844 mg), which contained the desired acid (^{1}H-NMR), in the form of sodium carboxylate salt (maximum of 173 mg of acid, 36% yield), and was used in the following step without further purification.

In a 25 mL round-bottomed flask equipped with magnetic stirrer, **62b** (844 mg of a crude that could contain a maximum of 173 mg of acid) was suspended in a mixture of EtOAc / DMF (7.7 mL, 10:1), and treated subsequently with EDC·HCl (140 mg, 0.73 mmol), Et_3N (0.34 mL, 2.43 mmol) and HOBt (99 mg, 0.73 mmol). After stirring for 10 min at r. t., a solution of the amine **54·HCl** (182 mg, 0.54 mg) in EtOAc / DMF (8.8 mL, 10:1) was added and the reaction mixture was stirred at r. t. overnight, then evaporated to dryness to give a brown oil (1.38 g), which was purified through column chromatography (silica gel 40–63 µm, 70 g, Ø = 4.5 cm; #1, 300 mL, CH_2Cl_2 / 50% aq. NH_4OH 100:0.4; #2, 1300 mL, CH_2Cl_2 / MeOH / 50% aq. NH_4OH 99:1:0.4; #3-91, 1000 mL, CH_2Cl_2 / MeOH / 50% aq. NH_4OH 98:2:0.4), to afford **68b** (#17-49, 132 mg, 45% yield) as a yellowish solid.

R_f = 0.5 (silica gel, 10 cm, CH_2Cl_2 / MeOH / 50% aq. NH_4OH 9.5:0.5:0.02)

Analytical sample of 68b·HCl

In a vial, **68b** (132 mg) was dissolved in CH_2Cl_2 (2 mL), filtered through a 0.2 µm PTFE filter, treated with excess of a solution of HCl in Et_2O (1 mL, 1.17 M), and evaporated to dryness. The resulting solid was washed with EtOAc (2 x 2 mL), hexane (2 x 2 mL), and pentane (2 x 2 mL), evaporated to dryness and dried at 45 °C/2 Torr for 5 days, to provide **68b·HCl** (72 mg) as a yellowish solid.

Melting Point: 195–197 °C

IR (ATR) ν: 3500–2500 (max at 3268, 3055, 2938, 2861, N–H, $^+$N–H, C–H st), 1683, 1635, 1557, 1507 (Ar–C–C, Ar–C–N st) cm^{-1}.

^{1}H NMR (400 MHz, CD_3OD) δ: 1.30–1.50 [m, 2H, piperidine 3(5)-H_a], 1.92–2.05 (complex signal, 6H, 2''-H_2, 3''-H_2, piperidine 3(5)-H_b], 2.15 (m, 2H, 3'-H_2), 2.68 (t, *J* = 6.4 Hz, 2'-H_2), superimposed in part 2.73 (m, 2H, 1''-H_2), 2.99 (m, 2H, 4''-H_2), superimposed in part 2.93 (m, 1H), 3.24 (ddd, *J* = 14.0 Hz, *J'* = 11.2 Hz, *J''* = 2.8 Hz, 1H), 3.92 (dm, *J* = 14.0 Hz, 1H), 4.41 (dm, *J* = 14.0 Hz, 1H) [piperidine 2(6)-H_a, piperidine 2(6)-H_b], 3.82 (m, 1H, piperidine 4-H), 4.02 (t, *J* = 6.8 Hz, 2H, 4'-H_2), 4.85 (s, NH, $^+$NH), 7.15 [d, *J* = 8.8 Hz, 2H, phenyl 3(5)-H], 7.43 [d, *J* = 8.8 Hz, 2H, phenyl 2(6)-H], 7.56 (dd, *J* = 9.6 Hz, *J'* = 2.4 Hz, 1H, 7''-H), 7.75 (d, *J* = 2.4 Hz, 1H, 5''-H), 8.53 (d, *J* = 9.6 Hz, 1H, 8''-H).

^{13}C NMR (100.6 MHz, CD_3OD) δ: 21.78 (CH_2), 22.88 (CH_2) (C2'', C3''), 24.88 (CH_2, C1''), 26.07 (CH_2, C3'), 29.28 (CH_2, C4''), 31.84 (CH_2, C2'), 33.03 (CH_2), 33.75 (CH_2) [piperidine C3(5)], 41.90 (CH_2), 45.45 (CH_2) [piperidine C2(6)], superimposed 45.45 (CH_2, C4'), 48.05 (CH, piperidine C4), 113.31 (C), 115.38 (C) (C8a'', C9a''), 119.00 (CH, C5''), 120.09 [2CH, phenyl C2(6)], 121.98 (C, q, $J_{C\text{-}F}$ = 254.5 Hz, CF_3), 122.62 [2CH, phenyl C3(5)], 126.66 (CH, C7''), 129.11 (CH, C8''), 140.06 (C, C6''), 140.09 (C, C10a''), 140.56 (C, phenyl C1), 145.02 (C, q, $J_{C\text{-}F}$ = 2.0 Hz, phenyl C4), 151.78 (C, C4a''), 157.21 (C, C9''), 157.80 (C), 173.08 (C) (C2, C1').

HRMS ESI:

Calculated for $[C_{30}H_{33}{}^{35}ClF_3N_5O_3 + H]^+$: 604.2297

Found: 604.2287

Synthesis of 1-{1-{5-[(6-chloro-1,2,3,4-tetrahydroacridin-9-yl)amino]pentanoyl}piperidin-4-yl}-3-[4-(trifluoromethoxy)phenyl]urea, 68c

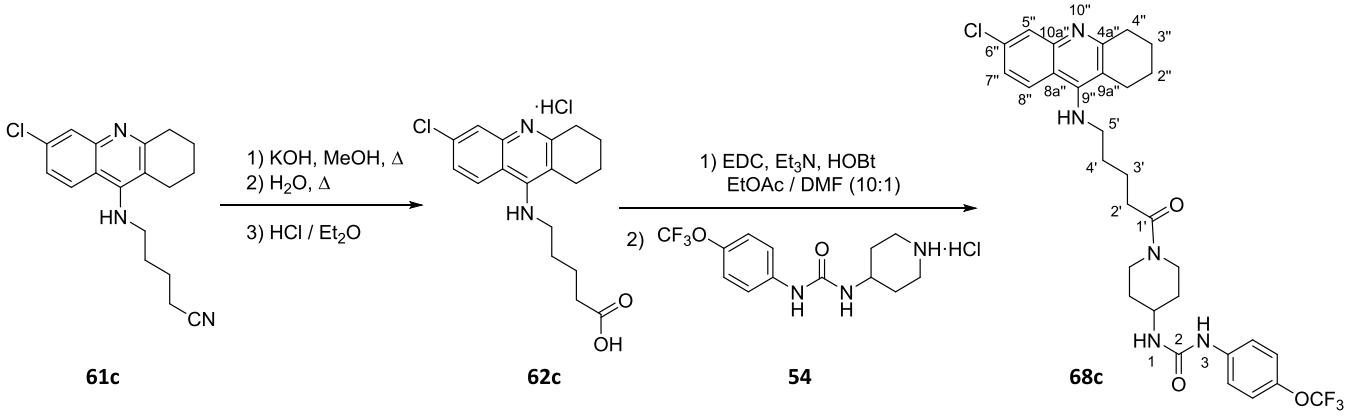

In a 50 mL round-bottomed flask equipped with magnetic stirrer and reflux condenser, **61c** (289 mg, 0.92 mmol) was dissolved in MeOH (1.5 mL), treated with a solution of KOH (40% in MeOH, 2.5 mL). The resulting suspension was stirred under reflux for 5 h, treated with water (4 mL) and stirred at reflux overnight. The resulting yellow solution was cooled down to r. t. and evaporated to dryness, then treated with excess of a solution of HCl in Et_2O (6 mL, 1.17 M) and evaporated to dryness, to afford a brilliant yellow solid (789 mg, maximum of 340 mg of acid), which contained the expected acid (^{1}H-NMR) in the form of quinoline hydrochloride salt, **62c·HCl**, and was used in the following step without further purification.

In a 50 mL round-bottomed flask equipped with magnetic stirrer, **62c·HCl** (789 mg of a crude that could contain a maximum of 340 mg of acid) was suspended in a mixture of EtOAc / DMF (13.2 mL, 10:1), and treated subsequently with EDC·HCl (265 mg, 1.38 mmol), Et_3N (0.64 mL, 4.6 mmol) and HOBt (188 mg, 1.38 mmol). After stirring for 10 min at r. t., a solution of the amine **54·HCl** (313 mg, 0.92 mg) in EtOAc / DMF (17.6 mL, 10:1) was added and the reaction mixture was stirred at r. t. overnight, then evaporated to dryness to give a brown oil (2.09 g), which was purified through column chromatography (silica gel 40 –63 µm, 82 g, Ø = 5 cm; #1, 400 mL, CH_2Cl_2 / 50% aq. NH_4OH 100:0.4; #2, 800 mL, CH_2Cl_2 / MeOH / 50% aq. NH_4OH 99.5:0.5:0.4; #3, 900 mL, CH_2Cl_2 / MeOH / 50% aq. NH_4OH 99:1:0.4; #4-51, 4800 mL, CH_2Cl_2 / MeOH / 50% aq. NH_4OH 98.5:1.5:0.4; #52-56, 400 mL, CH_2Cl_2 / MeOH / 50% aq. NH_4OH 97:3:0.4), to provide **68c** (#16-45, 452 mg, 79% yield) as an ochre solid.

R_f = 0.22 (silica gel, 10 cm, CH_2Cl_2 / MeOH / 50% aq. NH_4OH 9.6:0.4:0.04)

Analytical sample of 68c·HCl

In a 10 mL round-bottomed flask, **68c** (452 mg) was dissolved in CH_2Cl_2 (5 mL), filtered through a 0.2 µm PTFE filter, treated with excess of a solution of HCl in Et_2O (2 mL, 1.17 M), and evaporated to dryness. The resulting solid was washed with EtOAc (2 x 5 mL), hexane (2 x 5 mL), and pentane (2 x 5 mL), evaporated to dryness and dried at 45 °C/2 Torr for 5 days, to provide **68c·HCl** (411 mg) as a light brown solid.

Melting Point: 154–157 °C

IR (ATR) ν: 3500–2500 (max at 3279, 3062, 2936, 2871, N–H, $^+$N–H, C–H st), 1688, 1631, 1555, 1509 (Ar–C–C, Ar–C–N st) cm^{-1}.

^{1}H NMR (400 MHz, CD_3OD) δ: 1.30–1.47 [m, 2H, piperidine 3(5)-H_a], 1.73 (tt, *J* = *J'* = 6.8 Hz, 2H, 3'-H_2), 1.87 (tt, *J* = *J'* = 7.2 Hz, 2H, 4'-H_2), superimposed in part 1.90–2.05 [complex signal, 6H, 2''-H_2, 3''-H_2, piperidine 3(5)-H_b], 2.48 (m, 2H, 2'-H_2), 2.71 (m, 2H, 1''-H_2), 2.90 (ddd, *J* = 14.4 Hz, *J'* = 10.8 Hz, *J''* = 2.8 Hz, 1H), 3.22 (ddd, *J* = 14.4 Hz, *J'* = 11.2 Hz, *J''* = 2.4 Hz, 1H), 3.91 (dm, *J* = 14.0 Hz, 1H), 4.37 (dm, *J* = 14.0 Hz, 1H) [piperidine 2(6)-H_a, piperidine 2(6)-H_b], 3.00 (m, 2H, 4''-H_2), 3.81 (m, 1H, piperidine 4-H), 3.98 (t, *J* = 7.2 Hz, 2H, 5'-H_2), 4.85 (s, NH, $^+$NH), 7.15 [d, *J* = 8.4 Hz, 2H, phenyl 3(5)-H], 7.43 [d, *J* = 8.4 Hz, 2H, phenyl 2(6)-H], 7.56 (dd, *J* = 9.2 Hz, *J'* = 2.0 Hz, 1H, 7''-H), 7.76 (d, *J* = 2.0 Hz, 1H, 5''-H), 8.42 (d, *J* = 9.2 Hz, 1H, 8''-H).

^{13}C NMR (100.6 MHz, CD_3OD) δ: 21.76 (CH_2), 22.88 (CH_2) (C2'', C3''), 23.17 (CH_2, C3'), 24.79 (CH_2, C1''), 29.34 (CH_2, C4''), 30.83 (CH_2, C4'), 33.15 (CH_2, C2'), 33.04 (CH_2), 33.92 (CH_2) [piperidine C3(5)], 41.75 (CH_2), 45.47 (CH_2) [piperidine C2(6)], 48.08 (CH, piperidine C4), 48.89 (CH_2, C5'), 113.42 (C), 115.47 (C) (C8a'', C9a''), 119.10 (CH, C5''), 120.85 [2CH, phenyl C2(6)], 122.00 (C, q, $J_{C\text{-}F}$ = 254.5 Hz, CF_3), 122.62 [2CH, phenyl C3(5)], 126.81 (CH, C7''), 128.85 (CH, C8''), 140.10 (C, C6''), 140.15 (C, C10a''), 140.50 (C, phenyl C1), 152.07 (C, q, $J_{C\text{-}F}$ = 1.8 Hz, phenyl C4), 151.19 (C, C4a''), 157.19 (C, C9''), 157.92 (C), 173.26 (C) (C2, C1').

HRMS ESI:

Calculated for $[C_{31}H_{35}{}^{35}ClF_3N_5O_3 + H]^+$: 618.2453

Found: 618.2443

Synthesis of (+)-(7*R*,11*R*)-1-{1-{5-[(3-chloro-6,7,10,11-tetrahydro-9-methyl-7,11-methanocycloocta[*b*]quinolin-12-yl)amino]pentanoyl}piperidin-4-yl}-3-[4-(trifluoromethoxy)phenyl]urea, (+)-16

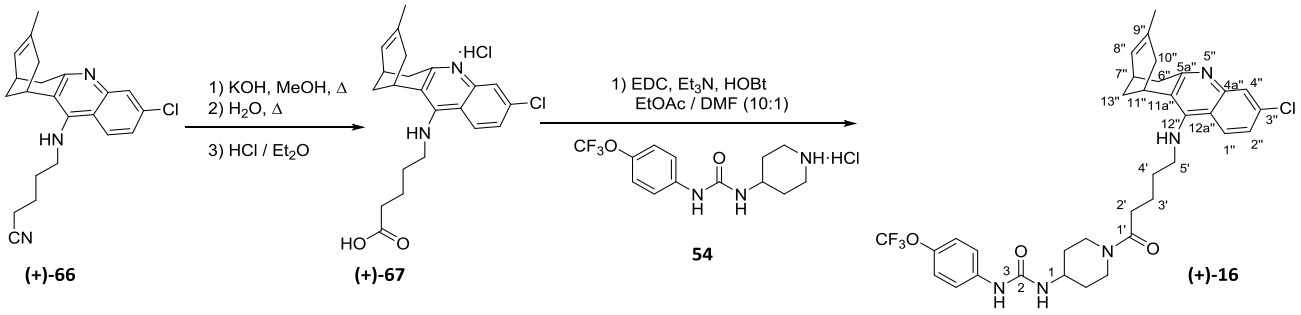

In a 25 mL round-bottomed flask equipped with magnetic stirrer and reflux condenser, **(+)-66** (102 mg, 0.28 mmol) was dissolved in MeOH (0.5 mL) and treated with a solution of KOH (40% in MeOH, 0.8 mL). The resulting suspension was stirred under reflux for 3 h, treated with water (1 mL) and stirred at reflux overnight. The resulting orange solution was cooled down to r. t., evaporated under reduced pressure, treated with excess of a solution of HCl in Et_2O (5 mL, 1.17 M) and evaporated to dryness, to afford a brilliant yellow solid (575 mg, maximum of 117 mg of acid), whose ^{1}H-NMR spectra was consistent with the presence of the desired acid, in the form of the quinoline hydrochloride salt, **(+)-67·HCl**, and was used in the following step without further purification.

In a 25 mL round-bottomed flask equipped with magnetic stirrer, **(+)-67·HCl** (575 mg of a crude that could contain a maximum of 117 mg of acid) was suspended in a mixture of EtOAc / DMF (5.5 mL, 10:1), and treated subsequently with EDC·HCl (80 mg, 0.42 mmol), Et_3N (0.18 mL, 1.28 mmol) and HOBt (57 mg, 042 mmol). After stirring for 10 min at r. t., a solution of the amine **54·HCl** (104 mg, 0.31 mg) in EtOAc / DMF (3.85 mL, 10:1) was added and the reaction mixture was stirred at r. t. overnight, then evaporated to dryness to give a brown oil (983 mg), which was purified through column chromatography (silica gel 40–63 µm, 39 g, Ø = 3.5 cm; #1, 300 mL, CH_2Cl_2 / 50% aq. NH_4OH 100:0.4; #2, 600 mL, CH_2Cl_2 / MeOH / 50% aq. NH_4OH 99.5:0.5:0.4; #3-29, 3800 mL, CH_2Cl_2 / MeOH / 50% aq. NH_4OH 99:1:0.4; #30-33, 300 mL, CH_2Cl_2 / MeOH / 50% aq. NH_4OH 98:2:0.4), to provide **(+)-16** (#14-31, 74 mg, 40% yield) as a light brown solid.

R_f = 0.68 (silica gel, 10 cm, CH_2Cl_2 / MeOH / 50% aq. NH_4OH 9.5:0.5:0.04)

Analytical sample of (+)-16·HCl

In a vial, **(+)-16** (74 mg) was dissolved in CH_2Cl_2 (1 mL), filtered through a 0.2 µm PTFE filter, treated with excess of a solution of HCl in Et_2O (1 mL, 1.17 M), and evaporated to dryness. The resulting solid was washed with EtOAc (2 x 5 mL), hexane (2 x 5 mL), and pentane (2 x 5 mL), evaporated to dryness and dried at 45 °C/2 Torr for 7 days, to provide **(+)-16·HCl** (58 mg) as a light brown solid.

Melting Point: 178–180 °C

$[\alpha]^{20}_D$ = +138 (*c* 0.54, MeOH)

IR (ATR) ν: 3500–2500 (max at 3272, 3073, 2935, 2860, N–H, $^+$N–H, C–H st), 1688, 1632, 1583, 1556, 1508 (C=O, Ar–C–C, Ar–C–N st) cm^{-1}.

^{1}H NMR (400 MHz, CD_3OD) δ: 1.28–1.48 [m, 2H, piperidine 3(5)-H_a], 1.58 (s, 3H, 9''-CH_3), 1.75 (tt, *J* = *J'* = 7.2 Hz, 2H, 3'-H_2), 1.91 (tt, *J* = *J'* = 6.8 Hz, 2H, 4'-H_2), superimposed in part 1.87–2.03 [complex signal, 4H, 10''-H_{endo}, 13''-H_{syn}, piperidine 3(5)-H_b], 2.09 (dm, *J* = 14.8 Hz, 1H, 13'-H_{anti}), 2.50 (t, *J* = 7.2 Hz, 2H, 2'-H_2), 2.57 (dd, *J* = 18.0 Hz, *J'* = 5.6 Hz, 1H, 10''-H_{exo}), 2.77 (m, 1H, 7''-H), 2.86 (br d, *J* = 18.0 Hz, 1H, 6''-H_{endo}), 3.20 (dd, *J* = 18.0 Hz, *J'* = 5.2 Hz, 1H, 6''-H_{exo}), 2.91 (m, 1H), 3.23 (m, 1H), 3.91 (dm, *J* = 14.0 Hz, 1H), 4.36 (dm, *J* = 14.0 Hz, 1H) [piperidine 2(6)-H_a, piperidine 2(6)-H_b], 3.50 (m, 1H, 11''-H), 3.82 (m, 1H, piperidine 4-H), 4.01 (t, *J* = 6.8 Hz, 2H, 5'-H_2), 4.85 (s, NH, $^+$NH), 5.58 (br d, *J* = 5.6 Hz, 1H, 8''-H), 7.14 [d, *J* = 8.8 Hz, 2H, phenyl 3(5)-H], 7.44 [d, *J* = 8.8 Hz, 2H, phenyl 2(6)-H], 7.56 (dd, *J* = 9.2 Hz, *J'* = 2.0 Hz, 1H, 2''-H), 7.75 (d, *J* = 2.0 Hz, 1H, 4''-H), 8.43 (d, *J* = 9.2 Hz, 1H, 1''-H).

^{13}C NMR (100.6 MHz, CD_3OD) δ: 23.21 (CH_2, C3'), 23.47 (CH_3, 9''-CH_3), 27.26 (CH, C11''), 27.88 (CH, C7''), 29.33 (CH_2, C13''), 30.81 (CH_2, C4'), 33.10 (CH_2, C2'), 33.06 (CH_2), 33.93 (CH_2) [piperidine C3(5)], 36.05 (CH_2), 36.21 (CH_2) (C6'', C10''), 41.75 (CH_2), 45.44 (CH_2) [piperidine C2(6)], 48.12 (CH, piperidine C4), 49.34 (CH_2, C5'), 115.69 (C, C12a''), 117.70 (C, C11a''), 119.04 (CH, C4''), 120.88 [2CH, phenyl C2(6)], 121.99 (C, q, $J_{C\text{-}F}$ = 254.6 Hz, CF_3), 122.64 [2CH, phenyl C3(5)], 125.07 (CH, C8''), 126.70 (CH, C2''), 129.56 (CH, C1''), 134.65 (C, C9''), 140.14 (C, phenyl C1), 140.23 (C, C3''), 140.97 (C, C4a''), 145.03 (C, q, $J_{C\text{-}F}$ = 2.1 Hz, phenyl C4), 151.19 (C, C5a''), 156.96 (C, C12''), 157.20 (C), 173.22 (C) (C2, C1').

HRMS ESI:

Calculated for $[C_{35}H_{39}{}^{35}ClF_3N_5O_3 + H]^+$: 670.2766

Found: 670.2762

Synthesis of (–)-(7*S*,11*S*)-1-{1-{5-[(3-chloro-6,7,10,11-tetrahydro-9-methyl-7,11-methanocycloocta[*b*]quinolin-12-yl)amino]pentanoyl}piperidin-4-yl}-3-[4-(trifluoromethoxy)phenyl]urea, (–)-16

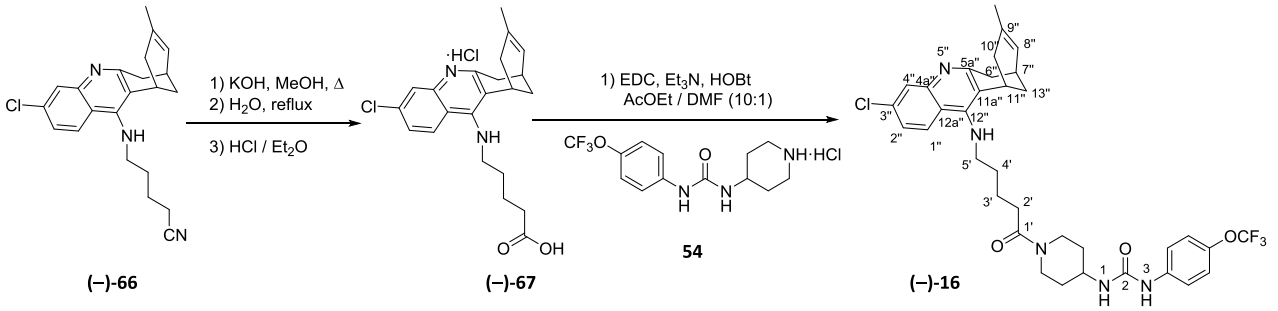

In a 25 mL round-bottomed flask equipped with magnetic stirrer and reflux condenser, **(–)-66** (206 mg, 0.56 mmol) was dissolved in MeOH (0.8 mL), treated with a solution of KOH (40% in MeOH, 1.6 mL). The resulting suspension was stirred under reflux for 3 h, treated with water (2 mL) and stirred at reflux overnight. The resulting yellow solution was cooled down to r. t. and evaporated to dryness. Because ^{1}H-NMR analysis of the reaction mixture showed that there was still a small amount of unreacted nitrile, the reaction was repeated. Thus, the crude was dissolved in MeOH (0.8 mL), treated with a solution of KOH (40% in MeOH, 1.6 mL) and stirred under reflux for 3 h, then treated with water (2 mL) and stirred at reflux overnight. The yellow solution was cooled down to r. t., evaporated under reduced pressure, treated with excess of a solution of HCl in Et_2O (10 mL, 1.17 M) and evaporated to dryness to afford a brilliant yellow solid (1.55 g, maximum of 236 mg of acid), whose ^{1}H-NMR spectra was consistent with the presence of the desired acid, in the form of the quinoline hydrochloride salt, **(–)-67·HCl**, and was used in the following step without further purification.

In a 25 mL round-bottomed flask equipped with magnetic stirrer, **(–)-67·HCl** (1.55 g of a crude that could contain a maximum of 236 mg of acid) was suspended in a mixture of EtOAc / DMF (9.9 mL, 10:1), and treated subsequently with EDC·HCl (161 mg, 0.84 mmol), Et_3N (0.39 mL, 2.8 mmol) and HOBt (114 mg, 0.84 mmol). After stirring for 10 min at r. t., a solution of the amine **54·HCl** (190 mg, 0.56 mg) in EtOAc / DMF (8.8 mL, 10:1) was added and the reaction mixture was stirred at r. t. overnight, then evaporated to dryness to give a brown oil (2.28 g), which was purified through column chromatography (silica gel 40–63 µm, 90 g, Ø = 5 cm; #1, 1000 mL, CH_2Cl_2 / 50% aq. NH_4OH 100:0.4; #2, 500 mL, CH_2Cl_2 / MeOH / 50% aq. NH_4OH 99.5:0.5:0.4; #3, 500 mL, CH_2Cl_2 / MeOH / 50% aq. NH_4OH 99:1:0.4; #4-55, 5000 mL, CH_2Cl_2 / MeOH / 50% aq. NH_4OH 98.5:1.5:0.4; #56-62, 500 mL, CH_2Cl_2 / MeOH / 50% aq. NH_4OH 98:2:0.4), to obtain **(–)-16** (#31-53, 286 mg, 76% yield) as a light brown solid.

R_f = 0.67 (silica gel, 10 cm, CH_2Cl_2 / MeOH / 50% aq. NH_4OH 9.5:0.5:0.04)

Analytical sample of (–)-16·HCl

In a 10 mL round-bottomed flask, **(–)-16** (286 mg) was dissolved in CH_2Cl_2 (5 mL), filtered through a 0.2 µm PTFE filter, treated with excess of a solution of HCl in Et_2O (2 mL, 1.17 M), and evaporated to dryness. The resulting solid was washed with EtOAc (2 x 5 mL), hexane (2 x 5 mL), and pentane (2 x 5 mL), evaporated to dryness and dried at 45 °C/2 Torr for 7 days, to provide **(–)-16·HCl** (234 mg) as a grey solid.

Melting Point: 177–180 °C

$[\alpha]^{20}_D$ = –145 (*c* 0.60, MeOH)

IR (ATR) ν: 3500–2500 (max at 3258, 3060, 2933, 2863, N–H, $^+$N–H, C–H st), 1682, 1633, 1583, 1554, 1509 (C=O, Ar–C–C, Ar–C–N st) cm^{-1}.

^{1}H NMR (400 MHz, CD_3OD) δ: 1.30–1.50 [m, 2H, piperidine 3(5)-H_a], 1.58 (s, 3H, 9''-CH_3), 1.75 (tt, *J* = *J'* = 7.2 Hz, 2H, 3'-H_2), 1.92 (tt, *J* = *J'* = 6.8 Hz, 2H, 4'-H_2), superimposed in part 1.85–2.03 (complex signal, 4H, 10''-H_{endo}, 13''-H_{syn}, piperidine 3(5)-H_b], 2.09 (m, 1H, 13'-H_{anti}), 2.51 (t, *J* = 7.2 Hz, 2H, 2'-H_2), 2.57 (dd, *J* = 18.0 Hz, *J'* = 5.2 Hz, 1H, 10''-H_{exo}), 2.77 (m, 1H, 7''-H), 2.86 (br d, *J* = 17.6 Hz, 1H, 6''-H_{endo}), 3.20 (dd, *J* = 17.6 Hz, *J'* = 5.2 Hz, 1H, 6''-H_{exo}), 2.91 (ddd, *J* = 14.4 Hz, *J'* = 11.2 Hz, *J''* = 2.8 Hz, 1H), 3.23 (m, 1H), 3.92 (dm, *J* = 13.6 Hz, 1H), 4.36 (dm, *J* = 13.6 Hz, 1H) [piperidine 2(6)-H_a, piperidine 2(6)-H_b], 3.51 (m, 1H, 11''-H), 3.82 (m, 1H, piperidine 4-H), 4.01 (t, *J* = 6.8 Hz, 2H, 5'-H_2), 4.85 (s, NH, $^+$NH), 5.58 (br d, *J* = 5.2 Hz, 1H, 8''-H), 7.14 [d, *J* = 9.2 Hz, 2H, phenyl 3(5)-H], 7.44 [d, *J* = 9.2 Hz, 2H, phenyl 2(6)-H], 7.56 (dd, *J* = 9.2 Hz, *J'* = 2.0 Hz, 1H, 2''-H), 7.76 (d, *J* = 2.0 Hz, 1H, 4''-H), 8.43 (d, *J* = 9.2 Hz, 1H, 1''-H).

^{13}C NMR (100.6 MHz, CD_3OD) δ: 23.21 (CH_2, C3'), 23.47 (CH_3, 9''-CH_3), 27.26 (CH, C11''), 27.88 (CH, C7''), 29.33 (CH_2, C13''), 30.81 (CH_2, C4'), 33.10 (CH_2, C2'), 33.06 (CH_2), 33.93 (CH_2) [piperidine C3(5)], 36.04 (CH_2), 36.22 (CH_2) (C6'', C10''), 41.75 (CH_2), 45.43 (CH_2) [piperidine C2(6)], 48.11 (CH, piperidine C4), 49.35 (CH_2, C5'), 115.69 (C, C12a''), 117.69 (C, C11a''), 119.09 (CH, C4''), 120.88 [2CH, phenyl C2(6)], 121.99 (C, q, $J_{C\text{-}F}$ = 254.4 Hz, CF_3), 122.64 [2CH, phenyl C3(5)], 125.08 (CH, C8''), 126.70 (CH, C2''), 129.55 (CH, C1''), 134.65 (C, C9''), 140.14 (C, phenyl C1), 140.23 (C, C3''), 140.97 (C, C4a''), 145.03 (C, q, $J_{C\text{-}F}$ = 2.1 Hz, phenyl C4), 151.19 (C, C5a''), 156.96 (C, C12''), 157.20 (C), 173.22 (C) (C2, C1').

HRMS ESI:

Calculated for $[C_{35}H_{39}{}^{35}ClF_3N_5O_3 + H]^+$: 670.2766

Found: 670.2762

Biological evaluation of amyloidogenic proteins aggregation.

A) General methods and materials

All the compounds evaluated were previously synthesised by our group and were used as hydrochloride salts, unless otherwise stated. General chemicals were purchased from Sigma-Aldrich. Compounds for bacterial media were purchased from Pronadisa. All the materials used were bought sterile or were previously autoclaved to ensure their sterility. Solutions were prepared in doubly distilled water, purified with a Milli-Q system (Millipore). The M9 minimal medium was prepared freshly every day and contained (per 100 mL): 10 mL salts 10X (0.68 g Na_2HPO_4, 0.30 g KH_2PO_4, 0.05 g NaCl, 0.10 g NH_4Cl), 0.2 mL 1 M $MgSO_4$, 0.2 mL 50 mM $CaCl_2$, 2.5 mL 20% glucose and 87.1 mL H_2O. Fluorescence and absorbance for the inhibition assay in *E. coli* cells were recorded using a Beckman Coulter DTX 880 Multimode Detector Microplate Reader. For the *in vitro* fluorescence assay, the Th-S and Th-T spectra were recorded on an Aminco Bowman series 2 luminescence spectrophotometer (Aminco-Bowman AB2, SLM Aminco, Rochester, NY) from 460 to 600 nm at 25 °C. For the *in vitro* assay with Congo red (CR), its spectrum was recorded in a Shimadzu UV-2401 PC UV−Vis spectrophotometer.

B) Transformation of competent cells

The first step in the biological assay is the incorporation in the *E. coli* cells of the plasmid with the DNA sequence encoding the targeted amyloid-prone protein. It must be mentioned that I did not perform this initial step of the biological assays, as the group had colonies of BL21 (DE3) previously transformed (bearing the desired plasmids) and stored in the freezer at −80 °C.

The procedure consisted of the transformation of *E. coli* BL21 (DE3) competent cells with the required pET vectors carrying the DNA sequence of each amyloid-prone protein. Because of the addition of the initiation codon ATG in front of genes, the overexpressed peptides contain an additional methionine residue at the N-termini. This procedure was performed for the overexpression of $A\beta_{42}$ peptide and other amyloidogenic proteins, except for tau protein. For the cloning and overexpression of full-length tau protein, *E. coli* BL21 (DE3) competent cells were transformed with the pTARA vector containing the RNA-polymerase gene of phage T7 (T7RP), under the control of the promoter PBAD. Then, *E. coli* BL21 (DE3) competent cells containing pTARA competent cells were transformed with the pRKT42 vector encoding four repeats of tau protein in two inserts.

C) Assay of antiaggregating properties

The evaluation of the antiaggregating properties of the compounds is realized in three consecutive days, even though more than one experiment can be performed in parallel.

Day 1: preparation of the overnight culture of bacteria

The first day, a culture of bacteria expressing the desired protein was prepared, in order to have enough amount of bacteria for the experiment. For a single overnight culture preparation, a colony of BL21 (DE3) cells bearing the adequate plasmid to be expressed was inoculated in 10–15 mL of M9 minimal medium containing the appropriate antibiotic or antibiotics for each protein (kanamycin and ampicillin at 50 µg / mL, and chloramphenicol at 12.5 µg / mL, **Table 8.1**) and ThS at 25 µM. The bacterial culture was grown at 37 °C with 250 rpm agitation overnight.

Table 8.1. Proteins and peptides studied with their corresponding antibiotic and inductor of protein expression.

Protein	Antibiotic	Inductor
$A\beta_{40}$	KAN[a]	IPTG[b]
$A\beta_{42}$	KAN	IPTG
tau	AMP[c] / CM[d]	Arabinose
htau (244-372)	KAN	IPTG
SynH	AMP / CM	IPTG
SynM	AMP / CM	IPTG
PrP	AMP / CM	IPTG
TTR	KAN	IPTG
hIAPP	AMP / CM	IPTG
PaHET-s PFD	KAN	IPTG
FgHET-s PFD	KAN / CM	IPTG
Sup35NM	AMP / CM	IPTG
HypFN	AMP / CM	IPTG

[a] Kanamycin
[b] 1-Thio-*β*-D-galactopyranoside
[c] Ampicillin
[d] Chloramphenicol

Day 2: preparation of the inhibition assay in microplates

At the second day, the experiment of inhibition of protein aggregation with the compounds took place. Firstly, 1.5 mL Eppendorf tubes were prepared containing the mixtures of components for the assay. Each Eppendorf tube was used for the determination of the inhibitory evaluation of one compound against one protein. A reference compound was always evaluated to ensure that the experiments worked. To induce the expression of proteins in bacteria, the adequate inducer (IPTG or arabinose, **Table 8.1**) was added to the M9 minimal medium. As negative controls (maximal amyloid presence, no inhibition) the same amount of DMSO without drug was used. In parallel, non-induced samples (in absence of inductor of protein expression) of each inhibitor / control / reference compound were prepared as positive controls (non-amyloid presence, no aggregation). These positive controls were also used to assess the potential intrinsic toxicity of the compounds and to confirm the correct bacterial growth.

The Eppendorf tubes were prepared with the following components:

- 15 µL of the inhibitor (previously diluted at 1 mM with DMSO) or 15 µL of DMSO (for negative control, absence of inhibition): final concentration 10 µM.
- 1185 µL M9 minimal medium. For the inhibition experiments: M9 minimal medium + antibiotics at previously mentioned concentrations + ThS at final concentration of 25 µM + the adequate inductor (1-thio-β-D-galactopyranoside (IPTG) at final concentration of 1 mM, arabinose at final concentration of 0.25%). For positive controls (absence of protein aggregation), the same mixture was prepared but without the inductor.
- 300 µL of the overnight bacterial culture.

Afterwards, a 96 well plate was filled with the Eppendorf tubes content (200 µL / well), sealed and incubated at 37 °C and 250 rpm agitation overnight. Normally, two identical plates are prepared with one overnight culture and this experiment was repeated three different days with three different overnight cultures, giving a total of 6 replicates per experiment. A model plaque for an experiment can be seen in **Table 8.2**.

Table 8.2. Model plaque for an experiment of antiaggregating properties. In this model, six different compounds, a negative control (with DMSO instead of compound) and a reference compound are evaluated against one single protein. In each plate there is always a negative control and a reference compound. The six induced replicates (+) for one compound come from the same Eppendorf tube and the same applies for the six non-induced (-) replicates.

		1	2	3	4	5	6	7	8	9	10	11	12
Control	**A**	+	+	+	-	-	-	+	+	+	-	-	-
Drug 1	**B**	+	+	+	-	-	-	+	+	+	-	-	-
Drug 2	**C**	+	+	+	-	-	-	+	+	+	-	-	-
Drug 3	**D**	+	+	+	-	-	-	+	+	+	-	-	-
Drug 4	**E**	+	+	+	-	-	-	+	+	+	-	-	-
Drug 5	**F**	+	+	+	-	-	-	+	+	+	-	-	-
Drug 6	**G**	+	+	+	-	-	-	+	+	+	-	-	-
Ref	**H**	+	+	+	-	-	-	+	+	+	-	-	-

Day 3: results measurement

Finally, the third day all the plaques prepared were read and the results were analysed. The fluorescence of Th-S was measured at 460–600 nm at 25 °C, with an excitation wavelength of 440 nm, a slit width of 4 nm and an emission wavelength of 485 nm. In addition, the bacterial concentration of each well was determined by absorbance measurement, as differences in bacterial cells concentration can slightly affect the Th-S relative fluorescence as a consequence of both bacterial membranes staining and scattering. So, Th-S fluorescence was normalized as a function of the bacterial concentration in each well. Moreover, the control samples of cells expressing the protein (only DMSO with inducer) were considered to correspond to 100% of relative fluorescence or 0% of inhibitory activity, whereas the control samples of cells non-expressing the protein (only DMSO, non-induced) were considered as 0% of relative fluorescence or 100% inhibition.

CHAPTER 9

Bibliography

1. *Global Health Estimates 2016: Deaths by Cause, Age, Sex, by Country and by Religion, 2000-2016*. Geneva, World Health Organization, **2018**.
2. C. Patterson. *World Alzheimer Report 2018: The state of the art of dementia research: New frontiers. Alzheimer's Disease International* **2018.**
3. Alzheimer's Association. *Alzheimer's & Dementia* **2018**, *14*, 367–429.
4. Alzheimer's Association. *Alzheimer's & Dementia* **2019**, *15*, 321–387.
5. P. Scheltens, K. Blennow, M. M. B. Breteler, B. de Strooper, G. B. Frisoni, S. Salloway, W.M. Van der Flier. *Lancet* **2016**, *388*, 505–517.
6. C. Reitz, R. Mayeux. *Biochem. Pharmacol.* **2014**, *88*, 640–651.
7. W. Shao, D. Peng, X. Wag. *J. Clin. Neurosci.* **2017**, *45*, 1–8.
8. a) A. Alzheimer. *Allgemeine Zeitschrift für Psychiatrie und Phychisch-Gerichtliche Medizin.* **1907**, *64*, 146–148. b) A. Rainulf, H. Stelzmann, N. Scnitzlein, F. R. Murtagh. *Clin. Anat.* **1995**, *8*, 429–431.
9. R. E. Tanzi, L. Bertram. *Cell* **2005**, *120*, 545–555.
10. P. Nelson, I. Alafuzoff, E. Bigio, C. Bouras, H. Braak, N. Cairns, R. Castellani, B. Crain, P. Davies. *J. Neuropathol. Exp. Neurol.* **2012**, *71*, 362–381.
11. K. Blennow, M. J. de Leon, H. Zetterberg. *Lancet* **2006**, *368*, 387–403.
12. P. Sharma, P. Srivastava, A. Seth, P. N. Tripathi, A. G. Banerjee, S. K. Shrivastava. *Prog. Neurobiol.* **2019**, *174*, 53–89.
13. D. M. Bowen, C. B. Smith, P. White, A. N. Davison. *Brain* **1976**, *99*, 459–496.
14. P. Davies, A. J. F. Maloney. *Lancet* **1976**, *2*, 1403.
15. A. Blokland. *Brain Res. Rev*. **1995**, *21*, 285–300.
16. R. T. Bartus, R. L. Dean 3rd, B. Beer, A. S. Lippa. *Science* **1982**, *217*, 408–414.
17. P. Francis, A. Palmer, M. Snape, G. Wilcock. *J. Neurol. Neurosurg. Psychiatry* **1999**, *66*, 137–147.
18. G. Benzi, A. Moretti. *Eur. J. Pharmacol.* **1998**, *346*, 1–13.
19. D. Volpato, U. Holzgrabe. *Molecules* **2018**, *23*, 3230.
20. J. A. Hardy, G. A. Higgins. *Science* **1992**, *256*, 184–185.
21. J. Hardy, D. Allsop. *Trends in Pharmac.* **1991**, *12*, 383–388.
22. D. J. Selkoe. *Neuron* **1991**, *6*, 487–498.
23. D. J. Selkoe. J. Hardy. *EMBO Mol. Med.* **2016**, *8*, 595–608.
24. J. Hardy, D. J. Selkoe. *Science*, **2002**, *297*, 353–356.
25. C. Morgan, M. Colombres, M. T. Nuñez, N. C. Inestrosa. *Prog. Neurobiol.* **2004**, *74*, 323–349.
26. T. Mohamed, A. Shakeri, P. P. N. Rao. *Eur. J. Med. Chem.* **2016**, *113*, 258–272.
27. D. J. Selkoe, D. Schenk. *Annu. Rev. Pharmacol. Toxicol*. **2003**, *43*, 545–584.

28. G. Thinakaran, E. H. Koo. *J. Biol. Chem.* **2008**, *283*, 29615–29619.
29. K. Sambamurti, N. H. Greig, D. K. Lahiri. *Neuromol. Med.* **2002**, *1*, 1–31.
30. Y. W. Zhang, R. Thompson, H. Zhang, H. Xu. *Mol. Brain*, **2011**, *4*, 3.
31. D. M. Walsh, D. J. Selkoe. *J. Neurochem.* **2007**, *101*, 1172–1184.
32. C. C. Chang, J. C. Althaus, C. J. Carruthers, M. A. Sutton, D. G. Steel, A. Gafni. *PLoS One*, **2013**, *8*, e82139.
33. C. A. lane, J. Hardy, J. M. Schott. *Eur. J. Neurol.* **2018**, *25*, 59–70.
34. S. T. Ferreira, W. L. Klein. *Neurobiol. Learn Mem.* **2011**, *96*, 529–543.
35. C. Haass, D. J. Selkoe. *Nat. Rev. Mol. Cell. Biol.* **2007**, *8*, 101–112.
36. P. T. Nelson, I. Alafuzoff, E. H. Bigio, C. Bouras, H. Braak, N. J. Cairns, R. J. Castellani, B. J. Crain, P. Davies, K. del Tedici, C. Duyckaerts, M. P. Frosch, V. Haroutunian, P. R. Hof, C. M. Hulette, B. T. Hyman, T. Iwatsubo, K. A. Jellinger, G. A. Jicha, E. Kövari, W. A. Kukull, J. B. Leverenz, S. Love, I. R. Mackenzie, D. M. Mann, E. Masliah, A. C. Mckee, T. J. Montine, J. C. Morris, J. A. Schneider, J. A. Sonnen, D. R. Thal, J. Q. Trojanowski, J. C. Troncoso, T. Wisniewski, R. L. Woltjer, T. G. Beach. *J. Neuropathol. Exp. Neurol.* **2012**, *71*, 362–381.
37. a) A. Mietelska-Porowska, U. Wasik, M. Goras, A. Filipek, G. Niewiadomska. *Int. J. Mol. Sci.* **2014**, *15*, 4671–4713. b) S. Biswal, D. Sharma, K. Kumar, T. C. Nag, K. Barhwal, S. K. Hota, B. Kumar. *Neurobiol. Learn. Mem.* **2016**, *133*, 157–170.
38. M. L. Billingsley, R. L. Kincaid. *Biochem. J.* **1997**, *323*, 577–591.
39. M. P. Mazanetz, P. M. Fischer. *Nat. Rev. Drug Discov.* **2007**, *6*, 464–479.
40. E. Kopke, Y. C. Tung, S. Shaikh, A. C. Alonso, K. Iqbal, I. Grundke-Iqbal. *J. Biol. Chem.* **1993**, *268*, 24374–24384.
41. S. Roy, B. Zhang, V. M. Lee, J. Q. Trojanowski. *Acta Neuropathol.* **2005**, *109*, 5–13.
42. D. A. Butterfield, C. B. Pocernich. *CNS Drugs* **2003**, 17, 641–652.
43. C. Tabone, M. Ramaswami. *Neuron* **2012**, *74*, 767–769.
44. J. W. Olney, D. F. Wozniak, N. B. Farber. *Arch. Neurol.* **1997**, *54*, 1234–1240.
45. a) A. F. Teich, R. E. Nicholls, D. Puzzo, J. Fiorito, R. Purgatorio, O. Arancio. *Neurotherapeutics* **2015**, *12*, 29–41. b) D. Y. Zhu, L. Lau, S. H. Liu, J. S. Wei, Y. M. Lu. *Proc. Natl. Acad. Sci. U.S.A.* **2004**, *101,* 9453–9457.
46. M. Parsons, L. Raymond. *Neuron* **2014**, *82*, 279–293.
47. B. Halliwell. *Drugs Aging* **2001**, *18*, 685–716.
48. H. W. Querfurth, F. M. LaFerla, *N. Engl. J. Med* **2010**, *362*, 329–344.
49. J. T. Coyle, P. Puttfarcken. *Science* **1993**, *262*, 689–695.
50. J. S. Aprioku. *J. Reprod. Infertil.* **2013,** *14*, 158.
51. K. Nowotny, T. Jung, A. Höhn, D. Weber, T. Grune. *Biomolecules* **2015**, *5*, 194–222.

52. W. J. Streit. *Front. Aging Neurosci*. **2010**, *2*, 1– 5.
53. J. M. Rubio-Perez, J. M. Morillas-Ruiz. *Sci. World J.* **2012**, *2012*, 1–15.
54. C. M. Henstridge, B. T. Hyman, T. L. Spire-Jones. *Nat. Rev. Neurosci.* **2019**, *20*, 94–108.
55. A. Cavalli, M. L. Bolognesi, A. Minarini, M. Rossini, V. Tumiatti, M. Recanatini, C. Melchiorre. *J. Med. Chem* **2008**, *51*, 347–372.
56. A. Carocci, A. Catalano, M. S. Sinicropi, G. Genchi. *Biometals* **2018**, *31*, 715–735.
57. D. J. R. Lane, S. Ayton, A. I. Bush. *J. Alzheimers Dis.* **2018**, *64*, 5379–5395.
58. J. T. O'Brien, T. Erkinjuntti, B. Reisberg, G. Roman, T. Sawada, L. Pantoni, J. V. Bowler, C. Ballard, C. DeCarli, P. B. Gorelick, K. Rockwood, A. Burns, S. Gauthier, S. T. DeKosky. *Lancet Neurol.* **2003**, *2*, 89–98.
59. B. Kim, E. L. Feldman, *Exp. Mol. Med.* **2015**, *47*, e149.
60. P. Sharma, P. Srivastava, A. Seth, P. N. Tripathi, A. G. Banerjee, S. K. Shrivastava. *Prog. Neurobiol.* **2019**, *174*, 53–89.
61. J. W. Lustbader, M. Cirilli, C. Lin, H. W. Xu, K. Takuma, N. Wang, C. Caspersen, X. Chen, S. Pollak, M. Chaney, F. Trinchese, S. Liu, F. Gunn-Moore, L. F. Lue, D. G. Walker, P. Kuppusamy, Z. L. Zewier, O. Arancio, D. Stern, S. S. Yan, H. Wu. *Science* **2004**, *304*, 448–452.
62. A. Caricasole, A. Copani, A. Caruso, F. Caraci, L. Iacovelli, M. A. Sortino, G. C. Terstappen, F. Nicoletti. *Trends Pharmacol. Sci.* **2003**, *24*, 233–238.
63. L. Xie, E. Helmerhorst, K. Taddei, B. Plewright, W. Van Bronswijk, R. Martins. *J. Neurosci.* **2002**, *22*, RC221.
64. B. L. Kagan, Y. Hirakura, R. Azimov, R. Azimova, M. C. Lin. *Peptides* **2002**, *23*, 1311–1315.
65. E. Tamagno, M. Parola, M. Guglielmotto, G. Santoro, P. Bardini, L. Marra, M. Tabaton, O. Danni. *Free Radical Biol. Med.* **2003**, *35*, 45–58.
66. M. E. Bamberger, G. E. Landreth. *Microsc. Res. Tech*. **2001**, *54*, 59–70.
67. M. M. Mesulam, M. A. Moran. *Ann. Neurol.* **1987**, *22*, 223–228.
68. R. Schliebs. *Neurochem. Res.* **2005**, *30*, 895–908.
69. M. C. Dinamarca, J. P. Sagal, R. A. Quintanilla, J. A. Godoy, M. S. Arrazola, N. C. Inestrosa. *Mol. Neurodegener.* **2010**, *5,* 4.
70. F. J. Muñoz, N. C. Inestrosa. *FEBS Lett.* **1999**, *450*, 205–209.
71. L. R. Fodero, S. S. Mok, D. Losic, L. L. Martin, M. I. Aguilar, C. J. Barrow, B. G. Livett, D. H. Small. *J. Neurochem.* **2004**, *88*, 1186–1193.
72. L. B. Willard, B. Hauss-Wegrzyniak, G. L. Wenk, *Neuroscience* **1999**, *88*, 193–200.
73. P. Eikelenboom, W. A. van Gool. *J. Neural Transm.* **2004**, *111*, 281–294.
74. J. D. Buxbaum, M. Oishi, H. I. Chen, R. Pinkas-Kramarski, E. A. Jaffe, S. E. Gandy, P. Greengard. *Proc. Natl. Acad. Sci. U.S.A.* **1992**, *89*, 10075–10078.

75. J. T. Rogers, L. M. Leiter, J. McPhee, C. M. Cahill, S. S. Zhan, H. Potter, L. N. Nilsson. *J. Biol. Chem.* **1999**, *274*, 6421–6431.
76. S. Roβner, J. Apelt, R. Schliebs, J. R. Perez-Polo, V. Bigl. *J. Neurosci. Res.* **2001**, *64*, 437–446.
77. T. Maas, J. Eidenmüller, R. Brandt. *J. Biol. Chem.* **2000**, *275*, 15733–15740.
78. X. Li, Y. Kumar, H. Zempel, E. M. Mandelkow, J. Biernat, E. Mandelkow. *EMBO J.* **2011**, *30*, 4825–4837.
79. F. Hernandez, J. Avila. *Cell. Mol. Life Sci.* **2007**, *64*, 2219–2233.
80. S. Varadarajan, S. Yatin, M. Aksenova, D. A. Butterfield. *J. Struct. Biol.* **2000**, *130*, 184–208.
81. S. Varadarajan, J. Kanski, M. Aksenova, C. Lauderback, D. A. Butterfield. *J. Am. Chem. Soc.* **2001**, *123*, 5625–5631.
82. D. A. Butterfield, D. Boyd–Kimball. *J. Alzheimers Dis.* **2018**, *62*, 1345–1367.
83. V. Rangachari, D. N. Dean, P. Rana, A. Vaidya, P. Ghosh. *BBA Biomembranes* **2018**, *1860*, 1652–1662.
84. F. De Felice, P. Velasco, M. Lambert, K. Viola, S. Fernandez. S. Ferreira, L. Klein. *J. Biol. Chem.* **2007**, *282*, 11590–11601.
85. R. Malinow. *Curr. Opin. Neurobiol.* **2012**, *22*, 559–563.
86. J. S. de Almeida, S. F. de A. Cavalcante, R. Dolezal, K. Kuca, K. Musilek, D. Jun, T. C. França. *J. Biomol. Struct. Dyn.* **2018**, *37*, 1–8.
87. H. Dvir, I. Silman, M. Harel, T. L. Rosenberry, J. Sussman. *Chem. Biol. Interact.* **2010**, *187*, 10–22.
88. V. N. Talesa. *Mech. Ageing Dev.* **2001**, *122*, 1961–1969.
89. Y. Madav, S. Wairkar, B. Prabhakar. *Brain Res. Bull.* **2019**, *146*, 171–184.
90. J. Patocka, D. Jun, K. Kuca. *Curr. Drug Metab.* **2008**, *9*, 332–335.
91. J. Coyle, P. Kershaw. *Biol. Psychiatry* **2001**, *49*, 289–299.
92. M. B. Colovic, D. Z. Krstic, T. D. Lazarevic-Pasti, A. M. Bondzic, V. M. Vasic. *Curr. Neuropharmacol.* **2013**, *11*, 315–335.
93. E. Giacobini. *Pharmacol. Res.* **2004**, *50*, 433–440.
94. J. S. Birks. *Cochrane Database Syst Rev* 2006, *1*, CD005593.
95. R. Raschetti, E. Albanese, N. Vanacore, M. Maggini. *PLoS Med.* **2007**, *4*, e338.
96. A. Contestabile. *Behav. Brain Res.* **2011**, *221*, 334–340.
97. D. Muñoz-Torrero. *Curr. Med. Chem.* **2008**, *15*, 2433–2455.
98. M. Mehta, A. Adem, M. Sabbagh. *Int. J. Alzheimers Dis.* **2012**, *2012*, 728983.
99. A. Astrup, S. Madsbad, L. Breum, T. J. Jensen, J. P. Kroustrup, T. M. Larsen. *Lancet* **2008**, *372*, 1906–1913.
100. W. Krall, J. Sramek, N. Cutler. *Ann. Pharmacother.* **1999**, *33*, 441–450.

101. L. Savini, A. Gaeta, C. Fattorusso, B. Catalanotti, G. Campiani, L. Chiasserini, C. Pellerano, E. Novellino, D. McKissic, A. Saxena. *J. Med. Chem.* **2003**, *46*, 1–4.
102. G. Reid, N. Chilukuri, S. Darvesh. *Neuroscience* **2013**, *234*, 53–68.
103. M. Mesulam, A. Guillozet, P. Shaw, B. Quinn. *Neurobiol. Dis.* **2002**, *9*, 88–93.
104. Y. Nicolet, O. Lockridge, P. Masson, J. C. Fontecilla-Camps, F. Nachon. *J. Biol. Chem.* **2003**, *278*, 41141–41147.
105. S. Darvesh, D. A. Hopkins, C. Geula. *Nat. Rev. Neurosci.* **2003**, *4*, 131–138.
106. C. H. Lee, W. Lü, J. C. Michel, A. Goehring, J. Du, X. Song, E. Gouaux. *Nature* **2014**, *511*, 191–197.
107. E. Karakas, H. Furukawa. *Science* **2014**, *344*, 992–997.
108. S. A. Lipton. *Nat. Rev. Drug Discov*. **2006**, *5*, 160–170.
109. R. McShane, A. Areosa Sastre, N. Minakaran. *Cochrane Database Syst. Rev.* **2006**, *2*, CD003154.
110. P. N. Tariot, M. R. Farlow, G. T. Grossberg, S. M. Graham, S. McDonald, I. Gergel. *JAMA* **2004**, *291*, 317–324.
111. J. J. Miguel-Hidalgo, I. A. Paul, V. Wanzo, P. K. Banerjee. *Eur. J. Pharmacol.* **2012**, *692*, 38–45.
112. E. Karran, J. Hardy. *Ann. Neurol.* **2014**, *76*, 185–205.
113. R. Vassar, B. D. Bennett, S. Babu-Khan, S. Kahn, E. A. Mendiaz, P. Denis, D. B. Teplow, S. Ross, P. Amarante, R. Loeloff. *Science* **1999**, *286*, 735–741.
114. J. Yuan, S. Venkatraman, Y. Zheng, B. M. McKeever, L. W. Dillard, S. B. Singh. *J. Med. Chem.* **2013**, *56*, 4156–4180.
115. M. Hernández-Rodríguez, J. Correa-Basurto, A. Gutiérrez, J. Vitorica, M. C. Rosales- Hernández. *Eur. J. Med. Chem.* **2016**. *124*, 1142–1154.
116. L. Hong, J. Tang. *Biochemistry* **2004**, *43*, 4689–4695.
117. B. Hitt, S. Riordan, L. Kukreja, W. Eimer, T. Rajapaksha, R. Vassar. *J. Biol. Chem.* **2012**, *287*, 38408–38425.
118. K. W. Menting, J. A. Claassen. *Front. Aging Neurosci.* **2014**, *6*, 1–19.
119. S. Hung, W. Fu. *J. Biomed. Sci.* **2017**, *24*, 1–47.
120. G. He, W. Luo, P. Li, C. Remmers, W. J. Netzer, J. Hendrick, K. Bettayeb, M. Flajolet, F. Gorelick, L. P. Wennogle. *Nature* **2010**, *467*, 95–98.
121. J. D. Grill, J. L. Cummings. *Expert Rev. Neurother.* **2010**, *10*, 711.
122. C. M. Carroll, Y. M. Li. *Brain Res. Bull.* **2016**, *126*, 199–206.
123. S. C. Mayer, A. F. Kreft, B. Harrison, M. Abou-Gharbia, M. Antane, S. Aschmies, K. Atchison, M. Chlenov, D. C. Cole, T. Comery. *J. Med. Chem.* **2008**, *51*, 7348–7351.
124. R. J. Andrew, K. A. Kellett, G. Thinakaran, N. M. Hooper. *J. Biol. Chem.* **2016**, *291*, 19235–19244.

125. K. Stromberg, S. Eketjall, B. Georgievska, K. Tunblad, K. Eliason, F. Olsson, A. C. Radesater, R. Klintenberg, P. I. Arvidsson, S. von Berg, J. Fälting, R. F. Cowburn, M. S. Dabrowski, *FEBS J.* **2015**, *282*, 65–73.

126. S. H. Barage, K. D. Sonawane. *Neuropeptides* **2015**, *52,* 1–18.

127. A. Lorenzo, B. A. Yankner. *Proc. Natl. Acad. Sci. U.S.A.* **1994**, *91*, 12243–12247.

128. B. Neddenriep, A. Calciano, D. Conti, E. Sauve, M. Paterson, E. Bruno, D. A. Moffet. *Open Biotechnol. J.* **2011**, *5*, 39–46.

129. L. D. Estrada, C. Soto. *Curr. Top. Med. Chem.* **2007**, *7*, 115–126.

130. a) P. S. Aisen, S. Gauthier, B. Vellas, R. Briand, D. Saumier, J. Laurin, D. Garceau. *Curr. Alzheimer Res.* **2007**, *4*, 473–478. b) C. Caltagirone, L. Ferrannini, N. Marchionni, G. Nappi, G. Scapagnini, M. Trabucchi. *Aging Clin. Exp. Res*. **2012**, *24*, 580–587.

131. D. S. Wang, D. W. Dickson, J. S. Malter. *J. Biomed. Biotechnol.* **2006**, *2006*, 58406.

132. N. N. Nalivaeva, C. Beckett, N. D. Belyaev, A. J. Turner. *J. Neurochem.* **2012**, *120*, 167–185.

133. J. Godyn, J. Jonczyk, D. Panek, B. Malawska. *Pharmacol. Rep.* **2016**, *68,* 127–138.

134. J. Moreth, C. Mavoungou, K. Schindowski. *Immun. Ageing* **2013**, *10*, 1–9.

135. C. Gao, C. Hölscher, Y. Liu, L. Li. *Rev. Neurosci.* **2012**, *23*, 1–11.

136. a) H. Hampel, M. Ewers, K. Burger, P. Annas, A. Mortberg, A. Bogstedt, L. Frolich, J. Schroder, P. Schonknecht, M. W. Riepe, I. Kraft, T. Gasser, T. Leyhe, H. J. Moller, A. Kurz, H. Basun. *J. Clin. Psychiatry* **2009***, 70*, 922–931. b) P. N. Tariot, P. Aisen, J. Cummings, L. Jakimovich, L. Schneider, R. Thomas, L. Becerra, R. Loy. *Alzheimers Dement.* **2009**, *5*, 84–85.

137. R. Anand, K. D. Gill, A. A. Mahdi. *Neuropharmacology* **2014**, *76*, 27–50.

138. K. R. Brunden, B. Zhang, J. Carroll, Y. Yao, J. S. Potuzak, A. M. Hogan, M. Iba, M. J. James, S. X. Xie, C. Ballatore, A. B. Smith 3rd, V. M. Lee, J. Q. Trojanowski. *J. Neurosci.* **2010**, *30*, 13861–13866.

139. S. Wegmann, S. Nicholls, S. Takeda, Z. Fan, B. T. Hyman. *J. Neurochem* **2016**, *139*, 1163–1174.

140. N. Badiola, V. Alcalde, A. Pujol, L. M. Munter, G. Multhaup, A. Lleo, M. Coma, M. Soler-Lopez, P. Aloy. *PLoS One* **2013**, *8*, e58837.

141. A. Boutajangout, J. Ingadottir, P. Davies, E. M. Sigurdsson. *J. Neurochem.* **2011**, *118*, 658–667.

142. C. H. van Dyck. *Biol. Psychiatry* **2018**, *83*, 311–319.

143. F. Grodstein, J. Chen, W. C. Willett. *Am. J. Clin. Nutr.* **2003**, *77*, 975–984.

144. N. Farina, M. G. Isaac, A. R. Clark, J. Rusted, N. Tabet. *Cochrane Database Syst. Rev.* **2012**, *11*, CD002854.

145. R. C. Petersen, R. G. Thomas, M. Grundman, D. Bennett, R. Doody, S. Ferris, D. Galasko, S. Jin, J. Kaye, A. Levey, E. Pfeiffer, M. Sano, C. H. van Dyck, L. J. Thal. *N. Engl. J. Med.* **2005**, *352*, 2379–2388.

146. M. W. Dysken, P. D. Guarino, J. E. Vertrees, S. Asthana, M. Sano, M. Llorente, M. Pallaki, S. Love, G. D. Schellenberg, J. R. McCarten, J. Malphurs, S. Prieto, P. Chen, D. J. Loreck, S. Carney, G. Trapp, R. S. Bakshi, J. E. Mintzer, J. L. Heidebrink, A. Vidal-Cardona, L. M. Arroyo, A. R. Cruz, N. W. Kowall, M. P. Chopra, S. Craft, S. Thielke, C. L. Turvey, C. Woodman, K. A. Monnell, K. Gordon, J. Tomaska, G. Vatassery. *Alzheimers Dement.* **2014**, *10*, 36–44.

147. C. P. Ramsey, C. A. Glass, M. B. Montgomery, K. A. Lindl, G. P. Ritson, L. A. Chia, R. L. Hamilton, C. T. Chu, K. L. Jordan-Sciutto. *J. Neuropathol. Exp. Neurol.* **2007**, *66*, 75–85.

148. R. A. Cherny, C. S. Atwood, M. E. Xilinas, D. N. Gray, W. D. Jones, C. A. McLean, K. J. Barnham, I. Volitakis, F. W. Fraser, Y. S. Kim. *Neuron* **2001**, *30*, 665–676.

149. P. A. Adlard, J. M. Parncutt, D. I. Finkelstein, A. I. Bush. *J. Neurosci.* **2010**, *30*, 1631–1636.

150. P. A. Adlard, R. A. Cherny, D. I. Finkelstein, E. Gautier, E. Robb, M. Cortes, I. Volitakis, X. Liu, J. P. Smith, K. Perez, K. Laughton, Q. X. Li, S. A. Charman, J. A. Nicolazzo, S. Wilkins, K. Deleva, T. Lynch, G. Kok, C. W. Ritchie, R. E. Tanzi, R. Cappai, C. L. Masters, K. J. Barnham, A. I. Bush. *Neuron* **2008**, *59*, 43–55.

151. C. Cornelius, J. Fastbom, B. Winblad, M. Viitanen. *Neuroepidemiology* **2004**, *23*, 135–143.

152. S. A. Reines, G. A. Block, J. C. Morris, G. Liu, M. L. Nessly, C. R. Lines, B. A. Norman, C. C. Baranak. *Neurology* **2004**, *62*, 66–71.

153. B. Schmitt, T. Bernhardt, H. J. Moeller, I. Heuser, L. Frölich. *CNS Drugs* **2004**, *18*, 827–844.

154. R. Morphy, Z. Rankovic. *J. Med. Chem.* **2005**, *48*, 6523–6543.

155. E. Viayna, I. Sola, O. Di Pietro, D. Muñoz-Torrero. *Curr. Med. Chem.* **2013**, *20*, 1623–1634.

156. A. Anighoro, J. Bajorath, G. Rastelli. *J. Med. Chem.* **2014**, *57*, 7874–7887.

157. M. Decker. *Curr. Med. Chem.* **2011**, *18*, 1464–1475.

158. E. Viayna, I. Sola, M. Bartolini, A. De Simone, C. Tapia-Rojas, F. G. Serrano, R. Sabaté, J. Juárez-Jiménez, B. Pérez, F. J. Luque, V. Andrisano, M. V. Clos, N. C. Inestrosa, D. Muñoz-Torrero. *J. Med. Chem.* **2014**, *57*, 2549–2567.

159. A. Badia, J. E. Baños, P. Camps, J. Contreras, D. M. Görbig, D. Muñoz-Torrero, M. Simón, N. M. Vivas. *Bioorg. Med. Chem.* **1998**, *6*, 427–440.

160. P. Camps, R. El Achab, D. M. Görbig, J. Morral, D. Muñoz-Torrero, A. Badia, J. E. Baños, N. M. Vivas, X. Barril, M. Orozco, F. J. Luque. *J. Med. Chem.* **1999**, *42*, 3227−3242.

161. D. Muñoz-Torrero, P. Camps. *Exp. Opin. Drug Discov.* **2008**, *3*, 65–81.

162. M. Pickhardt, Z. Gazova, M. V. Bergen, I. Khlistunova, Y. Wang, A. Hascher, E. -M. Mandelkow, J. Biernat, E. Mandelkow. *J. Biol. Chem.* **2005**, *280*, 3628–3635.

163. B. Bulic, M. Pickhardt, B. Schmidt, E. -M. Mandelkow, H. Waldmann, E. Mandelkow. *Angew. Chem. Int. Ed.* **2009**, *48*, 1740–1752.

164. X. Yang, G. Sun, C. Yang, B. Wang. *ChemMedChem* **2011**, *6*, 2294–2301.

165. F. G. Serrano, C. Tapia-Rojas, F. J. Carvajal, P. Cisternas, E. Viayna, I. Sola, D. Muñoz-Torrero, N. C. Inestrosa. *Curr. Alzheimer Res.* **2016**, *13*, 1017–1029.

166. L. Vázquez-Jiménez, M. Garrido, M. Miceli, E. Prats, A. Ferrer-Montiel, M. Teixidó, C. Jimeno, A. Messeguer. *Eur. J. Med. Chem.* **2016**, *123*, 788–802.

167. F. J. Pérez-Areales, M. Garrido, E. Aso, M. Bartolini, A. De Simone, A. Espargaró, T. Ginex, R. Sabate, B. Pérez, V. Andrisano, F. J. Luque, I. Ferrer, F. Ciruela, A. Messeguer, D. Muñoz-Torrero, submitted.

168. F. J. Pérez-Areales, N. Betari, A. Viayna, C. Pont, A. Espargaró, M. Bartolini, A. De Simone, J. F. R. Alvarenga, B. Pérez, R. Sabate, R. M. Lamuela-Raventós, V. Andrisano, F. J. Luque, D. Muñoz-Torrero. *Fut. Med. Chem.* **2017**, *9*, 965–981.

169. J. Liu, G. Hu, R. Xu, Y. Qiao, H. -P. Wu, X. Ding, P. Duan, P. Tu, Y. -J. Lin. *J. Asian Nat. Prod. Res.* **2015**, *15*, 756–763.

170. H. Pajouhesh, G. R. Lenz. *Neurotherapeutics* **2005**, *2*, 541–553.

171. O. Di Pietro, J. Juárez-Jiménez, D. Muñoz- Torrero, C. A. Laughton, F. J. Luque. *PLoS ONE* **2017**, *12*, e0190327.

172. G. L. Ellman, K. D. Courtney, V. Andres Jr., R. M. Featherstone. *Biochem. Pharmacol.* **1961**, *7*, 88–90.

173. E. Viayna, R. Sabaté, D. Muñoz-Torrero. *Curr. Top. Med. Chem.* **2013**, *13*, 1820–1842.

174. S. Pouplana, A. Espargaró, C. Galdeano, E. Viayna, I. Sola, S. Ventura, D. Muñoz-Torrero, R. Sabate. *Curr. Med. Chem*. **2014**, *21*, 1152–1159.

175. L. Di, E. Kerns, K. Fan, O. McConnell, G. Carter. *Eur. J. Med. Chem.* **2003**, *38*, 223–232.

176. C. Galdeano, E. Viayna, I. Sola, X. Formosa, P. Camps, A. Badia, M. V. Clos, J. Relat, M. Ratia, M. Bartolini, F. Mancini, V. Andrisano, M. Salmona, C. Minguillón, G. C. González-Muñoz, M. I. Rodríguez-Franco, A. Bidon-Chanal, F. J. Luque, D. Muñoz-Torrero. *J. Med. Chem.* **2012**, *55*, 661–669.

177. M. Hedberg, M. V. Clos, M. Ratia, D. Gonzalez, C. U. Lithner, P. Camps, D. Muñoz-Torrero, A. Badia, L. Giménez-Llort, A. Nordberg. *Neurodegener. Dis.* **2010**, *7*, 379–388.

178. R. Friedman, A. Caflisch. *Proteins* **2010**, *78*, 1575–1582.

179. A. A. Gorfe, A. Caflisch. *Structure* **2005**, *13*, 1487–1498.

180. J. W. Newman, C. Morisseau, B. D. Hammock. *Prog. Lipid Res.* **2005**, *44*, 1–51.

181. C. Morisseau, B. D. Hammock. *Annu. Rev. Pharmacol. Toxicol.* **2013**, *53*, 37–58.

182. A. Marowsky, J. Burgener, J. R. Falck, J.-M. Fritschy, M. Arand. *Neuroscience* **2009**, *163*, 646–661.

183. P. Sura, R. Sura, A. E. Enayetallah, D. F. Grant. *J. Histochem. Cytochem.* **2008**, *56*, 551–559.

184. C. Brenneis, M. Sisignano, O. Coste, K. Altenrath, M. J. Fischer, C. Angioni, I. Fleming, R. P. Brandes, P. W. Reeh, C. J. Woolf, G. Geisslinger, K. Scholich. *Mol. Pain* **2011**, *7*, 78.

185. B. Inceoglu, A. Bettaieb, F. G. Haj, A. V. Gomes, B. D. Hammock. *Prostaglandins Other Lipid Mediat.* **2017**, *133*, 68–78.

186. X. Liu, C. M. Davis, N. J. Alkayed. *Antioxid. Redox Signaling* **2018**, *28*, 987–1007.

187. A. A. Spector, X. Fang, G. D. Snyder, N. L. Weintraub. *Prog. Lipid Res.* **2004**, *43*, 55–90.

188. T. E. Rose, C. Morisseau, J. -Y. Liu, B. Inceoglu, P. D. Jones, J. R. Sanborn, B. D. Hammock. *J. Med. Chem.* **2010**, *53*, 7067–7075.

189. I. Sola, E. Aso, D. Frattini, I. López-González, A. Espargaró, R. Sabaté, O. Di Pietro, F. J. Luque, M. V. Clos, I. Ferrer, D. Muñoz-Torrero. *J. Med. Chem.* **2015**, *58*, 6018–6032.

190. O. Di Pietro, F. J. Pérez-Areales, J. Juárez-Jiménez, A. Espargaró, M. V. Clos, B. Pérez, R. Lavilla, R. Sabaté, F. J. Luque, D. Muñoz-Torrero. *Eur. J. Med. Chem.* **2014**, *84*, 107–117.

191. P. Camps, X. Formosa, C. Galdeano, T. Gómez, D. Muñoz-Torrero, L. Ramírez, E. Viayna, E. Gómez, N. Isambert, R. Lavilla, A. Badia, M. V. Clos, M. Bartolini, F. Mancini, V. Andrisano, A. Bidon-Chanal, Ó. Huertas, T. Dafni, F. J. Luque. *Chem. Biol. Interact.* **2010**, *187*, 411–415.

192. P. Camps, X. Formosa, C. Galdeano, T. Gómez, D. Muñoz-Torrero, M. Scarpellini, E. Viayna, A. Badia, M. V. Clos, A. Camins, M. Pallàs, M. Bartolini, F. Mancini, V. Andrisano, J. Estelrich, M. Lizondo, A. Bidon-Chanal, F. J. Luque. *J. Med. Chem.* **2008**, *51*, 3588–3598.

193. S. J. Burguess, A. Selzer, J. X. Kelly, M. J. Smilkstein, M. K. Riscoe, D. H. Peyton. *J. Med. Chem.* **2006**, *49*, 5623–5625.

194. M. de Souza, K. Pais, C. Kaiser, M. Peralta, M. Ferreira, M. Lourenço. *Bioorg. Med. Chem.* **2009**, *17*, 1474–1480.

195. N. M. Wolf, C. Morisseau, P. D. Jones, B. Hock, B. D. Hammock. *Anal. Biochem.* **2006**, *355*, 71–80.

196. a) A. Aguzzi, T. O'Connor. *Nat. Rev. Drug Discov.* **2010**, *9*, 237–248. b) L. Goldschmidt, P. K. Teng, L. Riek, D. Eisenberg. *Proc. Natl. Acad. Sci. U.S.A.* **2010**, *107*, 3487–3492.

197. F. Rousseau, L. Serrano, J. W. Schymkowitz. *J. Mol. Biol.* **2006**, *355*, 1037−1047.

198. F. Chiti, C. M. Dobson. *Annu. Rev. Biochem.* **2006**, *75*, 333−366.

199. D. Eisenberg, R. Nelson, M. R. Sawaya, M. Balbirnie, S. Sambashivan, M. I. Ivanova, A. O. Madsen, C. Riekel. *Acc. Chem. Res.* **2006**, *39*, 568−575.

200. I. W. Hamley. *Chem. Rev.* **2012**, *112*, 5147−5192.

201. a) M. Bartolini, C. Bertucci, M. L. Bolognesi, A. Cavalli, C. Melchiorre, V. Andrisano. *ChemBioChem* **2007**, *8*, 2152−2161. b) T. Akaishi, T. Morimoto, M. Shibao, S. Watanabe, K. Sakai-Kato, N. Utsunomiya-Tate, K. Abe. *Neurosci. Lett*. **2008**, *444*, 280−285.

202. S. W. Pimplikar. *Int. J. Biochem. Cell Biol.* **2009**, *41*, 1261−1268.

203. S. Ventura, A. Villaverde. *Trends Biotechnol.* **2006**, *24*, 179−185.

204. N. S. de Groot, R. Sabate, S. Ventura. *Trends Biochem. Sci.* **2009**, *34*, 408−416.

205. M. Carrió, N. González-Montalbán, A. Vera, A. Villaverde, S. Ventura. *J. Mol. Biol*. **2005**, *347*, 1025−1037.

206. A. Espargaró, R. Sabate, S. Ventura. *Mol. Biosyst.* **2012**, *8*, 2839−2844.

207. H. LeVine III. *Methods Enzymol.* **1999**, *309*, 274−284.

208. A. Espargaro, A. Medina, O. Di Pietro, D. Munoz-Torrero, R. Sabate. *Sci. Rep.* **2016**, *6*, 23349.

209. F. J. Pérez-Areales, A. L. Turcu, M. Barniol-Xicota, C. Pont, D. Pivetta, A. Espargaró, M. Bartolini, A. De Simone, V. Andrisano, Belén Pérez, R. Sabate, F. X. Sureda, S. Vázquez, D. Muñoz-Torrero. *Eur. J. Med. Chem.* **2019**, *180*, 613–626.

210. A. Espargaró, C. Pont, P. Gamez, D. Muñoz-Torrero, R. Sabate. *ACS Chem. Neurosci*. **2019**, *10*, 1311–1317.

211. O. Di Pietro, F. J. Perez-Areales, J. Juarez-Jimenez, A. Espargaro, M. V. Clos, B. Perez, R. Lavilla, R. Sabate, F. J. Luque, D. Muñoz- Torrero. *Eur. J. Med. Chem.* **2014**, *84*, 107−117.

212. D. Muñoz-Torrero, M. Pera, J. Relat, M. Ratia, C. Galdeano, E. Viayna, I. Sola, X. Formosa, P. Camps, A. Badia, M. V. Clos. *Neurodegener. Dis.* **2012**, *10*, 96−99.

213. C. Galdeano, E. Viayna, I. Sola, X. Formosa, P. Camps, A. Badia, M. V. Clos, J. Relat, M. Ratia, M. Bartolini, F. Mancini, V. Andrisano, M. Salmona, C. Minguillon, G. C. Gonzalez-Munoz, M. I. Rodriguez- Franco, A. Bidon-Chanal, F. J. Luque, D. Muñoz-Torrero. *J. Med. Chem.* **2012**, *55*, 661−669.

214. P. Spólnik, B. Stopa, B. Piekarska, A. Jagusiak, L. Konieczny, J. Rybarska, M. Król, I. Roterman, B. Urbanowicz, J. Zieba-Palus. *Chem. Biol. Drug Des.* **2007**, *70*, 491−501.

215. N. Darghal, A. Garnier-Suillerot, M. Salerno. *Biochem. Biophys. Res. Commun.* **2006**, *343*, 623−629.

CHAPTER 10

Communication of results

Scientific publications

F. J. Pérez-Areales, A. L. Turcu, M. Barniol-Xicota, **C. Pont**, D. Pivetta, A. Espargaró, M. Bartolini, A. De Simone, V. Andrisano, B. Pérez, R. Sabate, F. X. Sureda, S. Vázquez, D. Muñoz-Torrero. A novel class of multitarget benzohomoadamantane-chlorotacrine hybrids to confront the cholinergic and glutamatergic mechanisms of Alzheimer's disease**.** *Eur. J. Med. Chem.* **2019**, *180*, 613–626.

A. B. Caballero, A. Espargaró, **C. Pont**, M. A. Busquets, J. Estelrich, D. Muñoz-Torrero, P. Gamez, R. Sabate. Bacterial Inclusion Bodies for Anti-Amyloid Drug Discovery: Current and Future Screening Methods. *Curr Protein Pept Sci*. **2019**, 20, 563–576.

A. Espargaró*, **C. Pont***, P. Gamez, D. Muñoz-Torrero, R. Sabate. Amyloid pan-inhibitors: one family of compounds to cope with all conformational diseases. *ACS Chem. Neurosci.,* **2019**, *10*, 1311−1317.

* Equal contribution to the work

F. J. Pérez-Areales, N. Betari, A. Viayna, **C. Pont**, A. Espargaró, M. Bartolini, A. De Simone, F. J. Rinaldi Alvarenga, B. Pérez, R. Sabate, R. M. Lamuela-Raventós, V. Andrisano, F. J. Luque, D. Muñoz-Torrero. Design, synthesis and multitarget biological profiling of a second-generation anti-Alzheimer rhein-huprine hybrids. *Fut. Med. Chem.*, **2017**, *9*, 965–981.

Scientific patent

Inventors (by order): D. Muñoz-Torrero, S. Vázquez, **C. Pont**, S. Codony.
Title: Multitarget compounds for the treatment of Alzheimer's disease
Application Number: EP19382219.4 Priority country: Members of the European Patent Convention
Priority date: 28/03/2019
Patent Holder: UBAR - Universitat de Barcelona

Contributions to scientific meetings

Oral communications

C. Pont, N. Cristiano, A. Albalat, P. Martínez, M. Bartolini, A. de Simone, M. Barenys, D. Linares, J. Gomez, B. Pérez, R. Sabate, V. Andrisano, D. Muñoz-Torrero. "Synthesis and pharmacological evaluation of a novel class of multitarget huprine-based anti-Alzheimer hybrids". *Italian-Spanish-Portuguese Joint Meeting in Medicinal Chemistry (MedChemSicily 2018)*. July **2018**, Palermo (Italy).

Poster presentations

C. Pont, N. Martínez, T. Ginex, M. Bartolini, A. de Simone, M. Barenys, A. Matellone, M. Scheiner, J. Gomez, B. Pérez, R. Sabate, V. Andrisano, M. L. Bolognesi, M. Decker, F. J. Luque, D. Muñoz-Torrero. "Synthesis and biological profiling of multisite BACE-1/AChE inhibitors as potential anti-Alzheimer agents". *EFMC-ACSMEDI Medicinal Chemistry Frontiers 2019*. June **2019**. Krakow (Poland).

F. J. Pérez-Areales, A. L. Turcu, M. Barniol-Xicota, **C. Pont**, D. Pivetta, A. Espargaró, M. Bartolini, A. De Simone, V. Andrisano, B. Pérez, R. Sabaté, F. X. Sureda, S. Vázquez, Diego Muñoz-Torrero. "Novel multi-target agents tackling Alzheimer's disease through cholinesterases inhibition and NMDA receptor antagonism". *EFMC-ACSMEDI Medicinal Chemistry Frontiers 2019*. June **2019**. Krakow (Poland).

C. Pont, A. Espargaró, P. Gamez, D. Muñoz-Torrero, R. Sabaté. "Amyloid Pan-inhibitors: can a single compound treat all conformational diseases?". *2nd Molecules Medicinal Chemistry Symposium: Facing Novel Challenges in Drug Discovery*. May **2019**. Barcelona (Spain).

F. J. Pérez-Areales, A. L. Turcu, M. Barniol-Xicota, **C. Pont**, D. Pivetta, A. Espargaró, M. Bartolini, A. De Simone, V. Andrisano, B. Pérez, R. Sabaté, F. X. Sureda, S. Vázquez, Diego Muñoz-Torrero. "A novel class of cholinesterases- and NMDA receptor-directed multi-target anti-Alzheimer agents". *2nd Molecules Medicinal Chemistry Symposium: Facing Novel Challenges in Drug Discovery*. May **2019**. Barcelona (Spain).

C. Pont. "Design, synthesis and pharmacological profiling of a new class of anti-Alzheimer huprine-based hybrids". *XXXVIII European School of Medicinal Chemistry (ESMEC 2018)*. July **2018**. Urbino (Italy)

C. Pont, N. Cristiano, A. Albalat, P. Martínez, M. Bartolini, A. de Simone, M. Barenys, D. Linares, J. Gomez, B. Pérez, R. Sabate, V. Andrisano, D. Muñoz-Torrero. "Synthesis and multitarget biological profiling of a new generation of anti-Alzheimer hybrids". *V Symposium of Young Scientists (SEQT).* June **2018**. Madrid (Spain).

Publications and contributions not directly related with the present Thesis content

Scientific publications

N. Alencar, I. Sola, M. Linares, J. Juárez-Jiménez, **C. Pont,** A. Viayna, D. Vílchez, C. Sampedro, P. Abad, S. Pérez-Benavente, J. Lameira, J. M. Bautista, D. Muñoz-Torrero, F. J. Luque. First homology model of Plasmodium falciparum glucose-6-phosphate dehydrogenase: Discovery of selective substrate analog-based inhibitors as novel antimalarial agents. *Eur. J. Med. Chem.,* **2018**, *146*, 108–122.

Oral communications

C. Pont, N. Alencar, I. Sola, M. Linares, L. Di Palma, C. Barbaraci, C. Sampedro, J. Juárez-Jiménez, P. Abad, S. Pérez-Benavente, J. Lameira, J. M. Bautista, F. J. Luque, D. Muñoz-Torrero. "Design of Potential Antimalarial Agents Based on a Homology Model of Plasmodium falciparum Glucose-6-Phosphate Dehydrogenase". *1st Molecules Medicinal Chemistry Symposium (1st MMCS)*. September **2017**. Barcelona (Spain). Oral communication.

C. Pont, I. Sola, N. Alencar, M. Linares, C. Sampedro, J. Juárez-Jiménez, P. Abad, S. Pérez-Benavente, J. M. Bautista, F. J. Luque, D. Muñoz-Torrero. "Selective inhibitors of Plasmodium falciparum glucose-6-phosphate dehydrogenase as a new class of antimalarial agents". *Medicinal Chemistry of Tropical Diseases. XIIth SEQT Symposium*. November **2016**. Tres Cantos (Madrid, Spain). Flash Oral Communication.

Poster presentations

C. Pont, N. Alencar, I. Sola, M. Linares, L. Di Palma, C. Barbaraci, C. Sampedro, J. Juárez-Jiménez, P. Abad, S. Pérez-Benavente, J. Lameira, J. M. Bautista, F. J. Luque, D. Muñoz-Torrero. "Plasmodium falciparum glucose-6-phosphate dehydrogenase, a promising target in the search of novel selective antimalarial agents". *Hybrid Molecules and Polypharmacology in Drug Discovery*. November **2017**. Würzburg (Germany).

C. Pont, N. Alencar, I. Sola, M. Linares, L. Di Palma, C. Barbaraci, C. Sampedro, J. Juárez-Jiménez, P. Abad, S. Pérez-Benavente, J. Lameira, J. M. Bautista, F. J. Luque, D. Muñoz-Torrero. "Targeting Plasmodium falciparum glucose-6-phosphate dehydrogenase in the pursuit of novel antimalarial agents". *10th Joint Meeting on Medicinal Chemistry*. June **2017**. Dubrovnik (Croatia).

C. Pont, N. Alencar, I. Sola, M. Linares, L. Di Palma, C. Barbaraci, C. Sampedro, J. Juárez-Jiménez, P. Abad, S. Pérez-Benavente, J. Lameira, J. M. Bautista, F. J. Luque, D. Muñoz-Torrero. "Plasmodium falciparum glucose-6-phosphate dehydrogenase, a promising target in the search of novel selective antimalarial agents" *IV Symposium of Young Scientists (SEQT).* May **2017**. Barcelona (Spain). Best poster prize.

C. Pont, I. Sola, N. Alencar, M. Linares, C. Sampedro, J. Juárez-Jiménez, P. Abad, S. Pérez-Benavente, J. M. Bautista, F. J. Luque, D. Muñoz-Torrero. "Design, Synthesis and Biological Evaluation of a New Class of Antimalarial Agents" *III Symposium of Young Scientists (SEQT).* June **2016**. Barcelona (Spain).